ISSN 1512-1127

საქართველოს გეოფიზიკური საზოგადოების ჟურნალი

სერია ბ. ატმოსფეროს, ოკეანისა და კოსმოსური პლაზმის ფიზიკა

JOURNAL
OF THE GEORGIAN GEOPHYSICAL SOCIETY

Issue B. Physics of Atmosphere, Ocean and Space Plasma

ტომი 15ბ 2011-2012
vol. 15B 2011-2012

ISSN 1512-1127

საქართველოს გეოფიზიკური საზოგადოების ჟურნალი

სერია ბ. ატმოსფეროს, ოკეანისა და კოსმოსური პლაზმის ფიზიკა

JOURNAL
OF THE GEORGIAN GEOPHYSICAL SOCIETY

Issue B. Physics of Atmosphere, Ocean and Space Plasma

ტომი 15ბ 2011-2012
vol. 15B 2011-2012

საქართველოს გეოფიზიკური საზოგადოების ჟურნალი

სერია ბ. ატმოსფეროს, ოკეანისა და კოსმოსური პლაზმის ფიზიკა

მისამართი:

საქართველო, 0193, თბილისი, ალექსიძის ქ. 1,
საქართველოს მეცნიერებათა აკადემიის მ. ნოდიას სახ. გეოფიზიკის ინსტიტუტი
ტელ.: 33-28-67; 94-35-91; Fax; (99532 332867); e-mail: ***avtokor@ig.acnet.ge***

ჟურნალის შინაარსი:

ჟურნალი მოიცავს ატმოსფეროს, ოკეანისა და კოსმოსური პლაზმის ფიზიკის ყველა მიმართულებას. გამოქვეყნებული იქნება: კვლევითი წერილები, მიმოხილვები, მოკლე ინფორმაციები, დისკუსიები, წიგნების მიმოხილვები, განცხადებები.

გამოქვეყნების განრიგი და ხელმოწერა:

სერია (ბ) გამოიცემა წელიწადში ერთხელ.
ხელმოწერის ფასია (უცხოელი ხელმომწერისათვის) 50 დოლარი, საქართველოში – 10 ლარი, ხელმოწერის მოთხოვნა უნდა გაიგზავნოს რედაქციის მისამართით.

ЖУРНАЛ ГРУЗИНСКОГО ГЕОФИЗИЧЕСКОГО ОБЩЕСТВА

серия Б. Физика Атмосферы, Океана и Космической Плазмы

Адрес:

Грузия, 0193, Тбилиси, ул. Алексидзе, 1.
Институт геофизики им. М. Нодия АН Грузии
Тел: 33-28-67; 94-35-91; Fax: (99532) 332867; e-mail: *avtokor@ig.acnet.ge*

Содержание журнала:

Журнал охватывает все направления физики атмосферы, океана и космической плазмы. В журнале будут опубликованы научные статьи, обозрения, краткие информации, дискуссии, обозрения книг, объявления

Порядок издания и условия подписи:

Том серии (Б) издается по одному номеру в год.
Подписная цена 50 долларов США, включая стоимость пересылки.
Заявка о подписи высылается в адрес редакции.

JOURNAL OF THE GEORGIAN GEOPHYSICAL SOCIETY

Issue B. Physics of Atmosphere, Ocean and Space Plasma

Address:

M. Nodia Institute of Geophysics, Georgian Academy of Sciences, 1 Alexidze Str., 0193 Tbilisi, Georgia
Tel.: 33-28-67; 94-35-91; Fax: (99532) 332867; e-mail: ***avtokor@ig.acnet.ge***

Scope of the Journal:

The Journal is devoted to all branches of the Physics of Atmosphere, Ocean and Space Plasma. Types of contributions are: research papers, reviews, short communications, discussions, books reviews, announcements**.**

Publication schedule and subscription information:

One volume issue (B) per year is scheduled to be published.
The subscription price is 50 $, including postage.
Subscription orders should be sent to editor's address.

Journal of the Georgian Geophysical Society,
Issue B. Physics of Atmosphere, Ocean, and Space Plasma, v.15, 2011-2012, pp.3-13

Circulation processes in the easternmost part of the Black Sea in 2010-2012: Results of simulation and forecast

Avtandil A. Kordzadze, Demuri I. Demetrashvili, Vepkhia G. Kukhalashvili

M. Nodia Institute of Geophysics, 1,Alexidze Str., 0171, Tbilisi, Georgia,
e-mail: akordzadze@yahoo.com, demetr_48@yahoo.com

Abstract

Results of forecasts of the basic hydrophysical fields for 2010-2012 in the easternmost part of the Black Sea became the basis for studying of some features of inner-annual variability of regional circulating processes in this part of the sea basin. The forecast of a hydrological mode is carried out on the basis of the regional forecasting system developed at M. Nodia Institute of Geophysics in cooperation with oceanographic Centers of Black Sea riparian countries within the framework of EU international scientific - technical projects ARENA and ECOOP. The analysis of the data shows, that the easternmost water area of the Black Sea represents dynamically very active zone, where different circulating processes significantly distinguished from each other continuously develop.

1. Introduction

Since June 2010 3- days forecasts of a hydrological mode of the easternmost part of the Black Sea on a basis of the regional forecasting system are regularly carried out at M. Nodia Institute of Geophysics. The regional forecasting system is one of the parts of the basin-scale Black Sea Nowcasting/Forecasting system [1, 2] and enables to forecast 3-D fields of current, temperature and salinity with 1 km spacing in the regional area, which is limited to the Caucasian and Turkish coastal lines and the western liquid boundary coinciding with a meridian 39.08^0E. A core of the regional forecasting system is the regional mathematical model of Black Sea dynamics of M. Nodia Institute of Geophysics (RM-IG), which is nested in the Basin-scale model of Black Sea dynamics of Marine Hydrophysical Institute (MHI) of the National Academy of Sciences of Ukraine (Sevastopol). All input data required for calculation of marine forecasts are received in operative mode from MHI via Internet. The basic principles of functioning of the regional forecasting system and some results of forecast of hydrological fields for the easternmost part of the Black Sea are described in [3-5].

Nowadays a significant database is created by us, which contains results of modeling and 3-days forecasts of dynamic processes developed for 2010-2012 in the easternmost part of the Black Sea. The analysis of this material promotes to the best understanding of mechanisms of formation and evolution of hydro and thermodynamic processes in one of dynamically active regions of the Black Sea and enrichment ours knowledge about these processes.

The main goal of the present paper is the research of some features of inner-annual variability of regional dynamic processes for 2010-2012 in the easternmost part of the Black Sea.

2. Results of simulation and forecast of circulation processes

In numerical experiments, the results of which are showed below, a grid having 215 x 347 points on horizons with 1 km spacing were used. On a vertical the non-uniform grid with 30

calculated levels on depths: 2, 4, 6, 8, 12, 16, 26, 36, 56, 86, 136, 206, 306,…, 2006 m were considered. The time step was equal to 0.5 h.

Regular calculations of the regional forecasts for 2010-2012 show, that the easternmost part of the Black Sea including the Georgian water area, represents a dynamically active zone. Circulating processes here develop which are characterized by significant inner-annual variability.

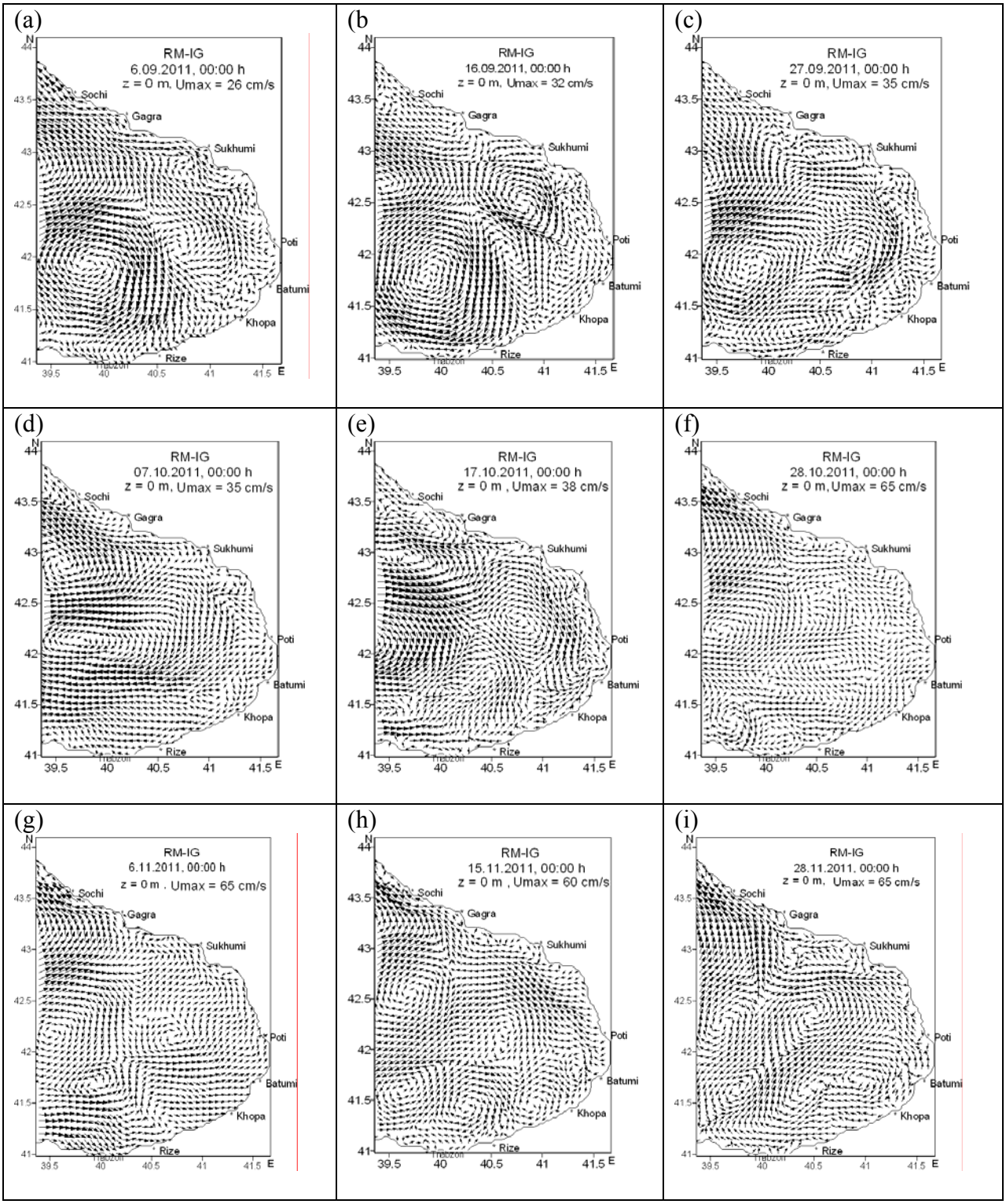

Fig.1. Simulated surface current fields in autumn 2011. (a) – 6 September , (b) – 16 September, (c) –27 September, (d) – 7 October, (e) – 17 October, (f) - 28 October, (g) – 6 November, (h) – 15 November, (i) – 28 November.

In Figs. 1-4 the calculated fields of surface currents for period since September 2011 till August 2012 are shown. Herewith for each month three circulation patterns are chosen which are more characteristic for the appropriate month.

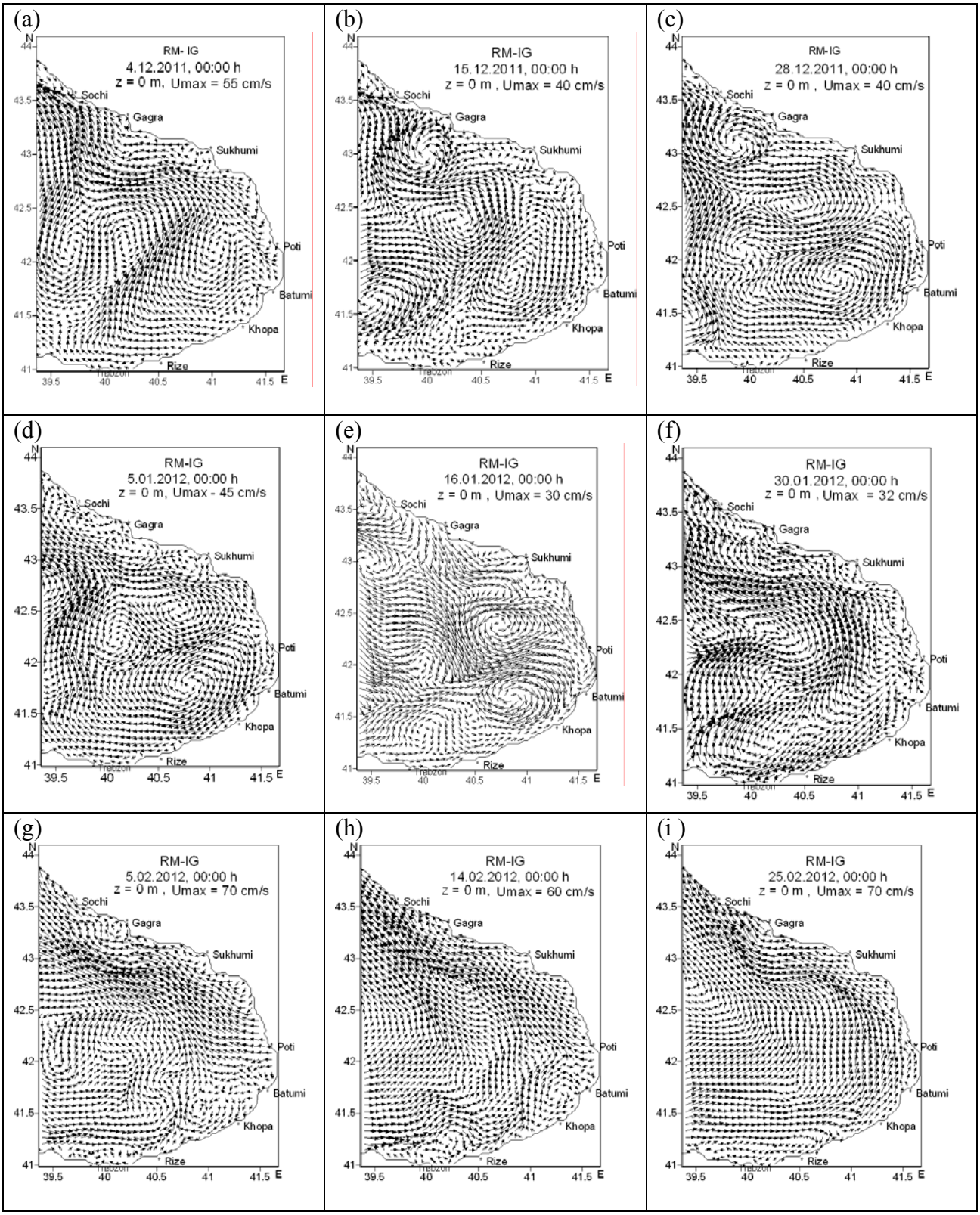

Fig.2. Simulated surface current fields in winter 2011-2012. (a) – 4 December 2011, (b) – 15 December 2011, (c) – 28 December 2011, (d) – 5 January 2012, (e) – 16 January 2012, (f) – 30 January 2012, (g) – 5 February 2012, (h) – 14 February 2012, (i) – 25 February 2012.

The main element of September circulation in 2011 is anticyclonic eddy with diameter about of 100-120 km (called the Batumi eddy), which is formed in the southwest part of the considered area.

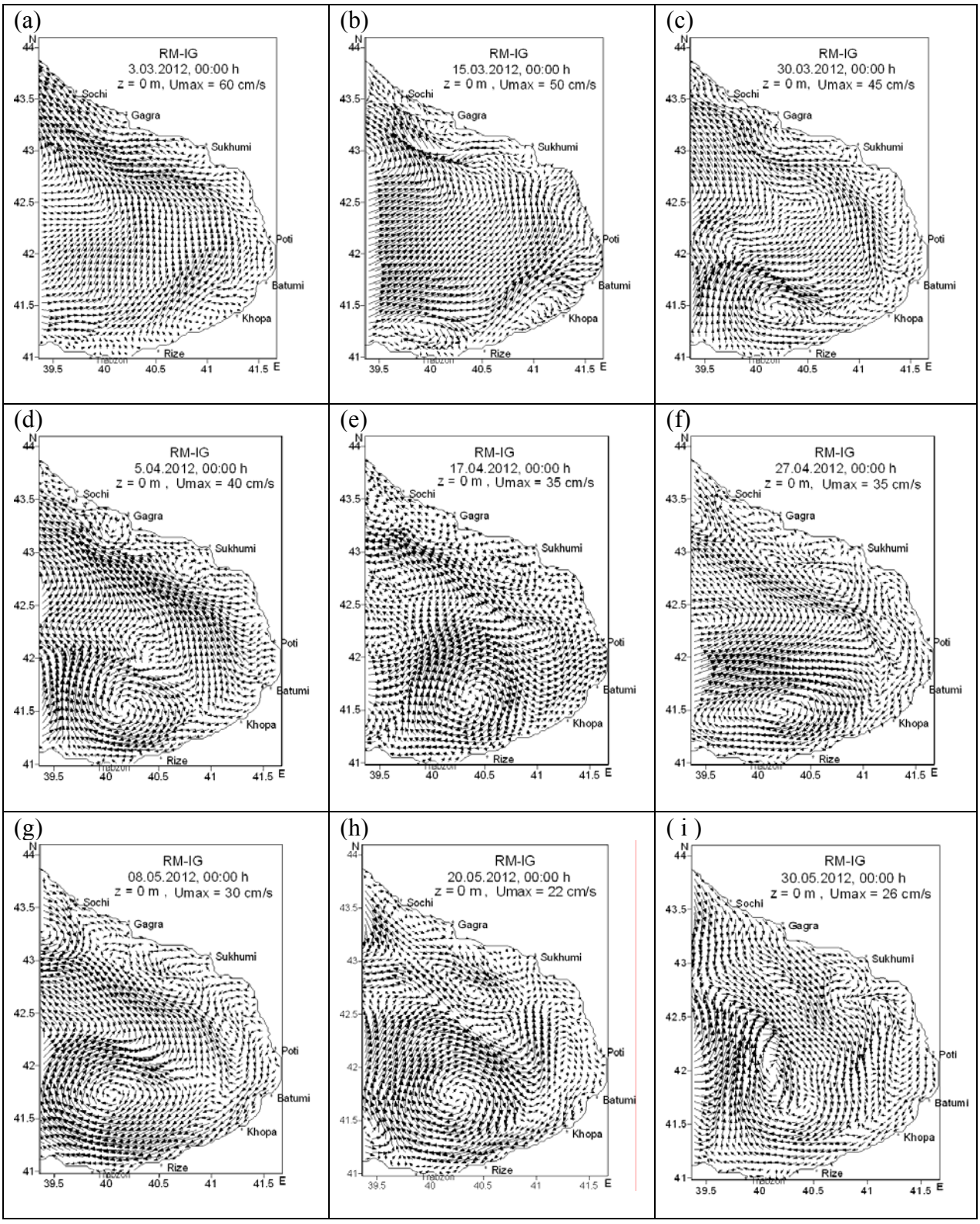

Fig.3. Simulated surface current fields in Spring 2012. (a) – 3 March , (b) – 15 March, (c) – 30 March, (d) – 5 April, (e) – 17 April, (f) - 27 April, (g) – 8 May, (h) – 20 May, (i) – 30 May.

The structure of this eddy undergoes some changes and by the end of the month substantially decreases in the sizes. from middle of September it is possible to observe also formation of the second anticyclonic eddy with rather smaller sizes, which is exposed to the certain changes. Along the Caucasian coast the narrow zone with width about of 20-25 km is formed which is characterized by intensive formation of small coastal unstable eddies, existence time of which are a few days. It should be noted that such coastal eddies of small sizes in coastal zones of the Black Sea are often observed [6-8]

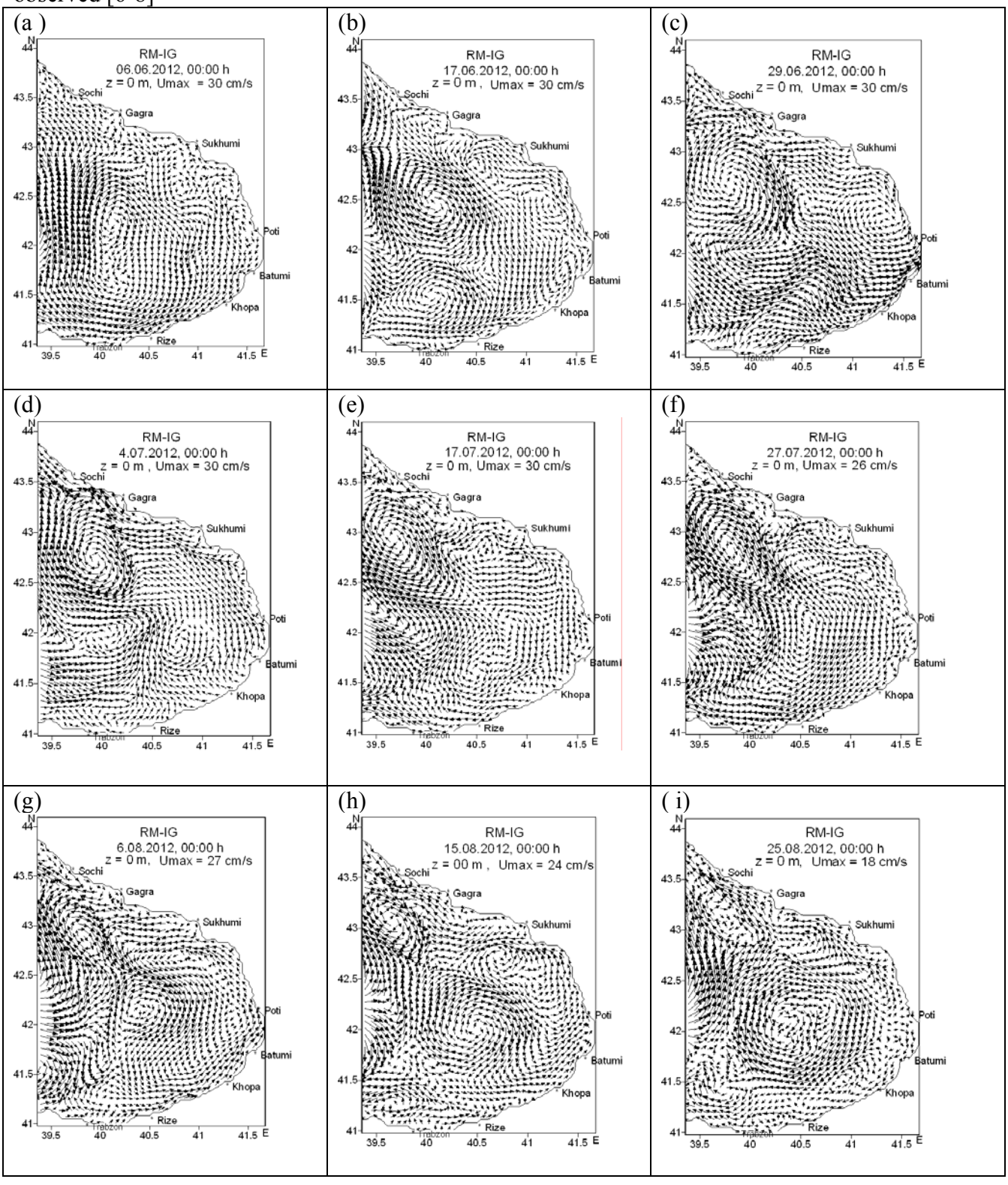

Fig. 4. Simulated surface current fields in Summer 2012. (a) – 6 June , (b) – 17 June, (c) – 29 June, (d) – 4 July, (e) – 17 July, (f) - 27 July, (g) – 6 August, (h) – 15 August, (i) – 25 August.

The transformation of a circulating mode proceeds within October. By the end of October the absence of a dominant direction and presence of several small anticyclonic and cyclonic eddies is characteristic for a circulating mode. The similar character of circulation takes place within November and here current speeds reach 60 cm/s.

The circulating mode in December 2011 differs from a mode of the previous month and is basically characterized by presence of the cascade of sharply expressed anticyclonic eddies. The January circulation in 2012 in the first half of month is similar in the certain degree with December circulation and the main elements of a circulating mode are obviously expressed cyclonic and anticyclonic eddies with characteristic diameter about of 30-40 km. East branch of the Rim Current is present at the majority of pictures of February circulation with the maximal speeds 60-70 m/c on its core. In general, Circulating mode of February 2012 is characterized by weak vorticity that is possible to explain by action of strong atmospheric winds, which develop in this period. An intense atmospheric circulation has smoothing influence on surface sea currents and promote disappearance of vortical formations [4].

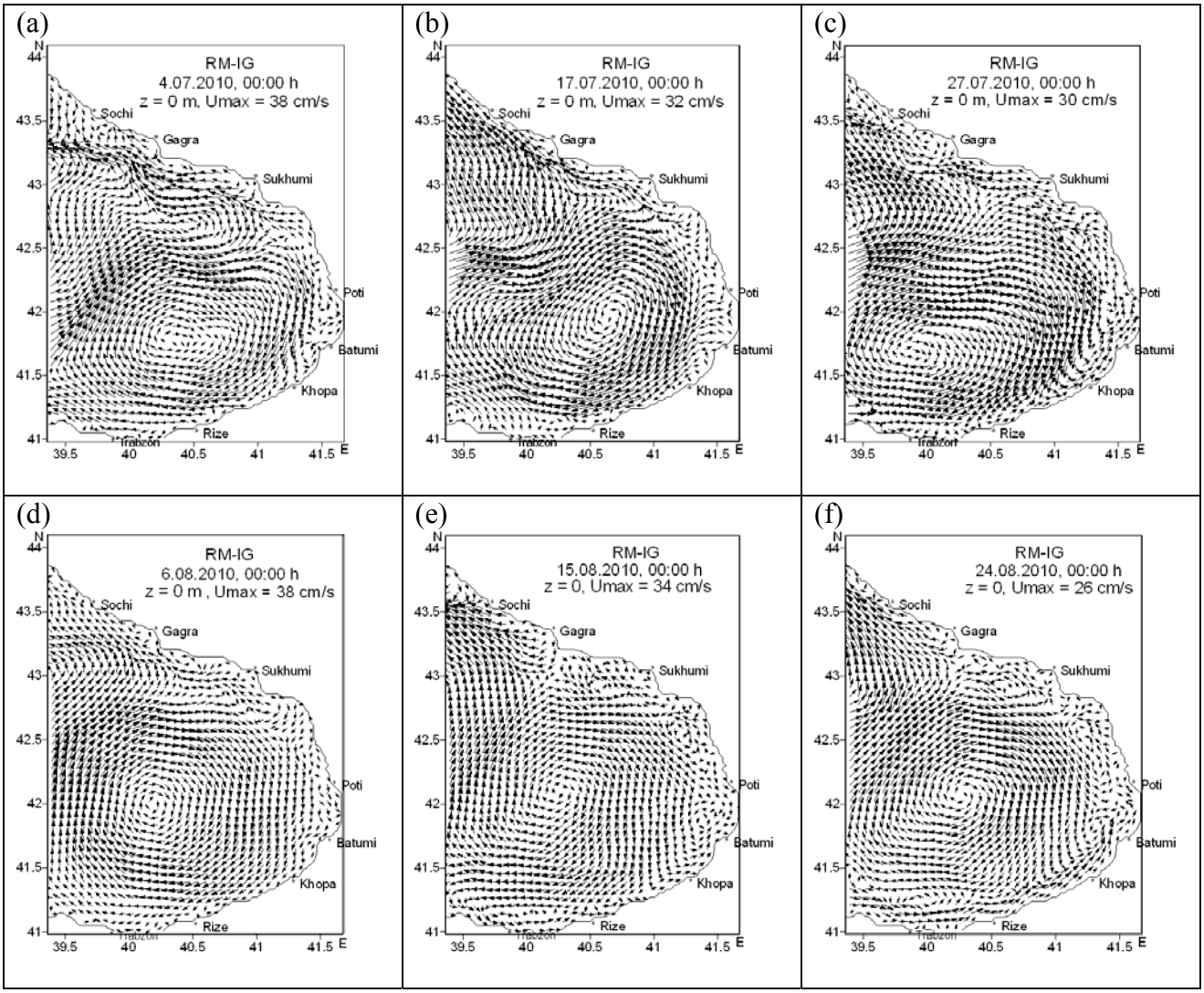

Fig.7. Simulated surface fields in Summer 2010. (a) – 4 July , (b) – 17 July, (c) – 27 July, (d) – 6 August, (e) – 15 August, (f) - 25 August.

The circulating mode of first half of March 2012 was characterized also basically by free-vortex movement (except for formation some coastal small eddies), but by the end of the month generation of anticyclonic vortical formation in the southwest part of the considered area is

observed. In April anticyclonic vortex grows in the sizes and it is present within all month. The narrow zone along the Caucasian coast is a zone of intensive vortex formation, where small coastal cyclonic and anticyclonic eddies are generated and transformed.

In middle of May the anticyclonic eddies amplifies, and by the end it weakens. The speeds of current decrease.

In the beginning of summer the anticyclonic eddy is stretched along a meridian and as a result in middle of June two anticyclonic eddies are formed. In June a zone of vortex formation along the Caucasian coast is well observed too. In local water area between Sukhumi and Poti the anticyclonic vortex with diameter about of 25 km is especially well observed.

In the beginning of July formation of the anticyclonic vortex in the northwest part of considered area is observed. This vortex by the end of July extends in the southern direction. In August formation of anticyclonic eddy takes place at the centre of the considered regional area and then gradually extends and covers the area with a diameter about of 80-90 km.

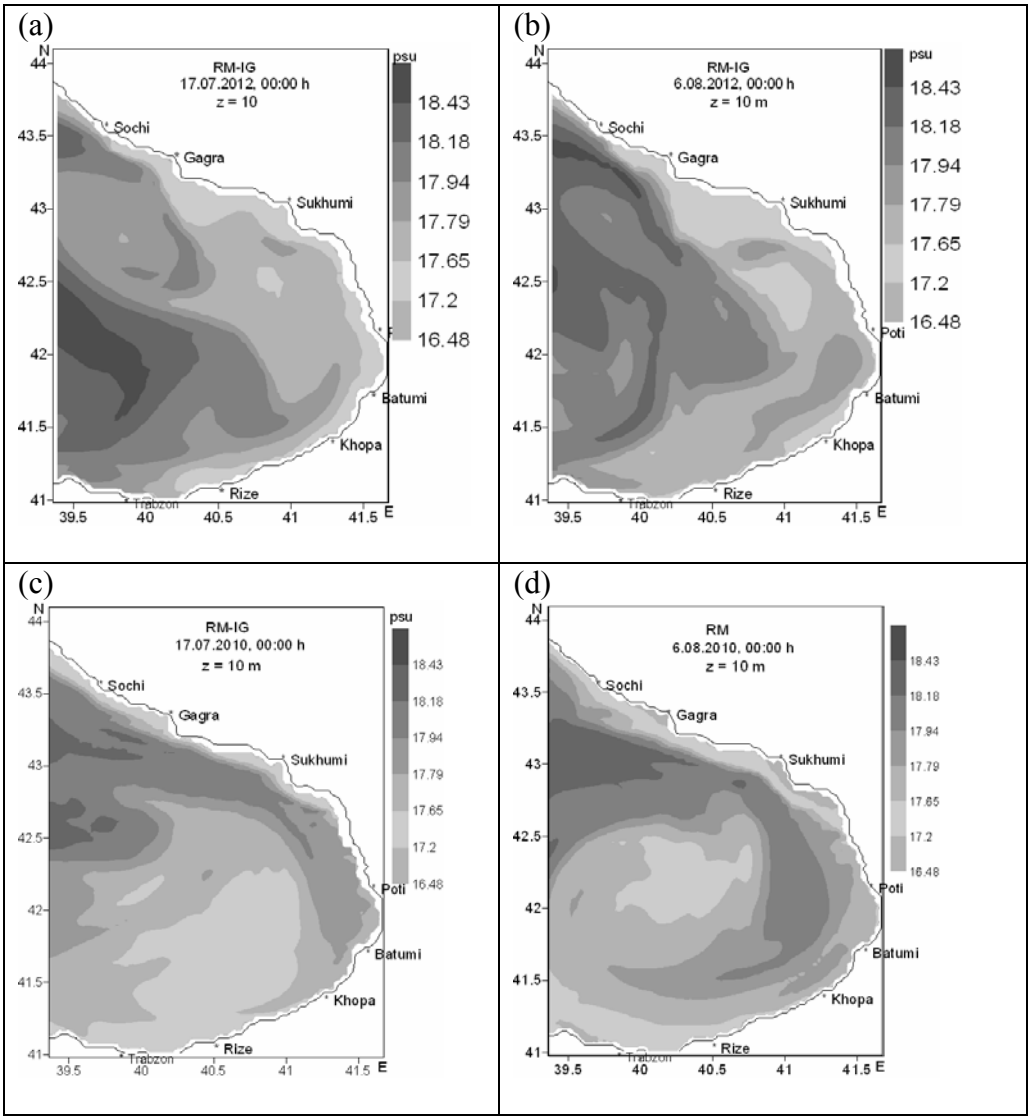

Fig.8. Simulated salinity fields on z = 10 m. (a) – 17 July 2012, (b) – 6 August 2012, (c) – 17 July 2010, (d) – 6 August 2010.

The analysis of the data of circulating modes for 2010-2012 shows that the circulating modes of the same season in the considered easternmost part of the Black Sea can considerably differ from each other per different years. There seems different meteorological conditions which are formed above the regional water area of the Black Sea promote this phenomenon. In confirmation of this

fact the comparison of summer circulating modes of 2010 (Fig. 7) and 2012 (Fig. 6) serves. The summer circulation in 2010, which significantly differs from summer circulation in 2012, was characterized by sharply distinguished features. The main feature of the regional circulation of 2010 was the existence of the Batumi anticyclonic eddy practically within all summer period. It was rather steady formation, which reached the maximal intensity in August and covered the significant part of the considered regional area. It is interesting to note, that under the information of synoptic-meteorologists the summer of 2010 in Georgia was abnormal hot for last decades. Temperature of air quite often reached and passed 40°C, and coastal waters of the sea were heated up more than 30°C. The abnormal temperature mode, obviously, has affected a mode of evaporation and precipitation and at the end thermochaline conditions of coastal waters have appeared favorable for formation intensive anticyclonic vortical formation.

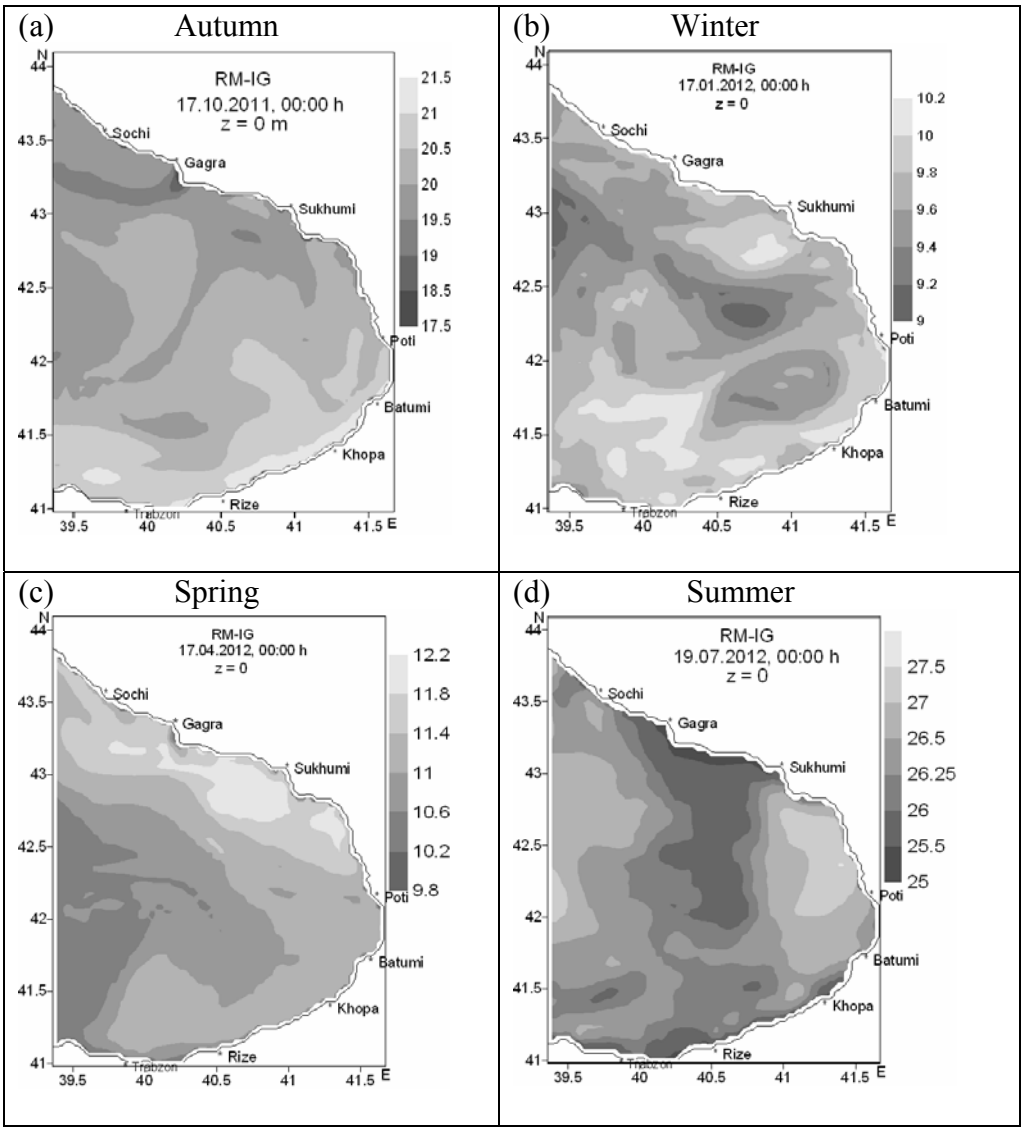

Fig. 9. Simulated surface temperature fields, corresponding to different seasons 2011-2012. (a) – 17 October 2011, (b) – 17 January 2012, (c) – 17 April 2012, (d) – 19 July 2012.

The analysis of the data for 2010-2012 shows that the distribution of the salinity field in the considered regional area underwent certain inner-annual changes. The general character of variability of the salinity field within one year depends both on inner-annual change of balance in system evaporation – precipitation, rivers' inflow and on the circulating characteristics. The analysis of our data confirms the known fact, that the salinity field well correlates with the field of circulation. General law is that anticyclonic eddies promote formation of waters with low salinity in

its central art, and cyclonic eddies - on the contrary. The ascending flows at the centre of a cyclone promote carry of more salty waters from deep layers in the upper layers, and the descending flows in the central part of anticyclonic eddy transfer less salt waters from upper layers downwards. Thus, the circulating mode in the greater degree determines structure of the salinity field in the easternmost regional area. This fact is especially precisely shown by comparison of pictures of salinity, corresponding to summer 2010 and 2012, when the circulating modes sharply differed from each other. From Fig. 8, where the calculated fields of salinity on horizon z = 10 м, corresponding to summer season 2010 and 2012 are shown, it is clearly visible that intensive Batumi anticyclonic eddy observable in the summer of 2010 has considerably affected a mode of salinity in the easternmost part of the basin. Here was observed rather lowered salinity on the significant central area of the Batumi eddy, and the peripheral current of the eddy promoted penetration of more salty waters from open area of the sea in the easternmost water area.

The certain impression about seasonal evolution of a surface temperature field gives Fig.9, where the distributions of the Black Sea surface temperature for four seasons are given. The temperature field undergoes both significant qualitative and quantitative seasonal changes and the character of its change in the upper layer is basically determined by heat exchange between the sea and atmosphere.

3. Summary

Summarizing the researches carried out in this work on the base of analysis of simulated hydrological fields for 2010-2012 it is possible to formulate briefly the basic features of inner-annual variability of dynamic processes in the easternmost water area of the Black Sea. During all seasons in the easternmost part of the Black Sea generation, deformation and disappearance of anticyclonic and cyclonic vortex formations continuously takes place. The analysis of calculated current fields again confirms the fact known from the Black Sea oceanographic literature [9], that the most intensive vortical formation is the Batumi anticyclonic eddy, which exists in the warm period of year. In most cases a narrow zone along the Caucasian coast with width about of 20-30 km is formed, where intensive vortex formation takes place. In this zone generation of small unstable eddies with diameters from 5 up to 20 km is observed. Vortex formation weakens in February when the atmospheric winds amplify having smoothing effect on sea current. In that case, when the Batumi eddy is intensive and occupies a significant part of considered water area, it forms the certain mode of salinity: salinity of waters considerably decreases in the central part of the Batumi eddy, but the peripheral current of the eddy promotes penetration of more salty waters from an open part of the Black Sea in the considered regional area.

References

[1]. Korotaev G. K., Oguz T., Dorofeev V. L. et al. Development of Black Sea nowcasting and forecasting system, Ocean Science, 7, 2011, P. 629-649, doi: 10.5194/os-7-629-2011.

[2]. Kubryakov A. I., Korotaev G. K., Dorofeev V. L. et al. Black Sea Coastal forecasting system. Ocean Science, 8, 2012, P. 183-196, doi: 10.5194/os-8-183-2012.

[3] Kordzadze A., Demetrashvili D. Some results of forecast of hydrodynamic processes in the Easternmost part of the Black Sea. J. Georgian Geophys. Soc., 2010, v.14b, pp. 37-52.

[4] Kordzadze A. A, Demetrashvili D. I. Operational forecast of hydrophysical fields in the Georgian Black Sea coastal zone within the ECOOP. *Ocean Science*, 2011, 7, *pp.* 793- 803, www.ocean-sci.net/7/793/2011/, doi: 10.5194/os-7-793-2011.

[5] Kordzadze A. A, Demetrashvili D. I. Operational regional forecasting system of state of the east part of the Black Sea. Ecological safety of coastal and shelf zones and comprehensive use of shelf resources. Collected scientific papers. Sevastopol, Iss. 25, vol.2, 2011, pp.136-146 (in Russian).

[6] Ivanov V. A., Tuchkovenko Yu. C. Applied mathematical modeling of water quality of shelf sea ecosystems. Sevastopol, Marine Hydrophysical Institute 2006, 368 p (in Russian).
[7] Demyshev C. G., Dovgaia C. V., Markova N. V. Numerical experiment on modeling of the thermogydrodynamics of the Black Sea in 2006. Ecological safety of coastal and shelf zones and comprehensive use of shelf resources. Collected scientific papers. Sevastopol, EKOCI-Gidrofizika, 2009, Iss.19, pp.32-45 (in Russian).
[8] Demyshev C. G. Numerical prognostic calculation in the Black Sea with high horizontal resolution. Marine Hydrophysical Journal. 2011, N 1, p.36-47 (In Russian).
[9] Korotaev G., Oguz T., Nikiforov A., Koblinsky,C. Seasonal, interannual, and mesoscale variability of the Black Sea upper layer circulation derived from altimeter data. J. Geophys. Res., 2003, v.108, No. C4, 3122, pp. 19-15.

(Received in final form 20 December 2012)

Циркуляционные процессы в восточной части Чёрного моря: Результаты моделирования и прогноза

Автандил Кордзадзе, Демури Деметрашвили, Вепхиа Кухалашвили

Резюме

Накопленные за 2010-2012 гг. результаты прогноза основных гидрофизических полей в крайне восточной части Чёрного моря явились основой для исследования особенностей внутригодовой изменчивости региональных циркуляционных процессов в этой части бассейна. Прогноз гидрологического режима производится на основе региональной прогностической системы, разработанной в Институте геофизики им. М. Нодиа в сотрудничестве с океанографическими центрами причерноморских стран в рамках международных научно-течнических проектов Евросоюза ARENA и ECOOP. Анализ материала, накопленного за отмеченный период, показывает, что крайне восточная акватория Чёрного моря представляет собой динамически довольно активной зоной, где в течение года непрерывно развиваются разные циркуляционные процессы, резко отличающиеся друг от друга.

ცირკულაციური პროცესები შავი ზღვის აღმოსავლეთ ნაწილში 2010-2012 წწ-ში: მოდელირების და პროგნოზის შედეგები

ავთანდილ კორძაძე, დემური დემეტრაშვილი, ვეფხია კუხალაშვილი

რეზიუმე

2010-2012 წლებში დაგროვილი ძირითადი ჰიდროფიზიკური ველების პროგნოზის შედეგები შავი ზღვის უკიდურესი აღმოსავლეთ ნაწილისათვის წარმოადგენენ საფუძველს რეგიონალური ცირკულაციური პროცესების შიდა წლიური ცვალებადობის თავისებურებათა გამოკვლევებისათვის ზღვის აუზის ამ ნაწილში.

ჰიდროლოგიური რეჟიმის პროგნოზი ხორციელდება რეგიონალური პროგნოზული სისტემის საფუძველზე, რომელიც შემუშავებულია მ. ნოდიას გეოფიზიკის ინსტიტუტში შავიზღვისპირა ქვეყნების ოკეანოგრაფიულ ცენტრებთან თანამშრომლობით ევროკავშირის სამეცნიერო-ტექნიკურ პროექტების ARENA და ECOOP ფარგლებში. აღნიშნულ პერიოდში არსებული მასალის ანალიზი გვიჩვენებს, რომ შავი ზღვის უკიდურესი აღმოსავლეთ აკვატორია წარმოადგენს დინამიკურად საკმაოდ აქტიურ ზონას, სადაც წლის განმავლობაში უწყვეტად ვითარდებიან ერთმანეთისაგან მკვეთრად განსხვავებული სხვადასხვა ცირკულაციური პროცესები.

Journal of the Georgian Geophysical Society,
Issue B. Physics of Atmosphere, Ocean, and Space Plasma, v.15, 2011-2012, pp 14-31.

On the effective numerical methods of solution of shallow water problem. Realization of the model for the easternmost part of the Black Sea

Avtandil A. Kordzadze, Demuri I. Demetrashvili, Vepkhia G. Kukhalashvili

M. Nodia Institute of Geophysics at. I. Javakhishvili Tbilisi State University , 1,Alexidze Str., 0171, Tbilisi,
Georgia, e-mail: akordzadze@yahoo.com, demetr_48@yahoo.com

Abstract

Two versions of the numerical method of solution of a shallow water equation system based on the two-cycle splitting method with realization for the easternmost water area of the Black Sea are presented. In the first version solution of the equation system, which is received as a result of splitting of the basic equation system with respect to physical processes (adaptation stage), is carried out with use of factorization method regarding to current velocity components. In the second version the equation system received on the adaptation stage is reduced to the oscillation equations of string, which are also solved by factorization method. The algorithms considered in the present paper do not require use of iterative methods, which considerably increase machine time for realization of a task.

1. Statement of the problem

In a 3-D area Ω $\{(x,y,z): x,y \in \Omega_0(t), -\zeta(x,y,z) \le z \le h(x,y)\}$ limited from above by the free surface $\zeta(x,y,z)$, from below - by the motionless bottom $h(x,y)$ and by the enough smooth lateral surface σ, let's consider a mathematical task describing dynamics of shallow water area. The area Ω represents coastal part of the deep sea or shallow lake with depth $H=-\zeta(x,y,z)+h(x,y)$. The boundary σ_0 of 2-D area Ω_0 is formed by crossing of the free surface with the bottom relief. The coordinate system is located so that the plane xoy coincides with undisturbed water surface, z is directed vertically downwards. By taken into consideration mobility of the boundary of the considered area the problem describes processes of drainage and flooding because of fluctuations of a see surface level. In other words, the problem consists in definition of the free surface level ζ and current characteristics averaged on a vertical

$$\bar{u}=\frac{1}{H}\int_{-\zeta}^{h} u\,dz \qquad \text{and} \qquad \bar{v}=\frac{1}{H}\int_{-\zeta}^{h} v\,dz\,,$$

where u and v are horizontal components of the current velocity vector on coordinates x and y, respectively.

With the purpose of reception of a shallow water problem the equations of movement and continuity for an incompressible liquid are considered, integration of which on a vertical from $z = -\zeta$ to $z= h(x,y)$ with use of appropriate transformations enables us to receive the system of differential equations of the shallow water theory [1-5]:

$$\frac{\partial U}{\partial t}+\frac{\partial \bar{u}U}{\partial x}+\frac{\partial \bar{v}U}{\partial y}-lV+gH\frac{\partial \zeta}{\partial x}=\nabla\mu\nabla U+f_1,$$

$$\frac{\partial V}{\partial t}+\frac{\partial \bar{u}V}{\partial x}+\frac{\partial \bar{v}V}{\partial y}+lU+gH\frac{\partial \zeta}{\partial y}=\nabla\mu\nabla V+f_2, \qquad (1)$$

$$\frac{\partial \zeta}{\partial t} + \frac{\partial U}{\partial x} + \frac{\partial V}{\partial y} = 0,$$

where $U = \bar{u}H$, $V = \bar{v}H$, $\nabla \mu \nabla = \nabla_x \mu \nabla_x + \nabla_y \mu \nabla_y$,

$$f_1 = \frac{1}{\rho}(\tau_{xz}^0 - \tau_{xz}^1) - \frac{gH}{\rho}\frac{\partial P_a}{\partial x}, \quad f_2 = \frac{1}{\rho}(\tau_{yz}^0 - \tau_{yz}^1) - \frac{gH}{\rho}\frac{\partial P_a}{\partial y}.$$

For a pressure of sea water the hydrostatic law is accepted

$$P = g\rho(\zeta + z) + P_a.$$

Here P_a is the atmospheric pressure above the free sea surface, g is the gravity acceleration, μ is the factor of turbulent viscosity, the density $\rho = const$, τ_{xz}^0 and τ_{yz}^0 are wind stress components on the free surface $z = -\zeta$, τ_{xz}^1 and τ_{yz}^1 are the bottom friction components on $z = h$.

The system of equations (1) is solved under the following boundary and initial conditions:

$$U = \tilde{U}(x, y, t), \quad V = \tilde{V}(x, y, t) \quad \text{on} \quad \sigma_2 , \tag{2}$$

$$U = 0, \quad V = 0 \quad \text{on} \quad \sigma_1 , \tag{3}$$

$$U = U^0(x, y) , \quad V = V^0(x, y) , \quad \zeta = \zeta^0(x, y) \quad \text{if} \quad t = 0, \tag{4}$$

where σ_1 is the lateral solid surface adjacent to the land, σ_2 is the liquid (open) boundary separating the sea basin from the remaining water area. On the open boundary σ_2 the vector of a complete flow is the given function of horizontal coordinates and time.

We assume that the input data of the given task have sufficient smoothness providing solvability of the task (1) - (4) [1, 4, 6, 7].

2. Numerical method of solution

2.1. Splitting of the problem with respect to physical processes

For numerical solution of the problem (1)-(4) the entire time interval (O, T), on which the solution is searched, is broken up into equal intervals $t_{j-1} \le t \le t_{j+1}$ and is supposed that on the each interval the components of the vector velocity $\vec{u}$ are known from the previous time step [8, 9, 10].

Let's consider vectors φ, Q, F, and matrixes A and B

$$\varphi = \begin{Vmatrix} U \\ V \\ \zeta \end{Vmatrix}, \quad Q = \begin{Vmatrix} f_1 \\ f_2 \\ 0 \end{Vmatrix}, \quad F = \begin{Vmatrix} U^0 \\ V^0 \\ \zeta^0 \end{Vmatrix}, \quad A = \begin{Vmatrix} \Pi & -l & gH\frac{\partial}{\partial x} \\ l & \Pi & gH\frac{\partial}{\partial y} \\ gH\frac{\partial}{\partial x} & gH\frac{\partial}{\partial y} & 0 \end{Vmatrix}, \quad B = \begin{Vmatrix} 1 & 0 & 0 \\ 0 & 1 & 0 \\ 0 & 0 & gH \end{Vmatrix}.$$

Here $\Pi = div\vec{u} - \nabla \mu \nabla$. Then the equation system (1) we shall write in the operator form

$$B\frac{\partial \varphi}{\partial t} + A\varphi = Q \tag{5}$$

and as the initial conditions we shall accept

$$B\varphi = BF \quad \text{if} \quad t = 0. \tag{6}$$

After scalar multiplying the equation (5) by φ, we shall receive

$$\frac{1}{2}\frac{\partial}{\partial t}(B\varphi,\varphi)+(A\varphi,\varphi)=(Q,\varphi),$$

where the scalar product is determined as follows

$$(a,b)=\sum_{i=1}^{3}\iint_{\Omega}a^{i}b^{i}d\Omega.$$

Here a^i and b^i are the vector components of functions a and b.

With taken into consideration uniform conditions corresponding to (2) and (3) it is easily to check up that the following ratio takes place:

$$(A\varphi,\varphi)\geq 0$$

Now we shall present the operator A as the sum of two operators

$$A=A_1+A_2,$$

where

$$A_1=\begin{Vmatrix}\Pi & 0 & 0\\ 0 & \Pi & 0\\ 0 & 0 & 0\end{Vmatrix},\qquad A_2=\begin{Vmatrix}0 & -l & gH\frac{\partial}{\partial x}\\ l & 0 & gH\frac{\partial}{\partial y}\\ gH\frac{\partial}{\partial x} & gH\frac{\partial}{\partial y} & 0\end{Vmatrix}$$

Similarly, it is possible to show that the following ratios take place

$$(A_1\varphi,\varphi)\geq 0,\qquad (A_2\varphi,\varphi)=0.$$

These conditions are necessary for construction of steady finite-difference schemes of splitting.

Let's now $t_j-t_{j-1}=\tau$ and on each extended time interval $t_{j-1}\leq t\leq t_{j+1}$ the two-cyclic method of splitting on physical processes to the task (5), (6) we shell apply. Then if we assume that φ^{j-1} is the solution of the task (5), (6) at the moment t_{j-1} then we receive the following tasks:

on the first time interval $t_{j-1}\leq t\leq t_j$ -

$$B\frac{\partial\varphi_1}{\partial t}+A_1\varphi_1=Q,\quad B\varphi_1^{j-1}=B\varphi^{j-1}. \tag{7}$$

on the time interval $t_{j-1}\leq t\leq t_{j+1}$ -

$$B\frac{\partial\varphi_2}{\partial t}+A_2\varphi_2=0,\quad B\varphi_2^{j-1}=B\varphi_1^{j}, \tag{8}$$

on the last time interval $t_j\leq t\leq t_{j+1}$ -

$$B\frac{\partial\varphi_3}{\partial t}+A_1\varphi_3=Q,\quad B\varphi_3^{j}=B\varphi_2^{j+1}. \tag{9}$$

In equations (7) and (9) values of functions $\bar{u}$ и $\bar{v}$ are taken the same within each time interval $t_{j-1}\leq t\leq t_{j+1}$ to obtain second -order accuracy in τ [9].

In the component form the tasks (7) - (9) will accept the following form:

on the time interval $t_{j-1}\leq t\leq t_j$

$$\left.\begin{aligned} \frac{\partial U_1}{\partial t}+\frac{\partial \bar{u}U_1}{\partial x}+\frac{\partial \bar{v}U_1}{\partial y}=\nabla\mu\nabla U_1+f_1\ , \quad U_1^{j-1}=U^{j-1} \\ \frac{\partial V_1}{\partial t}+\frac{\partial \bar{u}V_1}{\partial x}+\frac{\partial \bar{v}V_1}{\partial y}=\nabla\mu\nabla V_1+f_2\ , \quad V_1^{j-1}=V^{j-1} \end{aligned}\right\} \qquad (10)$$

with boundary conditions (2), (3) written for U_1 and V_1

$$U_1=0\,, \quad V_1=0 \qquad \text{on} \quad \sigma_1,$$

$$U_1=\bar{U}, \quad V_1=\bar{V} \qquad \text{on} \quad \sigma_2. \qquad (11)$$

On the time interval $t_{j-1}\le t\le t_{j+1}$ we have the differential equation system

$$\left.\begin{aligned} \frac{\partial U_2}{\partial t}-lV_2+gH\frac{\partial \zeta_2}{\partial x}=0 \\ \frac{\partial V_2}{\partial t}+lU_2+gH\frac{\partial \zeta_2}{\partial y}=0 \\ \frac{\partial \zeta_2}{\partial t}+\frac{\partial U_2}{\partial x}+\frac{\partial V_2}{\partial y}=0 \end{aligned}\right\} \qquad (12)$$

at following boundary and initial conditions

$$\begin{aligned} U_{2_n}&=0 \qquad \text{on} \quad \sigma_1\ , \\ \zeta_2&=\bar{\zeta} \qquad \text{on} \quad \sigma_2\ , \end{aligned} \qquad (13)$$

where U_{2_n} is normal component of velocity vector $\overrightarrow{U_2}$, and $\bar{\zeta}$ is known function,

$$U_2^{j-1}=U_1^j\ , \quad V_2^{j-1}=V_1^j\ , \quad \zeta_2^{j-1}=\zeta^{j-1}\ ; \qquad (14)$$

and, on the time interval $t_j\le t\le t_{j+1}$ -

$$\left.\begin{aligned} \frac{\partial U_3}{\partial t}+\frac{\partial \bar{u}U_3}{\partial x}+\frac{\partial \bar{v}U_3}{\partial y}=\nabla\mu\nabla U_3+f_1\ , \quad U_3^j=U_2^{j+1} \\ \frac{\partial V_3}{\partial t}+\frac{\partial \bar{u}V_3}{\partial x}+\frac{\partial \bar{v}V_3}{\partial y}=\nabla\mu\nabla V_3+f_2\ , \quad V_3^j=V_2^{j+1} \end{aligned}\right\} \qquad (15)$$

at the boundary conditions (2), (3) for functions U_3 and V_3 -

$$\begin{aligned} U_3=0\ , \quad V_3=0 \qquad &\text{на} \qquad \sigma_1\ , \\ U_3=\bar{U}\ , \quad V_3=\bar{V} \qquad &\text{на} \qquad \sigma_2. \end{aligned} \qquad (16)$$

Thus, as a result of application of the splitting method with respect to physical processes the task (1) - (4) is reduced to the consecutive solution of a set of more simple three tasks (10) - (11), (12) - (14) and (15) - (16).

2.2. Finite – difference approximation of the transfer-diffusion equation. A method of component –by-component splitting

As the differential equations (10) are same, we shall consider one equation

$$\frac{\partial \phi_1}{\partial t}+div\bar{\bar{u}}\phi_1=\nabla\mu\nabla\phi_1+f_1, \qquad \phi_1^{j-1}=\phi^{j-1} \qquad (17)$$

at boundary conditions (11) for function ϕ_1. Here ϕ_1 is any function of U_1 or V_1. An index "1" at function we shall omit for simplicity. Let

$$\mathcal{Z}\psi = \frac{\partial \bar{u}\psi}{\partial x} + \frac{\partial \bar{v}\psi}{\partial y} - \nabla\mu\nabla\psi\,.$$

It is easily to be convinced that in case of homogeneous boundary conditions the differential operator is positively determined.

For the finite-difference approximation of the differential operator $\mathcal{Z}$ let's consider a difference grid, which is received at crossing of coordinate lines $x = x_k$ и $y = y_l$. As a result we receive a set of basic nodes. Let's assume that indexes k and l change in limits Ω_0: $k^0 \le k \le k^1$ and $l^0 \le l \le l^1$. In addition, it is considered that the boundary points coincide with the boundary σ_0 of the solution area Ω_0. The set of such points we shall denote by σ_{0h}. Let's consider the basic points x_k, y_l, and the auxiliary points $x_{k+1/2}$, $y_{l+1/2}$, and we shall denote

$\Delta x_{k+1/2} = x_{k+1} - x_k$, $\Delta y_{l+1/2} = y_{l+1} - y_l$ and $\Delta x_k = \frac{1}{2}(\Delta x_{k+1/2} + \Delta x_{k-1/2})$,

$\Delta y_l = \frac{1}{2}(\Delta y_{l+1/2} + \Delta y_{l-1/2})$.

Now we use the scheme of the second -order accuracy

$$\mathcal{Z}^h\Phi_{kl} = (\mathcal{Z}_0^h + \mathcal{Z}_1^h)\Phi_{kl}\,,\quad \mathcal{Z}_0^h = \sum_{i=1}^{2}\mathcal{Z}_{0,i}^h,\quad \mathcal{Z}_1^h = \sum_{i=1}^{2}\mathcal{Z}_{1,i}^h\,, \qquad (18)$$

where

$$\mathcal{Z}_{0,1}^h\Phi_{kl} = \frac{u_{k+1/2,l}\Phi_{k+1,l} - u_{k-1/2,l}\Phi_{k-1,l}}{2\Delta x_k}\,,\quad \mathcal{Z}_{0,2}^h\Phi_{kl} = \frac{v_{k,l+1/2}\Phi_{k,l+1} - v_{k,l-1/2}\Phi_{k,l-1}}{2\Delta y_l}\,,$$

$$\mathcal{Z}_{1,1}^h\Phi_{kl} = -\frac{1}{\Delta x_k}\left[\frac{\mu_{k+1/2,l}}{\Delta x_{k+1/2}}\Phi_{k+1,l} - \left(\frac{\mu_{k+1/2,l}}{\Delta x_{k+1/2}} + \frac{\mu_{k-1/2,l}}{\Delta x_{k-1/2}}\right)\Phi_{k,l} + \frac{\mu_{k-1/2,l}}{\Delta x_{k-1/2}}\Phi_{k-1,l}\right],$$

$$\mathcal{Z}_{1,2}^h\Phi_{kl} = -\frac{1}{\Delta y_l}\left[\frac{\mu_{k,l+1/2}}{\Delta y_{l+1/2}}\Phi_{k,l+1} - \left(\frac{\mu_{k,l+1/2}}{\Delta y_{l+1/2}} + \frac{\mu_{k,l-1/2}}{\Delta y_{l-1/2}}\right)\Phi_{k,l} + \frac{\mu_{k,l-1/2}}{\Delta y_{l-1/2}}\Phi_{k,l-1}\right].$$

It is easily be convinced that the grid operators $\mathcal{Z}_{0,i}^h$ and $\mathcal{Z}_{1,i}^h$ with taken into consideration of homogeneous boundary condition are skew-symmetric and positively determined [4, 8, 9, 10]

$$(\mathcal{Z}_{0,i}^h\vec{\Phi}\,,\vec{\Phi}) = 0\,,\quad (\mathcal{Z}_{1,i}^h\vec{\Phi}\,,\vec{\Phi}) \ge 0\,,\quad i = 1,2$$

and

$$(\mathcal{Z}^h\vec{\Phi},\vec{\Phi}) \ge 0\,,\qquad \mu_{kl} \ge 0.$$

Here the scalar product is determined as

$$(a,b) = \sum_{kl} a_{kl}b_{kl}\Delta x_k\Delta y_l\,.$$

The summation is made on all internal points of the grid area Ω_{0h}.

With taken into consideration (18), the system of finite-difference equations approximating the task (17) with the second-order accuracy on space variables accepts the following operator form:

$$\frac{d\vec{\Phi}}{dt} + \mathcal{Z}^h\vec{\Phi} = \vec{F}, \qquad (19)$$

where $\vec{\Phi}$ and $\vec{F}$ are the vector-functions with components $\{\Phi_{kl}\}$ and $\{F_{kl}\}$, respectively, given in grid points Ω_{0h}.

Now, multiplying the equation (19) scalarly by $\vec{\Phi}$, we receive

$$\frac{1}{2}\frac{d(\vec{\Phi},\vec{\Phi})}{dt} + (z\vec{\Phi},\vec{\Phi}) = (\vec{F},\vec{\Phi}).$$

If in (19) we assume that $\mu_{k+1/2,l+1/2} = 0$ and grid vector-function $\vec{F}$ in the right part of the difference equation, caused by boundary conditions for the equation (17), is identically equal to zero then we receive

$$\frac{d(\vec{\Phi},\vec{\Phi})}{dt} = 0$$

Thus, the norm of grid solution

$$\left\|\vec{\Phi}^j\right\| = \sqrt{\left(\vec{\Phi}^j,\vec{\Phi}^j\right)}$$

is kept, i. e.

$$\left\|\vec{\Phi}^j\right\|^2 = \left\|\vec{\Phi}^{j-1}\right\|^2.$$

With taken into consideration the continuity equation for functions $\bar{u}_{k+1/2,l}$ and $\bar{v}_{k,l+1/2}$ the condition of conservation of substation on time takes place:

$$\frac{d(\vec{\Phi},\vec{e})}{dt} = \frac{d}{dt}\sum_{kl}\vec{\Phi}_{kl}\Delta x_k \Delta y_l = 0,$$

where $\vec{e}$ is the unit vector.

For approximation of the equation (19) in time on the time interval $t_{j-1} \le t \le t_j$ the Crank-Nicholson scheme by the subsequent application of a two-cycle splitting method is used. As a result, the problem is reduced to a sequence of more simple one-dimensional finite-difference equations which are effectively solved by a factorization method. These equations have the following form:

$$\frac{\vec{\Phi}^{j-1/6}-\vec{\Phi}^{j-1}}{\tau/2} + \left(Z^h_{0,1} + Z^h_{1,1}\right)\frac{\vec{\Phi}^{j-1/6}+\vec{\Phi}^{j-1}}{2} = 0,$$

$$\frac{\vec{\Phi}^{j-4/6}-\vec{\Phi}^{j-3/6}}{\tau/2} + \left(Z^h_{0,2} + Z^h_{1,2}\right)\frac{\vec{\Phi}^{j-4/6}+\vec{\Phi}^{j-3/6}}{2} = 0,$$

$$\frac{\vec{\Phi}^{j-2/6}-\vec{\Phi}^{j-4/6}}{\tau/2} = F,$$

$$\frac{\vec{\Phi}^{j-2/6}-\vec{\Phi}^{j-2/6}}{\tau/2} + \left(Z^h_{0,2} + Z^h_{1,2}\right)\frac{\vec{\Phi}^{j-2/6}+\vec{\Phi}^{j-2/6}}{2} = 0,$$

$$\frac{\vec{\Phi}^{j}-\vec{\Phi}^{j-2/6}}{\tau/2} + \left(Z^h_{0,1} + Z^h_{1,1}\right)\frac{\vec{\Phi}^{j}+\vec{\Phi}^{j-2/6}}{2} = 0.$$

Application of the two-cycle splitting method provides the second order accuracy in time. The received system of finite –difference equations is absolutely steady on the interval $0 \le t \le T$.

Thus, the considered scheme approximates the differential equation (17) with the second-order accuracy both on time and on spatial coordinates and is absolutely steady. The task (15),(16) is similarly solved.

2.3. Finite –difference approximation of equations of adaptation. Splitting of the problem

Let's consider on the time interval $t_{j-1} \le t \le t_{j+1}$ the problem of adaptation (12)-(14). index "2" at solution components we shall omit for simplicity. Here the finite –difference scheme approximates the differential problem with the second-order accuracy on spatial coordinates. The Crank-Nicholson scheme with the subsequent application of a two-cyclic method of splitting is used for approximation on time. As a whole, the scheme received here is absolutely steady and approximates (12) - (14) with the second order accuracy. Note that coefficients $\bar{u}_{k+1/2,l}$ and $\bar{v}_{k,l+1/2}$ which are in transfer-diffusion equations, are defined after solving of the adaptation problem. Before to consider the difference approximation of the system of differential equations (12) let's consider the operators A_l, A_x and A_y. We assume that

$$A_2 = A_l + A_x + A_y,$$

where

$$A_l = \begin{Vmatrix} 0 & -l & 0 \\ l & 0 & 0 \\ 0 & 0 & 0 \end{Vmatrix}, \quad A_x = \begin{Vmatrix} 0 & 0 & gH\frac{\partial}{\partial x} \\ 0 & 0 & 0 \\ gH\frac{\partial}{\partial x} & 0 & 0 \end{Vmatrix}, \quad A_y = \begin{Vmatrix} 0 & 0 & 0 \\ 0 & 0 & gH\frac{\partial}{\partial y} \\ 0 & gH\frac{\partial}{\partial y} & 0 \end{Vmatrix}.$$

Then the system of equations (12) in the operator form is

$$B\frac{\partial \varphi}{\partial t} + A_2\varphi = 0\,. \qquad (20)$$

Now if on the time interval $t_{j-1} \le t \le t_{j+1}$ we shell use the two-cycle splitting method for (20), then the problem is reduced to solution of a set of more simple problems:
on the time interval $t_{j-1} \le t \le t_j$ -

$$B\frac{\partial \varphi_1}{\partial t} + A_l\varphi_1 = 0, \qquad B\varphi_1^{j-1} = B\varphi_1^j, \qquad (\varphi_1^j \text{ is solution of (7) at moment } t = t_j),$$

$$B\frac{\partial \varphi_2}{\partial t} + A_x\varphi_2 = 0, \qquad B\varphi_2^{j-1} = B\varphi_1^j, \qquad (21)$$

$$B\frac{\partial \varphi_3}{\partial t} + A_y\varphi_3 = 0, \qquad B\varphi_3^{j-1} = B\varphi_2^j$$

and on the interval $t_j \le t \le t_{j+1}$ we have

$$B\frac{\partial \varphi_4}{\partial t} + A_y\varphi_4 = 0, \qquad B\varphi_4^j = B\varphi_3^j,$$

$$B\frac{\partial \varphi_5}{\partial t} + A_x\varphi_5 = 0, \qquad B\varphi_5^j = B\varphi_4^{j+1}, \qquad (22)$$

$$B\frac{\partial \varphi_6}{\partial t} + A_l\varphi_6 = 0, \qquad B\varphi_6^j = B\varphi_5^{j+1}.$$

The first equation from (21) and last equation from (22) we shall write in the component-by-component form for the basic grid points (grid points by integer indexes). As a result, we shall receive simple systems of the equations, analytical solution of which are:

$$U_{1_{ki}}^j = U_{1_{ki}}^{j-1}\cos lt + V_{1_{ki}}^{j-1}\sin lt,$$

$$V_{1kl}^{j} = V_{1kl}^{j-1}\cos lt - U_{1kl}^{j-1}\sin lt$$

and

$$U_{6kl}^{j+1} = U_{6kl}^{j}\cos lt + V_{6kl}^{j}\sin lt,$$

$$V_{6kl}^{j+1} = V_{6kl}^{j}\cos lt - U_{6kl}^{j}\sin lt .$$

For numerical solution of other tasks from (21),(22) let's consider their finite-difference approximation on space variables. With this purpose Let's consider approximation of the operators $\frac{\partial}{\partial x}$ и $\frac{\partial}{\partial y}$. Let the function U is given in points $x_{k^0+1/2}$ and $x_{k^1+1/2}$. Besides $U_{k^0+1/2} = a$, $U_{k^1+1/2} = b$ and $\zeta_{k^0} = c$. Then we shall use the following approximation

$$\frac{\partial U}{\partial x} \approx \nabla_k^- U \qquad \text{and} \qquad \frac{\partial \zeta}{\partial x} \approx \nabla_k^+ \zeta_k ,$$

where

$$\nabla_k^- U = \begin{cases} \dfrac{1}{\Delta x_{k^0}} U_{k^0+1/2} - \dfrac{a}{\Delta x_{k^0}} & , \ k = k^0 \\ \dfrac{1}{\Delta x_k}\left(U_{k+\frac{1}{2}} - U_{k-\frac{1}{2}}\right) & , k = k^0+1, k^0+2, \dots, k^1-1 \\ -\dfrac{1}{\Delta x_{k^1}} U_{k^1-1/2} + \dfrac{b}{\Delta x_{k^1}} & , \ k = k^1 \end{cases}$$

and

$$\nabla_k^+ \zeta_k = \begin{cases} \dfrac{1}{\Delta x_{k^0+1/2}} \zeta_{k^0+1} - \dfrac{c}{\Delta x_{k^0+1/2}} & , \ k = k^0 \\ \dfrac{1}{\Delta x_{k+1/2}} (\zeta_{k+1} - \zeta_k) & , k = k^0+1, k^0+2, \dots, k^1-1 \end{cases}$$

Operators ∇_l^+ and ∇_l^- are similarly determined, which approximate differential operator $\frac{\partial}{\partial y}$. Then finite-difference approximation of the differential operators A_x and A_y we will consider in the following form

$$A_x^h = \begin{Vmatrix} 0 & 0 & gH\nabla_k^+ \\ 0 & 0 & 0 \\ gH\nabla_k^- & 0 & 0 \end{Vmatrix}, \qquad A_y^h = \begin{Vmatrix} 0 & 0 & 0 \\ 0 & 0 & gH\nabla_l^+ \\ 0 & gH\nabla_l^- & 0 \end{Vmatrix}.$$

Similarly to operators A_x and A_y the operators A_x^h and A_y^h are skew-symmetric. These conditions are necessary for construction of absolutely steady finite –difference schemes.

Taking into consideration the finite-difference operators A_x^h and A_y^h in equations (21),(22) and using the Crank-Nicholson scheme for approximation on time, after the appropriate transformations we shall receive the following systems of the finite –difference equations

$$\left.\begin{aligned} U^{j-1/2}_{2_{k+1/2,l}} + \frac{\tau g H_{k+1/2,l}}{2}\nabla_k^+ \zeta^{j-1/2}_{2_{kl}} &= U^{j-1}_{2_{k+1/2,l}} \\ V^{j-1/2}_{2_{kl+1/2}} &= V^{j-1}_{2_{kl+1/2}} \\ \zeta^{j-1/2}_{2_{kl}} + \frac{\tau}{2}\nabla_k^- U^{j-1/2}_{2_{kl}} &= \zeta^{j-1}_{2_{kl}} \end{aligned}\right\} \qquad (23)$$

with the initial conditions

$$U^{j-1}_{2_{k+1/2,l}} = U^{j}_{1_{k+1/2,l}} \quad , \quad V^{j-1}_{2_{kl+1/2}} = V^{j}_{1_{kl+1/2}}, \quad \zeta^{j-1}_{2_{kl}} = \zeta^{j-1}_{1_{kl}}$$

and

$$\left.\begin{aligned} U^{j-1/2}_{3_{k+1/2,l}} &= U^{j-1}_{3_{k+1/2,l}} \\ V^{j-1/2}_{3_{kl+1/2}} + \frac{\tau g H_{kl+1/2}}{2}\nabla_l^+ \zeta^{j-1/2}_{2_{kl}} &= V^{j-1}_{3_{kl+1/2}} \\ \zeta^{j-1/2}_{3_{kl}} + \frac{\tau}{2}\nabla_l^- V^{j-1/2}_{3_{kl}} &= \zeta^{j-1}_{3_{kl}} \end{aligned}\right\} \qquad (24)$$

with the initial conditions

$$U^{j-1}_{3_{k+1/2,l}} = U^{j}_{2_{k+1/2,l}} \quad , \quad V^{j-1}_{3_{kl+1/2}} = V^{j}_{2_{kl+1/2}} \quad \zeta^{j-1}_{3_{kl}} = \zeta^{j}_{2_{kl}} .$$

Here $\Phi^{j-1/2} = (\Phi^j + \Phi^{j-1})/2$, Φ is any function of U_α, V_α or ζ_α $(\alpha = 2,3)$.

Now Let's consider the system of finite-difference equations (23). Then with use of the third equation we shall exclude from the first equation function $\zeta^{j-1/2}_{2_{kl}}$, as a result we shall receive one-dimensional finite-difference equation

$$U^{j-1/2}_{2_{k+1/2,l}} - \frac{\tau^2 g H_{k+1/2,l}}{4}\nabla_k^+\nabla_k^- U^{j-1/2}_{2_{kl}} = U^{j-1}_{2_{k+1/2,l}} - \frac{\tau g H_{k+1/2,l}}{2}\nabla_k^+ \zeta^{j-1}_{2_{kl}} . \qquad (25)$$

After salving of this equation from the third equation we shell determine the function $\zeta^{j-1/2}_{2_{kl}}$

$$\zeta^{j-1/2}_{2_{kl}} = -\frac{\tau}{2}\nabla_k^- U^{j-1/2}_{2_{kl}} + \zeta^{j-1}_{2_{kl}} .$$

The equation (25) is effectively solved by the factorization method.

Similarly to equation (25), from the equation system (24) for the function $V^{j-1/2}_{3_{kl+1/2}}$, we receive the following equation

$$V^{j-1/2}_{3_{kl+1/2}} - \frac{\tau^2 g H_{kl+1/2}}{4}\nabla_l^+\nabla_l^- V^{j-1/2}_{3_{kl}} = V^{j-1}_{3_{kl+1/2}} - \frac{\tau g H_{kl+1/2}}{2}\nabla_l^+ \zeta^{j-1}_{3_{kl}} . \qquad (26)$$

The equation (26) is salved similarly to (25).

On the time interval $t_j \le t \le t_{j+1}$, the systems of finite - difference equations (22) for grid function $U^{j+1/2}_{4_{k+1/2,l}}$, $V^{j+1/2}_{4_{k,l+1/2}}$, $\zeta^{j+1/2}_{4_{k,l}}$ and $U^{j+1/2}_{5_{k+1/2,l}}$, $V^{j+1/2}_{5_{k,l+1/2}}$, $\zeta^{j+1/2}_{5_{k,l}}$ are solved completely similarly previous systems.

Thus, the considered numerical scheme allows the solution of a shallow water problem reduce to solution of a set of more simple one-dimensional tasks which are effectively solved by the factorization method. The constructed scheme has the second-order approximation both on time and on horizontal coordinates and is absolutely steady.

At solution of the equation system (23),(24) it is possible from the continuity equation eliminate the functions $U^{j-1/2}_{2_{k+1/2,l}}$ and $V^{j-1/2}_{3_{k,l+1/2}}$, which are determined from the first and the second equations, respectively. As a result the three-point equations are received for $\zeta^{j-1/2}_{2_{k,l}}$ and $\zeta^{j-1/2}_{3_{k,l}}$, which are solved also by factorization method. Analogically are determined the grid functions $\zeta^{j+1/2}_{4_{k,l}}$ and $\zeta^{j+1/2}_{5_{k,l}}$ from (21),(22).

Now let's consider methodically other algorithm of solution of the adaptation task (the second version of the algorithm). With this purpose on the time interval $t_{j-1} \le t \le t_j$ we shall consider second and third equations from (21), and on the interval $t_j \le t \le t_{j+1}$ - the first and second equations from (22), which are approximated on spatial variable. The received equations in the component form will accept the following form:
on the time interval $t_{j-1} \le t \le t_j$ -

$$\left.\begin{aligned} \frac{dU_2}{dt} + gH\nabla_k^+\varsigma_2 = 0 \\ \frac{dV_2}{dt} = 0 \\ \frac{d\varsigma_2}{dt} + \nabla_k^- U_2 = 0 \end{aligned}\right\} \qquad (27)$$

with the initial conditions

$$U_2^{j-1} = U_1^j \;,\; V_2^{j-1} = V_1^j \;,\; \varsigma_2^{j-1} = \varsigma_1^j \qquad (28)$$

and

$$\left.\begin{aligned} \frac{dU_3}{dt} = 0 \\ \frac{dV_3}{dt} + gH\nabla_k^+\varsigma_3 = 0 \\ \frac{d\varsigma_3}{dt} + \nabla_k^- V_3 = 0 \end{aligned}\right\} \qquad (29)$$

with conditions

$$U_3^{j-1} = U_2^j,\; V_3^{j-1} = V_2^j,\quad \varsigma_3^{j-1} = \varsigma_2^j \,. \qquad (30)$$

On the time interval $t_j \le t \le t_{j+1}$ we have following tasks

$$\left.\begin{aligned} \frac{dU_4}{dt} = 0 \\ \frac{dV_4}{dt} + gH\nabla_k^+\varsigma_4 = 0 \\ \frac{d\varsigma_4}{dt} + \nabla_k^- V_4 = 0 \end{aligned}\right\} \qquad (31)$$

with conditions

$$U_4^j = U_3^j,\ V_4^j = V_3^j,\quad \varsigma_4^j = \varsigma_3^j \tag{32}$$

and

$$\left.\begin{aligned} \frac{dU_3}{dt} + gH\nabla_k^+\varsigma_3 &= 0 \\ \frac{dV_3}{dt} &= 0 \\ \frac{d\varsigma_3}{dt} + \nabla_k^- U_3 &= 0 \end{aligned}\right\} \tag{33}$$

with initial conditions

$$U_3^j = U_4^{j+1},\ V_3^j = V_4^{j+1},\ \varsigma_3^j = \varsigma_4^{j+1}. \tag{34}$$

It should be noted that the problems (27),(28) - (33),(34) may be received from (20), if on each time interval $t_{j-1} \le t \le t_{j+1}$ we shell use the two-cycle splitting method in case, when

$$A_2 = A_x + A_y$$

Thus, the specified tasks are received from the equation system

$$\left.\begin{aligned} \frac{dU_2}{dt} + gH\nabla_k^+\varsigma_2 &= 0 \\ \frac{dV_2}{dt} + gH\nabla_l^+\varsigma_2 &= 0 \\ \frac{d\varsigma_2}{dt} + \nabla_k^- U_2 + \nabla_l^- V_2 &= 0 \end{aligned}\right\} \tag{35}$$

with conditions

$$U_2^{j-1} = U_1^j,\ V_2^{j-1} = V_1^j,\quad \varsigma_2^{j-1} = \varsigma^{j-1} \tag{36}$$

(where U_1^j and V_1^j are solutions of the task on the stage taking into account the Coriolis force and ς^{j-1} is the initial condition of the basic problem).

The problem (35),(36) may be to reduce to the oscillation equation of a membrane. After the appropriate transformations on the interval $t_{j-1} \le t \le t_{j+1}$ we shall receive the equation [8]

$$\frac{d^2\varsigma_2}{dt^2} - \nabla_k^- c^2 \nabla_k^+ \varsigma_2 - \nabla_l^- c^2 \nabla_l^+ \varsigma_2 = 0 \tag{37}$$

with initial conditions at $t = t_{j-1}$

$$\varsigma_2^{j-1} = \varsigma^{j-1} \quad \text{и} \quad \frac{d\varsigma_2}{dt} = q, \tag{38}$$

where $C = \sqrt{gH}$ и $q = \nabla_k^- U_2^{j-1} + \nabla_l^- V_2^{j-1}$.

On the other hand from each problems (27),(28) - (33),(34) analogically one-dimensional problems are received:
on the interval $t_{j-1} \le t \le t_j$ -

$$\frac{d^2\varsigma_2}{dt^2} - \nabla_k^- c^2 \nabla_k^+ \varsigma_2 = 0\,, \qquad \varsigma_2^{j-1} = \varsigma^{j-1}\ ,\ \frac{d\varsigma_2}{dt} = q,$$

$$\frac{d^2\varsigma_3}{dt^2} - \nabla_l^- c^2 \nabla_l^+ \varsigma_3 = 0\,, \quad \varsigma_3^{j-1} = \varsigma_2^j \quad , \quad \frac{d\varsigma_3}{dt} = q \tag{39}$$

and on the interval $t_j \le t \le t_{j+1}$ the following problems

$$\frac{d^2\varsigma_4}{dt^2} - \nabla_l^- c^2 \nabla_l^+ \varsigma_4 = 0\,, \quad \varsigma_4^j = \varsigma_3^j \quad , \quad \frac{d\varsigma_4}{dt} = q,$$

$$\frac{d^2\varsigma_5}{dt^2} - \nabla_k^- c^2 \nabla_k^+ \varsigma_5 = 0\,, \quad \varsigma_5^j = \varsigma_4^{j+1} \quad , \quad \frac{d\varsigma_5}{dt} = q, \tag{40}$$

which as a whole give solution of the problems (27),(28) - (33),(34), i. e. of the problem (35),(36) or (36),(37).

As a result of solution of received one-dimensional problems, the grid functions ς_2^j, ς_3^j, ς_4^{j+1} and ς_5^{j+1} are determined, with help of which values of U_2^j, V_2^j, U_3^j, V_3^j, U_4^{j+1}, V_4^{j+1}, U_5^{j+1} and V_5^{j+1} are easily calculated.

As the one-dimensional tasks from (39),(40) are the same, a method of solution of the received tasks we shall consider on an example of the first task from (39).

Thus, on the time interval $t_{j-1} \le t \le t_j$ we consider the problem

$$\frac{d^2\varsigma_2}{dt^2} - \nabla_k^- c^2 \nabla_k^+ \varsigma_2 = 0\,, \tag{41}$$

$$\varsigma_2 = \varsigma^{j-1} \quad , \quad \frac{d\varsigma_2}{dt} = q \qquad \text{at} \qquad t = t_{j-1}. \tag{42}$$

With the purpose of approximation on time on the interval $t_{j-1} \le t \le t_j$ of the task (41),(42) we shall consider the implicit scheme, which is similar to the Crank-Nicholson scheme [8]

$$\frac{\varsigma_{2_{kl}}^j - 2\varsigma_{2_{kl}}^{j-\frac{1}{2}} + \varsigma_{2_{kl}}^{j-1}}{\frac{\tau^2}{4}} - \nabla_k^- C_{kl}^2 \nabla_k^+ \frac{\varsigma_{2_{kl}}^j + \varsigma_{2_{kl}}^{j-1}}{2} = 0$$

at initial conditions

$$\varsigma_{2_{kl}}^j = \varsigma_{kl}^{j-1}, \quad \frac{\varsigma_{2_{kl}}^{j-\frac{1}{2}} + \varsigma_{2_{kl}}^{j-\frac{3}{2}}}{\tau} = q_{kl}. \tag{43}$$

Further we shall consider approximation

$$\frac{\varsigma_{2_{kl}}^{j-\frac{1}{2}} - 2\varsigma_{2_{kl}}^{j-1} + \varsigma_{2_{kl}}^{j-\frac{3}{2}}}{\frac{\tau^2}{4}} - \nabla_k^- C^2 \nabla_k^+ \varsigma_{2_{kl}}^{j-1} = 0 \tag{44}$$

Then from (44) with use (43) we receive

$$\varsigma_{2_{kl}}^{j-1/2} = \varsigma_{2_{kl}}^{j-1} + \frac{\Delta\tau}{2} q_{kl} + \frac{\Delta\tau^2}{8} \nabla_k^- C^2 \nabla_k^+ \varsigma_{2_{kl}}^{j-1}.$$

Similarly we receive algorithm of solution for the first task from (40) on the time interval $t_j \le t \le t_{j+1}$. In this case we have

$$\frac{\varsigma_{4_{kl}}^{j+1} - 2\varsigma_{4_{kl}}^{j+\frac{1}{2}} + \varsigma_{4_{kl}}^{j}}{\frac{\tau^2}{4}} - \nabla_l^- C^2 \nabla_l^+ \frac{\varsigma_{4_{kl}}^{j+1} + \varsigma_{4_{kl}}^{j}}{2} = 0$$

$$\varsigma_{4_{kl}}^{j} = \varsigma_{3_{kl}}^{j} \quad , \quad \varsigma_{4_{kl}}^{j+1/2} = \varsigma_{4_{kl}}^{j} + \frac{\Delta\tau}{2} q_{kl} + \frac{\Delta\tau^2}{8} \nabla_l^- C_{kl}^2 \nabla_l^+ \varsigma_{2_{kl}}^{j} .$$

Concerning unknown grid functions $\varsigma_{3_{kl}}^{j}$ and $\varsigma_{3_{kl}}^{j+1}$ from (39) and (40) it should be noted that also the similar equations are received, which are effectively solved by the factorization method.

To the similarly previous algorithm (the first version), in this case received scheme is absolutely steady and has the second order accuracy on time and spatial variables. At all stages of splitting the received equations are effectively solved by the factorization method.

. .

2.4. Some questions of considered algorithms

As a result of using of the splitting method with respect to physical processes on each time interval $t_{j-1} \le t \le t_{j+1}$ the main problem is reduced to solution of set of more simple tasks on the intervals $t_{j-1} \le t \le t_j$, $t_{j-1} \le t \le t_{j+1}$ and $t_j \le t \le t_{j+1}$.

Thus it is assumed that coefficients $\bar{u}_{k+1/2,l}$ and $\bar{v}_{k,l+1/2}$ included in the transfer-diffusion equations (at the first and third stages of splitting of the basic task), are known and constant on all interval $t_{j-1} \le t \le t_{j+1}$. Thus, on the time interval $t_{j-1} \le t \le t_{j+1}$ the values of these coefficients are determined on the previous step $t_{j-2} \le t \le t_{j-1}$ at the adaptation stage of solution of the problem (12)-(14). For definition of grid functions the following approximation are also used

$$\bar{u}_{k+1/2,l} = \bar{u}_{2_{k+1/2,l}}^{j-1/2} + \bar{u}_{3_{k+1/2,l}}^{j+1/2} \quad \text{and} \quad \bar{v}_{k,l+1/2} = \bar{v}_{2_{k,l+1/2}}^{j-1/2} + \bar{v}_{4_{k,l+1/2}}^{j+1/2}$$

Coefficients of turbulent viscosity on the interval $t_{j-1} \le t \le t_{j+1}$ at the first and third stages of splitting (transfer-diffusion stages) of the basic task are also the same, which are determined on the previous time interval by the formula [12]

$$\mu^j = \Delta x.\Delta y \sqrt{2\left(\frac{\partial u}{\partial x}\right)^2 + \left(\frac{\partial u}{\partial y} + \frac{\partial v}{\partial x}\right)^2 + 2\left(\frac{\partial v}{\partial y}\right)^2}$$

where Δx and Δy are horizontal grid steps along x and y axes, respectively.

2.5. Numerical realization of the model for the easternmost part of the Black Sea

The shallow water model (SHWM) is included in the regional forecasting system for the easternmost part of the Black Sea [13-15], which is a part of the Basin-scale Black Sea nowcastong/forecstong system [16-17]. functioning of the regional forecasting system schematically is illustrated in Fig.1.

A Basin-scale model of Black Sea dynamics of Marine Hydrophysical Institute (MHI, Sevastopol) of the National Academy of Sciences of Ukraine provides RM-IG and SHWM of M. Nodia Institute of Geophysics with initial and boundary conditions on the liquid boundary. SHWM

requires also wind stress components and atmosphere pressure gradients along x and y axes, which are provided from atmospheric model ALADIN. All these data with one-hour time step frequency within the 4-days period are received operatively via ftp site from MHI. Test calculations on SHWM were carried out for the same regional area, for which are calculated marine forecasts by 3-D RM-IG [13-15]. This area is bounded with the Caucasus and Turkish shorelines and the western liquid (open) boundary coincident with 39.08°E. The grid parameters are also the same for both RM-IG and SHWM: a grid has 215 x 347 points on horizons with step 1 km.

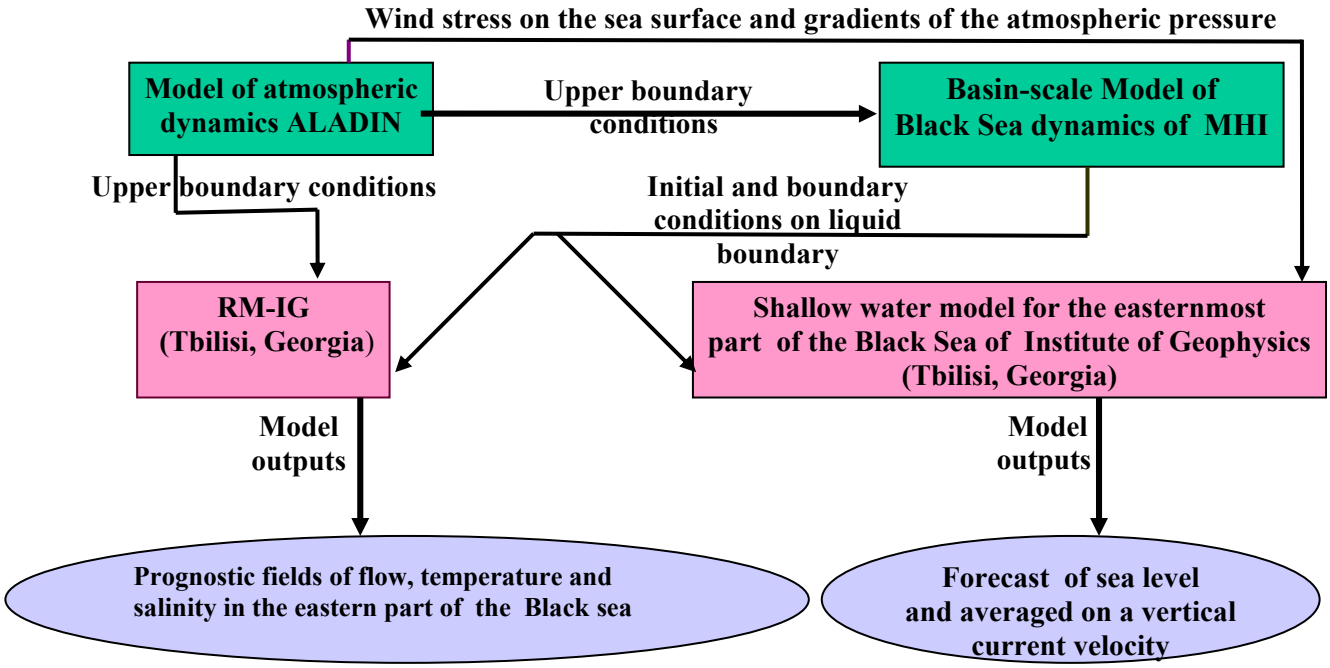

Fig.1. The scheme of functioning of the regional forecasting system.

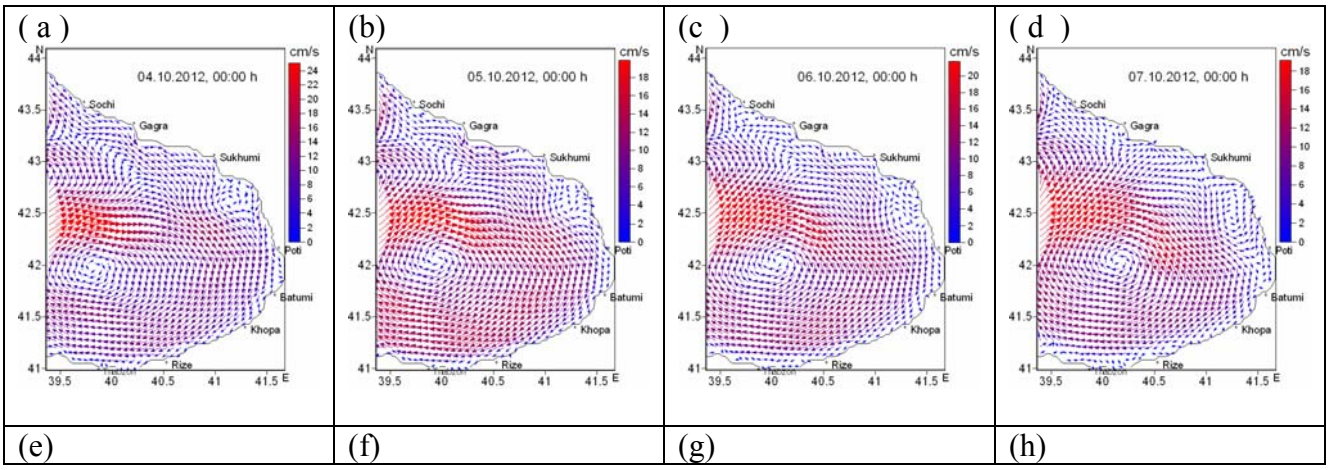

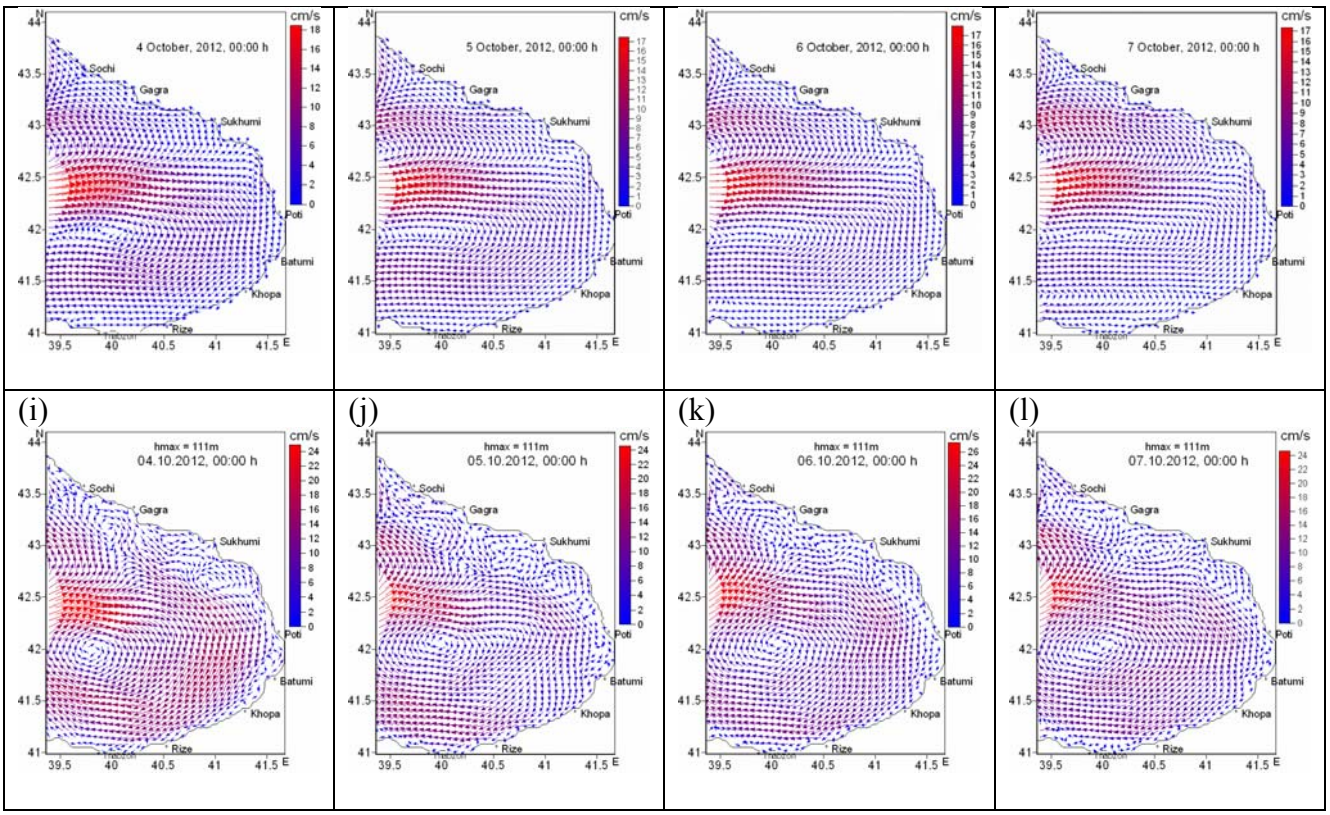

Fig.1.Simulated current fields within 4-7 October 2012. (a), (b), (c), (d) – calculated from SHWM (the first version of the algorithm), hmax = 111 m, dlt = 150 s; (e), (f), (g), (h) - calculated from SHWM (the second version of the algorithm), hmax = 111 m, dlt = 3 s; (i), (j), (k), (l) - averaged in the 111 m upper layer current fields calculated from 3-D RM-IG.

With the purpose of testing the SHWM numerical experiments were carried out by using of both versions of numerical algorithm, which are described in the previous section. The numerical experiments showed that realizations of the model with use of the second version of numerical algorithm of solution, when the equation systems at the stage of adaptation are reduced to the oscillation equations of a string, requires much less time step than in the first version. In both cases maximal depth equal to 111m was consider.

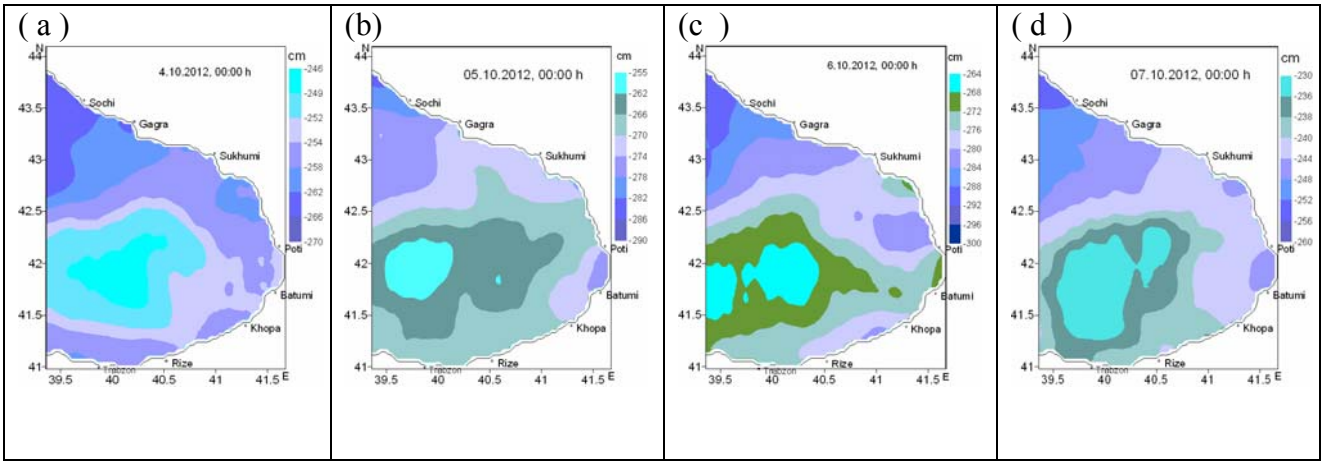

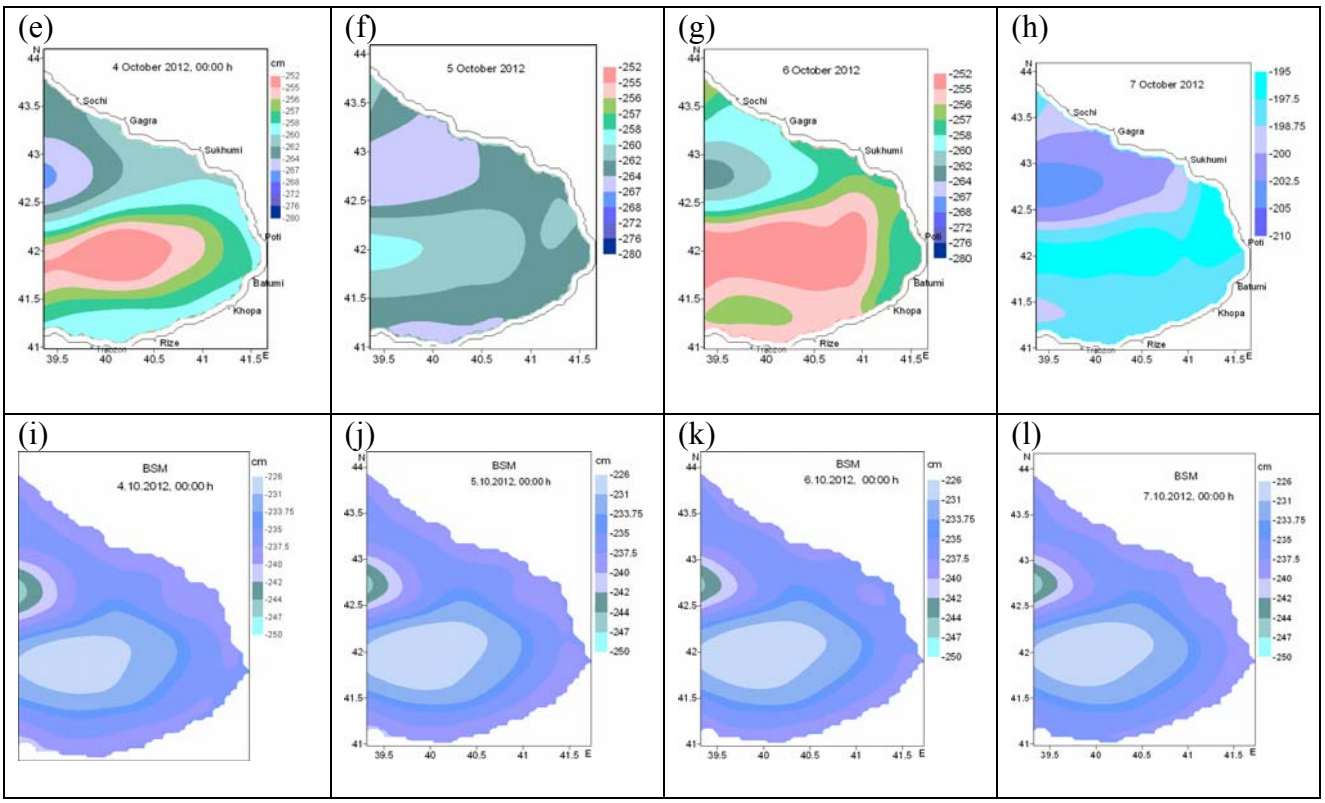

Fig.2. Simulated sea level changes (in cm) within 4-7 October 2012. (a), (b), (c), (d) – calculated from SHWM (the first version of the algorithm), hmax = 111 m, dlt = 150 s; (e), (f), (g), (h) - calculated from SHWM (the second version of the algorithm), hmax = 111 m, dlt = 3 s; (i), (j), (k), (l) - calculated from the 3-D model of Black Sea dynamics of MHI.

By SHWM the autumn circulation was simulated during 3-7 October 2012. The integration of the equations began at 00:00 h (Greenwich time), October 3 2012 and 4 days last, but we consider that the SHWM gives forecast only for three days as during the first day the coastal model runs in the prognostic mode only to have better adjustment of the fine resolution to the course initial conditions provided by the basin-scale model of MHI. At realization of the SHWM with use of the first version of the numerical algorithm for the easternmost area of the Black Sea the time step was equal to 150 s, but at realization with use of the second version the time step was 3 s.

With the purpose of illustrating in Fig.2 simulated currents are shown after 24, 48, 72, and 96 h after start of integration by the SHWM with use of the first version of the numerical algorithm (Fig.2a, b, c, d) and with use of the second version of the algorithm (Fig.2e, f, g, h), also averaged on a vertical within 111 m upper layer simulated currents by the 3-D RM-IG (Fig.2i, j, k, l). From Fig.2 it is clear that the main feature of the regional circulation for the considered time period is formation of the anticyclonic eddy (called the Batumi eddy), which covers the significant part of the considered regional area. Comparison of circulation patterns calculated from SHWM (with use of both versions of algorithm) and RM-IG shows that circulation patterns received from SHWM with use of the first version is more close to circulation patterns received from 3-D RM-IG.

In Fig.3 are illustrated simulated sea level changes after 24, 48, 72, and 96 h after start of integration using SHWM (with use of both versions of algorithm) and sea level changes received from the 3-D of MHI (Fig.2i, j, k, l). The change of the free surface level in many respects is caused by circulating features. From Fig.3 it is well visible, that in the considered area the decreasing of the sea level from the undisturbed level is observed during all time, but in the central part of the Batumi eddy the level rises. Comparison of results show that sea level patterns received from the first version of SHWM are more close to sea level patterns received from the 3-D of MHI.

Summarizing results of the carried out numerical experiments we come to opinion, that for simulation and forecast of sea coastal processes the first version of the numerical algorithm of

solution of equations of the shallow water theory is more acceptable than the second version, when solution of equations on the adaptation stage of splitting is reduced to the oscillation equations. In addition, the realization of the second version requires to use very small step in time. But the consideration of this algorithm has the significant interest, as it can appear very convenient and useful to tasks concerning fluctuations and wave processes in different environments.

Finally, it should be noted that the further improvement of a regional forecasting system is connected to inclusion of modeling of coastal processes connected to change of a sea level for the shallow part of the Georgian coast with the very high spatial resolution. Thus the results of models stated in the given paper, will be used as the input data. The model takes into account mobile lateral boundary with the land, which is determined on a free surface level. It enables to predict processes of drainage and flooding.

References

[1] Marchuk G. I., Kagan B. A. Ocean tide. Leningrad, Gidrometeoizdat, 1977, 266 p (in Russian).

[2] Backhaus J. Entwicklung eines numerischen modells zur reproduktion widangeregter bewegungsvorgo-nge in Flash-wassergebieten mit beweglichem Rand.-Diplomarbeit. Univ. Hmburg, 1975, 81 p.

[3] Cherkasov L. V. Hydrodynamics of surface and internal waves. Kiev, "Naukova dumka", 1976, 364 p (in Russian).

[4] Marchuk G. I., Dymnikov V. P., Zalesny V. B. Mathematical models of geophysical hydrodynamics and numerical methods of their realization. Leningrad, Gidrometeoizdat, 1987, 296 p (in Russian).

[5] Girgvliani A. G. On numerical modeling of shallow water problems. Preprint N454, Novosibirsk, VC CO AH CCCP, 1983, 18 p (in Russian).

[6] Kordzadze A. A. Mathematical questions of solution of ocean dynamics problems. VC CO AH CCCP, Novosibirsk, 1982, 148 p (in Russian).

[7] Bubnov M. A. Mathematical questions of modeling of tide and circulations in the baroclinic ocean. VC CO AH CCCP, Novosibirsk, 1984, 152 p (in Russian).

[8] Marchuk G. I. Methods of computer mathematics. Moscow, Nauka Press, 1977, 454 p (in Russian).

[9] Marchuk G. I. Numerical solution of problems of atmospheric and oceanic dynamics. Leningrad, Gidrometeoizdat, 1974, 303 p 90 (in Russian).

[10] Kordzadze A. A. Mathematical modeling of dynamics of sea currents (theory, algorithm, Numerical experiments), Moscow, OVM AH CCCP, 1989, 218 p (in Russian).

[11] Ilin V. P., Kordzadze A. A. About one iteration scheme of a splitting method for stationary tasks of ocean currents. In: methods of computing and applied mathematics. Differential and Integral equations. VC CO AH CCCP, Novosibirsk, 1977, pp.136-146 (in Russian).

[12] Zilitinkevich S. S., Monin A. S. Turbulence in dynamic models of the atmosphere. Nauka, Leningrad, 1971, 41 p (in Russian).

[13] Kordzadze A. A, Demetrashvili D. I. Operational forecast of hydrophysical fields in the Georgian Black Sea coastal zone within the ECOOP. *Ocean Science*, 2011, 7, *pp.* 793- 803, www.ocean-sci.net/7/793/2011/, doi: 10.5194/os-7-793-2011.

[14] Kordzadze A. A, Demetrashvili D. I. Operational regional forecasting system of state of the east part of the Black Sea. Ecological safety of coastal and shelf zones and comprehensive use of shelf resources. Collected scientific papers. Sevastopol, Iss. 25, vol.2, 2011, pp.136-146 (in Russian).

[15] Kordzadze A. A, Demetrashvili D. I., Kukhalashvili V. G. Circulation processes in the easternmost part of the Black Sea in 2010-2012. Results of circulation and forecast. J. Georgian Geoph. Soc., 2012 (in present journal).

[16] Korotaev G. K., Oguz T., Dorofeev V. L. et al. Development of Black Sea nowcasting and orecasting system, Ocean Science, 7, 2011, P. 629-649, doi: 10.5194/os-7-629-2011.

[17] Kubryakov A. I., Korotaev G. K., Dorofeev V. L. et al. Black Sea Coastal forecasting system. Ocean Science, 8, 2012, P. 183-196, doi: 10.5194/os-8-183-2012.

(Received in final form 20 December 2012)

Об эффективных численных методах решения задачи мелкой воды. Реализация модели для восточной части Чёрного моря

Автандил Кордзадзе, Демури Деметрашвили, Вепхиа Кухалашвили

Резюме

Предложены два варианта численного метода решения системы уравнений мелкой воды, основанного на методе двуциклического расщепления, которые реализованы для восточной акватории Черного моря. В первом варианте решение ситемы уравнений, полученной в результате расщепления основной системы уравнений по физическим процессам (этап адаптации) сводится к применению метода факторизации относительно компонентов скорости течения, а во втором варианте на этапе адаптации полученная система уравнений приводится к уравнениям колебании струны относительно координатных линий, которые решаются также методом факторизации. Предложенные в данной статье методы решения не требуют применения внутренних итераций, что значительно увеличивает эффективность их практического применения.

“მცირე” წყლის ამოცანის ამოხსნის ეფექტური რიცხვითი მეთოდების შესახებ. მოდელის რეალიზაცია შავი ზღვის აღმოსავლეთ ნაწილისათვის

ავთანდილ კორძაძე, დემური დემეტრაშვილი, ვეფხია კუხალაშვილი

რეზიუმე

განხილულია გახლეჩის ორციკლიან მეთოდზე დაფუძნებული “მცირე” წყლის თეორიის განტოლებათა სისტემის ამოხსნის რიცხვითი მეთოდის ორი ვარიანტი, რომლებიც რეალიზებულია შავი ზღვის აღმოსავლეთი აკვატორიისათვის. პირველ ვარიანტში ძირითად განტოლებათა სისტემის ფიზიკური პროცესების მიხედვით გახლეჩის შედეგად მიღებული განტოლებათა სისტემის (ადაპტაციის ეტაპი) ამოხსნა დაიყვანება ფაქტორიზაციის მეთოდის გამოყენებაზე დინების სიჩქარის კომპონენტების მიმართ, ხოლო მეორე ვარიანტში იგივე ადაპტაციის ეტაპზე განტოლებათა სისტემა დაიყვანება სიმის რხევის განტოლებებზე საკოორდინატო ღერძების მიმართ, რომლებიც ასევე ეფექტურად ამოიხსნება ფაქტორიზაციის მეთოდის გამოყენებით. შემოთავაზებული ამოხსნის მეთოდები არ მოითხოვს შიდა იტერაციების გამოყენებას, რაც მნიშვნელოვნად ზრდის მათი პრაქტიკული გამოყენების ეფექტიანობას.

Journal of the Georgian Geophysical Society,
Issue B. Physics of Atmosphere, Ocean, and Space Plasma, v.15, 2011-2012, pp. 32-45.

Numerical investigation of the modeling of transportation and deposition of the radioactive pollution in the Caucasian Region in case of the hypothetical accident on the Armenian Nuclear Power Plant

Aleksandre A. Surmava

Iv. Javakhishvili Tbilisi State University, M. Nodia Institute of Geophysics,
1, Aleksidze Str.,0173, Tbilisi, Georgia, e-mail:aasurmava@yahoo.com

Abstract

By means of regional model of development of atmospheric processes in the Caucasian Region and the equation of a substance transfer the spatial distributions of the radioactive pollution (^{131}I) and zones of radioactive deposition are investigated. In the model the radioactive decay and aerosols deposition processes are taken into account. The distribution of radioactive pollution is simulated in cases of the South, South West and South East background winds. The distribution of only one radionuclide aerosol ^{131}I with diameter 10 μm is considered.

It is shown, that the relief of the Caucasus significantly influences on the trajectory of the pollution distribution. The North West orientation of the Main Caucasian Range resists air motion to the north, constrains the radioactive pollution in the boundary layer to flow around the Main Caucasian Range from the west or east sides. It is obtained that the 48 hours are necessary for the radioactive cloud to overflow the South Caucasus and distribute over the territory of the North Caucasus. The radioactive pollution is falling out mainly in the central, southeast and northwest parts of the South Caucasus. The zone of the radioactive deposition is extended along the background wind and deformed by the influence of the relief. The maximum length of the zone of significant deposition of radioactive substance equals approximately 750 km in case of the background South East wind and 350 km in other cases. The maximum width of the zone approximately equals 150 km. It is obtained that the surface density of the deposited radioactive nuclide in the zone of significant radioactivity decreases from 360 a.u./m^2 down to 1 a.u./m^2 when the concentration of 10 μm aerosol ^{131}I in emission plume during 6 hours are equal to 100 a.u./m^3.

1. Introduction

The accidents of the Chernobyl, Fukushima and other power plants show that the nuclear reactors carry the great potential hazards for population and environment especially when plants are located in the seismic hazardous regions [1, 3].

The Armenian Nuclear Power Plant (ANPP) is one of such objects. It lies in the South Caucasus in Metsamor 20 km from the capital of Armenia Yerevan on one of the Earth's most earthquake-prone terrain. ANPP, as a very dangerous object, was closed after earthquake in Armenia in 1988 but was reopened in 1995. ANPP has one of just a few remaining Soviet nuclear power reactors that were built

without the primary containment structures. Consequently, the hazard of the radioactive pollution of the environment in the Caucasus becomes highly probable event. The neighbouring countries, Turkey and Azerbaijan, protest the operation renewal of ANPP, and Azerbaijan has called on the UN Security Council to suspend the operation of the nuclear power plant in Metsamor [4-6].

The radioactive aerosols, emitted in the atmosphere from the nuclear reactors, can be transferred on the large distance and produce a radioactive contamination of the underlying territory [3, 7]. Therefore, a preliminary determination of the possible trajectories of the radioactive pollution cloud and nuclear deposition in the various meteorological situations has a practical importance for the environmental safety services.

A prediction of the dispersion of the radioactive pollution is possible by means of numerical simulation of the radioactive substances transfer. The accident of the Chernobyl nuclear plant shows necessity of development of the hemispheric, long- and meso-scale transport models for radioactive substances. The existing numerical dispersion models of pollution were developed as well as some new models of transfer of radioactive pollutions were elaborated (ApSimon et al., 1987; Lange et al., 1988; Alberger at al., 1988; Hass at al., 1990; Ishikawa, 1991, 1995; Ishikawa and Chino, 1991; Brandt at al., 2002; Khatib, 2008; Winiarek and etc. [8 -17]).

The tasks of the article are the numerical simulation of the possible trajectories of the movement of the radioactive clouds hypothetically emitted from ANPP and determination of the possible zones of nuclear fallout in the Caucasus. G. Lazriev considered some issues of this problem [18].

In the present article G. Lazriev's approach is continued to be investigated on the basis of the use of the regional model of the atmospheric processes over Caucasus region elaborated at the M. Nodia Institute of Geophysics; it allows calculate the spatial distribution of the meteorological fields over the complex relief of the Caucasus [19]. We have simulated the dispersion of the radioactive pollution by using of the momentum equation.

2. Formulation of the problem

2.1. Basic equations

The main equations of the model describing variations of the meteorological fields are
(a) for the troposphere

$$
\begin{aligned}
&\frac{du}{dt} = -\frac{\bar{P}}{\rho}\frac{\partial \phi}{\partial x} + lv + g(1+0.61q)\vartheta\frac{\partial z}{\partial x} + \mu\Delta u + \frac{1}{\rho h^2}\frac{\partial}{\partial \zeta}\rho\nu\frac{\partial u}{\partial \zeta}\ ,\\
&\frac{dv}{dt} = -\frac{\bar{P}}{\rho}\frac{\partial \phi}{\partial y} - lu + g(1+0.61q)\vartheta\frac{\partial z}{\partial y} + \mu\Delta v + \frac{1}{\rho h^2}\frac{\partial}{\partial \zeta}\rho\nu\frac{\partial v}{\partial \zeta}\ ,\\
&\frac{\partial \phi}{\partial \zeta} = \frac{g}{R\bar{T}}(1+0.61q)\vartheta h\ , \qquad \frac{\partial h}{\partial t} + \frac{\partial uh}{\partial x} + \frac{\partial vh}{\partial y} + \frac{\partial \tilde{w}h}{\partial \zeta} + \frac{1}{\rho}\frac{d\rho}{dz}wh = 0\ ,\\
&\frac{\partial \vartheta'}{\partial t} + u\frac{\partial \vartheta}{\partial x} + v\frac{\partial \vartheta}{\partial y} + \tilde{w}\frac{\partial \vartheta}{\partial \zeta} + S\,w = \mu\Delta\vartheta + \frac{1}{\rho h^2}\frac{\partial}{\partial \zeta}\rho\nu\frac{\partial \vartheta}{\partial \zeta} + \frac{L}{\rho C_p}\varphi_{con} - \frac{\partial \theta}{\partial t}\ ,\\
&\frac{\partial q'}{\partial t} + u\frac{\partial q}{\partial x} + v\frac{\partial q}{\partial y} + \tilde{w}\frac{\partial q}{\partial \zeta} = \mu\,\Delta q + \frac{1}{\rho}\frac{\partial}{\partial \zeta}\rho\,\nu\frac{\partial q}{\partial \zeta} - \varphi_{con} - \frac{\partial Q}{\partial t}\ ,\\
&\frac{\partial m'}{\partial t} + u\frac{\partial m}{\partial x} + v\frac{\partial m}{\partial y} + \tilde{w}\frac{\partial m}{\partial \zeta} = \mu\,\Delta m + \frac{\partial}{\partial \zeta}\nu\frac{\partial m}{\partial \zeta} + \varphi_{con} - \frac{\partial N}{\partial t}\ , \qquad (1)\\
&w = \frac{\partial z}{\partial t} + u\frac{\partial z}{\partial x} + v\frac{\partial z}{\partial y} + \tilde{w}h\ , \quad z = \zeta\,\mathrm{h} + \delta\ ,
\end{aligned}
$$

$$\frac{d}{dt}=\frac{\partial}{\partial t}+u\frac{\partial}{\partial x}+v\frac{\partial}{\partial y}+\tilde{w}\frac{\partial}{\partial \zeta},\qquad \Delta=\frac{\partial}{\partial x^2}+\frac{\partial}{\partial y^2};$$

b) for the active layer of soil

$$\frac{\partial C}{\partial t}=\frac{\partial}{\partial z}D(C)\frac{\partial C}{\partial z}-\frac{\partial E(C)}{\partial z},\qquad \frac{\partial T_{soil}}{\partial t}=K_{soil}\frac{\partial^2 T_{soil}}{\partial z^2}\quad \text{at}\quad \delta_0>z>Z_{soil};\qquad (2)$$

c) for the layer of sea water

$$\frac{\partial T_{sea}}{\partial t}=K_{sea}\frac{\partial^2 T_{sea}}{\partial z^2}+\frac{1}{C_{sea}\,\rho_{sea}}\frac{\partial I}{\partial z}\ ,\quad \text{at}\quad \delta_0>z>Z_{sea},\qquad (3)$$

where t is time; x, y, and z are the axes of the Cartesian coordinate directed to the east, north and vertically upwards, respectively; $\zeta=(z-\delta)/h$ is the dimensionless vertical coordinate; $\delta=\delta_0(x,y)+50\,\text{m}$ is the surface layer height; δ_0 is the height of the relief; $H(t,x,y)$ is the height of the tropopause; $h=H-\delta$; u, v, w, and $\tilde{w}$ are the wind velocity components along the axes x, y, z, and ζ, respectively; $\vartheta=T'/\overline{T}$, and $\phi=P'/\overline{P}(z)$ are the analogues of temperature and pressure, respectively; $\overline{T}=300K$; T' and P' are the devotions of temperature and pressure from the standard vertical distributions

$T'(t,x,y,z)=T(t,x,y,z)-\overline{T}+\gamma\ z-\overline{\overline{T}}(t,x,y,z)$, $\mathrm{P'(t,x,y,z)=P(t,x,y,z)\ -\overline{P}(z)-\overline{\overline{P}}(t,x,y,z)}$;

T and P are the temperature and pressure of the atmosphere, respectively: $\overline{T}-\gamma\ z$ and $\overline{P}(z)$ are the standard vertical distributions of the temperature and pressure, respectively; γ is the standard vertical temperature gradient; $\overline{\overline{T}}$ and $\overline{\overline{P}}$ are the background deviations of the temperature and pressure from standard vertical distributions; ϑ and θ are the mesoscale and background components of the analogue of temperature, respectively; $\vartheta'=\vartheta-\theta$; q and Q are the mass fraction of water vapour and the background mass fraction of water vapour, respectively; $q'=q-Q$; m and M are the mass fraction of cloud water and the background mass of cloud water, respectively; $m'=m-M$; T_{soil} and T_{sea} are the temperatures of soil and seawater, respectively; C is the volume content of soil water; $\rho(z)$ and ρ_{sea} are the standard vertical distributions of the densities of dry air and seawater, respectively; $\sigma=-\rho^{-1}dp/dz$; g is the gravitational acceleration; R is the universal gas constant for dry air; C_p and C_{sea} are the specific heat capacities of dry air at constant pressure and seawater, respectively; S is the thermal stability parameter; L is the latent heat of condensation; ϕ_{con} is the condensation rate; $\partial N/\partial t$ is the intensity of prescription;

$\partial N/\partial t=(m-m_{cr})/\delta t$ *when* $m>m_{cr}$ *and* $=0$ *when* $m\le m_{cr}$; $\mathrm{m_{cr}}$ is the critical magnitude of the mass fraction of a cloud water; $\delta\,\mathrm{t}$ is the time of setting out of a surplus cloud water; D is the diffusion coefficient of water in soil; E is the filtration coefficient of water in a soil; I_{sea} is the total solar radiation flux in sea water; K_{soil} and K_{sea} are the thermal diffusivity coefficients of soil and sea water, respectively; μ and ν are the horizontal and vertical turbulent diffusion coefficients.

The equation of transport of the radioactive nuclide is

$$\frac{\partial Con,i}{\partial t}+u\frac{\partial Con,i}{\partial x}+v\frac{\partial Con,i}{\partial y}+(\widetilde{w}-\frac{W_{sed}}{h})\frac{\partial Con,i}{\partial \varsigma}=\mu\Delta Con,i+\frac{\partial}{\partial \varsigma}\nu\frac{\partial Con,i}{\partial \varsigma}-\alpha\, Con,i\ ,\quad (4)$$

where, Con,i is the concentration of radioactive nuclide i; the index $\alpha=\ln 2/T_{rad}$ is the radioactive-decay constant; T_{rad} is a decay period; W_{sed} is an aerosol deposition velocity. The equation (4) shows that any functions that equal to $Con,i\,(\mathrm{t,x,y},\zeta)\times const$ also obey the equation (4). Therefore we will consider $Con,i\,(\mathrm{t,x,y},\zeta)$ as unit value and then in order to obtain the real magnitude of concentration we are to multiply the calculated field of Con,i by $const$. The set of equations (1) and (2)-(4) are solved in the coordinate systems *(t, x, y,* ζ*)* and *(t, x, y, z)*, respectively.The initial and boundary conditions, the values of background fields, and methods of parameterization of the separate meteorological processes are selected in accordance with specific objectives of modeling.

2.2. Initial and boundary conditions, main parameters of the regional problem The initial and boundary conditions for the set of equations (1) - (4) are

The initial conditions at $t=0$ we have

a) for the system (1)

$$\vartheta'=q'=m'=0\,,\ u=\overline{\overline{u}}\,(0,\,x,\,y,\zeta)\,,\ \ v=\overline{\overline{v}}\,(0,\,x,\,y,\zeta)\,;\,,h=\overline{\overline{h}}\,(0,\,x,\,y)=9000-\delta\left(x,y\right)$$

b) for equations (2) and (3)

$$C=C_0(x,\,y,\,z)\,,\quad T_{sea}=T_{0,sea}(\,x,\,y,\,z)\,,\ T_{soil}=T_{0,soil}(\,x,\,y,\,z)\,,\qquad (5)$$

c) for equation (4)

$$Con,i=\begin{cases}Con,i^{0}(x,y,\zeta) & \text{if}\quad (\mathrm{x,y},\zeta)\in\Omega\\ 0 & \text{if}\quad (\mathrm{x,y},\zeta)\notin\Omega\end{cases}.$$

The vertical boundary conditions

d) for the system (1)

$$\frac{\partial\psi}{\partial\zeta}=0,\ \widetilde{w}=0,\ \varphi=\varphi_1(t,x,y)+(g/R\overline{T})\Delta\theta(h(t,x,y)-h(0,x,y))\quad \text{, at } \zeta=1,$$

$$\left.\begin{aligned}
&\nu\frac{\partial \mathrm{u}}{\partial\zeta}=\mathrm{A}|\mathrm{V}|\mathrm{uh}/\Delta\zeta_0\,, && \nu\frac{\partial \mathrm{v}}{\partial\zeta}=\mathrm{A}|\mathrm{V}|\mathrm{vh}/\Delta\zeta_0\,,\\
&\nu\frac{\partial \vartheta'}{\partial\zeta}=\mathrm{A}|\mathrm{V}|(\vartheta'-\vartheta'_0)\mathrm{h}/\Delta\zeta_0\,, && \nu\frac{\partial \mathrm{m}'}{\partial\zeta}=\mathrm{A}|\mathrm{V}|\mathrm{m}'\mathrm{h}/\Delta\zeta_0\\
&\nu\frac{\partial \mathrm{q}'}{\partial\zeta}=\mathrm{A}|\mathrm{V}|(\mathrm{q}'-\mathrm{q}'_0)\mathrm{h}/\Delta\zeta_0\,, && \widetilde{\mathrm{w}}=0\ ,
\end{aligned}\right\}\ \text{at}\ \ \zeta=0\,,\quad (6)$$

e) for equations (2) and (3)

$$\rho_e C_e K_e \frac{\partial T_e}{\partial z} - \rho C_p A|V|(T - T_e)/\Delta\zeta_0 - \rho L_q A|V|(q - q_e)/\Delta\zeta_0 = I_e$$

$$\begin{cases} C = C_{por}\,, & \text{at} \int_0^1 \partial N/\partial t \, d\zeta > 0 \\ D\dfrac{\partial C}{\partial z} = \dfrac{\rho_w}{\rho} A|V|(q - q_e), & \text{at} \int_0^1 \partial N/\partial t \, d\zeta \le 0 \end{cases}, \qquad \text{at } z = \delta_0 \qquad (7)$$

$$\frac{\partial T_e}{\partial z} = \frac{\partial C}{\partial z} = 0\,, \qquad \text{at } z = \delta_0 - 2\,\text{m};$$

f) for the equation (4) the concentration of radioactive pollution In the area of emission during an interval of time $0 - t$ is given by the formulae

$$Con,i = \begin{cases} Con,i^0 & \text{if } (x, y, \zeta) \in \Omega \quad \text{and } t \le t^0 \\ \dfrac{\partial Con,i}{\partial \zeta} = 0 & \text{if } (x, y, \zeta) \notin \Omega,\ \zeta = 0 \quad \text{and } t \le t^0 \\ \dfrac{\partial Con,i}{\partial \zeta} = 0 & \text{if } \zeta = 0 \quad \text{and } t > t^0 \end{cases}, \qquad (8)$$

$$\frac{\partial Con,i}{\partial \zeta} = 0 \quad \text{if} \quad \zeta = 1\,.$$

The lateral boundary conditions

$u = \overline{\overline{u}}(t, x, y, \zeta)$, $v = \overline{\overline{v}}(t, x, y, \zeta)$, $h = \overline{\overline{h}}(t, x, y)$, $\vartheta' = q' = m' = 0$,

$\partial\psi/\partial n = \partial h/\partial n = \partial Con,i/\partial n = 0$, if $x = 0,\ X;\ y = 0, Y$,

$$\begin{cases} \dfrac{\partial Con,i}{\partial n} = 0, & \text{if } x = 0,\ X;\ y = 0, Y \text{ and } v_n \text{ directed inward of the domain} \\ Con,i = 0, & \text{if } x = 0,\ X;\ y = 0, Y, \text{ and } v_n \text{ directed outward of the domain} \end{cases}, \qquad (9)$$

where $|V| = \left(u^2 + v^2\right)^{1/2}$; ϕ_1 is given function of time and coordinate and shows the magnitude of the pressure in the tropopause; $\Delta\zeta_0$ is non-dimensional thickness of the atmospheric surface layer; X and Y are the coordinates of lateral boundaries; n is a unit normal vector; $\psi = (u, v, \vartheta', q', m')$; index „0" indicates the value of the function at the level $z = \delta_0$; $q_0' = q_0 - q_{sat}$ on the sea surface and $q_0' = (q_0 - q_{sat})C/C_{por}$ on the soil surface; C_{por} is the porosity of the soil, index „e" indicates either „sea" or „soil" for the sea and soil surfaces; Ω is a rectangular prism area in vicinity of the lower boundary; Con,i^0 is a known initial magnitude of emitted radioactive ingredient; t_0 is duration of a radioactive emission; C_{soil} and ρ_{soil} are the specific heat capacity and soil density, respectively; C_0, $T_{0,sea}$ and $T_{0,soil}$ are average monthly values for the June of functions C, T_{sea} and T_{soil}, respectively; A and $\Delta\zeta_0$ are constant parameters; $\overline{\overline{u}}, \overline{\overline{v}}$, and $\overline{\overline{h}}$ are the background values of the wind velocity

components and atmosphere thickness, respectively; $\overline{\overline{u}}$ and $\overline{\overline{v}}$ are calculated by means of geostrophic wind and quasi-static equations using the known background values of temperature and pressure at the tropopause level $\overline{\overline{\theta}}(t,x,y,\zeta)$ and $\phi_1(t,x,y,1)$, respectively. By vary $\overline{\overline{h}}$, $\overline{\overline{\theta}}$ and ϕ_1 it is possible to obtain the necessary background winds.

Coefficient of vertical turbulence is decreasing in the vertical direction from the value at the surface layer from $5\,\mathrm{m}^2\cdot\mathrm{s}^{-1}$ up to 0.001 $\mathrm{m}^2\cdot\mathrm{s}^{-1}$ at a height of 3-4 km above the Earth's surface. At more high altitudes it equals to 0.001 $\mathrm{m}^2\cdot\mathrm{s}^{-1}$. Coefficient of the horizontal turbulence is equal to $5000\,\mathrm{m}^2\cdot\mathrm{s}^{-1}$. Background value of the relative humidity is equal to 40%, the background value of the water content mass concentration equals to zero.

Other meteorological parameters are the well known values characterizing middle latitudes.

3. Analyze of results

Numerical integration of equations (1) and (2)-(4) with the initial and boundary conditions (5)-(9) are carried out using both the explicit and implicit schemes. In the modelling domain the rectangular finite-difference grid is used with $108\times90\times17$ points having 10 km horizontal steps and the non-dimensional vertical step equalling 1/17. In the soil and sea the number of levels is equal 20, the vertical step equals 10 cm. The temporal step equals 4 min.

The background fields of temperature and pressure are selected in such a manner that they form the South, South-East and South-West background stationary geostrophic winds.

Since we limited ourselves by the Caucasus Region, the calculations were performed for a period up of 48 h. The transfer of the radioactive nuclide ^{131}I was modeled which during 6 h was being emitted in the atmosphere into rectangular prism area Ω (10 km×10 km×1.5km) in vicinity of ANPP (Fig.1). The initial concentration $Ccon,i^0$=100 arbitrary units (a.u.). The radius of the particles equals 10 μm and corresponding fall-out velocity calculated by Stokes formula is equal to W_{sed} = 1cm/s [21], the decay period T_{rad} =8,02 day.

Figures 2, 3 and 4 show the distribution of the concentration of I^{131} and the wind field obtained in case of the background south wind on the surface level $z = delta = \delta(x, y)+100\,\mathrm{m}$ and on the altitudes z = 1, 2, 4, 6, 8 km at the moment of the time t = 6, 24 and 48 h, respectively. In Fig. 2 we can note that during 6 h the radioactive emission forms the radioactive cloud over ANPP that by wind and atmosphere turbulence is stretched to the north along the direction of the background wind. The radioactive cloud is located into ellipsoid columns area with maximum horizontal sizes 100 km and

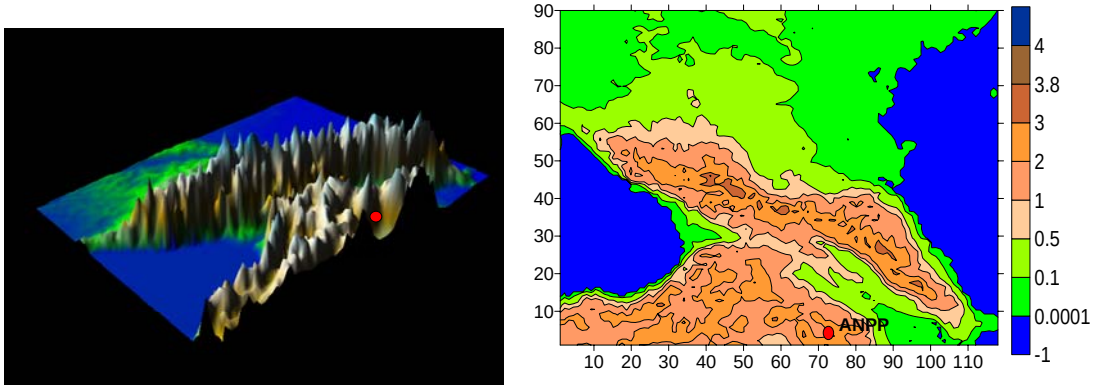

Fig. 1. The Caucasus Region relief and topography (heights in km) and the location of the ANPP (the red circle)

170 km along x and y coordinates, respectively, and with vertical width approximately equal 9 km. The magnitude of the concentration is equal to 100 a. u. into the emission plume in the 4 km layer and exponentially decreases on the periphery of this area.

After six hours the radioactive cloud increases step-by-step in size because of the movement along the wind and atmospheric turbulence; simultaneously the concentration of the pollutant substance decreases in result of the processes of dispersion, deposition, and radioactive-decay. The radioactive cloud in the surface layer at t = 24 h is obtained over the central part of the South Caucasus mainly up of the territory of the north part of the Armenia and the east part of Georgia. Over this surface layer the size of the polluted atmosphere volume gradually increases up to 6 km; the zone of the higher concentration is displaced from the South Caucasus to the North Caucasus (from the East Georgia to the Stavropol Kray). The magnitude of maximal concentration during the 24 hours is decreased down to 0.48 a. u. In the upper troposphere z > 6 km, the size of the polluted area and concentration of radioactive pollution is decreased, and the zone of pollution is wholly located over the North Caucasus.

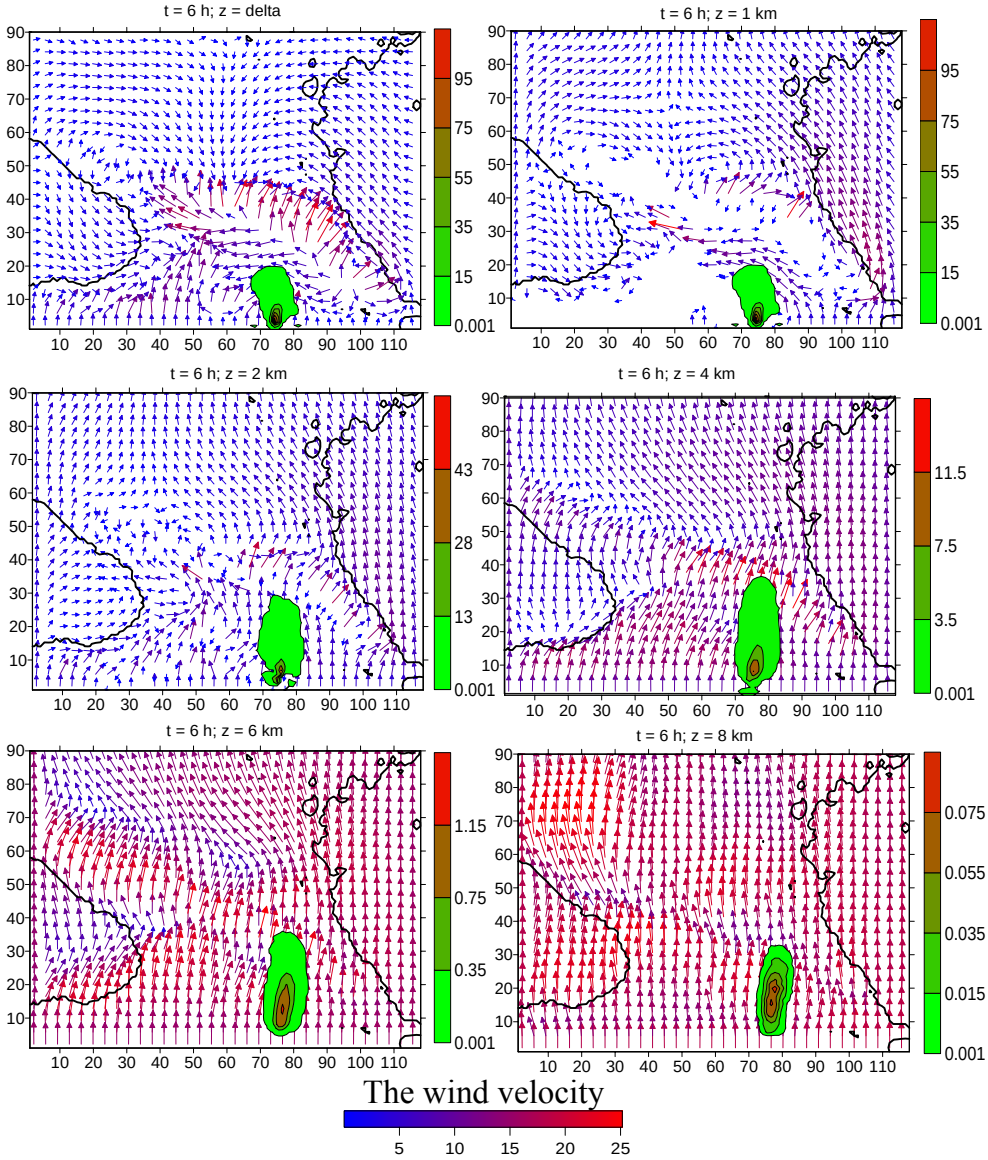

Fig. 2. The spatial distribution of the concentration *Con,i* and wind fields at *t* = 6h.

During two days (Fig. 4) the radioactive cloud mainly moves over territory of the North Caucasus and localizes over the Stavropol Kray. In the South Caucasus the radioactive cloud is obtained over a small territory of the central part of Georgia. The concentration there is small varying between 0.001 - 0.006 a.u. The maximal value of concentration in the plume of pollution caused by the processes of dispersion, deposition, and radioactive-decay is decreased about 2000 times from 100 a. u. to 0.05a.u. The spatial distribution of the radioactive deposition on the earth surface is shown in Fig. 5. As it is shown here, the main part of the radioactive dust falls on the territory of Armenia and Georgia into the stripe of 100 km in width and about 400 km in length. The radioactive ingredient up to 12 h falls out only on the territory of the South Caucasus. After this time the process of fallout begins also on the territory of the North Caucasus. After 20 h from the beginning of emission the radioactive fallout happens mainly on the territory of the North Caucasus and at t = 48 h the surface density of ^{131}I on the territory of the north slope of the Main Caucasus Range reaches 10 a.u. on 1 m^2. The radioactive deposition on the territory of the South Caucasus ends after 30 h.

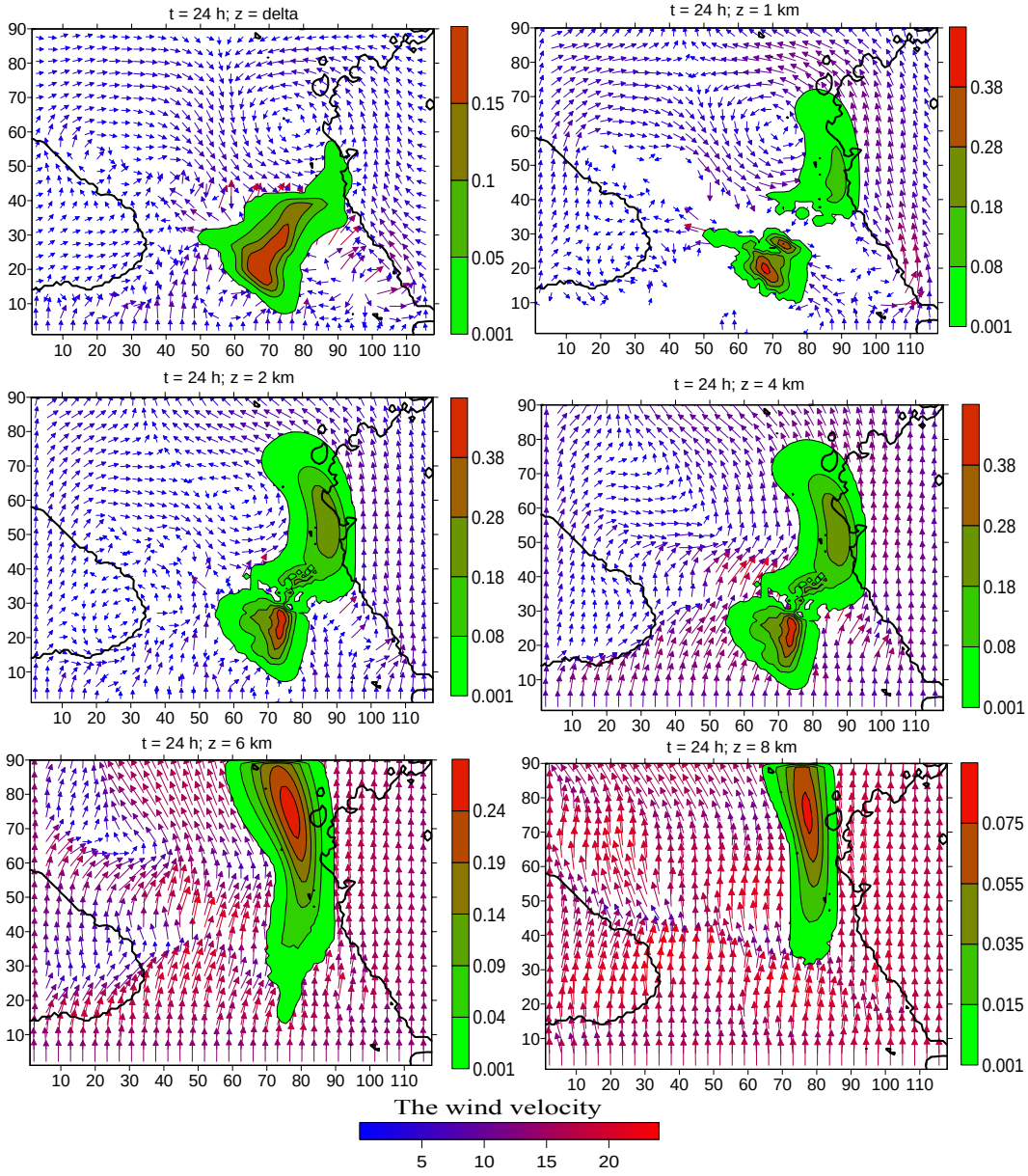

Fig. 3. The spatial distribution of the concentration *Con,i* and wind fields at t = 24 h.

The results of the numerical modeling of the radioactive diffusion when the background south-east wind is considered are shown in Fig. 6. The calculation shows that the radioactive pollution moves to the north firstly on the territory of Armenia and then over the central and north-west parts of the Caucasus Region. At t = 24 h the main part of atmosphere over Georgia is polluted by radioactive ingredient. Further the radioactive cloud falls over the Main Caucasus Range, splits in two parts and at t = 48 h we obtain two zones of the radioactive pollution. One of these zones is located over the Black Sea and another over the north slope of the Main Caucasus Range. The radioactive deposition obtained at t =0, 24 h and 48 h are also shown in Fig. 6. We see that in 48 h the radioactive fallout mainly happens on the territory of the north part of Armenia, the south, central, and north-west parts of Georgia. The small amounts of the radioactivity are also deposited on the territories of Turkey and Russian.

The maximal magnitude of he surface density at t = 48 h is equal to 360 a.u./m^2 and is obtained in vicinity of source of emission.

When the background south-west wind blows, the radioactive pollution diffuses in the atmosphere over the north-east part of Armenia, whole territory of Azerbaijan, Republic, Dagestan, and the Caspian Sea (Fig. 7). The atmosphere in vicinity of east border of the Georgia will be polluted also.

4. Discussion

This article is our first investigation about of the possible radioactive pollution of the Caucasus territory in case of the accident takes place in ANPP. In this article, the problem of distribution of the radioactive element ^{131}I with diameter 10 μm is discussed. Such modeling can be made for other radioactive radionuclides.

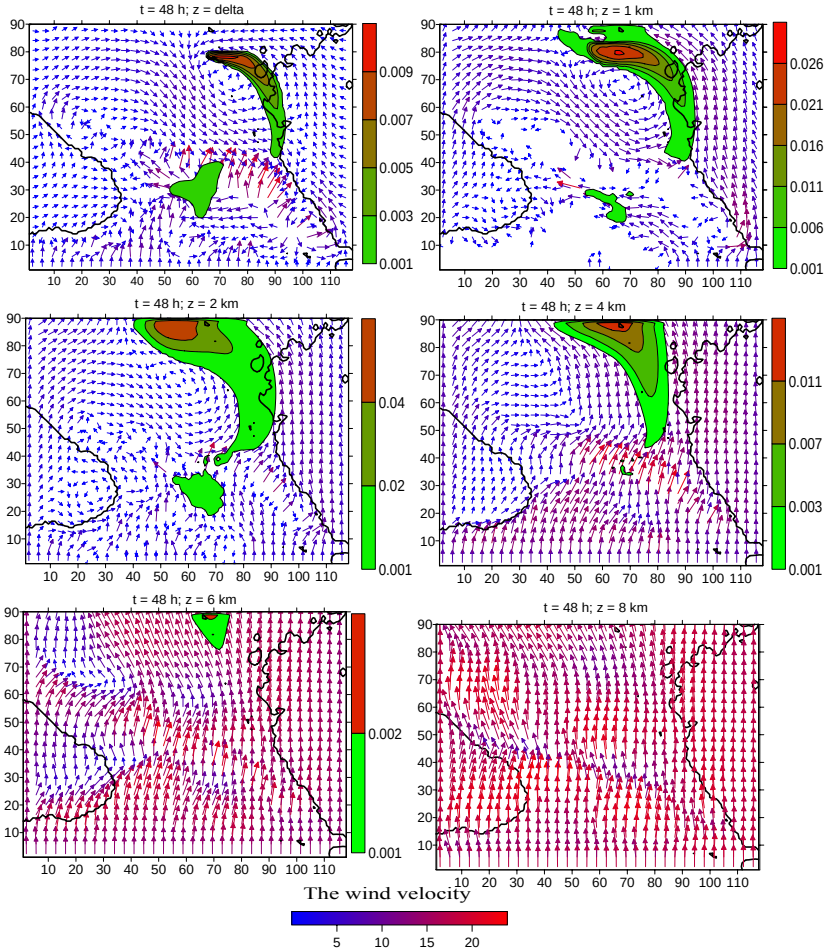

Fig. 4. The spatial distribution of the concentration *Con,i* and wind fields at *t* = 48 h.

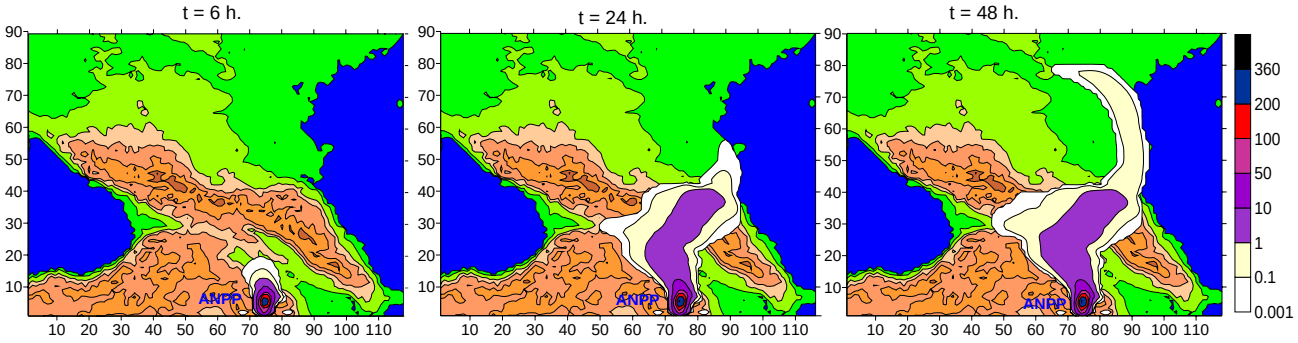

Fig. 5. Distribution of the surface density of the radioactive deposition at t = 6, 24 and 48 h

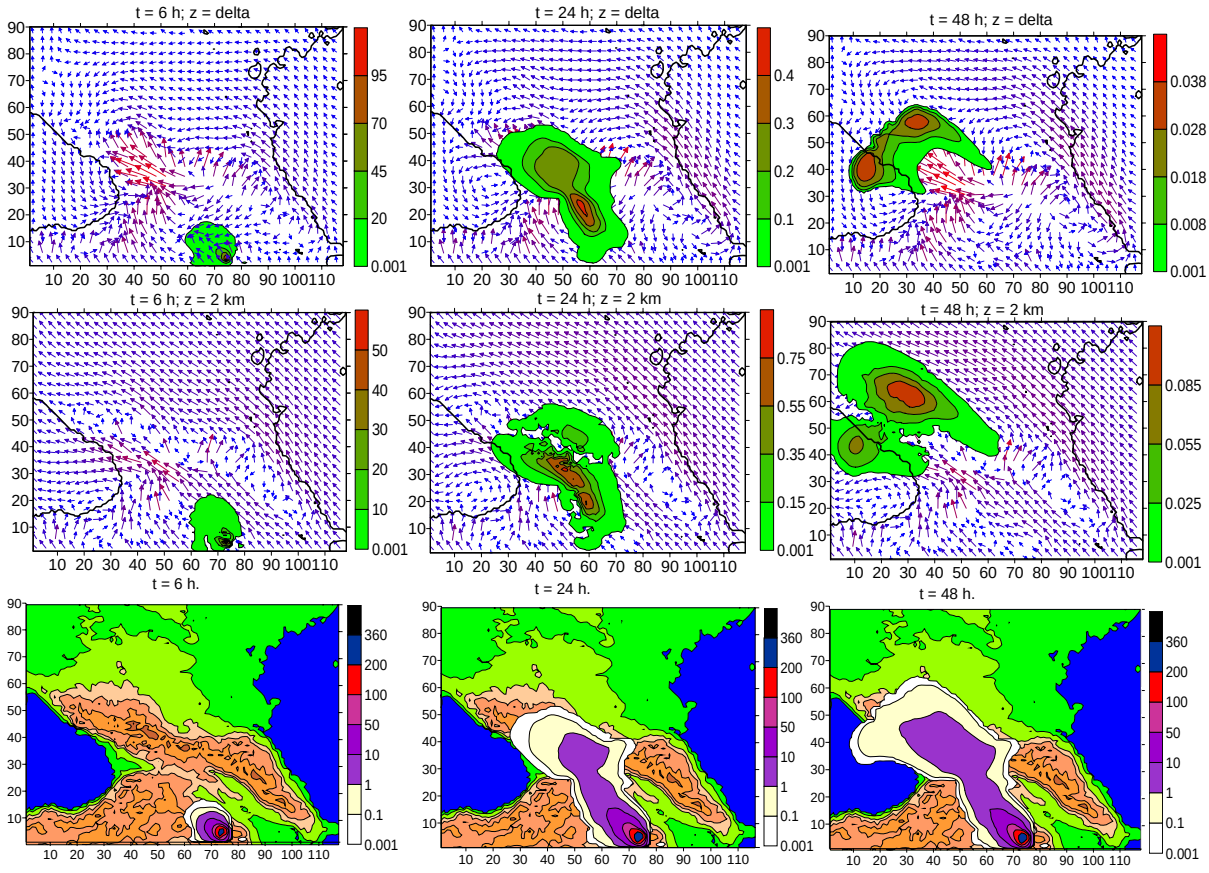

Fig. 6. Concentration of the radioactive substance in the atmosphere (upper six figures) and surface density of the radioactive deposition of ^{131}I (lower three figures) in case of the south-east background wind.

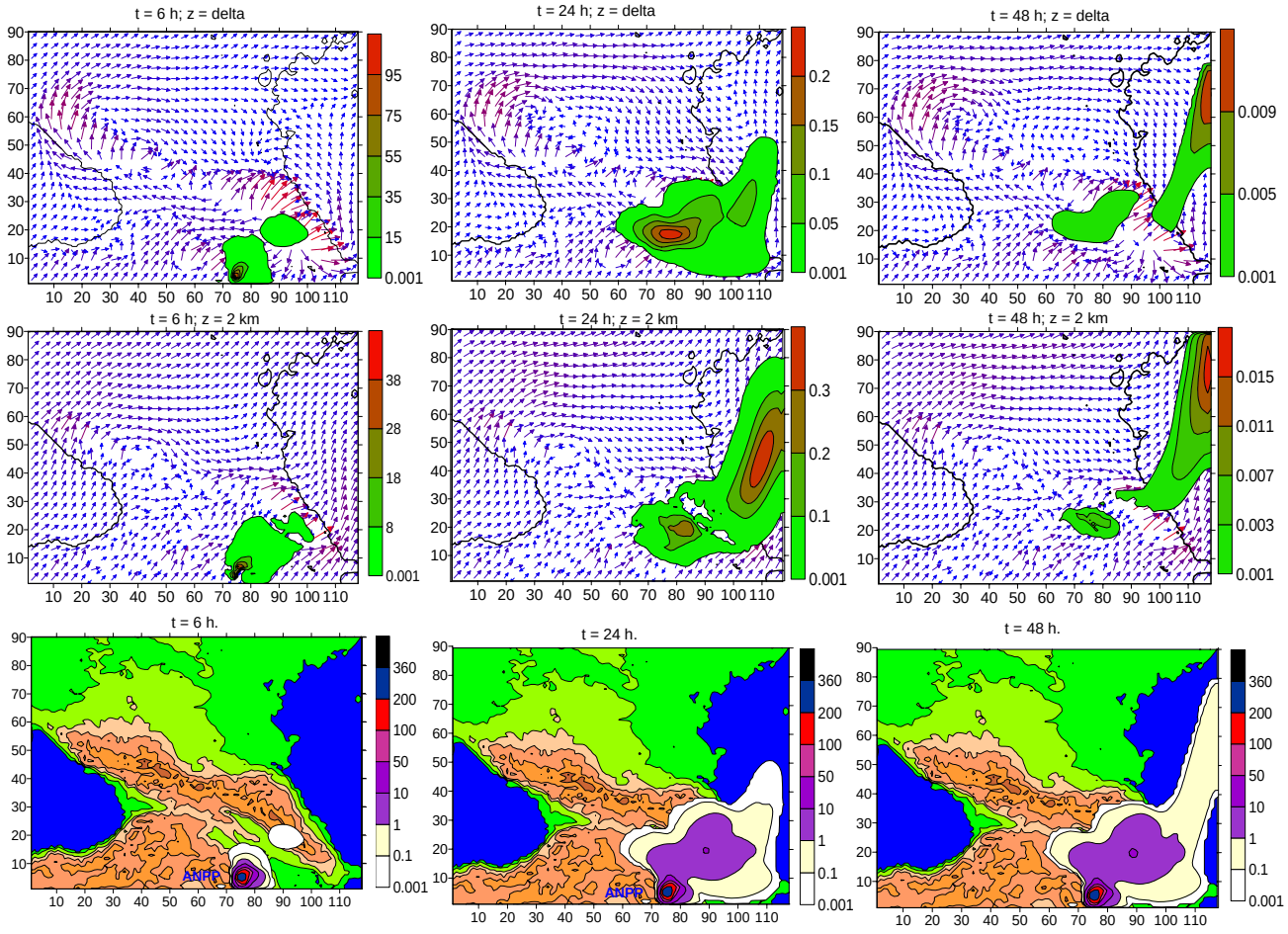

Fig. 7. Concentration of the radioactive substance in the atmosphere (upper six figures) and a surface density of radioactive deposition of ^{131}I (lower three figures) in case of the south-west background wind

It is evident, that the sum of obtained concentrations and radioactivities will give us the main picture of the possible radioactive contamination.

The radioactive pollution falls out mainly on the central, southeast, and northwest parts of the South Caucasus. The zone of radioactive deposition is extended along the background wind and deformed by influence of the relief. In case of the background southeast wind the maximal length of the zone of significant deposition of radioactive substance is approximately equal 750 km and – 350 km in other cases. The maximal width of this zone equals approximately 150 km. The concentration of deposited radioactive element in the zone of radioactive fall-out decreases from 360 a.u./m^2 down to 1 a.u./m^2.

For the reason of the absence of the observation data it isn't possible to estimate a quantitative reality of the obtained results. But, having compared the trajectory and shape of the radioactive cloud obtained in this article and in other works [1, 10, 15-17], it may be concluded that the obtained results properly describe the main features of the radioactive dispersion process in the Caucasus. Therefore, the model and results obtained here can be considered as first approximation for the further investigation and practical use. In addition, in our opinion, the spatial grid step 10 km is rather large for adequate description of studied process over complex terrain of Caucasus. We intended simulating the diffusion processes of radioactive pollution with the horizontal step approximately equal to 1-5 km in the atmosphere of the Caucasus.

Acknowledgement: The author is grateful to Dr. Sci. A. Gvelesiani for discussion the results and valuable comments.

References

[1] UNSCEAR, 1988 REPORT. Annex D. Exposures from the Chernobyl accident. http://www.unscear.org/docs/reports/1988annexd.pdf

[2] Fukushima Accident 2011. http://www.world-nuclear.org/info/fukushima_accident_inf129.html.

[3] Sources and Effects of Ionizing Radiation. United Nations Scientific Committee on the Effects of Atomic Radiation. UNSCEAR - 2008. Peported to General Assembly with Scientific Annexes/ 179 p. http://www.unscear.org/docs/reports/2008/11-80076_Report_2008_Annex_D.pdf

[4] Turkey's Energy Minister: "Metsamor Nuclear Power Plant in Armenia must be closed" http://en.apa.az/news.

[5] Turkey warns Armenia about 40-year old nuclear plant http://www.trdefence.com/2011/04/18 /turkey-warns-armenia-about-40-yo-nuclear plant/.

[6] Azerbaijan Urges UN to Halt Armenian Nuclear Plant *http://en.rian.ru/world/20120423/ 172992199.html*.

[7] ApSimon, H. M., J. J. N. Wilson, S. Cuirguis, and P. A. Stott. Assessment of the Chernobyl release in the immediate aftermath of the accident. Nucl. Energy, 1987, v. 26, pp. 295- 301.

[8] Albergel, A., D. Martin, B. Strauss, and, J.M. Gross. The Chernobyl accident: Modelling of dispersion over Europe of the radioactive plume and comparison with air activity measurements. Atmos. Environ., 1988, v. 22, pp. 2431-2444.

[9] Environmental Accident and their Remediation: Twenty years of Experiences. Report of the Chernobyl Forum Expert Group " Environment" http://chernobyl.info/Portals/0/Docs/en/pdf_en/EnvRep_Pub1239_web.pdf.

[10] J. Brandt, J. H. Christensen, and L. M. Frohn. Modelling transport and deposition f cesium and iodine from Chernobyl accident using the DREAM model. Atmos. Chem. Phys. Discuss. 2002, v. 2, pp. 828-874. www. Atmos-che-phys.org/acpd/2/825 /.

[11] Y. Roustan, C. Birman, M. Bocquet, Camille Birman, P. Tran. Atmospheric dispersion of radionuclides from the Fukushima-Daichii nuclear power plant. Map of ground deposition of caesium-137 for the Fukushima-Daichii accident. http://cerea.enpc.fr/en/fukushima.html.

[12] Hass, H., M. Memmesheimer, H. Geiss', H. J. Jakobs, M. Laube, and A. Ebel, Simulation of Chernobyl radioactive cloud over Europe using EURAD model. Atmos. Environ., 1990, v. 24A, pp. 673-692.

[13] Ishikawa, H., and M. Chino, Development of regionally extended/worldwide version of environmental emergency dose information: WSPEEDI, (II) Long-rage transport model and its application to dispersion of Cesium-137 from Chernobyl. J. Nucl. Sci. Technol. 1991, v. 28, pp. 642-655.

[14] Piedelivere, J. P., L. Musson-Genon, and FBompay, MEDIA- An Eulerian model for atmospheric dispersion: First validation on the Chernobyl release. J. Appl. Meteor.1990, v. 29, pp. 1205-1220.

[15] Ishikava H. Evaluation of the effect of horizontal diffusion on the long-range atmospheric transport simulation with Chernobyl data. J. Appl. Meteor.1995, v. 34, pp. 1653-1665.

[16] A. Khatib. Transport of radioactive particles in the Middle East following a hypothetical nuclear realize. J. Appl. Sci. Environ. Sanit. 2008, v. 2, No. 2. pp. 51-62.

[17] V. Winiarek, M. Bocquet, Y. Roustan, C. Birman, P. Tran. Atmospheric dispersion of

radinuclides from the Fukushima-Daichii nuclear power plant. Map of ground deposition of caesium-137 for the Fukushima-Daichii accident. http://cerea.enpc.fr/en/fukushima.html
[18] G. Lazriev. Estimation of the radioactive situation on the territory of Georgia and of the environment pollution simulation in case of the possible accident in the Armenia Nuclear Power Plant. Report of Hydrometeorology Institute of Georgia, 2003, Tbilisi, Georgia. 49 pp. (manuscript, in Georgian)
[19] A. Surmava, A. A. Kordzadze, D. I. Demetrashvili, V. G. Kukhalashvili. Numerical investigation of the influence of the Caucasus relief on the distribution of hydrometeorological fields. Izvestia, Atmospheric and Oceanic Physics, 2007, v. 43, No. 6, pp. 722-730.
[20] Berliand M. E. The current problems of the atmospheric diffusion and diffusion of atmosphere.Gidrometeoizdat, Leningrad. 1975, 448 pp.

(Received in final form 20 December 2012)

Численное исследование модельного распространения и осаждения радиоактивного загрязнения (^{131}I) в случае гипотетической аварии на Армянской атомной электростанции

А. А. Сурмава

Резюме

С помощью региональной модели развития атмосферных процессов в Кавказском регионе и уравнения переноса примеси исследовано пространственное распределение радиоактивного загрязнения (^{131}I) в атмосфере в случае возможной гипотетической аварии на Армянской атомной электростанции. В модели учтены процессы радиоактивного распада и осаждения на подстилающую поверхность. Распространение радиоактивного загрязнения смоделировано для случаев южного, юго-западного и юго-восточного ветров и радоактиного аэрозоля с диаметром 10 мкм.

Показано, что рельеф Кавказа в приземном слое атмосферы существенно влияет на траекторию распространения радиоактивной примеси. Ориентированный на северо-запад Большой кавказский хребет, препятствуя перемещению воздуха на север, заставляет основную часть загрязнения обтекать препятствие с северо-взападной или с северо-восточной стороны, и далее распространиться над территорией Северного кавказа. Получено, что радиоактивному облаку необходимо проблизительно 48 часов для перетекания через Южный кавказ. Основная часть радиоактивного загрязнения выпадает над центральной, северо-западной и юго-восточной частями Южного кавказа. Зоны радиоактивного осаждения вытянуты вдоль фоновых ветров и частично деформированы под влиянием рельефа территории. Максимальная длина зоны значительного выпадения радиоактивного вещества приблизительно равна 750 км в случае фонового юго-восточного ветра и - 350 км для других направлений фоновых ветров. Получено, что когда в течение первых 6 часов концентрация частиц с диаметром 10 мкм равна 100 п.е./м^3 (произвольная единица/м^3), тогда поверхностная плотность выпавшего радиоактивного вещества в зоне максимального загрязнения уменьшается от максимального значения 360 п. е./м^2 до 1 п. е./м^2.

რადიაქტიური დაბინძურების (^{131}I) გავრცელების და დალექვის რიცხვითი გამოკვლევა სომხეთის ატომური ელექტროსადგურის ჰიპოთეტური ავარიის შემთხვევაში

ა. სურმავა

რეზიუმე

კავკასიაში ატმოსფერული პროცესების განვითარების რეგიონალური რიცხვითი მოდელისა და მინარევის გავრცელების განტოლების გამოყენებით შესწავლილია სომხეთის ატომური ელექტროსადგურიდან ატმოსფეროში ჰიპოთეტური შესაძლო ავარიის შედეგად ამოფრქვეული რადიოაქტიური ელემენტის ^{131}I-ის გავრცელება ფონური სამხრეთის, სამხრეთ-დასავლეთის და სამხრეთ-აღმოსავლეთის ქარების შემთხვევაში. გათვალისწინებულია რადიოაქტიური დაშლისა და აეროზოლის დალექვის პროცესები. განხილულია მხოლოდ 10 მკმ დიამეტრის რადიოაქტიური ნუკლიდის გავრცელება.

ნაჩვენებია, რომ კავკასიის რეგიონის რელიეფი ძლიერად მოქმედებს მინარევების გავრცელებაზე. პარალელის გასწვრივ ორიენტირებული კავკასიონის ქედი, ეწინააღმდეგება რა ჰაერის ჩრდილოეთით მოძრაობას, აიძულებს რადიოაქტიური ნივთიერების ძირითად ნაწილს, გარსშემოედინოს მთავარ კავკასიონის ქედს დასავლეთის ან აღმოსავლეთის მხრიდან და შემდგომ გავრცელდეს ჩრდილოეთ კავკასიაში. გამოთვლებით ნაჩვენებია, რომ დაახლოებით 48 საათია საჭირო იმისათვის, რომ რადიოაქტიური ღრუბელი გადაევლოს სამხრეთ კავკასიას და გავრცელდეს ჩრდილოეთ კავკასიაში. რადიოაქთიური ნივთიერება ძირითადად ილექება სამხრეთ კავკასიის ჩრდილო-დასავლეთ, ცენტრალურ და ჩრდილო-აღმოსავლეთ ნაწილებში ფონური სამხრეთ-აღმოსავლეთის, სამხრეთის და სამხრეთ-დასავლეთის ქარების შემთხვევებში, შესაბამისად. დიდი რაოდენობით დალექვის ზონის სიგრძე დაახლოებით 750 კმ-ის ტოლია სამხრეთ აღმოსავლეთის ფონური ქარის დროს, და – 350 კმ-ის სხვა შემთხვევებში. ამ ზონის სიგანე დაახლოებით 150 კმ-ს უდრის. მიღებულია, რომ როდესაც 10 მკმ ზომის აეროზოლის ამონაფრქვევის კონცენტრაცია ამონაფრქვევ ჭავლში 6 სთ-ის განმავლობაში 100 პ.ე./მ^3–ის (პირობითი ერთეული/მ^3) ტოლია, მაშინ დალექილი რადიაქტიური ნივთიერების ზედაპირული სიმკვრივე მაქსიმალური დალექვის ზონაში მცირდება 360 პ.ე./მ^2-დან 1 პ.ე./მ^2-მდე.

Journal of the Georgian Geophysical Society,
Issue B, Physics of Atmosphere, Ocean, and Space Plasma, v.15, 2011-2012, pp. 46-51

A numerical simulation of the soil salinity reduction

Aleksandre A. Surmava

Iv. Javakhishvili Tbilisi State University, M. Nodia Institute of Geophysics,
1, *Aleksidze Str.,0173, Tbilisi, Georgia, e-mail:aasurmava@yahoo.com*
Georgian Technical University, Institute of Hydrometeorology,

Abstract

Using the filtration and kinetic equations of the chemical reaction between the carbonate sodium and calcium sulfate, the soil salinity change is numerically simulated. It is shown that an application of external sorbent intensifies reduction of sodium in the upper 20 cm layer of the soil on 10%. The process of infiltration causes a displacement of liquid phase of sodium carbonate in the lower depths (z > 2 m) from the upper levels and rise its concentration in the lower levels.

1. Introduction

Salinization of the soils is a serious problem for agriculture of the East Georgia. In the arid and semi-arid regions of Georgia, the salted soils occupied a significant territory – about 250 thousand hectare [1].These territories aren't used or are small used in agriculture of the republic. Therefore, an elaboration of the soil salinity reduction method for the Georgian soils has a practical importance.

An equitable treatment of the problem of soils salinization is available from the FAO [2]. The complex computer simulation packages SALTMOOD and PESTFADE are elaborated to describe the movement of water and solutes in soil system [3, 4].

In the practice, the salinity reduction processes are doing by several ways (a) by leach of the saline soils, (b) by application of a external sorbent – calcium sulfate or others salts, (c) by using the some solinity consumptive plants (xerophyte, arid glasswort, and etc.), and (d) by means of combining of the noted above methods.

The theoretical basis for use of the practical methods was elaborated in [4- 11]. A tries of such investigation for the Georgian soils were made in [12, 13]. In the presented article, these theoretical investigations are continued. Here is simulated the soil salinity reduction by action of the external sorbent and following it a watering of the soil.

2. Formulation of the Problem

In the agriculture, the gypsum drag-in process for reduction of the salinization of the sodic soils is used. The corresponding chemical reaction for the humid environment of the soil may be writing by the following way:

$$CaSO_4 + Na_2CO_3 \longrightarrow CaCO_3 + Na_2SO_4 . \qquad (1)$$

After drag-in of the gypsum in the sodic soil, the sodium ion is substituting with calcium ion, and it is obtained the calcium carbonate and sodium sulfate. By means of this reaction, the sodium carbonate is reduced and the small amount of sodium sulfate appears. In small amounts, the sodium

sulfate aren't difficult for plants and it can be moved in deep layers of soil and leached from the root zone by irrigation water.

These chemical and hydrological processes can be described by following equations of diffusion and kinetic:

$$\frac{\partial W}{\partial t}+\frac{\partial \mathrm{W}\,\mathrm{K}(W+V_{Na_2CO_3}+V_{Na_2SO_4})}{\partial \mathrm{z}}=\frac{\partial}{\partial z}\left[D(W+V_{Na_2CO_3}+V_{Na_2SO_4})\frac{\partial W}{\partial z}\right],$$

$$\frac{\partial V_{Na_2CO_3}}{\partial t}+\frac{\partial V_{Na_2CO_3}\mathrm{K}(W+V_{Na_2CO_3}+V_{Na_2SO_4})}{\partial \mathrm{z}}=\frac{\partial}{\partial z}\left[D(W+V_{Na_2CO_3}+V_{Na_2SO_4})\frac{\partial V_{Na_2CO_3}}{\partial z}\right]$$

$$-S_{Na_2CO_3}(V_{Na_2CO_3}-V_{Na_2CO_3,sat})-RM_{Na_2CO_3}/M_{Ca\mathrm{SO}_4},$$

$$\frac{\partial V_{Na_2SO_4}}{\partial t}+\frac{\partial V_{Na_2SO_4}\mathrm{K}(W+V_{Na_2CO_3}+V_{Na_2SO_4})}{\partial \mathrm{z}}=\frac{\partial}{\partial z}\left[D(W+V_{Na_2CO_3}+V_{Na_2SO_4})\frac{\partial V_{Na_2SO_4}}{\partial z}\right]$$

$$-S_{Na_2SO_4}(V_{Na_2SO_4}-V_{Na_2SO_4,sat})+RM_{Na_2SO_4}/M_{Ca\mathrm{SO}_4},$$

(2)

$$\frac{\partial Q_{Na_2CO_3}}{\partial t}=S_{Na_2CO_3}(V_{Na_2CO_3}-V_{Na_2CO_3,sat})-S_{Na_2SO_4}(V_{Na_2SO_4}-V_{Na_2SO_4,sat}),$$

$$\frac{\partial Q_{CaCO_3}}{\partial t}=RM_{CaCO_3}/M_{Ca\mathrm{SO}_4},\quad \frac{\partial Q_{Na_2SO_4}}{\partial t}=S_{Na_2SO_4}(V_{Na_2SO_4}-V_{Na_2SO_4,sat}),$$

$$\frac{\partial Q_{CaSO_4}}{\partial t}=-R,\quad R=C_{CaSO_4,Na_2CO_3}\times Q_{Ca\mathrm{SO}_4}V_{Na_2CO_3},$$

$$\sigma=1-M-Q_{CaSO_4}-Q_{Na_2CO_3}-\mathrm{Q}_{CaCO_3}-Q_{Na_2SO_4},$$

$$S_x=\begin{cases}C_xV_x(W-W_0) & \text{if } V_x>V_{x,sat}\\ C_xQ_x(W-W_0) & \text{if } V_x\le V_{x,sat}\end{cases},$$

where t is the time; z is the vertical coordinate directed from the ground surface into soil; x denotes the chemical substance; W is the volumetric content of the soil water; $V_{Na_2CO_3}$ and $V_{Na_2SO_4}$ are the volumetric content of the soluted parts of sodium carbonate and sodium sulfate, respectively; $V_{Na_2CO_3,sat}$ ao $V_{Na_2SO_4,sat}$ are the saturated volumetric content of sodium carbonate and sodium sulfate, respectively; $Q_{Na_2CO_3}$, $Q_{Na_2SO_4}$, $Q_{Ca_2CO_3}$, and $Q_{Ca_2SO_4}$ are the volumetric content of the solid phase of sodium carbonate, sodium sulfate, calcium carbonate, and calcium sulfate, respectively; σ is the porosity of the soil; M is the volumetric content of another fractions of the solid soil; $C_{Na_2CO_3}$ and $C_{Na_2SO_4}$ are the velocity of dissolution of volumetric content of the correspondent soils; C_{CaSO_4,Na_2CO_3} is the time of an appearance of one unit calcium carbonate the chemical reaction; S_x is the kinematic coefficient; $M_{Na_2SO_4}$, $M_{Ca\mathrm{SO}_4}$, M_{CaCO_3}, and $M_{Na_2CO_3}$ are the molar masses of the correspondent soils; K and D are the velocity of filtration and diffusion coefficient of the soil water and soluted soils [14]:

$$K(y)=K_{\max}R(y),\ D(y)=D_{\max}R(y),\ R=\left(\frac{y-W_0}{\sigma-W_0}\right)^{3.5},$$

where y is the volumetric content of a sum of water and soluted parts of the substances, K_{max} and D_{max} are the maximal magnitude of the coefficients of the velocity of filtration and diffusion, respectively; W_0 is the volumetric content of the bound water.

The system (2) is soluted by using the following initial and boundary conditions:

$$W = W_0,\ V_{Na_2CO_3} = V_{Na_2SO_4} = 0\ ,\quad Q_{CaCO_3} = Q_{Na_2SO_4} = 0\ ,$$

$$Q_{Na_2CO_3} = Q_{Na_2CO_3,0}\ ,\ Q_{Ca_2SO_4} = Q_{Ca_2SO_4,0}\ , \qquad \text{if} \quad t = 0,$$

$$W(t,0) = \begin{cases} \sigma & \text{if } t \le 1\,\text{day} \\ W_0 & \text{if } t > 1\,\text{day} \end{cases}\ ,\quad \partial V_{Na_2CO_3}/\partial z = \partial V_{Na_2SO_4}/\partial z = 0, \qquad \text{if} \quad z = H, \quad (3)$$

$$\partial W/\partial z = \partial V_{Na_2CO_3}/\partial z = \partial V_{Na_2SO_4}/\partial z = 0, \qquad \text{if} \quad z = H,$$

where $W_0 = 0.0001$. Expression of W(0, t) describes the model situation when during one first day the soil is irrigated. After of this interval of time, the soil surface becomes dry. $Q_{Na_2CO_3,0}$ and $Q_{Ca_2SO_4,0}$ are the known distributions of sodium carbonate and sodium sulfate into solid soil: H = 500 cm is the depth of the soil.

The solution of the equation system (2) with the initial and boundary conditions (3) is made, using the Krankl-Nikolson implicit scheme with temporary and spatial steps equals 6 s and 1 cm, respectively.

It is considered a middle soluted sodic soil. In the upper layer of soil (with 20 cm thicknes), the external sorbent the gypsum is drag-in. In Table 1, the magnitudes of some parameters used in the model are shown.

Table 1. The hydrological and hydrochemical parameters of soil

depths (cm)	poros-ity σ	$Q_{Ca_2SO_4,0}$	$Q_{Na_2CO_3,0}$	coefficient of filtration K_{max} (cm/s)	coefficient of diffusion D_{max} (cm^2/s)
0-20	0.7	0.025	0.0025	8×10^{-5};	5×10^{-4};
20-500	0.5	0	0.0025	8×10^{-5};	5×10^{-4};

The magnitudes of the other parameters are following: $C_{Na_2CO_3} = 83.79\times 10^{-6}\ s^{-1}$; $C_{Na_2SO_4} = 3.83\times 10^{-6}\ s^{-1}$; $C_{CaSO_4,\,Na_2CO_3} = 5\times 10^{-6}\ s^{-1}$;

3. Results of calculations

The numerical simmulation was made for the interval of time equal to one month of physical time. In the Fig. 1, the calculated water cotent in the soil is shown. This figure shows that by means of action of the process of filtration and diffusion the water is distributed in the soil. During the first day, when the soil is irrigated the water saturates the upper 70 cm layer of the soil. After stopping of the irrigation process, the water content in the upper part of the soil decreases.Then, the water distributes into the depth of the soil and simultaneously increases the width of the water-containing layer of soil.

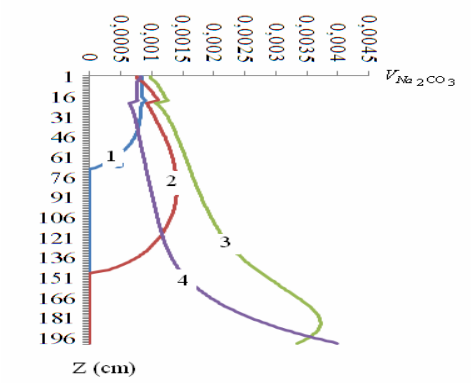

Fig. 1. The volumetric contet of water in the soil obtained for t = 1, 3, 15, and 30 day – lines 1-4, respectively.

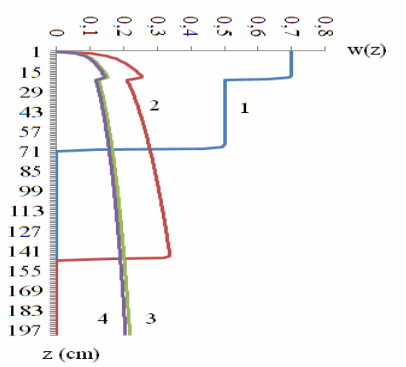

Fig. 2. The volumetric content of liquid sodium carbonate in the soil obtained for t = 1, 3, 15, and 30 days – lines 1-4, respectively.

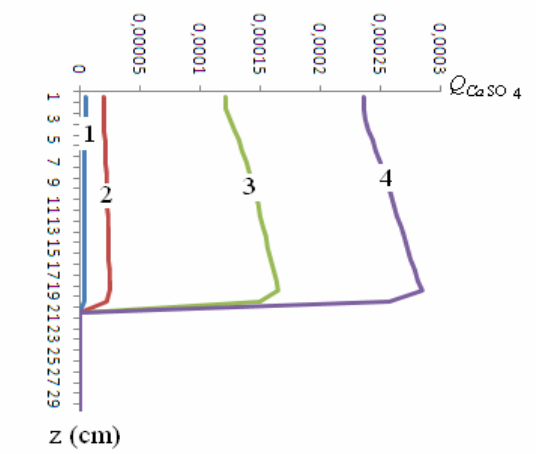

Fig. 3. The volumetric contet of summary sodium carbonate in the soil for t = 1, 3, 15, and 30 days – lines 1- 4, respectively.

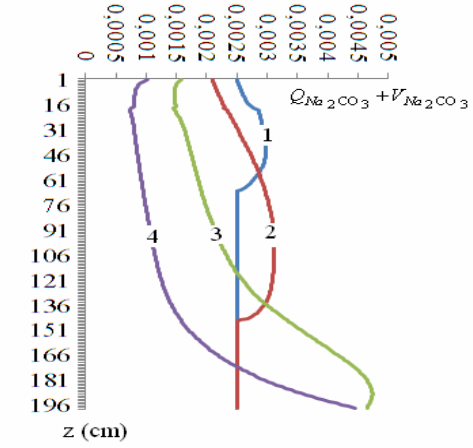

Fig. 4. The magnitude of decrease of volumetric content of gypsum in the soil for t = 1, 3, 15, and 30 days – lines 1- 4, respectively.

The calculation shows that during one month the content of the gypsum in the soil is decreased about 10% (Fig. 4). Simultaneously the small amount of calcium carbonate and sodium sulfate are arised (Figs. 5-6).

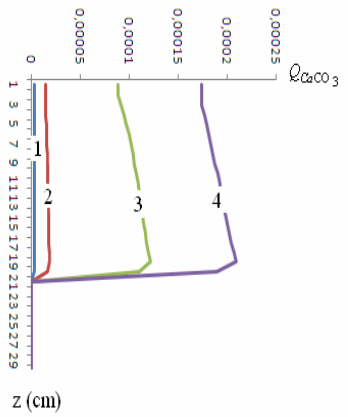

Fig. 5. The volumetric content of calcium carbonate in the soil obtained for t = 1, 3, 15, and 30 days – lines 1- 4, respectively.

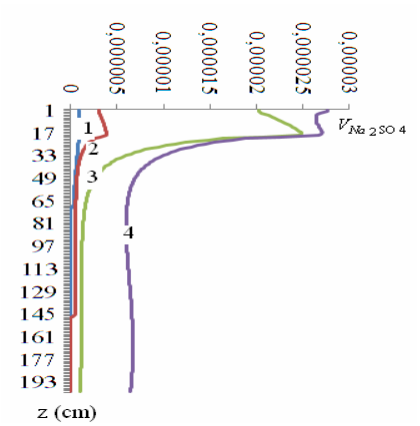

Fig. 6. The volumetric content of sodim sulfate in the soil obtained for t =1, 3, 15, and 30 days – lines 1- 4, respectively.

4. Discussion

The numerical simulation shows that the irrigation and followed it leaching of soil are the main procedures that can cause reduction of soil salinity in the upper part of siol. An application of the external sorbent – gypsum promotes to intensify this process by 10% . In the issue of action of noted above two processes the salinization of soil can be decreased in the upper 2 m layer. The liquid part of sodium carbonate through infiltration dissolved salt from upper levels can be accumulated in soil below 2 m and cause a grow their concentration.

The results obtained in this article have quantitative meaning, because we couldn't find the real measured magnitudes for kinematic parameters of processes of dissolution and chemical reaction. Parameters, used in the article, were taken from some handbooks and they can be used only as approximately values for soil of Georgia. Therefore, for further development of the theoretical investigation of considered task it is nessesury to determine experimentally the real magnitudes of the kinematic, filtration and hydrochemical parameters for salinited soils of Georgia.

References

[1] Sabashvili M. Soils of Georgian SSR. Tbilisi: Metsniereba, 1967, 372 p. (in Georgian).

[2] Salt-Affected Soils and their Management, FAO, Soils Bulletin 39, http://www.fao.org/docrep/x5871e/x5871e00.htm.

[3] SALTMOD. Description Principles, User Manual, and Examples of Application. www.waterlog.info/saltmod.htm.

[4] Clemente, R. S.,Prasher, S. O., Salehi, F. Performance testing and validation of PESTFADE. http://ideas.repec.org/a/eee/agiwat/v37y1998i3p205-224.html

[5] Robbins, C.W., R.J. Wagenet and J.J. Jurinak. A combined salt transport-chemical equilibrium model for calcareous and gypsiferous soils. Soil Sci. Soc. Amer. J. 1980.v. 44, pp.1191-1194.

[6] Haith D. A. A mathematical model for estimating pesticide losses in runoff. Journal Environmental Quality. 1980, v. 9, pp. 428-433.

[7] Breseler E. Transport of salts in soils and subsoils. Agricultural Water Management. 1981, v. 4, pp. 35-62.

[8] Denisov Y. M. Mathematical model of the water- and salt transfer processes in the soils. Mathematical Modeling of the hydrodynamic processes. Novosibirsk, 1984, pp. 49-55. (in Russian).

[9] Addiscott, T.M. and R.J. Wagenet. Concepts of solute leaching in soils: a review of modelling approaches. Journal of Soil Science. 1985, v. 36, pp. 411-424.

[10] Nour el-Din, M.M., I.P. King, K.K. Tanji. Salinity management model: I. Development. ASCE Journal of Irrigation and Drainage Engineering. 1988, 113(4), pp. 440-468.

[11] Relks L. M., Yakirevich A. M. Calculation of the moisture, heat and salts transfers in the saturated and non-saturated zones of the soils. http://rex.vniigim.ru/TWSR02/Rex5.htm

[12] Surmava A. A. Mathematical modeling of movement solute in soil. Proceedings of ZakNIGMI, v. 86(93), 1988, pp. 3-9.(in Georgian)

[13] Surmava A. A., Tugushi N. K., Shavliashvili L. U., Intskirveli L. K. Numerical modeling of a salinity loss of soil. Proceedings of M. Nodia Institute of Geophysics. 2008, v. LX.

[14] Chailds E. . Physical basis of soils hydrology. L. Gidrometeoizdat, 1973, pp . 427.(in Russian)

(Received in final form 20 December 2012)

Численное моделирование уменьшения солёности почвы

А. А. Сурмава

Резюме

С помощью уравнения фильтрации и уравнения кинетики для химической реакции карбоната натрия с сульфатом кальция численно смоделировано изменение солёности почвы. Показано, что внесение сорбента интенсифицирует уменьшение натрия в 20см слое почвы на 10%. Процесс инфильтрации вызывает перемещение жидкой фазы сульфата натрия из верхних уровней в нижние уровни *(z > 2 м)* и рост его содержания на нижных уровнях почвы.

ნიადაგის მარილიანობის შემცირების რიცხვითი მოდელირება

ა. ა. სურმავა

რეზიუმე

სითხის ფილტრაციისა და ნატრიუმის კარბონატის კალციუმის სულფატთან ქიმიური რეაქციის კინეტიკის განტოლების გამოყენებით რიცხობრივად მოდელირებულია ნიადაგის მარილიანობის ცვლილება. ნაჩვენებია, რომ სორბენტის შეტანა იწვევს განმარილიანების პროცესის ინტენსიფიცირებას დაახლოებით 10%-ით ნიადაგის ზედა 20 სმ ფენაში. ინფილტრაცია იწვევს გახსნილი ნატრიუმის სულფატის გადატანას ნიადაგის ზედა ნაწილიდან ქვედაში და ქვედა ფენაში (z > 2 მ) მისი კონცენტრაციის ზრდას.

Journal of the Georgian Geophysical Society,
Issue (A). , Physics of Atmosphere, Ocean, and Space Plasma, v. 15, 2011-2012, pp. 52-64

On the convective motions in different geophysical media

Anzor I. Gvelesiani

Iv. Javakhishvili Tbilisi State University, M. Nodia Institute of Geophysics
1, Alexidze Str., 0193 Tbilisi, Georgia, e-mail:
<anzor_gvelesiani@yahoo.com>

Abstract

From the unified point of view, this paper discusses some known and new results of theoretical and experimental investigations of slow mesoscale convective motions in the neutral and conductive gas and liquid mediums, and a mantle. Specific thermo-hydrodynamic regime conditions of the considered mediums were taken into account for determination of onset of convection and the vertical velocity of arisen heat thermal.

1. Introduction.

Turbulent heat- and mass-transfer processes are well known, and their research represents great interest for specialists, dealing with investigations of the geophysical and various practical problems. In that consequence, some known of other authors and some original results and discussions of the problems will be considered below [1-14]. This paper is sequential of the article [15].

.

2. Double convective diffusion in an ocean. Thermal and haline convection.

2.1. Theoretical analysis of Benard's experiments was made by Rayleigh, which issued linearized thermo-hydrodynamic equations of incompressible viscous liquid in the Boussinesq approximation [5, 7]

$$\frac{\partial v_i}{\partial t} = -\frac{1}{\rho_0}\frac{\partial p'}{\partial x_i} + \nu\Delta v_i + g\alpha T\delta_{i3}, \quad \frac{\partial \theta}{\partial t} = -Aw + \nu_\theta \Delta\theta, \ \frac{\partial v_i}{\partial x_i} = 0, \qquad (1)$$

where $A = (T_2 - T_1)/h$, $T = T_0(z) + \theta$, $T_0 = T_1 + Az$.
For solution of the Benard problem Rayleigh introduces the idea of free layer without tension forces at its boundaries:

$$\theta = w = \frac{\partial^2 w}{\partial z^2} = 0 \quad \text{at} \quad z = 0 \text{ and h.} \qquad (2)$$

Seeking the solution in the form normal modes Rayleigh found exact solution and obtained the critical values of the introduced parameter $Ra = g\alpha\Delta Th^3/\nu\nu_\theta$, $Ra_c = 27\pi^4/4 = 657.511$ (of the onset of thermal instability), and wave parameters ($|k|, n$) of the most fast growing perturbation.

$$(v_i, p', \theta) = e^{-\lambda t + i(k_1x_1 + k_2x_2)}(\hat{v}'(z), \hat{p}'(z), \hat{\theta}(z)), \qquad (3)$$

$$\hat{w}(z) = w_0 \sin n\pi z . \qquad (4)$$

Breaking stability depends on the form and dimensions of convective motions, perturbations scale, conditions at the boundaries of convective layer etc. The Rayleigh criterion is a criterion of onset and evolution of the cellular convection. At the critical value of the Rayleigh number, periodical relative to the spatial values stationary convective motions are arisen.

2.2. The temperature and salinity of sea water has non-uniform distribution. Most essential peculiarity of the sea water is influence of heat and salt on the density and characteristic property of heat and salt. Their opposite action upon the density of the sea water is reflected in expression $\Delta\rho / \rho_0 = \beta\Delta S - \alpha\Delta T$. Diffusion of a heat and salt in the sea water is determined by the thermal diffusivity ($\nu_T \approx 1.5 \cdot 10^{-3}\ cm^2 s^{-1}$) and the diffusion constant ($\nu_S \approx 1.3 \cdot 10^{-5}\ cm^2 s^{-1}$), $\nu_T / \nu_S \approx 115$. Brilliant mental experiment of Stommel-Arons-Blanchard (1956) [6], short report "An oceanographical curiosity: the perpetual salt fountain" become basic work initiated and stimulated study of convection in the presence of double diffusion process. The authors also suggested a scheme of operation.

In the sea, where the double convective diffusion takes place, the Archimedes force of total buoyancy has following form [7]:

$$g\frac{\Delta\rho}{\rho_0} = g(\alpha\Delta T - \beta\Delta S), \qquad R = \frac{\alpha|\Delta T|}{\beta|\Delta S|}, \qquad (5)$$

where $\Delta\rho = \rho - \rho_0$, $\Delta T = T - T_0$, $\Delta S = S - S_0$, here ρ_0, T_0, S_0 are means of the density, temperature and salinity at the layer lower boundary, $\Delta\rho$, ΔT, ΔS are increments of the density, temperature and salinity at the layer upper boundary; α and β are coefficients of volumetric expansion and its salt analogue, respectively; R is so called relation of buoyancy, which characterizes influence of two diffusive components upon the density change.

It is said that the layer is stably stratified if $\Delta\rho < 0$; when $\Delta\rho = 0$, stratification of layer is neutral; when $\Delta S = S = 0$ – thermal convection (heating from below), then $\Delta T < 0$ and $\Delta\rho > 0$ stratification of layer is unstable; when $\Delta T = 0$ – isothermal salt convection (salinization from above), then $\Delta S > 0$ and $\Delta\rho > 0$ – stratification of layer is unstable, too.

In the non-trivial double-convection case when $\Delta T \neq 0$, $\Delta S \neq 0$ it is evident that four cases of the temperature and salinity drops may be considered (salinization and heating of the water layer from above or from below):

(1) The salinization and heating from above: $\Delta S > 0$, $\Delta T > 0$, $\Delta\rho / \rho_0 = -\beta\Delta S(R-1)$;

(1a) $R > 1$, $\Delta\rho < 0$, stable stratification, (1b) $R < 1$, $\Delta\rho > 0$, unstable stratification.

(2) The salinization and heating from below: $\Delta S < 0$, $\Delta T < 0$, $\Delta\rho / \rho_0 = \beta\Delta S(1-R)$;

(2a) $R < 1$, $\Delta\rho < 0$, stable stratification, (2b) $R > 1$, $\Delta\rho > 0$, unstable stratification;

(3) The salinization from above and heating from below. $\Delta S > 0$, $\Delta T < 0$, $\Delta\rho / \rho_0 = \beta\Delta S(R+1)$

– stratification always is unstable;

(4) The salinization from below and heating from above. $\Delta S < 0$ $\Delta T > 0$, $\Delta\rho / \rho_0 =$

$= \beta\Delta S(R+1) < 0$ – stratification always is stable.

Expressions for convective vertical velocity and effective Reynolds number have following form [7]

$$w = \frac{2a_T k_\perp}{\tau\delta}\left[\left(1+\delta^2\right)\left(\sqrt{r}-1\right)\right]^{1/2}, \quad \text{or} \quad w = \frac{2a_s k_\perp}{\delta}\left[\left(1+\delta^2\right)\left(\sqrt{r}-1\right)\right]^{1/2}, \qquad (6)$$

where $\delta = l^*/H$, $k_\perp = \pi/H$, $\sigma = \Pr = \nu/a_T$, $\tau = a_T/\nu_s$, $r = \frac{\tau}{R} = \frac{a_T}{a_s}\frac{\beta\gamma_s}{\alpha\gamma_T}, \gamma_T = \frac{dT}{dz}, \gamma_s = \frac{ds}{dz}$,

where

$\Pr \approx 6.93$, $\tau \approx 115$; for $T_0 = 20^0 C$, $s_0 = 40\%$, $\beta = 0.72$, $\alpha = 2.1\cdot 10^{-4}(^0C)$. (7)

In the laboratory experiments modeling a double-convection in the systems heat-salt and sugar-salt (similar systems NaCl-KCl) no diffusing components loss takes place.

According to measurements in the upper layer of the ocean the vertical velocity of convectional motion changes from 0.04 $cm\cdot s^{-1}$ at the surface (h = 0 m.) of the ocean to 0.91 $cm\cdot s^{-1}$ at the depth h = 600 m.

$$w = 0.04 \div 0.91 \ cm\cdot s^{-1}, \quad h = 0 \div 600 \ m. \qquad (8)$$

2.2.2. In the presence of vertical velocity shear of the main fluid flow dU/dz in the layer of the water with heterogeneous density with a thickness equals to h^* respective Rayleigh number Ra^* is, [8],

$$Ra^* = \frac{h^{*3}}{h^4}\frac{1}{\nu}\left|\frac{dU}{dz}\right| Ra; \qquad Ra^* \le Ra. \qquad (9)$$

Here h is the initial thickness of the free convection layer. Positive values of the Rayleigh number $Ra^* > 0$ characterizes instability of the layer h^*.

3.1. Two-phase flows [16]. Equation of a turbulent energy balance in the shearing motion containing solid particles of sparse distribution takes up the form [15]

$$\rho < u'w' > \frac{\partial u}{\partial z} + \rho\varepsilon_t + < \rho'w' > g = 0; \qquad (10)$$

it is convenient to rewrite the aforecited equation in a following shape

$$< u'w' > \frac{\partial u}{\partial z}(1 - Ko) + \varepsilon_t = 0, \qquad (11)$$

where the non-dimensional **K**olmogorov parameter, *Ko***,**

$$Ko = -\frac{\overline{\rho'w'}\,g}{\rho\,\overline{u'w'}\,u_z} = -\frac{\sigma g\,\overline{s'w'}}{\overline{u'w'}\,u_z}, \qquad 0 < Ko < 1, \qquad (12)$$

u', w', ρ', and s' are pulsations of horizontal and vertical components of velocity, density of mixture, and mean volume concentration, s, of the particles, respectively; $\sigma = (\rho_p - \rho)/\rho$, ρ_p is the density of particles, and $u_z = \partial u/\partial z$. The Kolmogorov number shows a turbulent energy

consumption of the flow to the weighing of particles. When the Kolmogorov number *Ko* ~1, the particles influence on the dynamics of the flow is great, i.e., the Kolmogorov parameter *Ko* becomes an additional parameter determining influence of the stratification. **Thus**, **the Kolmogorov parameter, *Ko*, is similar to Richardson's one in the theory of temperature stratification.**

3.2. The energetic layer of an ocean.

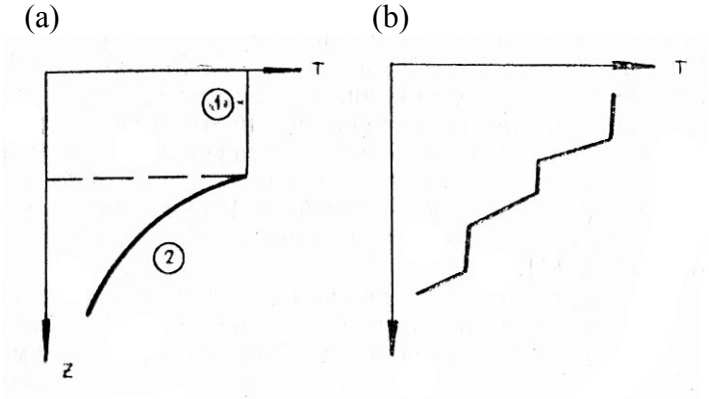

Fig. 1. Temperature distribution in the upper layer of the ocean:
(a) schematic profile of temperature: (1) is the upper uniform layer,
(2) is the upper thermocline [16]; (b) precise measuring profile [17].

Upper energetic layer of an ocean is uniform (in it the temperature and salinity. and, therefore, the density are constant) is connected with the turbulent mixing (see Fig.1). The mixing is realized by the wind shear and convection: descending heavy particles to swim with the current from the upper layer, cooled and salted, as a result of evaporation from the surface and also of breaking of the surface waves. The depth of this layer depends on the season: it increases in winter and decreases in spring. The upper uniform layer is supported by the region with sharply changed temperature (Fig. 1a) – upper thermocline to the depth about 200-250 m. Here a seasonal temperature changing does not become apparent. An analysis of temperature distributions in the strong and stable stratified upper thermocline shows that in the upper thermocline the turbulent diffusivity coefficient is of order $æ_t \sim (10^{-1} \div 1)\, cm^2/s$, intermediate value between the upper turbulent uniform layer's value equal to $æ_t \sim 10^3\, cm^2/s$, and the value of the molecular thermal diffusivity, $æ \sim 10^{-3} cm^2/s$. More precise measurements [17] obtain, that instantaneous temperature stratification has stepped character: the range of constant temperature changed by region with great gradients (Fig. 1b). That results from turbulence in the turbulent flow with steady stratification is spread in the form of pots and connected with internal waves [18].

3.3. Laboratory experiments [19]. Free convective motions inside of the heterogeneity liquids are one of main processes giving rise to generation of fine structure of ocean, atmosphere, and, seemingly, only mechanism of stratification of Antarctida' Lake Vanda type closed basins. Laboratory experiments (provided under lateral heating) showed that general property of the spatial structure (SS) of convective motions inside stratified liquid (SL) is generation periodic vertical circular layers. These layers separated by thin plates of still liquid having great gradients of temperature and salinity, shear of velocity. The convective processes inside of SL are convenient model for study of periodical SS dynamics inside of heterogeneity media. In this case, the temperature is "fast" variable and salinity is "slow" variable, spatial dispersion caused by difference of their kinetic coefficients – the thermal diffusivity $\chi = 1.43 \cdot 10^{-3} cm^2/s$ and diffusion of a salt $k_s = 1.41 \cdot 10^{-5} cm^2/s$ [19].

4. Golitsyn's approximate theory of the roll convection [11].

4.1. The Ū-Ra-Nu relation.An interest to this problem was arisen under attempts to estimate the motion velocities in the Earth upper mantle, which cause displacements of the lithospheric

plates of the Earth's crust. From the formula for the energy dissipation (under equal derivatives of the velocity components) and the character scale equal to the thickness of the layer d (roll convection) the mean values of the velocity components are [11]:

$$\overline{u} \approx \overline{w} \approx \frac{1}{a}\left(\frac{\varepsilon}{\nu}\right)^{1/2} d = \frac{d}{a}\left(\frac{agf}{\mu c_p}\frac{Nu-1}{Nu}\right)^{1/2}, \qquad (13)$$

or

$$\overline{u} \approx \overline{w} \approx \frac{\kappa}{ad}\left(Ra(Nu-1)\right)^{1/2}, \qquad Nu >> 1. \qquad (14)$$

i.e. for sufficiently developed convection, when the Raynolds number $\mathrm{Re} \geq 1500$, the Rayleigh number $Ra \sim 10^7$ and between them is following relation:

$$\mathrm{Re} = 0.5 a_1 P^{-2/3} Ra^{4/9}, \qquad (15)$$

where a_1 is experimental constant, κ is the coefficient of thermal diffusivity.

The author using the McKenzie et al. (1974) [11] recommendations for values of the material parameters: $\alpha = 2 \cdot 10^{-5} K^{-1}$, $c_p = 1.2 \cdot 10^3 J/(kg \cdot K)$, $\rho = 3.6 t./m^3$, $\nu = 2 \cdot 10^{17} m^2/s$, obtains for the geothermal flux of heat value $f = 6 \cdot 10^{-2} Wt/m^2$, for thickness of the upper mantle value $d = 7 \cdot 10^5 m = 700 km$, and for mean velocity (14) following value

$$\overline{u} \approx 1 cm/year. \qquad (16)$$

According to Elsasser et al. (1979) ([11]) all mantle with thickness $d \approx 3000 km$ takes part in convection process. Then

$$\overline{u} \approx 5 cm/year, \qquad (17)$$

what is near to real situation

$$\overline{u} \approx 10 cm/year. \qquad (18)$$

Another available conclusion for study fluid motions in the mental is that under small Raynolds' numbers the self-similarity of convection follows from these conceptions [12, 13]. *There is possibility of laboratory modeling of such motions under small Reynolds number* [11]. In detail, results of the laboratory investigations of this problem are discussed in the large paper [14].

4.2. The Nu-Ra relation.

Thermal conductivity equation in a fluid without internal sources,

$$\frac{\partial T}{\partial t} + v_i \frac{\partial T}{\partial x_i} = \kappa \frac{\partial^2 T}{\partial x_i^2}, \qquad (19)$$

is a homogeneous equation relative to the choice of the temperature scale. Introduce the scales of the length, d, velocity, U, and time, d/U. Then before the Laplacian in r.h.s. is appeared a factor, Pe^{-1} (where Pe is the Peklet number),

$$Pe = Ud/\kappa. \qquad (20)$$

It is evident that when $Pe >> 1$ the thermal boundary layer of the thickness

$$\delta \approx d\, Pe^{-1/2},\ (\frac{d}{\delta} \approx Pe^{1/2}),\qquad (Nu \sim \frac{d}{\delta}),\qquad (21)$$

is generated, but in the main part of liquid its temperature must little change.

A lot of laboratory and numerical experiments [20] confirm this picture and show that at the developed convection the temperature changes about $\Delta T/2$ near the boundaries and in main volume the liquid is isothermal, practically.

From the heat flux continuity through the liquid it is evident that $f/\rho c_p \approx \kappa \Delta T/2\delta$. Using (21) and $fd = \rho c_p \kappa \Delta T + HG$, $H = c_p/\alpha g$, the author obtained the relation [11]:

$$Nu \approx Pe^{1/2}/2. \qquad (22)$$

Choose the scale of velocity in form of (14), then instead of (22) we have

$$Nu \approx [Ra(Nu-1)]^{1/4}/2a^{1/2}. \qquad (23)$$

At small supercritical values of the Rayleigh number $Ra(Nu-1) \sim Ra - Ra_c$, i.e.

$$Nu \sim (Ra - Ra_c)^{1/4}. \qquad (24)$$

For Nu>>1, from (23) we have that

$$Nu \sim 2^{-4/3} a^{-2/3} Ra^{1/3}. \qquad (25)$$

These heat-transfer principles are well-known experimentally and the last one also has theoretical substantiations [20, 21]. *These formulas (22)-(25) are free from several assumptions of other authors*. Coefficient $2^{-4/3}a^{-2/3} = 0.1$ at $a = 9$ and 0.08 at $a = 12$.

According to [22], in case of plane surface for $Ra > 10^9$ at united laminar and turbulent convection $Nu = 0.13Ra^{1/3}$, for $Ra\ 10^4 \div 10^9$ at a natural laminar convection the dependence is lower $Nu = 0.59Ra^{1/4}$, but according to [14] $Nu \approx 0.1Ra_\gamma^{1/3}$. Last investigations reviewed in [14] confirm Nu - Ra relation obtained by [11].

4.3. The K-Qτ relation..

For non-dimensional kinetic energy of convection, K, it is obtained the formula

$$K = \frac{1}{2}(\overline{u}^2 + \overline{w}^2) \approx \frac{Ra(Nu-1)}{a^2}, \qquad (26)$$

in dimensional form

$$K \approx \frac{\gamma f}{a^2}\frac{d^2}{\nu} = \frac{G}{a^2}\tau_{rel}, \qquad (27)$$

where $G = \gamma f$ is the velocity of the kinetic energy generation from potential one (mechanical power), $\gamma = dT/dz$, f is the heat flux through the liquid without internal sources of heat, $\tau_{rel} = d^2/\nu$ is the viscous relaxation time.

For density convection in (14) instead of $G = \gamma f$ one can substitute $G = \gamma_g mgd$, where γ_g is the velocity of the kinetic energy generation, m is the flux of density through the layer, mgd is the mechanical power introducing into the flux under a stationary density convection.

In the inertial interval (homogeneous isotropic interval) for kinetic energy of the volume with a mass $M = \rho d^3$ relative to similar neighbour volumes the kinetic energy of convection

$$K \approx M(\varepsilon d)^{2/3} = Q_m d(\varepsilon d)^{-1/3}, \qquad (28)$$

where $Q_m = \rho \varepsilon d^3$ is the incoming total power of energy from the external scale of turbulence and dissipating into the viscous interval. Because of $(\varepsilon d)^{1/3} \approx U$, the mean square different of velocities in two points of the area divided by the distance equals to d, than $d(\varepsilon d)^{-1/3} = \tau_U$ is suggested as the character time life of the vortex of the scale d.

$$K \approx Q_m \tau_U . \qquad (29)$$

The kinetic energy of circulation on the slowly revolving planet may be written in similar form

$$K \approx Q \tau_e , \qquad (30)$$

where $Q = 4\pi a^2 q$ is a total energy surge to the planet of radius a, q is a mean solar energy surge to the area element of a planet surface, $\tau_e = a / c_e$ is a character time of propagation of disturbance in global scale, c_e is the isothermal speed of sound at the equilibrium temperature $T_e = (q/\sigma)^{1/4}$, and σ is the Stephan-Boltzmann constant.

Last formulas show that the total kinetic energy of large quantity of forced flows is determined by the product of the energy input into the liquid and the character time of relaxation. It is of importance that in all considered cases above mentioned time is the least among all times which may construct from parameters of the problem (having at one's disposal). Taking into account the hypothesis of self-similarity, that time is generally single one. Golitsyn introduces the rule of the fastest reaction which he names as "*principle of the fastest reaction*": *the kinetic energy of constant forced flow is of the order of power input multiplied by the minimal relaxation time character for the system.* This rule allows without recourse to the similarity theory to write the expression for total kinetic energy of the system.

5. The mantle plumes.

5.1. A simple model for planetary mantle convection is the Bénard convection in a fluid with a temperature-dependent viscosity. In the Bénard problem, dissipative processes play an essential role. Bénard was particularly interested in the role of viscosity. He found that when the temperature of the lower surface was gradually increased, at a certain instant, the layer became reticulated and revealed its dissection into cells [9]. This problem is one of the actual problems of the Geophysics and Physics of the Earth.

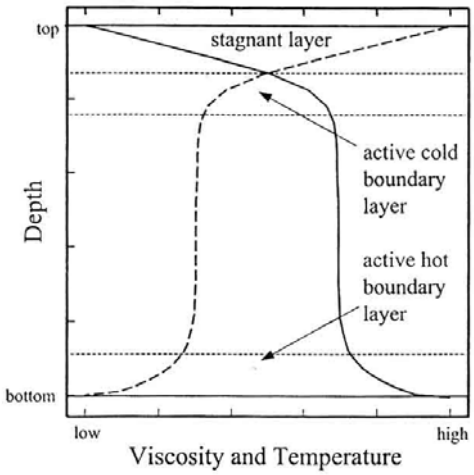

Fig. 3. A schematic illustration of the horizontally averaged variation of temperature (solid line) with depth during an experiment. Also shown are the active thermal boundary layers (thin dashed lines) at the top and bottom of the fluid layer. The high viscosity of the coldest region makes the upper part of the cold thermal boundary layer stagnant. Resultant weak cooling keeps the actively convecting region nearly isothermal and, in turn, the viscosity ratio across the hot thermal boundary layer small [14].

5.2. According to [23] the main unknown parameters are viscosity values within mantle layers whose number and thickness are prescribed in the models developed during the past two decades. These parameters are estimated by comparing observations and predictions of relative sea level change at various sites over the past 18,000 years. Secular changes of length of day and the Earth's gravitational oblateness also contain information on the depth-varying mantle viscosity. The upper mantle viscosity is fixed here at $5 \cdot 10^{20}$ Pa s. Comparison of theoretical oblateness- viscosity curve and observational one with each other leads to a lower mantle viscosity around $2 \cdot 10^{21}$ Pa s. (The author suggests the range $1 - 5 \cdot 10^{21}$ Pa s that fits the geological observations). This evident is conformed to the diagram in Fig. 3 [14].

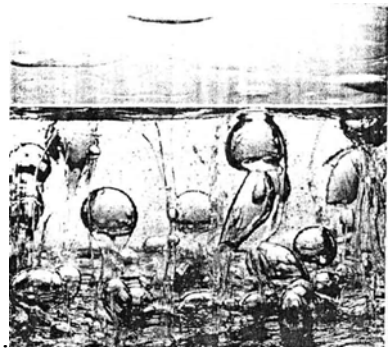

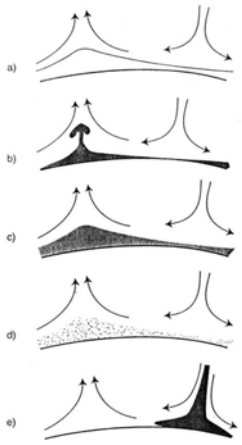

Fig. 3. Fig. 4.

Fig. 3 (left). A laboratory experiment with compositional convection in which low-viscosity water is injected through a permeable plate into high-viscosity glucose syrop. In a way that is dynamically similar to thermal convection, water collects in a gravitationally unstable compositional boundary layer at the base of the syrup and then drains intermittently as plumes with large heads and narrow underlying conduits. Despite the presence of robust low-viscosity conduits, complicated interactions among rising plumes prevent their becoming long-lived stable features [14].

Fig. 4 (right). Schematic illustration of several models for D″. Within the context of plate tectonics, D″ has been explained variously as (a) a phase change, (b) a thermal boundary layer, (c) a compositional boundary layer, (d) ponded chemical dregs from subducted lithosphere, and (e) a slab graveyard [14].

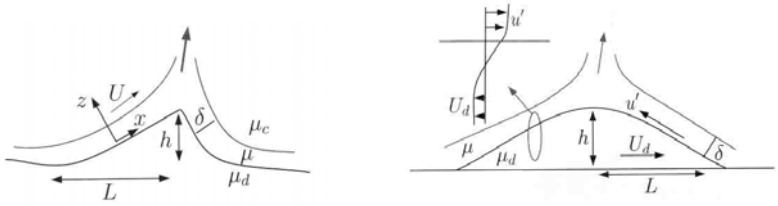

(a) (b)

Fig. 5. (a) Schematic cross section of the deformed dense layer defining variables and the geometry of the problem – dense layer topography and long-lived plumes. This scheme was constructed on the basis of laboratory experiments which showed as the dense layer is deformed by flow into a nascent plume instability showing the different regions of the flow. (b) Schematic cross section of the deformed dense layer defining variables and the geometry of the problem – height of topography. In order for topography to be stable $U_d \sim u'$ [14].

5.3**.** According to [26] lubrication theory analysis the perturbed velocity of fluids [14]

$$u(z) = U + u'(z), \tag{31}$$

where U is the velocity at the boundary between the interior and thermal boundary layer fluid, $u'(z)$ describes the variations in velocity within the boundary layer. The *x*-component of the momentum equation is

$$\frac{\partial p}{\partial x} = \mu \frac{\partial^2 u'}{\partial z^2}, \quad \text{and} \quad \frac{\partial p}{\partial x} \approx \frac{\Delta \rho g h}{L}, \tag{32}$$

where *p* is dynamic pressure, we have

$$u' \sim \frac{\Delta \rho g h \delta^2}{\mu L}, \tag{33}$$

Continuity of viscous stresses at the interface between the cold interior fluid and the thermal boundary layer demands that $\mu_c U / L \sim \mu u' / \delta$ and thus that

$$U \sim \frac{\Delta \rho g h \delta}{\mu_c}. \tag{34}$$

The criterion for stable plumes is that the velocity *U* must be greater than the speed, at which a thermal can rise through the mantle,

$$U_{th} \sim \frac{\Delta \rho g \delta^2}{\mu_c}, \tag{35}$$

where $\Delta\rho$ is the difference between the density of thermal boundary layer fluid and interior fluid, g is gravity μ_c is the viscosity at the cold boundary, δ is the thermal boundary layer's thickness, h is the dense layer's height. This condition leads to the requirement that $h/\delta > const$ (in the experiments $h/\delta \approx 0.6$).

Long-lived plumes are located on top of topographic peaks on the dense layer. In order for a plume conduit to become fixed on top of such a feature it is clear that thermal boundary layer fluid must flow along the interface with the dense layer faster than it can rise vertically into the interior as a new thermal. Said differently, the timescale for thermal boundary layer fluid to flow laterally from the center of an embayment to a peak must be less than the timescale for a new convective instability to grow.

The scheme Fig. 5a was constructed on the basis of laboratory experiments which showed as the dense layer is deformed by flow into a nascent plume instability showing the different regions of the flow. Knowing the height of the topography on the dense layer is critical for determining the stability of plumes. One dynamical requirement for stable topography is that the lateral flow of boundary layer fluid must be balanced by the opposing flow of dense layer material (Fig. 5b). The condition implies that $U_d \sim u'$, where $U_d \sim \Delta\rho g h\delta^2 / L\mu$ and thus that

$$\frac{h}{\delta} \sim \left(\frac{\Delta\rho}{\Delta\rho_c}\right)^{1/2} \sim \left(\frac{1}{B}\right)^{1/2}. \qquad (36)$$

6. Some remarks.

For comparison with the above mentioned picture of air bubbles generation (Fig. 3), below it is given the similar picture of air babbles, generated in super-cooled water drop after its freezing. Water drops of about 2-3 mm in diameter were frozen on the ice in the original micro-cold-store engineered in Geophysical Institute of Georgian Acad. Sci. [28].

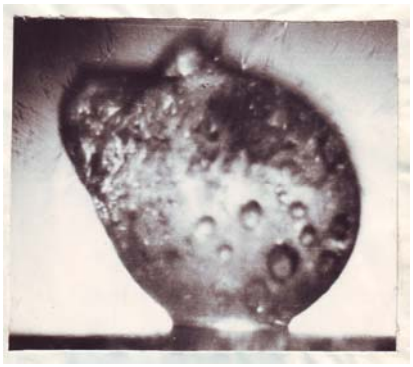

Fig. 6. Internal bubble structure of frozen supercooled water drop of about 2-3 mm in size [28].

were used. After freezing maximal air babbles' diameter was about 0.3 mm. The speed of spreading of the crystallization front $G \approx 3.48 \cdot 10^{-3}\, cm \cdot s^{-1}$; temperature drop of air in the cold store $\Delta T = -10^0$, thermal conductivity of air $\lambda_a = 5.63 \cdot 10^{-5}\, cal(cm \cdot sec \cdot K)^{-1}$, solubility of air in water in mole fractions is $D \sim 1.3 \div 1.8 \cdot 10^{-5}$; diffusion of a heat in the water $\nu_T \approx 1.5 \cdot 10^{-3}\, cm^2 s^{-1}$. The sizes of the air bubbles and thickness of initial ice layers in the freezing drop correlate with D/G. The thickness of first clear layer of ice is about 0.1-0.2 mm, and diameters of air bubbles ~ 0.12-0.16 mm.

6.1. It necessary to note, that criterion $B = \Delta\rho / \rho\alpha\Delta T$ in [14] may be obtained as ratio of criteria Archimedes, $Ar = (gl^3 / \nu^2)\Delta\rho / \rho$, and Grashof criteria, $Gr = (gl^3 / \nu^2)\alpha\Delta T$:

$$Ar : Gr = B = \Delta\rho / \rho\alpha\Delta T . \qquad (37)$$

When the Reynolds number $\mathrm{Re} = Ul / \nu$ equals to the Archimedes number $Ar = (gl^3 / \nu^2)\Delta\rho / \rho$, then for an ascending motion velocity of the warm mass of liquid we have the following formula:

$$U = \frac{\Delta\rho g l^2}{\rho\nu}; \qquad (38)$$

Using the relation $U / L \approx u' / h$ or $U \approx u'L / h$, i.e. we have that $u'L / h \approx \Delta\rho g l^2 / \rho\nu$ or $u' \approx \Delta\rho g h l^2 / \rho\nu L$. Having suggest $l = \delta$, one can obtain the expression (35) for the velocity variation in the boundary layer according to the modeling experiments [14]:

$$U_{th} \sim \frac{\Delta\rho g \delta^2}{\mu_c} .$$

6.2. Let compare Golitsyn's formula (22) with Jellinek-Manga's one (36):

$$Nu \approx \frac{d}{\delta} \sim Pe^{1/2} \quad \text{and} \quad \frac{h}{\delta} \sim B^{-1/2},$$

we obtain dependence between the Peklet number, and the form-factor *B*

$$Pe \sim B^{-1}$$

here $d = h$ $Pe = Ud / \kappa$, and $B = \Delta\rho_c / \rho\alpha\Delta T_i$ is the stabilizing buoyancy effect of the dense layer.

6.3. The theory of thermal instability in fluid spheres and in spherical shells has bearings on a number of geophysical questions [9]. Though applications of the theory are not universally subscribed, it cannot be doubted that convective motions in the fluid core are relevant to all theoriesconcerned with the origin of the earth's magnetic field and its secular variations.
But the theory of thermal instability has not been worked out with sufficient generality for these purposes. Even the effect of rotation has been examined only in a very preliminary way; and the onset of instability as overstability – which should be expected to be the rule rather than the exception with liquid metals requires investigation. And in addition to rotation, the effect of a magnetic field has also to be considered. The case of a uniform magnetic field presents no formal difficulty; but this is hardly appropriate for the problems in view. Without further knowledge, the choice of an initial field is so wide that the selection becomes almost arbitrary. It is, indeed, likely that the theory of the convective motions in the earth's core cannot be dissociated from the theory of the origin of the earth's magnetic field.

7. Conclusion.

In the above considered cases of convective motions we practically deal with the Bénard problem: (a) for a single fluid when the instability has a simple mechanical interpretation and (b) for a mixture in which the motion gets complicated by the diffusion processes. In the linear

stability theory, it is generally assumed that the most general perturbation can be represented as a complete set of normal modes. This approach of the problem, as is well known, was carefully developed by Chandrasekhar [9], and analyzed later, for example, in the monographs [10, 27]), especially by Joseph [10].

Being first step in analysis of the convective motions the linear theory cannot answer a number of essential questions. First of all, that is a question about stabilization of the rapidly increasing perturbations, secondly, a question about the structure of convective cells and their stability. Only by means of non-linear theory it is possible to answer these questions.

References

[1] Rumford C. On the propagation of heat in fluids. Complete Works, American Academy of Arts and Sciences, 1870, v. 1, p. 239.

[2] Thomson J. T. On a changing tessellated structure in certain liquids. Proc. Glasgow Philos. Soc, 1881, v. 2.

[3] Bénard M. Les tourbillons cellularies dans une nappe liquide. Revue General de Sciences, 1900, v. 12, pp. 1261-1309.

[4] Bénard M. Les tourbillons cellularies dans une nappe liquide transportant de la chaleur par convection en regime permanent. Ann. de Chimie et de Physique. 1901, v. 23, p. 62.

[5] Rayleigh O. M. On convection currents in a horizontal layer of fluid when the higher temperature is on the under side. Philos. Mag. and J. Sci., 1916, v. 32, N192, pp. 529-546.

[6] Stommel H., Arons A., Blanchard D. An oceanographical curiosity: the perpetual salt fountain. Deep-Sea Res., 1956, v. 3, N 2, pp. 152-153.

[7] Veliev A. A. Hydrodynamic theory of double-convective diffusion. Baku: University "Odlar Yurdu", 1997, 279 p.

[8] Bulgakov N. P. Convection in the ocean. M.: Nauka, 1975, 272 p.

[9] Chandrasekhar S. Hydrodynamic and hydromagnetic stability. Clarendon Press, Oxford, England, 1961, 652 p.

[10] Joseph D. D. Stability of fluid motions. Springer-Verlag, Berlin-Heidelberg-New York, 1976 ; M: Mir, 1981, 638 p.

[11] Golitsyn G. S. Energy of convection. Non-linear waves: Stochasticity and Turbulence. Gorky: AN SSSR, IPF, 1980, pp. 131-139.

[12] Golitsyn G. S. Study of convection with geophysical application and analogues. L.: Gidrometeoizdat, 1981.

[13] Golitsyn G. S. DAN SSSR, 1978, v. 240, N 5, p. 1054.

[14] Jellinek A. M., Manga M. Links between long-lived hot spots, mantle plumes, D″, and plate tectonics. Reviews of Geophysics, 2004, v. 42, RG3002, pp. 1-35.

[15] Gvelesiani A. I. On the convective motions in different layers of atmosphere. J. Georgian Geophys. Soc., 2010, v. 14B, pp. 161-182.

[16] Barenblatt G. I. Some phenomena of turbulence in liquid with strongly stable stratification. Stochasticity and Turbulence. Gorky: AN SSSR, IPF, 1980, pp. 89-114.

[17] Fyodorov K. N. Light thermohaline structure of the ocean waters. L.: Gidrometeoizdat. 1976, 184 p.

[18] Phillips O. M. Energy loss mechanisms from low mode waves. Soviet-American Conference on the Internal Waves. Novosibirsk, December, 1976.

[19] Chashechkin Yu. D. Stochasticity of convective flows in a stratified liquid. Non-linear waves: Stochasticity and Turbulence. Gorky: AN SSSR, IPF, 1980, pp. 131-139.

[20] Busse F. H. Rep. Progr. Phys., 1978, v. 41, p. 1929.

[21] Кутателадзе С. С. Основы теории теплообмена. Новосибирск: Наука, 1970

[22] Bennett C. O., Myers J. E. Momentum, heat and mass transfer. M.: Nedra, 1966, Ch. 26, 726 p.

[23] Cazenave A. and Nerem R. S. Present-day sea level chance: observations and causes. Rev. Geophys., 2004, v. 42, RG3001, doi:10.1029/2003RG00139.

[24] Forte A. M. and Peltier W. R. Viscous flow models of global geophysical observables: 1. Forward problems. J. Geophys. Res., 1991, v. 96(B12), pp. 20, 131-20,159.
[25] Hager B. H. and Clayton R. W. Constraints on the structure of mantle convection using seismic observations, flow models and the geoid. In Mental Convection, Plate Tectonics and Global Dynamics (edited by Peltier W. R.),1989, pp. 765-816, Gordon and Breach, Newark, N. J.
[26] Koch D. M., Koch D. L. Numerical and theoretical solution for a drop spreading below a free fluid surface. J. Fluid Mech., 1995, v. 287, pp. 251-278.
[27] Glansdorff P., Prigogine I. Thermodynamic theory of structure, stability and fluctuations. John Wiley, London-New York-Sydney-Toronto, 1971, 306 p.
[28] Gvelesiani A. I. Some aspects of the hail particles evolution. Ph.D. Thesis, Leningrad: LHMI, 1970, 211 p.

(Received in final form 20 December 2011)

О конвективных движениях в различных геофизических средах

Анзор И. Гвелесиани

С единой точки зрения рассматриваются результаты теоретических и экспериментальных исследований медленных мезамасштабных конвективных движений в атмосфере, океане и мантии. Учтена специфика режимов рассматриваемых сред при определении условий возникновения конвекции и нахождении аналитических формул для вертикальной скорости восходящего термика.

კონვექციური მოძრაობების შესახებ სხვადასხვა გეოფიზიკურ გარემოში

ანზორ ი. გველესიანი

რეზიუმე

განხილულია ოკეანესა და მანტიაში ნელი კონვექციური მეზომასშტაბური მოძრაობების თეორიული და ექსპერიმენტული შესწავლის შედეგები. კონვექციის წარმოშობის პირობებისა და აღმავალი თერმიკის ვერტიკალური სიჩქარის ანალიზური ფორმულების განსაზღვრისას გათვალისწინებულია განხილულ გარემოთა რეჟიმების სპეციფიკა.

Journal of the Georgian Geophysical Society,
Issue (B), Physics of Atmosphere, Ocean, and Space Plasma, v.15, 2011-2012, pp. 65-94

Generation, intensification and self-organization of internal-gravity wave structures in the Earth's ionosphere with directional wind shear

Aburjania G.D., Chargazia K. Z.

M. Nodia Institute of Geophysics at I .Javakhishvili Tbilisi State Univerity,
1 Aleksidze str., 0193 Tbilisi, Georgia

E-mail: aburj@mymail.ge, khatuna.chargazia@gmail.com

Abstract

The linear mechanism of generation, intensification and further nonlinear dynamics of internal gravity waves (IGW) in stably stratified dissipative ionosphere with non-uniform zonal wind (shear flow) is studied. In case of the shear flows the operators of linear problem are non-selfadjoint, and the corresponding Eigen functions - nonorthogonal. Thus, canonical - modal approach is of less use studying such motions. Non-modal mathematical analysis becomes more adequate for such problems. On the basis of non-modal approach, the equations of dynamics and the energy transfer of IGW disturbances in the ionosphere with a shear flow is obtained. Necessary conditions of instability of the considered shear flows are obtained. The increment of shear instability of IGW is defined. Exact analytical solutions of the linear as well as the nonlinear dynamic equations of the problem are built. It is revealed that the transient amplification of IGW disturbances due time does not flow exponentially, but in algebraic - power law manner. The frequency and wave-number of the generated IGW modes are functions of time. Thus in the ionosphere with the shear flow, a wide range of wave disturbances are produced by the linear effects, when the nonlinear and turbulent ones are absent. The effectiveness of the linear amplification mechanism of IGW at interaction with non-uniform zonal wind is analyzed. It is shown that at initial linear stage of evolution IGW effectively temporarily draws energy from the shear flow significantly increasing (by order of magnitude) own amplitude and energy. With amplitude growth the nonlinear mechanism of self-localization turns on and the process ends with self-organization of nonlinear solitary, strongly localized IGW vortex structures. Therefore, a new degree of freedom of the system and accordingly, the path of evolution of disturbances appear in a medium with shear flow. Depending on the type of shear flow velocity profile the nonlinear IGW structures can be the pure monopole vortices, the transverse vortex chain or the longitudinal vortex street in the background of non-uniform zonal wind. Accumulation of these vortices in the ionosphere medium can create the strongly turbulent state.

Keywords: Gravity waves; Shear flow; IGW transient amplification; nonlinear vortex structures

1. Introduction

In recent years an increasing interest is paid to investigation of the properties of internal gravity waves (IGW), arising as a result of vertical density stratification of the gas, and play an important role in the dynamics of both the lower and upper atmosphere and ionosphere of the earth and other planets. Grown interest, first of all, is caused primarily due to the understanding of the fact that these waves can

propagate over hundreds or thousands of kilometers from the source without significant attenuation. Propagating with group velocity the IGW provide an efficient transfer of energy, heat and momentum from the troposphere into the upper atmosphere (which exceeds even the energy supplied by the solar wind), where they influence on the thermal and dynamic regimes (Francis, 1975; Kim and Mahrt, 1992; Nakamura et al., 1993; Rishbeth

and Fukao, 1995; Fritts et al., 2006; Alexander et al., 2008; Hecht et al., 2009; Alexander, 2010). Latest numerical experiments (Gavrilov and Fukao, 2001; Alexander and Rosenlof, 2003; Alexander et al., 2010) show that an adequate description of climate change and the circulation of the middle atmosphere requires taking into account the accelerations of the background flows and heat inflows generated by the waves (especially by IGW) propagating from the troposphere.

Numerous theoretical and experimental studies have established that the source of IGW motions in the atmosphere and ionosphere can be: an earthquake (Liperovsky et al, 1992; Hayakawa, 1999), volcanic eruption (Cheng, Huang, 1991), magnetic and sea storms (Testud , 1970; Golitsyn et al, 1975), hurricanes, typhoons, tornadoes, (Kuester et al., 2008; Ming et al., 2010), the solar eclipse (Chimonas and Hines, 1971), jet flows (Bertin, et al. , 1978), the terminator (Burmaka et al, 2003), spans of meteors (Pokhotelov et al., 1995), launching of powerful rockets (Burmaka et al, 2003), the polar and equatorial current systems (Chimonas and Hines, 1970), as well as industrial, military and nuclear explosions of big strength (Tolstoy and Herron, 1970; Drobjev et al, 1986; Shaefer et al., 1999)).

One of the important properties of IGW is their significant influence on the distribution of the electromagnetic waves in atmospheric-ionosphere layers (Rastogi, 1981; Gershman, 1974). Consequently, ionosphere electric currents and electromagnetic fields may re-influence the wave properties of IGW at ionosphere altitudes. In the ionosphere, in contrary to the lower layers of the atmosphere, investigating the dynamics of wave processes non-uniform and non-stationary properties of the wind process, the turbulent state of the lower ionosphere and the influence of non-uniform electromagnetic forces should be taken into account. These factors, which are due to the low density medium in the ionosphere and the relatively high conductivity of the ionosphere gas, are strongly pronounced and they can sufficiently affect the propagation characteristics of wave patterns. Consequently, the general circulation in the ionosphere must have specific features that are absent in the troposphere.

The stationary problem of the existence of ionosphere wave disturbances in case of rectilinear uniform medium flow (for large-scale Rossby type waves) has been discussed for the first time in the work of Dokuchaev (1959). It has been revealed that in the theoretical study and interpretation of the dynamics of the winds above 100 km it is necessary to consider the possible deviations from the geostrophic winds associated with the action of electromagnetic forces. Further, a number of other works have appeared (Hines and Reddy, 1967; Aburdjania and Khantadze, 2002; Aburjania et al., 2005; Aburjania et al., 2006 and others), which studied the non-stationary evolution of wind structure in the conducting ionosphere medium under the influence of the spatially non-uniform geomagnetic field.

The action of the geomagnetic field, on the one hand, leads to the inductive damping of the waves associated with Pedersen or transverse (with respect to the geomagnetic field) conductivity, on the other one - to the gyroscopic effect due to the Hall conductivity of the ionosphere acting on the perturbation like the Coriolis force. As a result of the joint action of spatially non-uniform Coriolis and electrodynamic (related to the geomagnetic field) forces the new type waves with different characteristics from the usual waves in the neutral medium may exist in the ionosphere. These waves can be called as magnetized waves.

The results of long-term observations (Gossard and Hook, 1975; Kazimirovskii and Kokourov, 1979; Pedloski, 1979) also show that at the atmospheric-ionospheric layers the spatially non-uniform zonal winds - the shear flows are permanently present, produced by nonuniform heating of the atmospheric layers by the solar radiation. In this context the problem of the generation and evolution of

ordinary and magnetized waves at different layers of the atmosphere during their interaction with non-uniform zonal wind (shear flow) becomes urgent.

Interest to the shear flows, in general, is due to their widespread implementation in the near-Earth space (as noted above), astrophysical objects (galaxies, stars, jet emissions, oceans, etc.), and in the laboratory and technical equipments (pipelines, gas pipelines in the plasma magnetic traps, magnetohydrodynamic generators, etc.). The shear velocity represents a powerful source of various energy-consuming processes in the continuum. Canonical (modal) approximation of the linear wave processes - the spectral decomposition of the perturbations according to time with further analysis of Eigen values in the shear flows looses from the sight very important physical processes such as: transient amplification and mutual transformation of the linear wave modes (Reddy et al., 1993; Trefenthen et al., 1993).

A rigorous mathematical description of the specifics of the shear flows found out (Reddy et al., 1993) that at the canonical (modal) analysis of the linear processes the operators in the dynamic equations are not self-adjoint (Trefenthen et al., 1993) and, consequently, the eigen functions do not create orthogonal system, they hardly interfere with each other. This circumstance, for correct description of the phenomena, makes it necessary to estimate the results of interference of the eigen functions, which sometimes presents a huge problem.

There is another approach - so-called non-modal analysis of linear processes in the shear flows. In this approach a modified initial value problem (Cauchy problem) is solved by tracing the temporal evolution of spatial Fourier harmonics (SFH) perturbations without any spectral expansion in time (Graik and Criminale, 1986; Chagelishvili et al., 1996). Being the optimal language, the non-modal approximation greatly simplifies the mathematical description of the linear dynamics of disturbances in shear flows and allows identification of the key events (due to the non-orthogonality of the linear dynamics) that escaped from the view in a modal analysis.

In this paper we study the linear and nonlinear stages of evolution of IGW in shear zonal flows (winds) in different regions of the ionosphere. At the initial linear stage in the dynamic equations the perturbed hydrodynamic quantities are given by SFH, which corresponds to non-modal analysis in a moving coordinate system along the background wind. Non-modal mathematical analysis allows replacement of the spatial non-uniform nature of the perturbed quantities, associated with the basic zonal flow, by temporal one in the basic equations and trace the evolution of SFH disturbances according to time.

Currently, the results of numerous observations and experiments reveal the wave motion in a wide range of frequencies from the acoustic to the planetary ones in the atmosphere-ionosphere environment on almost all altitudes. In atmospheric acoustics the focus is laid on the study of internal gravity waves (IGW), representing fluctuations of atmospheric and ionospheric layers, the nature of which is mostly determined by gravity force. These oscillations are going with the frequency, at which the wave speed is comparable with the acceleration of gravity force. Therefore, for definiteness, we assume that their periods range from 5 minutes to 3 hours, and the wavelengths - from 100 m to 10 km.

In this paper, a property of internal gravity waves presents particular interest to us - propagating vertically up quite easily in an isothermal atmosphere, IGW tends to increase the amplitude of the hydrodynamic velocity exponentially with height, which follows from the conservation of energy when the density of the medium decreases with height growth (Hines, 1960; Gossard and Hook, 1975). Thus, even for the waves, the initial amplitude of which is small, the nonlinear effects at sufficiently high altitude becomes significant and must be taken into account. Indeed, it is clear that this growth can not be continued indefinitely. At some heights velocity becomes so large that the nonlinear effects can join the game. These effects stop the growth of the oscillation amplitude through the nonlinear interaction between the modes, the perturbations' energy redistribution (saturation of the waves) and, for example, self-organization of IGW vortex structures (Aburdjania, 1996, 2006). Nonlinear vortex structures transfer the trapped particles of the medium. Reaching the critical heights, the IGW structures, interacting with each other and medium, may form the atmospheric turbulence (Waterscheid and

Schubert, 1990), that creates real threats to aviation safety, but also leads to a mix of chemicals, released from the lower atmosphere, chemical reactions between them and the formation of potentially harmful compounds (Friedrich et al., 2009). Therefore, the IGW structures may also influence the formation of "space weather" by generating irregularities in the ionosphere (Schunk and Sojka, 1996).
The aim of this paper is theoretical investigation of the peculiarities of generation; intensification and further nonlinear stage of evolution of IGW structures due to the presence of local inhomogeneous zonal wind (shear flow). Section 2 explains the model of the medium and basic hydrodynamic equations for the lower ionosphere. In Sec. 3 we briefly outline the main principles of non-modal mathematical analysis and simulation results of the generation and intensification of magnetized IGW in the linear stage. In section 4, a model of the nonlinear hydrodynamic equations for the lower ionosphere is displayed, which describes the interaction of magnetized IGW structures with a shear flow. In Sec. 5 we examine the issue of the stability of the waves in shear flow and derive a necessary condition for instability. Generation mechanism of nonlinear vortex structures by non-uniform zonal wind is analyzed in Section 6. In Section 7 we study the characteristics of energy transfer by the IGW structures in the dissipative ionosphere with the shear flow. Discussion of the results is carried out in Section 8.

2. Model of environment and initial dynamic equation

Let's introduce a local system of Cartesian coordinates x, y, z with the axis x directed to the east, y axis − to the north and the z axis −vertically. We are interested in low-frequency wave motions in the ionosphere medium (consisting of electrons, ions and neutral particles) with $\omega << kc_s$ (where ω and k− the characteristic frequency and wave number of perturbation, respectively; $c_s = (\gamma P_0 / \rho_0)^{1/2}$ −the speed of sound, $\gamma = c_p / c_V$ −the ratio of specific heats, P_0 −the equilibrium gas-kinetic pressure, ρ_0 −the equilibrium density of the medium) with a horizontal spatial scale L_h of order of 10km, the vertical scale L_v is much smaller than the scale height H ($L_v << H = d\ln\rho_0 dz = c_s^2/(\gamma g)$) and the time scale τ of the order of 5 minutes $\le \tau <$ 3 hours. Herewith, the dynamic properties of this medium, and movements of the large step anew are determined by a neutral component, because of the condition $N_{e,i} / N_n << 1$ (where $N_e, N_i = N$ and N_n- the concentration of electrons, ions and neutral components, respectively). The presence of charged particles causes the electrical conductivity of the medium and the appearance of the electromagnetic Ampere force.
For considered class of perturbations the effective magnetic Reynolds number is relatively small $R_{eff} \approx \mu_0 \sigma_{eff} V \cdot L << 1$ (where μ_0 is the permeability of free space, σ_{eff} is the effective conductivity of the ionosphere, V and L- characteristic values of velocity and perturbations, respectively), which is quite well done almost right up to F-layer of the ionosphere (Gershman, 1974; Dokuchaev, 1959; Kamide and Chian, 2007). Consequently, for the lower ionosphere, we can neglect the induced magnetic field $\mathbf{b} \approx R_{eff}\,\mathbf{B}$ and the vortical electric field $E_v \sim R_{eff}(VB)$ that arise by virtue of variation of $\mathbf{b}$. Consequently, for the class of wave perturbations the magnetic field can be assumed given and equal to the external, spatially non-uniform geomagnetic field $\mathbf{B_0}(\mathbf{B} = \mathbf{b} + \mathbf{B_0} \approx \mathbf{B_0}, \mathbf{E_v} \to 0)$. It satisfies the equation $\mathrm{div}\mathbf{B}_0 = 0,\ \mathrm{rot}\mathbf{B}_0 = 0.$ At such induction free approximation consideration only of the current $\mathbf{j}$ is sufficient, arisen in the medium, ignoring the magnetic field generated by this current. In this case, the effect of geomagnetic field $\mathbf{B}_0$ on the induced current $\mathbf{j}$ in the ionosphere

plasma leads to consideration of the electromagnetic Ampere force $\left[\mathbf{j}\times\mathbf{B}_0\right]$ in the known equations of the dynamics of the ionosphere (in addition to forces: pressure, Coriolis and viscous frictions). This force causes the inductive damping (due to Pedersen currents) in the ionosphere of the earth, not less significant than usually viscous damping, especially in **F** region (Gershman, 1974; Dokuchaev, 1959). Based on the above discussion, the basic properties of internal gravity waves in the ionosphere is advisable to consider as the initial equation that for two-dimensional motion in the plane (x, z) ($\partial/\partial y = 0$; with velocity $\mathbf{V}(V_x, 0, V_z)$, where it's assumed the acceleration to be defined due to the gravity acceleration, pressure gradient, Coriolis forces, the volumetric electrodynamic and viscous frictions (Gershman, 1974; Dokuchaev, 1959; Gossard and Hook, 1975).

$$\frac{\partial \mathbf{V}}{\partial t} + (\mathbf{V}\nabla)\,\mathbf{V} = -\frac{\nabla \mathbf{P}}{\rho} + \mathbf{g} - 2\left[\mathbf{\Omega}_0 \times \mathbf{V}\right] + \frac{1}{\rho}\left[\mathbf{j}\times\mathbf{B}_0\right] + \nu\Delta\,\mathbf{V}, \qquad (1)$$

For exclusion of high-frequency acoustic modes, let's use the condition of incompressibility of medium

$$\nabla \cdot \mathbf{V} = 0. \qquad (2)$$

Then, the continuity equation can be chosen as the equation of medium density in the form:

$$\frac{d\rho}{dt} = \frac{\partial \rho}{\partial t} + \left(\mathbf{V}\nabla\right)\rho = 0 \qquad (3)$$

and the medium state equation:

$$\frac{\partial P}{\partial t} + \left(\mathbf{V}\nabla\right)P = 0. \qquad (4)$$

Here, as usual, $\rho = N_n M = \rho_0(z) + \rho'(x,z,t)$ is the density, $P = P_0(z) + P'(x,z,t)$ −pressure, $\mathbf{g} = -g\,\mathbf{e_z}$ − the gravity acceleration; $\mathbf{e_z}$ − the unit vector along the vertical direction, i.e. along the axis z. Variables with index zero mean atmospheric parameters in the unperturbed state, and values with a prime − the disturbed ones (hereinafter, for simplicity, the primes are omitted from the quantities). M is a mass of the ion and neutral particles (molecules), ν - kinematic viscosity, $\Delta = \partial^2/\partial x^2 + \partial^2/\partial z^2$ − two-dimensional Laplacian. Electromagnetic force $\left[\mathbf{j}\times\mathbf{B}_0\right]$ largely determines the specificity of ionosphere motions (Aburjania et al., 2006). Induced current density is determined from the generalized Ohm's law for the ionosphere (Gershman, 1974):

$$\mathbf{j} = \sigma_{\parallel}\,\mathbf{E}_{d\parallel} + \sigma_{\perp}\,\mathbf{E}_{d\perp} + \frac{\sigma_H}{B_0}[\mathbf{B}_0 \times \mathbf{E}_d], \qquad (5)$$

where the parallel $\sigma_{\parallel}$ (in the direction of the magnetic field $\mathbf{B}_0$), Pedersen or transverse σ_P (transverse to $\mathbf{B}_0$) and the Hall conductivities σ_H are determined by the following expressions

$$\begin{aligned}
\sigma_{\parallel} &= e^2 N\left(\frac{1}{m\nu_e} + \frac{1}{M\nu_{in}}\right),\\
\sigma_P &= e^2 N\left\{\frac{\nu_e}{m\left(\nu_e^2 + \omega_{Be}^2\right)} + \frac{\nu_{in}}{M\left(\nu_{in}^2 + \omega_{Bi}^2\right)}\right\}, \qquad (6)\\
\sigma_H &= e^2 N\left\{\frac{\omega_{Be}}{m\left(\nu_e^2 + \omega_{Be}^2\right)} - \frac{\omega_{Bi}}{M\left(\nu_{in}^2 + \omega_{Bi}^2\right)}\right\},
\end{aligned}$$

where e, m, $\nu_e = \nu_{ei} + \nu_{en}$, $\omega_{Be} = eB_0/m$ are charge, mass, frequency of collisions between electrons and ions and neutral molecules and electron cyclotron frequency, respectively; ν_{in} and $\omega_{Bi} = eB_0/M$ the corresponding values for the ions. Assuming the ionosphere to be quasi-neutral with a high degree of accuracy, we have neglected the electrostatic $\mathbf{E}_e = -\nabla\Phi$ (Φ - electrostatic potential) and vortex parts $\mathbf{E}_v$ of the electric field. Thus, in Eq. (5) the electric field strength, taking into account the medium motion, is determined only by dynamo - field (Gershman, 1974; Dokuchaev, 1959)

$$\mathbf{E}_d = [\mathbf{V} \times \mathbf{B}_0]. \qquad (7)$$

Geomagnetic field $\mathbf{B}_0(B_{0x}, B_{0y}, B_{0z})$ is considered to be dipole, which in chosen coordinate system has the following components (Dokuchaev, 1959)

$$B_{0x} = 0, \quad B_{0y} = -B_e \sin\theta', \quad B_{0z} = -2B_e \cos\theta', \qquad (8)$$

where $B_e \approx 3,5 \times 10^{-5}$ Tesla (T) is a value of the geomagnetic field induction at the equator. In this case, the full geomagnetic field induction is $B_0 = B_e\left(1 + 3\cos^2\theta'\right)^{1/2}$ and $\theta' = \pi/2 - \varphi'$, φ' – geomagnetic latitude. In the same coordinate system for the components of the angular velocity of the Earth rotation $\mathbf{\Omega}_0\left(\Omega_{ox}, \Omega_{oy}, \Omega_{oz}\right)$ it can be written

$$\Omega_{0x} = 0, \quad \Omega_{0y} = \Omega_0 \sin\theta, \quad \Omega_{0z} = \Omega_0 \cos\theta \qquad (9)$$

Further it's assumed that the geographic $\phi = \pi/2 - \theta$ and geomagnetic φ' latitudes are coinciding and the perturbation is located near latitude $\varphi_0 = \pi/2 - \theta_0$.

The equilibrium density of the medium is stratified due to gravitational forces. Therefore, in the thermosphere, the equilibrium density ρ_0 varies exponentially according to altitude

$$\rho_0(z) = \rho(0)\exp\left(-\frac{z}{H}\right) \qquad (10)$$

For definiteness, we will consider ionosphere E-region, which is located at altitudes of $80-150$ kilometers from the Earth's surface. In this region the equilibrium parameters of the medium have the following hierarchy: $\nu_e \approx \nu_{en}$; $\omega_{Be}\omega_{Bi} >> \nu_{in}\nu_{en}$ and $\nu_{in} >> \omega_{Bi}$, which allows simplification of the expression for the induced current (5). Herewith, the condition $\nu_{in} >> \omega_{Bi}$ means that the ions are un-magnetized and their speed across the geomagnetic field coincides with the velocity of the neutrals (Aburjania et al., 2005), i.e. ions are completely entrained by the neutral ionospheric winds. However, the electrons are magnetized $\omega_{Be} >> \nu_{en}$, and they are frozen in the geomagnetic field. In this case, the Hall $\sigma_H = en/B_0$ and Pedersen σ_P conductivities are subject of the following inequality $\sigma_P \approx \sigma_H\omega_{Bi}/\nu_{in} << \sigma_H$ (Aburjania et al., 2005). For numerical calculations we use typical values of the medium parameters (Gershman, 1974; Ginzburg and Rukhadze, 1975): $N/N_n \sim 10^{-8} - 10^{-6}$, $\nu_{ei} \sim 10^3 c^{-1}$, $\nu_{en} \sim 10^4 c^{-1}$, $\nu_{in} = 10^3 c^{-1}$, $\nu_{en} \sim 10^4 c^{-1}$, $\omega_{Be} \sim 10^7 c^{-1}$, $\omega_{Bi} \sim 10^2 s^{-1}$, $\sigma_H \approx 3\times10^{-4} S/m$ and $\sigma_P \approx 10^{-4} S/m$. In the equation of the ionosphere motion (1) the part of the contribution of the Lorentz force eNB_0/ρ_0 is associated with the Hall currents and the total contribution of the Coriolis force $2\Omega_0$ has the same order $\sim 10^{-4} s^{-1}$. In addition, we take into consideration that the ratio N/ρ_0 does not depend on the vertical coordinate (height) z (Gershman, 1974). Herewith, the characteristic frequency of IGW ($\omega \sim 10^{-2} c^{-1}$) is significantly higher than the Coriolis and Hall's gyroscopic frequencies. Based on these estimations, we can conclude that the contributions of the full Coriolis and

Lorentz forces, associated with the Hall currents, have negligible impact on the dynamic properties of IGW. However, inductive damping, stipulated by Pedersen conductivity (especially in the F-region), as well as viscous damping, can not be neglected how small they can be. In investigation of the dynamics of wave disturbances in shear flows they are important as a way of redistribution of energy of the system that provides sustainable self-maintaining of the nonlinear solitary structures in the medium.
Further, the motion equation can still be more simplified if we consider the fact, that perturbation of the medium density by internal gravity waves does not exceed $3-4\%$ (Gossard and Hook, 1975; Gill, 1982). Accordingly, ratio of the perturbed density with the unperturbed one has the order $\rho'/\rho_0 \sim (1-4)\times 10^{-2}$. Based on the aforementioned, in the initial equation of motion (1) we can neglect ρ' in comparison with $\rho_0(z)$ before the inertial, Coriolis and viscous terms and using the Boussinesq approximation, we obtain the following motion equation:

$$\rho_0(z)\left(\frac{\partial \mathbf{V}}{\partial t}+(\mathbf{V}\nabla)\mathbf{V}\right)=-\nabla P+\rho\,\mathbf{g}-\sigma_P B_0^2\left(\mathbf{V}-B_0\frac{(\mathbf{V}\cdot B_0)}{B_0^2}\right)+\rho_0(z)\nu\Delta\mathbf{V} \qquad (11)$$

The system of equations (3), (4) and (11) presents the initial closed system of equations for both linear and nonlinear dynamics of IGW in their interaction with the geomagnetic field in the dissipative ionosphere (D, E, and F -regions).

3. Generation and intensification of IGW at linear stage of evolution

To study the linear stage of interaction of internal gravity waves with the local non-uniform zonal wind and geomagnetic field, let's linearize the system of equations (3), (4) and (11) on the background of a plane zonal shear flow (wind), which has the velocity $\mathbf{V}_0(z)$, non-uniform along the vertical: $\mathbf{V}=\mathbf{V}_0(z)+\mathbf{V}(x,z,t)$, $\rho=\rho_0(z)+\rho(x,z,t)$, $P=P_0(z)+P(x,z,t)$. Here $\mathbf{V}_0(z)$ is the background zonal wind velocity which for the vertical shear flow is given as:

$$\mathbf{V}_0(z)=v_0(z)\,\mathbf{e_x}=A\cdot z\cdot\mathbf{e_x}, \qquad (12)$$

where $A>0$ - constant parameter of the wind shear, $\mathbf{e_x}$ - a unit vector directed along the axis x.
In the selected local rectangular coordinate system for the components (11), (2), (3) and (4) we obtain the following system of linear equations:

$$\rho_0\left(\frac{\partial}{\partial t}+v_0(z)\frac{\partial}{\partial x}\right)V_x=-\frac{\partial P}{\partial x}-\rho_0 v_0'(z)V_z-\sigma_P B_0^2 V_x+\rho_0\nu\Delta_\perp V_x, \qquad (13)$$

$$\rho_0\left(\frac{\partial}{\partial t}+v_0(z)\frac{\partial}{\partial x}\right)V_z=-\frac{\partial P}{\partial z}-\rho_0 g-\sigma_P B_y^2 V_z+\rho_0\nu\Delta_\perp V_z, \qquad (14)$$

$$\left(\frac{\partial}{\partial t}+v_0(z)\frac{\partial}{\partial x}\right)\rho=-\frac{d\rho_0}{dz}V_z, \qquad (15)$$

$$\left(\frac{\partial}{\partial t}+v_0(z)\frac{\partial}{\partial x}\right)P=-\frac{dP_0}{dz}V_z, \qquad (16)$$

$$\frac{\partial V_x}{\partial x}+\frac{\partial V_z}{\partial z}=0. \qquad (17)$$

Here $v_0'(z)=dv_0(z)/dz$. In this system of five equations (13) - (17) any four of them creates a closed system. To facilitate further research, we choose equation (13), (14), (15) and (17) as a closed system.

3.1. *The local dispersion equation*

The system of equations (13) - (17) presents partial differential equations with variable coefficients, depending on the spatial coordinate z. Therefore, to analyze the existence of nontrivial solutions at least at the initial stage of the evolution of wave disturbances, a local approximation is necessary, when the coefficients of equations (13) - (17) can be assumed locally uniform (constant). Then, for analyzes of the spectral characteristics, described by these equations of the disturbances, the Fourier expansion should be performed according to the spatial and temporal variables (Mikhailovskii, 1974). In Consequence to the exponential fall of the equilibrium density of the medium (10) with height, we seek a solution of equations (13) - (17) in the form of plane waves (Hines, 1960; Golitsyn, 1965; Gossard and Hook, 1975):

$$V_{x,z}(x,z,t) = \int V_{x,z}(k_x,k_z)\exp\{i[k_x x + (k_z - i/2H)z - \omega t]\}dk_x dk_z,$$
$$(P,\rho)(x,z,t) = \int (P,\rho)(k_x,k_z)\exp\{i[k_x x + (k_z + i/2H)z - \omega t]\}dk_x dk_z, \qquad (18)$$

where the spatial Fourier expansion of the wave disturbances is carried out; $\mathbf{k}\,(k_x,0,k_z)$ — wave vector and $\omega\,(k_x,k_z)$ - frequency of the waves. Inserting (18) into equations (13) - (15) and (17), we obtain the following dispersion equation:

$$(\omega - k_x v_0)^2 - \frac{k_x^2}{K^2}\omega_g^2 + i\frac{(\omega - k_x v_0)}{K^2}\left[k_x^2\left(\frac{\sigma_P B_{0y}^2}{\rho_0} + \nu K_1^2\right) - k_x\left(k_z + \frac{i}{2H}\right)v_0' + \left(k_z^2 + \frac{1}{4H^2}\right)\left(\frac{\sigma_P B_0^2}{\rho_0} + \nu K_1^2\right)\right] = 0. \qquad (19)$$

Here, we introduce the notation: $\omega_g = (g/H)^{1/2} > 0$ — frequency of Brunt-Vaisala for stably stratified incompressible isothermal atmosphere; $K^2 = k_x^2 + k_z^2 + 1/(4H^2)$, $K_1^2 = K_2^2 - ik_z/H$, $K_2^2 = k_x^2 + k_z^2 - 1/(4H^2)$, . Assuming the wave number K to be real and frequency $\omega = \omega_0 + i\gamma$, $|\gamma| << \omega_0$ to be complex, from (19) we get the expressions for the spectrum of linear fluctuations

$$\frac{\omega_0}{k_x} = v_0 - \frac{v_0'}{4K^2H^2} \pm \frac{\omega_g}{K}\sqrt{1 + \frac{v_0'^2}{16K^2H^2\omega_g^2}}, \qquad (20)$$

and decrement (increment) of the perturbations

$$\gamma = -\frac{k_x^2\left(\frac{\sigma_P B_{0y}^2}{\rho_0} + \nu K_2^2\right) + \left(k_z^2 + \frac{1}{4H^2}\right)\left(\frac{\sigma_P B_0^2}{\rho_0} + \nu K_2^2\right) - k_x k_z v_0'}{2K^2\left[1 + \frac{k_x v_0'}{4K^2H(\omega_0 - k_x v_0)}\right]} \qquad (21)$$

In the absence of shear flow the formula (20) transforms into the expression for the frequency of ordinary internal gravity waves (Golitsyn, 1965):

$$\omega_0 = \pm\frac{k_x\omega_g}{\left(k_x^2 + k_z^2 + 1/(4H^2)\right)^{1/2}}. \qquad (22)$$

Formula (21) expresses the damping decrement of IGW due to induction (Pedersen) and viscous damping in the ionosphere medium:

$$\gamma = -\frac{k_x^2\left(\frac{\sigma_P B_{0y}^2}{\rho_0}+\nu K_2^2\right)+\left(k_z^2+\frac{1}{4H^2}\right)\left(\frac{\sigma_P B_0^2}{\rho_0}+\nu K_2^2\right)}{2K^2}, \qquad (23)$$

According to (22), phase velocity of linear IGW is in the range:

$$-V_{max} \le V_p \le V_{max}, \qquad (24)$$

where $V_{max} = 2H\omega_g = 2(gH)^{1/2}$ in incompressible atmosphere. IGW is a low-frequency branch of acoustic-gravity waves (AGW), occupying an intermediate position between the frequency of inertial oscillations $\omega_i = 2\Omega_0$ and the frequency of the Brunt-Vaisala for stably stratified incompressible isothermal atmosphere ω_g, $\omega_i < \omega_0 < \omega_g$ (Gershman, 1974; Gossard and Hook, 1975). For the height of the uniform atmosphere $H \approx 4.5 \div 6$ km, we can estimate the value of maximal phase velocity of linear IGW $V_{max} \approx 440$ m/s, the frequency $\omega_g \approx 1.7\times10^{-2}$ and $\Omega_0 \approx 10^{-4}$. So, IGW disturbances cover the following range of low-frequency oscillations $10^{-4}\,c^{-1} < \omega < 1.7\times10^{-2}\,c^{-1}$ - and can be supersonic $V_p \ge c_s \approx 330$ m/s.

Considered waves have frequency limit ω_g and gravitational effects play an important role for them, as reflected in their name - IGW. From (22), it follows that for practically important case of relatively short waves, $k_z^2 >> k_x^2$ and $k_z H >> 1$, and phase ($\mathbf{V_p} = (\omega/k^2)\,\mathbf{k}$) and group ($\mathbf{V_g} = \nabla_{\mathbf{k}}\omega$) the velocities of IGW in the windless atmosphere are given by:

$$V_{px} = \frac{\omega_g k_x^2}{k_z^3}, \quad V_{pz} = \frac{\omega_g k_x}{k_z^2}; \quad V_{gx} = \frac{\omega_g}{k_z}, \quad V_{gz} = -\frac{\omega_g k_x}{k_z^2}. \qquad (25)$$

It is evident that short IGW possess strong spatial dispersion. The direction of the phase velocity is close to vertical, $|V_{pz}| >> |V_{px}|$, and the group speed is almost horizontal, $|V_{gx}| >> |V_{gz}|$. In the long-wave case $k_z H << 1$, IGW is almost dispersion-less.

Let's estimate appropriate wavelengths for IGW in the dissipative ionosphere. At ground level the kinematic molecular viscosity is determined as $\nu_0 \approx 1.3\times10^{-5}\,m^2/s$, at the level of the E-layer (~110 km) $-\nu_{110} \approx 1.3\times10^{2}\,m^2/s$ and at the level of the F-layer ((250-300)km) $-\nu_{300} \approx 1.3\times10^{6}\,m^2/s$ (Gossard and Hook, 1975). Appropriate minimal lengths of IGW with period 10 minute in the presence of kinematic viscosity for near Earth regions is $\lambda_0 \sim 10^{-1}$ m and with the height growth will increase correspondingly an appropriate minimal IG wavelength and for E-layer it would be $\lambda_{110} \sim 10$ m, for F-layer $-\lambda_{300} \sim 10$ km (Gossard and Hook, 1975). Coming through this and taking into account that the turbulent viscosity in the low atmosphere increases the IGW scale [Gossard and Hook, 1975], further we will consider the gravitational waves, the wavelengths of which fall into the range 100 m $\le \lambda \le 10$ km.

Let us estimate the damping rate of IGW. For ground level the parameters of the medium and the waves are $\sigma_p \cong 5\times10^{-7}$ S/m, $\rho_0 = 1.3$ kg/m^3, $B_0 = 0.5\times10^{-4}$ T, $\lambda \approx 10^4$ m, $\nu_0 \approx 1.3\times10^{-5}\,m^2/s$ and according to (21), viscous damping decrement of IGW structures is $\gamma_{\nu,0} \approx k^2\nu \sim 5\times10^{-12}$ s^{-1}, the decrement of the induction decay $-\gamma_{\sigma,0} \approx \sigma_p B_0^2/\rho_0 \sim 10^{-15}$ s^{-1}. For E-layer the parameters of the medium and the waves are $\sigma_p \cong 3\times10^{-4}$ S/m, $\rho_0 = 10^{-10}$ kg/m^3, $B_0 = 0.5\times10^{-4}$ T, $\lambda \approx 10^4$ m,

$\nu_{110} \approx 1.3\times10^{2}\,\mathrm{m^2/s}$: $\gamma_{\nu,110} \approx k^2\nu \sim 5\times10^{-5}\ \mathrm{s^{-1}}$, $\gamma_{\sigma,110} \approx \sigma_p B_0^2/\rho_0 \sim 10^{-3}\ \mathrm{s^{-1}}$. For F-layer we use the typical values of parameters $\sigma_H \approx en/B_0 \sim 10^{-4}$ S/m, $\sigma_p \approx \sigma_H\omega_{ci}/\nu_{in} \sim \sigma_H$, $\omega_{ci} \sim 3\times10^{2}\ \mathrm{s^{-1}}$, $\nu_{in} \le 10\ \mathrm{s^{-1}}$, $\nu_{300} \approx 1.3\times10^{6}\,\mathrm{m^2/s}$. For damping rates we obtain correspondingly: $\gamma_{\nu,300} \sim 10^{-1}\ \mathrm{s^{-1}}$, $\gamma_{\sigma,300} \sim 10^{-3}\ \mathrm{s^{-1}}$. So, at the different levels of ionosphere the values of the viscous and induction damping of IG structures are different, and it should be considered in dynamic problems involving IGW structures.

It should be noted, that according to (20), the non-uniform zonal wind greatly expands the range of IGW in the ionosphere. Moreover, the shear flow feeds the medium with energy (see formula (21)), which is responsible for the generation-swing of IGW and development of linear shear instability with a characteristic growth rate:

$$\gamma_A \sim \frac{k_x k_z}{K^2} A\,. \qquad (26)$$

From (23) it's obvious, that considered ionospheric shear flow can become the source of the instability at the condition $\gamma_A \ge \gamma_\nu, \gamma_\sigma$. According to (26), for generation of the IGW structures it is necessary the shear flow velocity to have even first derivative according to the vertical coordinate, different from zero ($v_0'(z) = A \ne 0$). As it was mentioned in the works (Margetroyd, 1969; Mayer et al., 1990), the typical value of the dimensional parameter of the shear flow $(A)\ \mathrm{s^{-1}}$ for the ionospheric F-region equals $A = v_0' \approx (0.015 \div 0.15)\mathrm{s^{-1}}$ as well. Taking it into account from (26) we obtain $\gamma_A \ge 10^{-1}\mathrm{s^{-1}}$. Thus, the condition of the generation and amplification of IGW perturbations (inequality $\gamma_A \ge \gamma_\nu, \gamma_\sigma$) in the different levels of the ionosphere (especially, in D and E -regions) can be satisfied and the shear instability can be developed. This conclusion can be made by virtue of above used modal (local - spectral) approach, which can't give more information about the features of the shear flow instability. But this doesn't mean that such instability always arises and remains in such form. This is exactly due to non-adequacy of modal approach at investigation of the features of shear flows, which is already considered in the introduction. In shear flows the modal approach can detect only possibility of instability. But for investigation of instability generation conditions and its temporal development in the ionosphere an alternative approach, namely, non-modal mathematical analysis becomes necessary.

As it will be shown in the next section on the basis of more adequate method for such problems –non-modal approximation, shear flows can become unstable transiently till the condition of the strong relationship between the shear flows and wave perturbations is satisfied (Chagelishvili et al., 1996; Aburjania et al., 2006), e. i. the perturbation falls into amplification region in the wave number space. Leaving this region, e. i. when the perturbation passes to the damping region in the wave vector space, it returns an energy to the shear flow and so on (if the nonlinear processes and self-organization of the vortex structure will not develop before) (Aburjania et al., 2010). The experimental and observation data shows the same (Gossard and Hooke, 1975; Pedlosky, 1979; Gill, 1982).

Thus, non-uniform zonal wind or shear flow can generate and/or intensify the internal gravity waves in the ionosphere and provoke transient growth of amplitude, i.e. transient transport the medium into an unstable state. In the next subsection we confirm this view by using a different, more self-consistent method for the shear flow.

3.2. *Non-modal analysis of shear instability of the waves in the ionosphere*

Deriving (19) - (21) we used so-called local approximation, i.e. it is assumed that v_0, v_0', ρ_0 and P_0 are locally uniform and we have provided the Fourier expansion of the physical quantities. Local approximation has limited applicability in non-uniform environment, and especially in the shear flows

(Mikhailovskii, 1974). In particular, the results received at such approximation are applicable only for the initial stage of evolution of the perturbations. In general, if the background flow is spatially non-uniform along the vertical, then we are not to provide Fourier expansion along the axis z. According to the papers (Graik et al., 1986; Reddy et al., 1993; Trefenthen et al., 1993; Chagelishvili et al., 1996; Aburjania et al., 2006), when studying the evolution of wave disturbances in shear flows at the linear stage the non-modal mathematical analysis is better to be used than a modal approach (i.e. direct Fourier expansion). Therefore, further analysis of the features of magnetized IGW wave at the linear stage in the ionosphere should be conducted in accordance with a non-modal approach. For this purpose, the moving coordinate system $X_1O_1Y_1$ is more convenient with origin O_1 and the axis Y_1, which coincides with the same characteristics of the equilibrium local system XOY, the axis X_1 flowing along the unperturbed (background) wind. In our problem, this transformation of the coordinate system is equivalent to the following replacement of the variables:

$$x_1 = x - azt, \quad y_1 = y, \quad t_1 = t, \tag{27}$$

or

$$\frac{\partial}{\partial t} = \frac{\partial}{\partial t_1} - az\frac{\partial}{\partial x_1}, \quad \frac{\partial}{\partial x} = \frac{\partial}{\partial x_1}, \quad \frac{\partial}{\partial z} = \frac{\partial}{\partial z_1} - at_1\frac{\partial}{\partial x_1}. \tag{28}$$

With these new variables equation (13), (14), (15) and (17) take the form

$$\rho_0\frac{\partial V_x}{\partial t_1} = -\frac{\partial P}{\partial x_1} - \rho_0 v_0' V_z - \sigma_P B_0^2 V_x + \nu\rho_0\left\{\frac{\partial^2}{\partial x^2} + \left(\frac{\partial}{\partial z_1} - at_1\frac{\partial}{\partial x_1}\right)^2\right\}V_x, \tag{29}$$

$$\rho_0\frac{\partial V_z}{\partial t_1} = -\left(\frac{\partial}{\partial z_1} - At_1\frac{\partial}{\partial x_1}\right)P - \rho_0 g - \sigma_P B_{0y}^2 V_z + \nu\rho_0\left\{\frac{\partial^2}{\partial x^2} + \left(\frac{\partial}{\partial z_1} - at_1\frac{\partial}{\partial x_1}\right)^2\right\}V_z, \tag{30}$$

$$\frac{\partial\rho}{\partial t_1} = \frac{\rho_0}{H}V_z, \tag{31}$$

$$\frac{\partial V_x}{\partial x} + \left(\frac{\partial}{\partial z_1} - At_1\frac{\partial}{\partial x_1}\right)V_z = 0. \tag{32}$$

Coefficients of the initial system of linear equations (13) - (16) depended on the spatial coordinate z. Such mathematical transformations replace this spatial non-uniform property into temporal one (see eq. (29) - (32)). Thus, the initial-boundary problem is reduced to the initial problem of Cauchy type. Since now the coefficients of (29) - (32) are independent of spatial variables, the Fourier transformation of these equations with respect to spatial variables x_1, z_1 is already possible without any local approximation, the temporal evolution of these spatial Fourier harmonics (SFH) we consider independently:

$$\begin{Bmatrix} V_x, z(x_1, z_1, t_1) \\ \rho, P(x_1, z_1, t_1) \end{Bmatrix} = \int_{-\infty}^{\infty}\int dk_{x_1} dk_{z_1} \begin{Bmatrix} \tilde{V}_{x,z}(k_{x_1}, k_{z_1}, t_1) \\ \tilde{\rho}, \tilde{P}(k_{x_1}, k_{z_1}, t_1) \end{Bmatrix} \times \exp(ik_{x_1}x_1 + ik_{z_1}z_1). \tag{33}$$

Here the factors with a tilde (for example $\tilde{V}_x$) indicate spatial Fourier harmonics (SFH) of the relevant physical quantities. Inserting (33) into equations (29) - (32), and passing to dimensionless variables,

$$\tau \Rightarrow \omega_g t_1; \quad V_{x,z} \Rightarrow \frac{\tilde{V}_{x,z}}{\omega_g H}; \quad \rho \Rightarrow \frac{\tilde{\rho}}{\rho_0}; \quad P \Rightarrow \frac{-i\tilde{P}}{\rho_0\omega_g^2 H^2};$$

$$(x, z) \Rightarrow \frac{(x_1, z_1)}{H}; \quad S \Rightarrow \frac{A}{\omega_g}; \quad k_{x,z} \Rightarrow k_{x_1,z_1}H; \quad k_z = k_z(0) - k_x S\tau;$$

$$k^2(\tau) = (k_x^2 + k_z^2(\tau)); \nu \Rightarrow \frac{\nu}{\omega_g H^2}; \; b_0 \Rightarrow \frac{\sigma_P B_0^2}{\rho_0 \omega_g}; b_y \Rightarrow \frac{\sigma_P B_y^2}{\rho_0 \omega_g}; \tag{34}$$

for each SFH perturbed quantities, we obtain

$$\frac{\partial V_x}{\partial \tau} = -SV_z + k_x P - [b_0 + \nu k^2(\tau)]V_x, \tag{35}$$

$$\frac{\partial V_z}{\partial \tau} = k_z(\tau)P - \rho - [b_y + \nu k^2(\tau)]V_z, \tag{36}$$

$$\frac{\partial \rho}{\partial \tau} = V_z, \tag{37}$$

$$k_x V_x + k_z(\tau)V_z = 0. \tag{38}$$

Closed system of equations (35) - (38) describes the linear interaction of IGW with a shear flow and the evolution of the generated disturbances in the dissipative ionosphere medium. We note once again that after these transformations the wave vector $k(k_x, k_z(\tau))$ of the perturbation became dependent on time: $k_z(\tau) = k_z(0) - k_x S \cdot \tau$; $k^2(\tau) = (k_x^2 + k_z^2(\tau))$. Variation of the wave vector according to time (i.e. splitting of the disturbances' scales in the linear stage) leads to significant interaction in the medium even of such perturbations, the characteristic scale of which are very different from each other at the initial time (Aburjania et al., 2006).

On the basis of (35) - (37) an equation of energy transfer of the considered wave structures can be obtained, which gives possibility to identify the pattern of energy density variation with time:

$$\frac{dE(\tau)}{d\tau} = -\frac{S}{2}\left(V_x^*(\tau) \cdot V_z(\tau) + V_x(\tau) \cdot V_z^*(\tau)\right) - b_1(\tau)|V_x|^2 - b_2(\tau)|V_z|^2, \tag{39}$$

Here the asterisk denotes the complex conjugate values of the indignations, $b_1(\tau) = b_0 + \nu k^2(\tau)$, $b_2(\tau) = b_y + \nu k^2(\tau)$ and the density of the total dimensionless energy of the wave perturbations $E(\tau)$ in the wave number space is given by:

$$E[k(\tau)] = \frac{1}{2}\left(|V_x|^2 + |V_z|^2 + |\rho|^2\right). \tag{40}$$

It's obvious that the transient evolution of wave energy structures in the ionosphere is due to the shear flow $(S \neq 0, \; A \neq 0)$, dissipative processes - induction decay ($b_0 \neq 0, \; b_y \neq 0$) and viscosity ($\nu \neq 0$). In the absence of shear flow $(S = 0, \; A=0)$, and dissipative processes $(\nu = 0, \sigma_P = 0)$, the energy of the considered wave disturbances in the ionosphere conserves $dE(\tau)/d\tau = 0$. The total energy density of the perturbations (40) consists of two parts: $E[k] = E_k + E_t$, where the first term is the kinetic energy of perturbation $E_k = \left(\left|V_x\right|^2 + \left|V_z\right|^2\right)/2$, and the second - thermobaric energy $E_t = |\rho|^2/2$, stipulated due to the elasticity of perturbations.

To emphasize the pure effect of shear flow on the evolution of IGW, for simplicity, we consider non-dissipative ionosphere, i.e. we suppose that $(\nu = 0, \sigma_P = 0)$. Further, we determine on the basis of equation (39) what actually leads the evolution of the energy of the wave disturbance to – does their energy increase or decrease? To answer we must calculate the right-hand side part of equation (39). For this purpose we must find the solutions of equations (35) - (38) at $b_1 = b_2 = 0$. Differentiating (36) with respect to time and using (35) (37) and (38), we obtain the second-order equation for the vertical velocity components:

$$\frac{d^2V_z}{d\tau^2} + R_1(\tau)\frac{dV_z}{d\tau} + R_2(\tau)V_z = 0, \tag{41}$$

where

$$R_1(\tau) = -4Sk_x\frac{k_z(\tau)}{k^2(\tau)}, \quad R_2(\tau) = (2S^2+1)\frac{k_x^2(\tau)}{k^2(\tau)}. \tag{42}$$

Equation (41) can be simplified by introducing a new variable (Magnus, 1976). Assuming

$$V_z = V\exp\left[-(1/2)\int R_1(\tau')d\tau'\right]. \tag{43}$$

Let's transform (41) to the equation of a linear oscillator with time dependent parameters:

$$\ddot{V} + \Omega^2(\tau)V = 0, \tag{44}$$

where

$$\ddot{V} = \frac{d^2V}{d\tau^2}; \quad \Omega^2(\tau) = R_2(\tau) - \frac{1}{2}\dot{R}_1(\tau) - \frac{1}{4}R_1^2(\tau) = \frac{k_x^2}{k^2(\tau)}. \tag{45}$$

The equation (44) is well known in mathematical physics. This is an equation of linear oscillations of a mathematical pendulum, length of which changes. The value $\Omega(\tau)$ determines the angular velocity of the pendulum.

We solve the equation (44) in the adiabatic approximation (Zeldovich and Mishkis, 1972), i.e. when dependence of $\Omega(\tau)$ on time is adiabatically slow:

$$\left|\dot{\Omega}(\tau)\right| << \Omega^2(\tau). \tag{46}$$

Taking into account the definition of the parameter $\Omega(\tau)$ the equation (46) can be rewritten as

$$S\cdot\left|k_z(\tau)\right| << \left[k_x^2 + k_z^2(\tau)\right]^{1/2}. \tag{47}$$

For the real ionospheric shear flow $S << 1$ (see definition (34)), so it can be said that the condition (47) holds for a wide range of variations of wave numbers $\left|k_z(\tau) = k_z(0) - k_xS\tau\right|$. In other words, when the temporary variation of $\left|k_z(\tau)\right|$ is due to the linear drift of the wave vector in the space of wave numbers, the condition (46) or (47) is valid in all stages of the evolution of IGW. In this case, an approximate solution of homogeneous equation (44) can be represented as:

$$V = \frac{C}{\sqrt{\Omega(\tau)}}\exp\left[i\varphi(\tau)\right], \tag{48}$$

where $C = \text{const}$ and

$$\varphi(\tau) = \int_0^\tau \Omega(\tau')d\tau' = \frac{1}{S}\ln\left|\frac{k_z(0)+k(0)}{k_z(\tau)+k(\tau)}\right|.$$

Substituting (48) in (43), and then - into the equations (35) - (38), we can finally construct the solutions for physical quantities:

$$V_z(\tau) = \frac{V_z(0)\cdot k^2(0)}{k_x^{1/2}\cdot k^{3/2}(\tau)}\exp\left[i\varphi(\tau)\right], \tag{49}$$

$$V_x(\tau) = -\frac{V_x(0)\cdot k_z(\tau)\cdot k^2(0)}{k_x^{3/2}\cdot k^{3/2}(\tau)}\exp\left[i\varphi(\tau)\right], \tag{50}$$

$$\rho(\tau) = -i\frac{\rho(0)\cdot k^2(0)}{k_x^{3/2}\cdot k^{1/2}(\tau)}\exp\left[i\varphi(\tau)\right], \tag{51}$$

$$P(\tau) = \frac{P(0)\cdot k^2(0)}{k_x^{3/2}\cdot k^{5/2}(\tau)}\left[2Sk(\tau) - ik_z(\tau)\right]\exp\left[i\varphi(\tau)\right], \qquad (52)$$

$$k_x V_x(0) + k_z(0)V_z(0) = 0\,. \qquad (53)$$

Here, in the expressions (49) - (53) for the values of physical quantities are considered the real parts. Substituting (49) - (51) into equations (39) and (40), we obtain an expression for the normalized energy density of the Fourier harmonics:

$$\overline{E}(\tau) = \frac{E(\tau)}{E(0)} = \frac{\left(1+k_0^2\right)^2}{\left[1+(k_0 - S\tau)^2\right]^{1/2}}, \qquad (54)$$

and for the IGW energy transport equation (at $b_1 = b_2 = 0$)

$$\frac{d\overline{E}(\tau)}{d\tau} = \frac{\left(1+k_0^2\right)^2\cdot(k_0 - S\tau)}{\left[1+(k_0 - S\tau)^2\right]^{3/2}}. \qquad (55)$$

Here for the convenience of numerical analysis a new parameter $k_0 = k_z(0)/k_x$ is introduced.

Using equations (54) and (55) we can determine an expression for the increment (decrement) of the shear instability $\Gamma(\tau) = (1/\overline{E}(\tau))\cdot d\overline{E}(\tau)/d\tau$ in the non-dissipative ionosphere:

$$\Gamma(\tau) = \frac{k_0 - S\tau}{1 + (k_0 - S\tau)^2}. \qquad (56)$$

Evolution of the dimensionless normalized energy density of the SFH (54) and the increment of shear instability (56) are presented in Figures 1,2. In the initial stage of evolution when $k_0 = k_z(0)/k_x > 0$ (when $k_z(\tau) > 0$) over time τ, $0 < \tau < \tau^* = k_z(0)/(Sk_x)$, the denominator (54) decreases and, accordingly, the energy density of IGW increases monotonically and reaches its maximum value (exceeding its initial value by an order) at the time $\tau = \tau^*$. Further, at $\tau^* < \tau < \infty$ the energy density begins to decrease (when $k_z(\tau) < 0$), and monotonically returns to its initial approximately constant value. In other words, in the early stages of evolution, temporarily, when $k_z(\tau) > 0$ and IGW perturbations are in the intensification region in wave-number space, the disturbances draw energy from the shear flow and increase own amplitude and energy by an order during the period of time $0 < \tau < \tau^* = k_z(0)/(Sk_x) = 100$. Then (if the nonlinear processes and the self-organization of the wave structures are not turned on), when $k_z(\tau) < 0$, IGW perturbation enters the damping region in wave number space and the perturbation returns energy back to the shear flow over time $\tau^* < \tau < \infty$ (Fig. 1, 2) and so on. Such transient redistribution of energy in the medium with the shear flow is due to the fact that the wave vector of the perturbation becomes a function of time $k = k(\tau)$, i.e. disturbances' scale splitting takes place. The structures of comparable scales effectively interact and redistribute free energy between them. Taking into account the induction and viscous damping (see equation (39)) the perturbation's energy reduction in the time interval $\tau^* < \tau < \infty$ is more intensive than that shown on fig. 1, the decay curve in the region $\tau^* < \tau < \infty$ becomes more asymmetric (right-hand side curve becomes steeper), and part of the energy of the shear flow passes to the medium in the form of heat.

Thus, even in a stable stratified ionosphere ($\omega_g^2 > 0$), temporarily, during the time interval $0 < t^* \approx 100/(\omega_g) \sim 5\cdot 10^3\,s \approx 1.5$ hour IGW-intensively draws energy from the shear flow and increases own energy and amplitude by an order. Accordingly, the wave activity will intensify in the given region of the ionosphere due to the shear flow (inhomogeneous wind) energy.

4. Nonlinear model dynamic equation for internal gravity waves in the ionosphere

For further analysis of the evolution of the IG wave disturbances it's necessary to construct a self-consistent simplified nonlinear dynamic equation on the basis of equations (11) and (3), that takes into account the presence of non-uniform zonal wind with velocity $\mathbf{V}_0(z) = v_0(z)\,\mathbf{e_x}$ in the ionosphere medium. With this purpose writing equation (11) for horizontal V_x and vertical V_z velocity components, and differentiating the first equation according to the coordinate z and the second equation – according to the coordinate x, subtracting the second equation from the first one, we get:

$$\left(\frac{\partial}{\partial t}+v_0(z)\frac{\partial}{\partial x}\right)\Delta\psi - v_0''(z)\frac{\partial\psi}{\partial x}+J(\psi,\Delta\psi) = -\frac{g}{\rho_0}\frac{\partial\rho}{\partial x} -$$
$$\frac{d\ln\rho_0}{dz}\left[\left(\frac{\partial}{\partial t}+v_0(z)\frac{\partial}{\partial x}\right)\frac{\partial\psi}{\partial z} - v_0'(z)\frac{\partial\psi}{\partial x}+J(\psi,\frac{\partial\psi}{\partial z})\right] -$$
$$\frac{1}{\rho_0}\frac{\partial}{\partial z}\left(\sigma_P B_0^2\right)\cdot\frac{\partial\psi}{\partial z} - \frac{\sigma_P B_0^2}{\rho_0}\cdot\frac{\partial^2\psi}{\partial z^2} - \frac{\sigma_P B_{0y}^2}{\rho_0}\cdot\frac{\partial^2\psi}{\partial x^2}+\nu\Delta^2\psi\,. \qquad (57)$$

Similarly, we transform the continuity equation (3):

$$\left(\frac{\partial}{\partial t}+v_0(z)\frac{\partial}{\partial x}\right)\rho + J(\psi,\rho) = -\frac{d\rho_0}{dz}\cdot\frac{\partial\psi}{\partial x}. \qquad (58)$$

Here, according to incompressibility condition of the considered two-dimensional perturbation ($\nabla\cdot\mathbf{V}=0$) (2), the stream function introduced as

$$V_x = -\frac{\partial\psi}{\partial z},\quad V_z = \frac{\partial\psi}{\partial x}, \qquad (59)$$

and the operator of the Jacobian $J(a,b) = \partial a/\partial x\cdot\partial b/\partial z - \partial a/\partial z\cdot\partial b/\partial x$.

For convenience of the further analysis, we turn to usual field variables for an isothermal atmosphere (Hines, 1960; Gossard and Hook, 1975):

$$\psi = \overline{\psi}\exp\left(\frac{z}{2H}\right),\ \rho = \overline{\rho}\exp\left(-\frac{z}{2H}\right). \qquad (60)$$

Substituting (60) into (57) and (58), replacing the factor by $\exp[z/(2H)]\approx 1$ before the nonlinear term (i.e. $k_z >> 1/(2H)$ - short wavelength waves due to vertical), considering that the parameter $(\sigma_P B_0^2/\rho_0)$ does not depend on the coordinate z (Gershman, 1974) and introducing a new variable $R = g\overline{\rho}/\rho_0(0)$, we obtain the following closed system of equations:

$$\left(\frac{\partial}{\partial t}+v_0(z)\frac{\partial}{\partial x}\right)\left(\Delta\overline{\psi}-\frac{\overline{\psi}}{4H^2}\right)+\left(\frac{v_0'(z)}{H}-v_0''(z)\right)\frac{\partial\overline{\psi}}{\partial x}+J(\overline{\psi},\Delta\overline{\psi}) = -\frac{\partial R}{\partial x} -$$
$$\frac{\sigma_P B_0^2}{\rho_0}\cdot\left(\frac{\partial^2\overline{\psi}}{\partial z^2}-\frac{\overline{\psi}}{4H^2}\right)-\frac{\sigma_P B_{0y}^2}{\rho_0}\cdot\frac{\partial^2\overline{\psi}}{\partial x^2}+\nu\Delta^2\overline{\psi}\,, \qquad (61)$$

$$\left(\frac{\partial}{\partial t}+v_0(z)\frac{\partial}{\partial x}\right)R + J(\overline{\psi},R) = \omega_g^2\cdot\frac{\partial\overline{\psi}}{\partial x}. \qquad (62)$$

Here $\omega_g = (g/H)^{1/2} > 0$ — frequency of Brunt-Vaisala for stably stratified incompressible isothermal atmosphere, $v_0'(z) = dv_0(z)/dz$ and $v_0''(z) = d^2v_0(z)/dz^2$.

The system of equations (61) and (62) describes the nonlinear interaction of internal gravity structures with an inhomogeneous zonal wind and the geomagnetic field in an incompressible isothermal dissipative ionosphere.

5. IGW stability criteria in the ionosphere with an inhomogeneous zonal wind

Nature of plane shear flow greatly defines the evolution of wave disturbances in the environment. Herewith, the shear flows in hydrodynamics and magneto-hydrodynamics are often unstable (Mikhailovskii, 1974; Gossard and Hook, 1975; Timofeev, 2000). The presence of the terms proportional to v_0' and v_0'' in equation (61) is related to the instability criterion (condition) of the shear flow**.** In the linear approximation for small perturbations of the form $(\overline{\Psi}(x,z,t), R(x,z,t)) = (\Psi_1(y), R_1(y))\exp(ik_x x - i\omega t)$, from the equations (61) and (62) follows an equation of the Orr-Sommerfeld

$$-i\left[\nu\left(\frac{d^2}{dz^2}-k_x^2\right)^2 + b_{0y}k_x^2 - b_0\left(\frac{d^2}{dz^2}-\frac{1}{4H^2}\right)\right]\Psi_1 + (\omega - k_x V_0)\left[\frac{d^2}{dz^2}-k_x^2-\frac{1}{4H^2}\right]\Psi_1 - \left[k_x\left(\frac{v_0'}{H}-v_0''\right)-\frac{k_x^2\omega_g^2}{\omega-k_x v_0}\right]\Psi_1 = 0. \qquad (63)$$

Neglecting the dissipation effects ($\sigma_P,\ \nu \to 0$) from the equation (63) we get

$$\Psi_1'' - \left[k_x^2 + \frac{1}{4H^2} + \frac{k_x(v_0'/H - v_0'')}{\omega - k_x V_0} - \frac{k_x^2\omega_g^2}{(\omega - k_x v_0)^2}\right]\Psi_1 = 0, \qquad (64)$$

where $\Psi_1'' = d^2\Psi_1/dz^2$. Equation (64) is a modification of the well-known Rayleigh equation (Timofeev, 2000) (at $1/H \to 0, \omega_g \to 0$). To determine the shear flow instability criterion in our case, we multiply (64) by Ψ_1^*, subtract the complex-conjugate expression from the result, and integrate the resulting expression in the borders from z_1 to z_2 of the plasma flow:

$$\int_{z_1}^{z_2}\frac{d}{dz}\left(\Psi_1^*\frac{d\Psi_1}{dz} - \Psi_1\frac{d\Psi_1^*}{dz}\right)dz - \int_{y_1}^{y_2}\left[\frac{1}{\omega - k_x v_0} - \frac{1}{\omega^* - k_x v_0}\right]k_x(v_0/H - v_0'')|\Psi_1|^2\,dz - \int_{z_1}^{z_2}\left[\frac{k_x^2\omega_g^2}{(\omega - k_x v_0)^2} - \frac{k_x^2\omega_g^2}{(\omega^* - k_x v_0)^2}\right]|\Psi_1|^2\,dz = 0. \qquad (65)$$

Assuming that the perturbation frequency is complex $\omega = \omega_0 + i\gamma$ (where ω_0 is eigen frequency of linear IGW), and the wave vector k_x - the real value, the imaginary part of equation (65) can be written as:

$$2\gamma\int_{z_1}^{z_2}\left[\frac{2\omega_1 k_x^2\omega_g^2}{(\omega_1^2+\gamma^2)^2} + \frac{k_x(v_0'' - v_0'/H)}{\omega_1^2+\gamma^2}\right]|\Psi_1|^2\,dz = 0, \qquad (66)$$

where $\omega_1 = \omega_0 - k_x v_0$. In the case of $\omega_1,\ \gamma,\ |\Psi_1^2| > 0$ from (66) the condition of linear instability of a shear flow it follows:

$$\frac{2\omega_1 k_x^2 \omega_g^2}{(\omega_1^2+\gamma^2)} + k_x\left(v_0'' - \frac{v_0'}{H}\right) = 0. \qquad (67)$$

For a critical level of the ionosphere, where the phase velocity $V_p = \omega / k_x$ matches the speed of wind v_0, $V_p = v_0(z)$ (i.e. $\omega_1 = \omega_0 - k_x v_0 \approx 0$), equality (67) can be rewritten as:

$$v_0''(y) - v_0' / H = 0. \qquad (68)$$

Conditions (67) and (68) can be called as modified Rayleigh condition ($v_0'' = 0$) for IGW at the appropriate parameters of the zonal flow, waves and environments. Implementation of this equation (67) (or (68)) in a resonant point $z = z_r$ of the shear flow is a necessary condition for instability.

In the Earth's atmosphere, the value v_0' / H can be both larger and smaller than v_0''. So, according to (68) the disturbance of the zonal wind may arise occasionally, such that in a critical layer $z = z_r$ the condition $\left|v_0''\right| = \left|v_0' / H\right|$ is fulfilled. This causes instability for some time, after which the zonal wind is reconstructed and becomes stable again, etc.

Let's briefly discuss the features and consequences of instability in simple shear flow of the ionosphere, where the rate of the local wind in the environment varies linearly - $v_0(z) = S \cdot z$, where $S > 0$ - constant parameter of the wind shear. For such wind velocity profile the necessary condition for the development of shear instability (67) is fulfilled at $\left|\omega_0\right| < \left|k_x v_0\right|$. In this case, according to section 3, shear instability develops even in a stable stratified ionosphere and temporarily, during the time interval $0 < t^* \approx 62{,}5/(\omega_b) \sim 3 \cdot 10^4$ IGW intensively draws energy of shear flow and increases own energy and amplitude by an order**.** Accordingly, the wave activity will intensify in this region of the ionosphere due to the energy of the shear flow (non-uniform wind).

6. Nonlinear vortex structures governed by the shear flow

As noted above, the spontaneously excited internal gravity waves at different layers of the ionosphere intensively draw energy from the shear flow at a certain point (in particular, for a time interval $0 < \tau \le \tau^*$) in their evolution. Receiving energy, amplitude of IGW increases (by an order of magnitude) and, accordingly, the nonlinear processes come into play. In this case, in the initial dynamic equation (61) and (62) the nonlinear terms can no longer be neglected and the full nonlinear system has to be investigated.

We proceed to study the influence of nonlinear effects on the dynamics of IGW structures in dissipative ionosphere. The results of the observations and targeted experiments show (Bengtsson and Lighthill, 1985; Chmyrev et al., 1991; Nezlin, 1994; Sundkvist, et al., 2005) that nonlinear solitary vortex structures can be generated at different layers of the atmosphere-ionosphere-magnetosphere. These structures transfer trapped rotating medium particles. Moreover, the ratio of the rotational speed of the particles U_c to the speed of motion of nonlinear structures U is given by $U_c / U \ge 1$ (Monin, 1978).

We introduce the characteristic time T and spatial scales L of the nonlinear structures. Using equation (11), (61) we can establish the relation between quantities: $U_c \sim V$, $U \sim L / T$. Similarly, for the ratio of the nonlinear term with the inertial one, we have: $(V\nabla)V / (\partial V / \partial t) \sim V / (L / T) \sim U_c / U$. Thus, the nonlinearity plays an essential role for wave processes satisfying the condition $U_c \ge U$. This estimation shows that nonlinear effects play a crucial role in the dynamics of IGW-type wave, the initial linear

stage of development of which is considered in previous section. Inequality $U_c \geq U$ coincides with the anti-twisting condition (Williams and Yamagata, 1984). Satisfying just the latter condition the initial nonlinear dynamic equations (61) and (62) may have the solitary (vortex) solutions (Williams, Yamagata, 1984; Nezlin, Chernikov, 1999).

From the general theory of nonlinear waves is well known the fact (Whitham, 1977) that if in the system the nonlinear effects are significant, then the principle of superposition can't be applied and the solution in the form of a plane wave is unjust. Nonlinearity distorts the wave profile and the wave form differs from a sinusoid. If in a nonlinear system the dispersion (or non-uniform equilibrium parameters of the medium) is lacked, all small-amplitude waves with different wave numbers k propagate with the same speed and have the opportunity for a long time interaction with each other. So, even a small nonlinearity leads to the accumulation of distortions. Such nonlinear distortion, as a rule, leads to the wave front curvature growth and its upset (breaking) or to the formation of the shock wave. In the presence of dispersion the phase velocities of waves with different k vary with the latter, the waves with different k propagate with different velocities and virtually unable to interact with each other. Therefore, the wave packet tends to spreading. For not very large amplitude the wave dispersion can compete with the nonlinearity. Because of this before breaking the wave may split into separate nonlinear wave packets, and the shock wave will not form. Indeed, in the real atmosphere, the shock wave, as a rule, (spontaneously, without external influence) is not formed spontaneously. Primarily, this means that in the atmosphere-ionosphere medium dispersion effects are strongly pronounced and significantly compete with nonlinear distortion. If the nonlinear steepening of the wave is exactly compensated by the dispersion spreading, there may appear the stationary waves such as solitary vortices propagating in a medium without changing its shape.

It should be noted also, that the results of ground and satellite observations show clearly that in the different layers of the ionosphere the zonal winds (currents) are permanently present, which are non-uniform along the vertical (Gershman 1974; Gossard and Hook, 1978; Kazimirovskii and Kokourov, 1979). As noted in section 3, at interaction with non-uniform zonal flow the wave disturbance obtains an additional dispersion as well as a new source of amplification and the nonlinear effects come into play in their dynamics. Thus, the ionospheric medium with shear flow creates a favorable condition for the formation of nonlinear stationary solitary wave structures.

So, we want to find a solution of the nonlinear equations (61) and (62) (a non dissipative case $\nu = \sigma_P = 0$) in the form of stationary regular waves $\overline{\psi} = \psi(\eta, z)$ and $R = R(\eta, z)$, propagating along the parallel (along the x-axis) with a constant velocity U = const without changing its form, where $\eta = x - U\tau$. Moreover, we consider the case when the wave structures propagate on the background mean zonal wind, which has the non-uniform velocity.

In the non-dissipative case ($\nu = \sigma_P = 0$), passing to above mentioned auto model variables η and z and considering that in this case $\partial / \partial\tau = -U\partial / \partial\eta$, the system of equations (61), (62) can be written as:

$$-U\frac{\partial}{\partial\eta}\left(\Delta\Psi - \frac{\Psi}{4H^2}\right) + \frac{\partial R}{\partial\eta} + J(\Psi, \Delta\Psi) = 0, \tag{69}$$

$$-U\frac{\partial R}{\partial\eta} - \omega_g^2\frac{\partial\Psi}{\partial\eta} + J(\Psi, R) = 0. \tag{70}$$

Here we have introduced a new feature of the stream function

$$\Psi(\eta, z) = \Phi_0(z) + \overline{\psi}(x, z), \tag{71}$$

and the velocity potential $\Phi_0(z)$ of the background zonal shear flow through the notation:

$$v_0(z) = -\frac{d\Phi_0(z)}{dz}. \tag{72}$$

Providing the so-called vector integration, according to (Aburjania, 2006), the general solution of equation (70) can be presented as:

$$R(\eta, z) = \omega_g^2 z + F(\Psi + Uz), \tag{73}$$

where $F(\xi)$ is the arbitrary function of its argument. Next, substituting (73) into (69) and performing the similar transformation we get a nonlinear equation in the form of the Jacobian:

$$J\left(\Delta\Psi + U\int\frac{dz}{4H^2} + \frac{dF(\Psi + Uz)}{d(\Psi + Uz)}z, \Psi + Uz\right) = 0. \tag{74}$$

The general solution of (74) has the form (Aburjania, 2006):

$$\Delta\Psi + U\int\frac{dz}{4H^2} + \frac{dF(\Psi + Uz)}{d(\Psi + Uz)}z = G(\Psi + Uz), \tag{75}$$

where $G(\xi)$ - a new arbitrary function of its argument.

As it was mentioned earlier, the results of observations and experiments show that vortex streets of various forms can be generated in ordinary liquid and plasma environment in the presence of the shear flow, as a consequence of the nonlinear saturation of Kelvin-Helmholtz instability. Such structures may occur if the asymptotic form of the function $G(\xi)$ in equation (75) is nonlinear (Petviashvili and Pokhotelov, 1992; Aburjania, 2006).

We assume that the nonlinear structure move by a velocity U that satisfies the following condition:

$$U\int\frac{dz}{4H^2} + \frac{dF(\Psi + Uz)}{d(\Psi + Uz)}z = 0. \tag{76}$$

It is obvious that (76) holds for IGW at only case when the function $F(\xi)$ is a linear function of its argument over the plane $x,\ z$, i.e. $F = -U(\Psi + Uz)/(4H^2)$. In this case, choosing an arbitrary function G as the following nonlinear function $G(\xi) = \psi_0^0\kappa^2(\exp(-2\xi/\psi_0^0)$ (Petviashvili and Pokhotelov, 1992; Aburjania, 2006), equation (75) reduces to:

$$\Delta(\Psi + Uz) = \psi_0^0\kappa^2\exp[-2(\Psi + Uz)/\psi_0^0]. \tag{77}$$

Now let's choose an expression for the stream function of the background shear flow in the form:

$$\Phi_0(z) = Uz + \psi_0^0\ln(\kappa_0 z). \tag{78}$$

Here ψ_0^0 characterizes the amplitude of the background structure, but $2\pi/\kappa$ и $2\pi/\kappa_0$ presents the characteristic size of the vortex structure and parameter of non-uniform background shear flow, respectively.

Given (71) and using (78), the vorticity equation (77) can be transformed into:

$$\Delta\overline{\psi} = \psi_0^0\kappa_0^2\left[\frac{\kappa^2}{\kappa_0^2}e^{-2\overline{\psi}/\psi_0^0} - 1\right]. \tag{79}$$

This equation has the solution (Mallier and Maslow, 1993):

$$\overline{\psi}(\eta, z) = \psi_0^0\ln\left[\frac{\mathrm{ch}(\kappa z) + \sqrt{1-\kappa_0^2}\cos(\kappa\eta)}{\mathrm{ch}(\kappa_0 z)}\right], \tag{80}$$

which is a street of the oppositely-rotating vortices. Substituting (80) and (78) into expression (71), we finally obtain the solution:

$$\Psi(\eta, z) = Uz + \psi_0^0\ln[\mathrm{ch}(\kappa z) + \sqrt{1-\kappa_0^2}\cos(\kappa\eta)]. \tag{81}$$

From equations (81), (78) and (59) we obtain the following expressions for the components of the medium velocity and shear flow, respectively:

$$V_x(\eta,z) = -U - \psi_0^0 \kappa \frac{sh(\kappa z)}{ch(\kappa z) + \sqrt{1-\kappa_0^2}\cos(\kappa\eta)}, \quad (82)$$

$$V_z(\eta,z) = -\psi_0^0 \kappa \frac{\sqrt{1-\kappa_0^2}\sin(\kappa\eta)}{ch(\kappa z) + \sqrt{1-\kappa_0^2}\cos(\kappa\eta)}, \quad (83)$$

$$v_0(z) = -U - \psi_0^0 \kappa_0 th(\kappa_0 z), \quad (84)$$

At $\kappa_0 = 1$ the solution (81) describes the background flow to the type of shear zonal flow (84). At $\kappa_0^2 < 1$ in the middle of the zonal flow (84) the longitudinal vortex street will form (Fig. 3). Solution (82), (83) with closed streamlines in the form of "cat's eyes" was first obtained by Lord Kelvin.

It must be mentioned that the nonlinear stationary equations (74), (75) also have an analytical solution in the form of a Larichev-Reznik type dipole pair of cyclone-anticyclone (Petviashvili and Pokhotelov, 1992; Aburjania, 2006) and vortex transverse chains (Aburjania et al., 2005).

7. Energy transfer by the vortex structures

In the dynamic equations of IGW structures (61) and (62) the source of convergence of external energy due to shear flow (non-uniform wind), the terms with $v_0(y)$, and divergence sources of energy due to dissipative processes in the environment - terms of induction σ_P and viscous ν damping are included obvious. The above mentioned nonlinear solitary vortex structures can self-sustain only at the existence of an appropriate balance between the convergence and divergence of energy in the wave perturbations in the ionosphere medium.

Further, we obtain the energy transport equation for the IGW vortex structures. With this purpose we multiply the equation (61) by $\overline{\Psi}$ and (62) – by ‘R, then integrate them according to x and z. After performing simple transformations of obtained relations we finally get the regularities of the dynamics of energy of the IGW structures:

$$\frac{\partial E}{\partial t} = \int v_0'(z)\frac{\partial\overline{\Psi}}{\partial x}\frac{\partial\overline{\Psi}}{\partial z}dxdz - \frac{\sigma_p B_{0y}^2}{\rho_0}\int\left(\frac{\partial\overline{\Psi}}{\partial x}\right)^2 dxdz - \frac{\sigma_p B_0^2}{\rho_0}\int\left[\left(\frac{\partial\overline{\Psi}}{\partial z}\right)^2 + \frac{\overline{\Psi}^2}{4H^2}\right]dxdz -$$

$$\nu\int\left[\left(\frac{\partial^2\overline{\Psi}}{\partial x^2}\right) + \left(\frac{\partial^2\overline{\Psi}}{\partial z^2}\right)^2 + 2\left(\frac{\partial^2\overline{\Psi}}{\partial x\partial z}\right)^2\right]dxdz, \quad (85)$$

where

$$E = \frac{1}{2}\int\left[\left(\nabla\overline{\Psi}\right)^2 + \frac{\overline{\Psi}^2}{4H^2} + \frac{R^2}{\omega_g^2}\right]dxdz, \quad (86)$$

presents energy of the nonlinear internal-gravity vortex structure.

Let’s mention, that the equation (85) is valid for linear as well as for nonlinear stage of evolution of IGW perturbations. In this equation the first term of the right hand side describes transient sway-generation of the IGW structures due to the shear instability; the second and the third terms – an induction damping of the wave disturbances due to Pedersen conductivity, and the last term describes the viscous damping of the perturbations. According to (85), for generation of the structures it is necessary the velocity of the shear flow to have at least the first derivative with respect to vertical coordinate different from zero ($v_0'(z) \neq 0$).

As noted in section 3.1, the considered IGW perturbations in the linear mode have eigen frequencies (22) and propagate along the Earth's parallel (along the x axis). The induction and viscous damping takes energy from these IGW structures and heat the ionospheric environment with a decrement γ (23), where $k_x \approx 2\pi / L_x$, $k_z \approx 2\pi / L_z$. In this case, shear flow temporarily supply the medium with energy, causing generation - swing of IGW structures and the development of shear instability with a characteristic growth increment γ_A (26).

Thus, the non-uniform zonal wind or shear flow can transiently generate and / or intensify the internal gravity structures in the ionosphere and contribute to self-sustaining of IGW vortices when $\gamma_A \geq \gamma$. According to section 3.1, the condition of nonlinear self-sustaining of IGW vortex structures at the levels of F-region of the ionosphere the condition ($\gamma_A \geq \gamma$) is fulfilled, even with some reserve, and considered vortex structures are long-lived.

Thus, the revealed internal gravity vortices in the ionosphere are sufficiently long-lived, so they can play a significant role in the transport of solid matter, heat, energy and form strong turbulence state in the medium (Aburjania et al., 2009).

8. Discussion and conclusion

In this article the linear stage of generation and further nonlinear evolution of IGW structures in the dissipative stably stratified ($\omega_g^2 > 0$) ionosphere in the presence of shear flow (non-uniform zonal wind) is studied. A model system of dynamic nonlinear equations describing the interaction of internal gravity structures with viscous ionosphere, non-uniform local zonal wind, and the geomagnetic field is obtained. On the basis of analytical solutions and theoretical analysis of the corresponding system of dynamic equations a new mechanisms of linear transient pumping of shear flow energy into that of the wave perturbation, wave amplification (multiple times), self-organization of nonlinear wave perturbations into the solitary vortex structures and the transformation of the perturbation energy into heat is revealed.

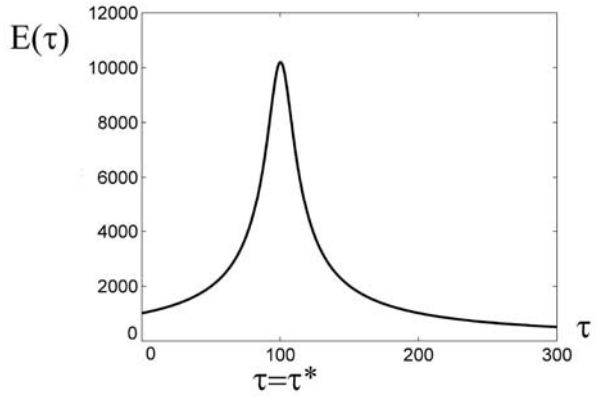

Fig. 1. Evolution of the non-dimensional energy density $E(\tau)$ (formulae (54)) for the initial parameters: $k_0 = 10$, $S = 0.1$.

A necessary condition for shear instability of IGW at their interaction with local non-uniform zonal wind, which is a generalization of the Rayleigh condition, is obtained.

The equation of energy transfer by nonlinear wave structure in the dissipative ionosphere is established. Based on the analysis of this equation it is revealed that the IGW structure effectively interacts with the local background non-uniform zonal wind and self-sustained by the shear flow energy in the ionosphere.

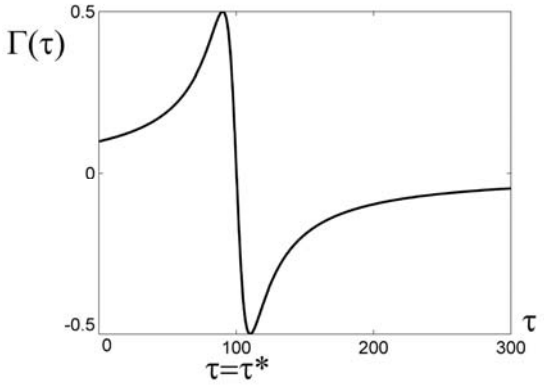

Fig. 2. Increment of shear instability $\Gamma(\tau)$ (formulae (56)), as function of time for the parameters: $k_0 = 10$, $S = 0.1$.

Linear amplification of IGW perturbation is not exponential as in the case of the AGW in the inverse-unstably stratified ($\omega_g < 0$, when IGW can not be generated) atmosphere (Aburjania, 1996)), but in algebraic-power law manner. Intensification of IGW is possible temporarily, for certain values of environmental parameters, shear and waves, which form an unusual way of heating of the shear flow in the ionosphere: the waves draw their energy from the shear flow through a linear drift of SFH in the wave number space (fragmentation of disturbances due to scale) and pump energy into the region of small-scale perturbations, i.e. in the damping region. Finally, the dissipative processes convert this energy into heat. The process is permanent and can lead to strong heating of the medium. Intensity of heating depends on the level of the initial disturbance and the parameters of the shear flow.

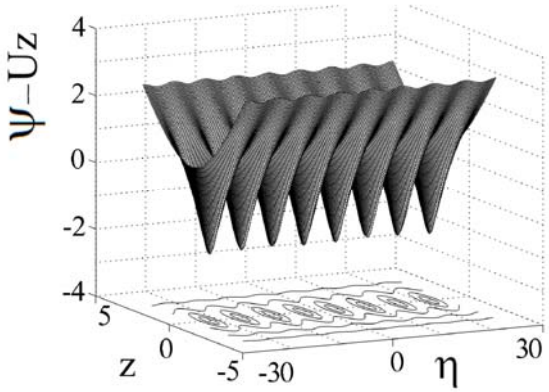

Fig. 3. Relief and current lines in the rest frame of the vortices $\Psi(\eta, y) - Uy$, calculated from formula (81) for $\psi_0^0 = 1$, $k = 1$, $æ_0 = 0.5$ (the longitudinal vortex street).

A remarkable feature of the shear flow is the dependence of the frequency and wave number of perturbations on time $k_z = k_z(0) - k_x S\tau$, $k(\tau) = (k_x^2 + k_z^2(\tau))^{1/2}$. In particular, frequency and wave number transient growth leads to a reduction of scales of the wave disturbances due to time in the linear regime and, accordingly, to energy transfer into a short scale region - the dissipation region. On the other hand a significant change in the frequency range of the generated disturbances stipulates in the environment the formation of a broad range of spectral lines of the perturbations, which is linked to the linear interactions and not to the strong turbulent effects. Moreover, amplification of the SFH perturbation and broadening of wave modes' spectra occur in a limited period of time (transient interval), yet satisfied the relevant conditions of amplification and a strong enough interaction between the modes.

It should be emphasized that the detection of the mechanism of the intensification and broadening of the spectrum of perturbations became possible within the non-modal mathematical analysis (these processes are overlooked by more traditional modal approach). Thus, non-modal approach, taking into account the nonorthogonality of the eigenfunctions of the linear wave dynamics, proved to be more appropriate mathematical language to study the linear stage of the wave processes in shear flows.

The frequency of considered linear IGW perturbations varies in the interval of $10^{-4}\,c^{-1} < \omega_0 < 1.7\times10^{-2}\,c^{-1}$ and includes low-frequency range of AGW. Wavelength lies in the interval $\lambda \sim 100м \div 10km$, the period – from 5 minutes to - 3 hours. Considering intermediate values of the IGW wavelengths ($k \sim 1/H$, $H \sim 10$ km; $\omega \sim \omega_g \sim 10^{-2}s^{-1}$) we find that the group and phase velocities are of the same order $V_g \sim V_p \sim \omega_g H \sim 10^{-2}s^{-1}\times10^4 m \sim 10^2 m/s$. This estimation agrees with existing observations and they move with velocity ($0.1 \div 200$) m/s in a random direction along the horizontal lines, depending on daytime and nighttime conditions. IGW is characterized by an exponential growth of the amplitude of the perturbed velocity at the vertical propagation in an environment with exponentially decaying vertical equilibrium density and pressure (Hines, 1960; Gossard, Hook, 1978). According to observational data, IGW disturbances manifest themselves in a wide range of heights - from the troposphere to the upper ionosphere heights $z \le 600$ km (Gossard and Hook, 1975; Francis, 1975; Rishbet and Fukao, 1995; Hecht et al., 2010). At ionospheric altitudes (above 90 km) the conductive medium strongly impacts on the IGW, causing its remarkable damping due to local Pedersen currents.

On the basis of analytical solutions of nonlinear dynamical equations it's shown that the internal-gravity waves organize themselves (due to the shear flow energy) in the form of stationary solitary vortex structures. The solution of the nonlinear equations has an exponential asymptotic behavior $\sim \exp(-\kappa|r|)$ at $|r| \to \infty$, i.e. structures are strongly localized along the plane transverse to the Earth's surface. Depending on the type of velocity profile of the zonal shear flow (wind) $v_0(z)$, the generated nonlinear structures maybe the monopole solitons, cyclone, anticyclone, dipole cyclone-anticyclone pair, longitudinal vortex streets or transverse vortex chain in the background of non-uniform zonal wind (see also Aburjania, et al., 2005). The presence of spatially non-uniform winds in the ionosphere gives IGW the properties of self-organization and self-sustaining in the form of the aforementioned nonlinear solitary vortex structures of different shapes.

Phase velocity of linear IGW occupies a range: $-V_{max} \le V_p \le V_{max}$ in an incompressible atmosphere, where $V_{max} = 2H\omega_g = 2(gH)^{1/2}$. This means that if the source (for example, the above mentioned nonlinear vortex structure) moves along x axes at a velocity greater than V_{max}, the source does not come in resonance with the linear internal gravity waves. Nonlinear vortices, moving faster than the corresponding linear waves, can retain their nonlinear amplitude as far as they do not lose energy by radiation of linear waves. It means that these sources can not excite a linear wave due to

Cherenkov mechanism and can retain its initial energy (Stepanyants and Fabrikant, 1992). Thus, these vortex structures can be generated, self-sustained and propagated with velocity $|U| > V_{max}$ along the horizon in any direction. For the height of the atmosphere $H \approx 4.5 \div 6$ km, we can estimate the value of maximal speed of linear IGW - $V_{max} \approx 440$ m / sec. Thus, the identified vortex structures are supersonic and do not loose energy by radiation of linear IGW in the velocity $|U| < V_{max}$ m / s region.

It should be noted that the discussed nonlinear two-dimensional vortex structures are very different from the atmospheric Rossby-type vortices (Larichev and Resnick, 1976; Aburjania, 2006). The main difference is that the motion velocity of our vortices is completely symmetric, i.e. the structures can move with velocities greater than the maximum phase velocity of linear waves in any horizontal direction. While Rossby vortices can move to the west only at the velocities exceeding the maximum velocity of Rossby waves. In the East such vortices can move with any speed as far as the linear Rossby waves do not propagate in this direction. In addition, we assumed that the atmospheric-ionospheric medium is isothermal. In case, when the equilibrium temperature T_0 of the medium is not constant, in the expression of maximum velocity of linear IGW $V_{max} = 2c_s(\gamma - 1)^{1/2}/\gamma$, the term $\gamma - 1$ must be replaced by $\gamma - 1 + H(dT_0/dz)/T_0$. Then, for temperatures, coinciding instability threshold (i.e. $d \ln T_0 / dz < 0$) (Stenflo and Stepaniants,1995), and for $\gamma = 1.4$ we get $V_{max} < |U| << c_s \approx 330$ m/s a nonlinear stationary IGW structure can be generated in atmospheric-ionospheric media .

Nonlinear vortex structures of large amplitude, very similar to those theoretically identified by us, were found at atmosphere-ionosphere layers with satellite and ground observations and analyzed in the papers (Bengtsson and Lighthill, 1985; Ramamurthy et al., 1990; Cmyrev et al., 1991; Nezlin, 1994; Shaefer et al., 1999). The motion of medium particles trapped by vortex structures is characterized by a non-zero vorticity $\nabla \times \mathbf{V} \neq 0$, i.e. particles rotate along the closed trajectories in the nonlinear structures. Characteristic value of rotational velocity U_c is of the order or greater than the structure velocity as a whole U, $U_c \geq U$. In this case, the structures trap the medium particles (whose number is comparable to the number of passing particles) and moving in the environment, transfer these rotating trapped particles. Therefore, being long-lived entities, IGW vortex structures can play a significant role in the process of transfer of mass, heat, energy and in the creation of macro turbulent state of ionosphere (Aburjania et al., 2009). In particular, the vortex structure can play the role of "turbulent agent" or elements of horizontal macroscopic turbulent exchange processes in general circulation of the ionosphere. Coefficient of horizontal turbulent eddy exchange can be estimated using the Obukhov-Richardson formula (Monin and Yaglom, 1967): $K_T \approx 10^{-6} d^{4/3}$ m^2/s. So, for the typical size of vortices $d \sim 10$ km, we find that $K_T \approx 10^2$ m^2/s. This estimate (which must be regarded as an upper limit) shows that the exchange processes between the upper and lower latitudes, the meridional heat transport from north to south in the ionosphere can have macro-turbulent vortex nature (note that in the ionosphere, the polar region is warmer than equatorial).

IGW structures are eigen degrees of freedom of the ionospheric resonator. Therefore, influence of external sources on the ionosphere above or below (magnetic storms, earthquakes, artificial explosions, etc.) will excite these modes (or intensified) in the first, (Aburjania and Machabeli, 1998). For a certain type of pulsed energy source the nonlinear solitary vortical structures will be generated (Aburdjania, 1996; Aburdjania, 2006), which is confirmed by experimental observations (Ramamurthy et al., 1990; Cmyrev et al., 1991; Nezlin, 1994; Shaefer et al., 1999; Sundkvist et al., 2005). Thus, these wave structures can also be the ionospheric response to natural and artificial activity.

Acknowledgments

The research leading to these results has received funding from the European Union Seventh Framework Program [FP7/2007-2013] under grant agreement № 269198 - Geoplasmas (Marie Curie International Research Staff Exchange Scheme).

Referens

Aburjania, G.D., Chargazia, Kh.Z., Kharshiladze, O.A. Shear flow driven magnetized planetary wave structures in the ionosphere. Journal of Atmospheric and Solar Terrestrial Physics. V. 72. P. 971-981.doi: 10.1016/j.jastp. 2010.05.008. 2010.

Aburjania, G.D., Chargazia, Kh.Z., Zeleny, L. M., Zimbardo, G. Model of strong stationary vortexturbulence in the space plasma. Nonlinear Process. Geophys. 16, 11-22. 2009.

Aburjania, G.D., 2006. Self-organization of the vortex structures and the vortex turbulence in the dispersed media. Komkniga, URSS, Moscow . 2009 (in Russian).

Aburjania, G.D., Chargazia, Kh.Z., Khantadze, A.G., Kharshiladze, O.A. Mechanism of the planetary Rossby wave energy amplification and transformation in the ionosphere with an inhomogeneous zonal smooth shear wind. J.Geophys.Res.111. A09304. Doi:10.1029/ 2005JA011567. 2006.

Aburjania, G.D., Chargazia, Kh.Z., Jandieri, G.V., Kharshiladze, O.A.Generation and propagation of the ULF planetary-scale electromagnetic wavy structures in the ionosphere. Planet. Space. Sci. 53, 881-901. 2005.

Aburjania, G.D., Khantadze, A.G. Large-scale electromagnetic wave structures in E-region of the ionosphere. Geomang. Aeron. 42 (2), 245-51. 2002.

Aburjania, G.D., Machabeli, G.Z. Generation of electromagnetic perturbations by acoustic waves in the ionosphere. J. Geophys. Res. A. 103, 9441-9447.1998.

Aburjania, G.D., 1996. Self-organization of acoustic gravity vortices in the ionosphere before the earthquake. Plasma Phys. Rep. 22 (10), 954-959.

Alexander, M.J. Chapter 5. Gravity waves in the stratosphere, in: "The Stratosphere: Dynamics, Chemistry and Transport". L.M. Polvani, A. Sobel, D.W. Waugh (Eds.). Geophys. Monogr. Ser. Doi: 10. 1029/ 2009GM000887. 2010.

Alexander, M.J., Geller, M., McLandress, C. et al., 2010. Recent developments in gravity wave effects, in climate models and global distribution of gravity wave momentum flux from observations and models. Q. J. R. Meteorol. Soc. 136, 1103-1124.

Alexander, M.J., Gille, J. Cavanaugh, C. et al. Global estimates of gravity wave momentum flux from High Resolution Dynamics Limb Sounder observations. J Geophys. Res.113,D15S18. Doi:10.1029/2007JD008807. 2008.

Alexander, M.J., Rosenlof, K.H. Gravity wave forcing in the stratosphere: Observational constraints from the Upper Atmosphere Research Satellite and implications for parametrization in global models. J Geophys. Res.108, D19,4597. Doi:10.1029/2003JD003373. 2003.

Bengston, L., lighthill, J. (Eds.). Intense Atmospheric Vortices. Springer-Verlag, Beerlin-Heidelberg. 1982.

Bertin, F., Testud, J., Kerby, L., Rees, P.The meteorological jet stream as a sourse of medium scale gravity waves in the thermosphere: an experimental study. J. Atmos. Terr. Phys. 40 (10/11), 1161-1183. 1978.

Burmaka, V.P., Kostrov, L.S., Chernogor, L.F.Statistical characteristics of Doppler HF radar signals at sounding of mid-latitude ionosphere medium, perturbed by satellite launches and solar terminators. Radiophysics, Radioastr., 8 (2), 143-162. 2003.

Chagelishvili, G.D., Rogava, A.D., Tsiklauri, D.G. Effect of coupling and linear transformation of waves in shear flow. Phys. Rev. E. 53 (6), 6028-6031. 1996.

Cheng, K., Huang, Y.-N. Ionospheric disturbances observed during the period oh Mount Pinatubo eruptions in June 1991. J. Geophys. Res. 97, 16,995-17,004. 1991.
Chimonas, G., Hines, C.O. Atmospheric gravity waves induced by a solar eclipse. J. Gephys. Res. 76, (28),. 703-705. 1971.
Chimonas, G., Hines, C.O. Atmospheric gravity waves launched by auroral currents. Planet. Space Sci. 18 (4), 565-612. 1970.
Cmyrev, V.M., Marchenko, V.A., Pokhotelov, O.A. et al.Vortex structures in the ionosphere and magnetosphere of the Earth. Planet. Space Sci. 39, 1025-1030. 1991.
Cowling, T.C. Magnetohydrodynamics. Monograph on Astronomical Subject, Hilger, Bristol, U.K.1976.
Dokuchaev, V.P. On the impact of the Earth's geomagnetic field on the winds in the ionosphere. Izv. AS SSSR, Phys. of Atmos. and Ocean., 5, P.783-787. 1959.
Drobjev, V.I., Molotov, G.F., Rudina, M.P., et al. Ionosphere response on the perturbation due to artificial explosions. Ionospheric Investigations, 39, 61-71. 1986.
Francis, S.H. Global propagation of atmospheric gravity waves: a review. Journal of Atmospheric and Terrestrial Physics. 37,1011-1054. 1975.
Friedrich, M., Torkar, K.M., Singer, W., et al. Signatures of mesospheric particles in ionospheric data. Ann. Geophys. 27, 823-829. 2009.
Fritts, D.C., Janches, D., Riggin, D.M. et al. Gravity waves and momentum fluxes in the mesosphere and lower thermosphere using 430 MHz dual-beam measurements at Aresibo: 2. Frequency spectra, momentum fluxes, and variability. J Geophys. Res. 111, D18108. Doi:10.1029/2005JD006883. 2006.
Gavrilov, N.M., Fukao, S. Hydrodynamic tropospheric wave sources and their role in gravity wave climatology of upper atmosphere from the MU radar observations. J. Atmos. Solar-Terr. Physics. 63, 931-943. 2001.
Gershman, B.N. Dynamics of ionosphere plasma. Nauka, Moscow . 1974 (in Russian).
Gill, A. Atmosphere- Ocean Dynamics. Academic Press, London. 1982.
Ginzburg, V.L., Rukhadze, A.A. Waves in Magnetoactive Plasma. Nauka, Moscow. 1975 (in Russian).
Golitsin, G. S., Romanova, N.N., Chunchuzov, E.P. On generation of internal waves in the atmosphere by sea choppiness. Izv. AS SSSR, Phys. of Atmos. and Ocean, 12, 319-323. 1975.
Golitsin, G. S. Damping of small scale oscillations in the atmosphere due to viscosity and thermal conductivity. Izv. AS SSSR, Phys. 0f Atmos. and Ocean, 1 (2), 136-149. 1965.
Gossard, E., Hooke, W. Waves in the Atmosphere. Elsevier, Amsterdam. 1975.
Graik, A.D.D., Criminale, W.O. Evolution of wavelike disturbances in shear flow: a class of exact solutions of the Navier-Stokes equations. Proc. Roy. Soc. London. Ser. A. 406, 13- 21. 1986.
Hayakawa, M. (Edit). Atmospheric and Ionospheric Electromagnetic Phenomena Associated with Earthquakes. Terra Sci., Tokyo. 1999.
Hecht, J.H., Alexander M.J., Walterscheid R.L. et al. Imaging of atmospheric gravity waves in the stratosphere and upper mesosphere using satellite and ground-based observations over Australia during the TWPICE campaign. J. Geophys. Res. A . 114 (17), D 18123, Doi: 10. 1029/2008 JD011259. 2009.
Hines, C.O., Reddy, C.A. On the propagation of atmospheric gravity waves trough region of wind shear. J. Geophys. Res. 72 (3), 1015-1034. 1967.
Hines, C.O. Internal atmospheric gravity waves at ionospheric heights. Canad. J. Phys.38 (11), 1441-1481. 1960.
Kamide, Y., Chian, A. (Eds.). Handbook of the Solar-Terrestrial Environment. Springer-Verlag, Berlin, Heidelberg. 2007.
Kazimirovskii, E.S., Kokourov, V.D. Motions in the Ionosphere. Nauka, Novosibirsk (in Russia).
Kim, J., Mahrt, L., 1992. Momentum transport by gravity waves. J. Atmos. Sci. 49, 735-748. 1979.
Kuester, M.A., Alexander, M.J., Ray, E.A., 2008. A model study of gravity waves over Huricane Humbert (2001). J. Atmos. Sci. 65, 3231-3246.

Larichev, V.D., Reznik, G.M. On the two-dimensional solitary Rossby waves. Soviet Physics Doklady, 21, 581-585. 2008.
Liperovskii, V.A., Pokhotelov, V.A., Shalimov, S.A. Ionospheric Precoursors of the Earthquakes. Nauka, Moscow. 1992.
Magnus, K. Schwingungen. B.G. Teubner Verlagsgesellschaft mbH, Stuttgart. 1976.
Mallier, R., Maslowe, S.A. A row of counter-rotating vortices// Phys. Fluids. A5, 1074-1075. 1993.
Margetreud, R., 1969. Winds in mesosphere and low termosphere. In Book.: The Wind in the Ionosphere. Gidrometisdat, Leningrad. 1969 (in Russian).
Mayr, H.G., Harris, I., Herraro, F.A. et al. Thermospheric gravity waves: observations and interpretation using the transfer function model (TFM). Space Sci. Rev. 54, 297-375. 1990.
Mikhailovskii, A.B. Theory of plasma Plasma Instabilities. V.2. Consultants Bureau, New York. 1974.
Ming, F.C., Chen, Z., Roux, F. Analysis of gravity-waves produced by intense tropical cyclones. Ann. Geophys. 28, 531-547. 2010.
Monin, A.S. (Ed.). Physics of Ocean. V.2. Hydrodynamics of Ocean. Nauka, Moscow. 1978 (in Russian).
Monin, A.S., Iaglom, A.N. Stastical Hydrodynamics. V.2. Nauka, Moscow. 1967 (in Russian).
Nakamura, T., Tsuda, T., Yamamoto, et. Al. Characteristic of gravity waves iv the mesosphere observed with the middle and upper atmosphere radar. 1. Momentum flux. J. Geophys. Res. 98 (B5), 8899-8910. 1993.
Nezlin, M.V., Chernikov, G.P. Analogies of the drift vortices in plasma and geophysical hydrodynamics. Plasma Phys. Rep., 21 (11), 975-999. 1999.
Nezlin, M.V. Rossby solitary vortices, on giant planets and in the laboratory. CHAOS. 4,187-202.
Pedlosky, J., 1979. Geophysical Fluid Dynamics.Springer-Verlag, New York. 1994.
Petviashvili, V.I., Pokhotelov, O.A. Solitary Waves in Plasmas and Atmosphere.Gordon and Breach, London. 1992.
Pokhotelov, O.A., Parrot, M., Fedorov, E.N. et al. Response of the ionosphere to natural and man-made acoustic sources. Ann. Geophys. 13, 1197-1210. 1995.
Ramamurthy, M.K., Collins, B.P., Rauber, R.M. et al. Evidence of very-large-amplitude solitary waves in the atmosphere. Nature. 348, 314-317. Doi: 10.1038/348314A0. 1990.
Rastogi, P.K.. Radar studies of gravity waves and tides in the atmosphere, a review. J. Atmos. Terr. Phys. 43 (5/6), 511- 524. 1981.
Reddy, S.C., Schmid, P.J., Hennigson, D.S. Pseudospectra of the Orr-Sommerfeld operator. SIAM. J. Appl. Math. 53,15-23. 1993.
Rishbeth, H., Fukao, S., 1995. A review of MU radar observation of the thermosphere and ionosphere. J. Geomag. Geoelectr. 47, 621-637.
Schunk, R.W., Sojka, J.J. Ionosphere thermosphere space weather issues. J. Atmos. Terr. Physics. 58. (14), 1527-1574. 1996.
Shaefer, L.D., Rock, O.R., Levis, T.P. Detection of explosive events by monitoring acoustically-induced geomagnetic perturbations. Lawrence Livermore Laboratory. CA USA, 94550. 1999.
Stenflo, L., Stepaniants, Yu.A. Acoustic-gravity modons in the atmosphere. Ann. Geophys. 13, 973-975. 1995.
Stepaniants, Yu., Fabrikant, A.L. Features of Cherenkov emission of the drift waves in hydrodynamics and plasma. Soviet Physics Journal of Experimetal and Theoretical Physics, 102 (5), 1512-1523. 1992.
Sundkvist, D., Vaivads, A., Andre, M. et al. Multi-spacecraft determination of wave characteristics near the proton gyrofrequency in high-altitude cusp. Ann. Geophys. 23, 983-995. 2005.
Testud, J. Gravity wave generated during magnetic substorms. J. Atmos. Terr. Phys. 32, 1793-1805. 1970.
Timofeev, A.V. Resonance Phenomena in Plasma Oscillations.Physmatlit, Moscow. 2000 (in Russian).

Tolstoy, I., Herron, T.J. Atmospheric gravity waves from nuclear explosions. J. Atmos. Sci. 27, 55-61. 1970.
Trefenthen, L.N., Trefenthen, A.E., Reddy, S.C., Driscoll, T.A. Hydrodynamic stability without eigenvalues. Science. 261, 578-584. 1993.
Waterscheid, R.L., Schubert, G. Nonlinear evolution of an upward propagating gravity wave: Overturning, Convection, Transience and Turbulence. J. Atmos. Sci. 47 (1), 101-125. 1990.
Whitham, G.B. Linear and Nonlinear Waves. John Wiley, New York. 1977.
Williams, G.P., Yamagata, T. Geostrophic regimes, intermediate solitary vortices and Jovian Eddies. J. Atmos. Sci. 41, 453-468. 1984.
Zeldovich, I.B., Mishkis, A.D. Elements of Applied Mathematics. Nauka, Moscow. 1972 (in Russian).

(Received in final form 20 December 2011)

Генерация, интенсификация и само-организация внутренних-гравитационных волновых структур в земной ионосфере с направленным сдвиговым ветром

Г. Абурджаниа, Х. Чаргазиа

Резюме

Изучена генерация, интенсификация и дальнейшая нелинейная динамика внутренних гравитационных волн (ВГВ) в устойчиво-стратифицированной диссипативной ионосфере с неоднородным зональным ветром (сдвиговым течением). В сдвиговых течениях операторы линейных задач являются несамосопряженными, а соответствующие собственные функции – неортогональными, поэтому канонически-модальный подход мало пригоден при изучении таких движений. Более адекватным для таких задач становится немодальный математический анализ. На основе немодального математического анализа получены уравнения динамики и переноса энергии ВГВ возмущений в ионосфере со сдвиговым течением. Выводится необходимое условие критерий неустойчивости сдвигового течения в ионосферной среде. Найдено точное аналитическое решение как линейных, так и нелинейных динамических уравнений рассматриваемых задач. Найден инкремент сдвиговой неустойчивости ВГВ. Выявлено, что временное усиление ВГВ возмущений происходит не экспоненциально, а алгебраическим – степенным образом. Частота и волновой вектор генерируемых ВГВ мод являются функциями времени. Так что, в ионосфере со сдвиговым течением, волновые возмущения с широким спектром порождаются с линейным эффектом даже тогда, когда отсутствуют нелинейные и турбулентные эффекты. Проанализирована эффективность линейного механизма усиления ВГВ при их взаимодействии с неоднородным зональным ветром. Показано, что ВГВ эффективно черпают энергию сдвигового течения в линейной стадии эволюции и существенно увеличивают (на порядок) свою энергию и амплитуду. С увеличением амплитуды включается нелинейный механизм самолокализации, и процесс заканчивается сам-организацией нелинейных, сильно локализованных ВГВ вихревых структур. Тем самим появляется новая степень свободы системы и путь эволюции возмущений в среде со сдвиговым течением. В зависимости от вида профиля скорости сдвигового течения нелинейные ВГВ структуры могут

быть или чисто монопольным вихрем, или вихревой дорожкой, или вихревой цепочкой на фоне неоднородного зонального ветра. Накопление таких вихрей в ионосферной среде может создавать сильнотурбулентное состояние.

შიდა-გრავიტაციული ტალღური სტრუქტურების გენერაცია, ინტენსიფიკაცია და თვით-ორგანიზაცია დედამიწის იონოსფეროში არაერთგვაროვან ქარებთან ურთიერთქმედებისას

გ. აბურჯანია, ხ. ჩარგაზია

რეზიუმე

შესწავლილია შიდა-გრავიტაციული ტალღების (შგტ) გენერაცია, ინტენსიფიკაცია და შემდგომი არაწრფივი დინამიკა მდგრადად სტრატიფიცირებულ დისიპაციურ იონოსფეროში, რომელზეც ზემოქმედებს არაერთგვაროვანი ზონალური ქარი (წანაცვლებითი დინება). წანაცვლებითი დინებების წრფივი დინამიკის აღმწერ წრფივ განტოლებებში შემავალი ოპერატორები არ არიან თვით-შეუღლებულნი და შესაბამისი საკუთარი ფუნქციები არიან არაორთოგონალურნი. ამიტომ, ასეთი მოძრაობის აღსაწერად კანონიკური, მოდალური მიდგომა ნაკლებად გამოდგება. მზგავსი ამოცანების ამოსახსნელად უფრო ადექვატური გამოდგა ე.წ. არამოდალური მათემატიკური ანალიზი. არამოდალური მიდგომის საფუძველზე მიღებულია შგტ შეშფოთებების დინამიკის აღმწერი და ენერგიის გატანის განტოლებები არაერთგვაროვანი ქარებით მართულ იონოსფეროში. მიღებულია წანაცვლებითი დინებების იონოსფეროში არამდგრადობის აუცილებელი პირობა-კრიტერიუმი. განსაზღვრულია წანაცვლებითი არამდგრადობის ინკრემენტი. აგებულია ამოცანის აღმწერი წრფივი და არაწრფივი დინამიკურ განტოლებათა სისტემის ზუსტი ანალიზური ამონახსნები. გამოვლენილია, რომ შგტ შეშფოთებების გაძლიერება დროის მიხედვით ხდება არა ექსპონენციალურად, არამედ ალგებრულად-ხარისხობრივად. გენერირებული მოდების სიხშირე და ტალღური ვექტორი ხდებიან დროის ფუნქცია. ასე, რომ წანაცვლებითი დინებებისას იონოსფეროში წრფივი პროცესებით ეფექტურად აღიძვრებიან ფართო დიაპაზონის ტალღური შეშფოთებები მაშინაც კი, როცა არაწრფივი და ტურბულენტური პროცესები არ წარმოიშობიან. გაანალიზებულია შგტ გაძლიერების ეფექტურობა მათი არაერთგვაროვან ზონალურ ქარებთან ურთიერთქმედებისას. ნაჩვენებია, რომ საწყის წრფივ სტადიაზე შგტ დროებით მაგრამ ეფექტურად ართმევს ენერგიას წანაცვლებით დინებას და შესამჩნევად ზრდის (რიგით) თავის ამპლიტუდას და ენერგიას. ამპლიტუდის ზრდისას თამაშში ერთვება არაწრფივი თვითლოკალიზაციის ეფექტი და პროცესი მთავრდება არაწრფივი, ძლიერად ლოკალიზებული შგტ გრიგალური სტრუქტურების თვითორგანიზაციით. მაშასადამე, წანაცვლებითი დინებები სისტემას ანიჭებს ახალ თავისუფლების ხარისხს და შესაბამისად, აჩენს შეშფოთებების ევოლუციის ახალ გზას. წანაცვლებითი დინებების სიჩქარის პროფილისაგან დამოკიდებულებით შგტ სტრუქტურები შეიძლება იყონ ან სუფთა მონოპოლური გრიგალები, ან განივი გრიგალური ჯაჭვები ან და გასწვრივი გრიგალური ბილიკები არაერთგვაროვანი

ზონალური ქარის ფონზე. ასეთი გრიგალური სტრუქტურების იონოსფეროში დაგროვებამ შეიძლება წარმოქმნას ძლიერად ტურბულენტური მდგომარეობა.

Journal of the Georgian Geophysical Society,
Issue (B), Physics of Atmosphere, Ocean, and Space Plasma, v.15, 2011-2012, pp. 95-108

The magnetic boundary layer of the Earth as an energy-supplying channel for the processes inside the magnetosphere

[1]Marina Chkhitunidze, [2]Nino Dzhondzoladze

[1]*I.Javakhishvili Tbilisi State University, M.Nodia Institute of Geophysics,1 Aleqsidze str. ,0171,Tbilisi*
[2]*I.Gogebashvili Telavi State University*

Abstract

Quasi-viscous interaction between the solar wind plasma and the geomagnetic field regularly takes place at the boundary of the magnetosphere. Like the effect of reconnection of force lines of the Earth magnetic field and the interplanetary magnetic field (IMF) transported by the solar wind the intensity of the quasi-viscous interaction depends on the magnetic viscosity of the plasma. Anomalous increase of the value of this parameter in the MHD boundary layer of the Earth, the magnetopause is analogized with which, is connected with the variation of the solar wind perturbation. In such circumstances for presenting the development process of the magnetopause dynamics the numerical and analytical methods of mathematical modeling have been used. Their effectiveness depends on the quality of the model describing the energy transmission process from the solar wind to the magnetopause. Usually, adequacy of a model for the development dynamics of the phenomena inside the magnetosphere is assessed in this way. In this work one of such theoretical models is considered. This model is based on the Zhigulev "magnetic" equation of the MHD boundary layer, which is simplified by means of the Parker velocities kinematic model. In order to clearly show the physical mechanisms stipulating the energy transmission process from the magnetosphere boundary to its inner structures some new characteristics of the MHD boundary layers are presented: thicknesses of magnetic field induction and the energy driven into the magnetopause. Besides, in the magnetic field induction equation several models of impulsive time variation of the magnetic viscosity of the solar wind is used and by means of the sequent approximation method an analytical image of quasi-stationary variation of the magnetopause parameters correspondent to these models is presented.

1. Introduction

At the boundary of the Earth magnetosphere there is a distinguished structure called magnetopause – an area where the solar wind plasma screens the geomagnetic field. According to the physical properties the magnetopause may be analogized with the magnetohydrodynamic (MHD) boundary layer that is usually created during overflow of a solid surface magnetized by fluid or gas characterized with finite electric conductivity [1]. Similarity between the magnetized

surface and the magnetosphere boundary is especially obvious at the boundary of the dayside of the magnetosphere. In its central area the flow of the solar wind plasma ramifies and a focal area is formed. Generally, the image of the overflow of the magnetosphere is spatial and asymmetric. According to various theoretical models the asymmetric character of the overflow of the magnetosphere is caused by the MHD nature of the flow of the solar wind plasma [2-4]. Experimentally this theoretical result is more or less proved by the work [5], and more completely- by results of computer simulations carried out recently [6].

Usually, energy dissipation always takes place in any type boundary layer (dynamic, temperature, magnetic). Therefore, during overflow of a solid surface stipulated by fluid or gas some part of the thermal flux formed by the dissipation in the boundary layer will penetrate into the overflowing body. It is natural that such an effect occurs during MHD overflow as well. Though, due to the specific nature of the overflow of the magnetosphere, thermal flux is substantially impossible on the magnetopause due to extremely low density of the solar wind. At the same time temperature change in the components of this extremely low density plasma is quite presumable. Change of the size as well as the direction of the induction flow of the magnetic field is also possible. The result of the former may appear in development of anomalous electric resistance effect in the plasma characterized with very high electric conductivity before interaction with the magnetosphere. This, in its turn, will intensify dissipation processes in the magnetopause. Both effects are connected with deceleration of the solar wind near the magnetosphere boundary. Invasion of additional flow of the magnetic field from the magnetopause into the magnetosphere is especially seen during sharp change in the distribution of the geomagnetic field induction in the MHD boundary layer. In such a case a change in the energy balance inside the magnetosphere is especially felt and it is linked with the reconnection of the force lines of the interplanetary magnetic field and the geomagnetic field [7]. Consequent to this process the corpuscular flow caused by erosion of the magnetosphere boundary will be distributed into different structures of the magnetosphere causing intensification of the radiation belts of the Earth.

Thus, analogizing the magnetopause with the magnetic boundary layer of the Earth is approved by physical similarity between the solid magnetized surface and the magnetosphere boundary. Such a view is especially suitable for analysis of the mechanisms directing the energy transition from the solar wind to the magnetosphere. However, for reliability of its qualitative physical image to strengthen it by quantitative assessments is very important. In its turn, it requires mathematically correct modeling of MHD effects developed in the magnetosheath (transitional area) before the magnetosphere and in its boundary. For the case of the magnetopause the basis for such modeling is the so called Zhigulev equation system of the plane magnetic boundary layer that corresponds to the main sections of the magnetosphere. In particular, the Zhigulev first category boundary layer corresponds to the meridional section of the magnetosphere that is directed along the central boundary force line of the geomagnetic field, and the second category magnetic boundary layer corresponds to the perpendicular equatorial section of the magnetosphere. The difference between the MHD equation systems that correspond to these layers is caused by the direction to each other of the components of the magnetic and velocity fields [1,3]. The reason for this difference is the flat characteristic of the equation system of the boundary layer and has no

substantial meaning from the viewpoint of similarity of the physical processes taking place in the magnetopause.

Like any equations of the boundary layer, it is possible to solve the equations of the MHD boundary layer by numerical as well as analytical methods. At the same time, it is to be taken into account that to receive a precise analytical solution, except in the cases that are very simple and less interesting in the physical viewpoint, is almost impossible. This is connected with the problem of self-consistency of the magnetic and velocity fields that is a huge problem for tasks of MHD overflow. Therefore, the hydrodynamic image of the solar wind flow is primarily determined by means of any kinematical model. Generally, the purpose of the mathematical modeling of the boundary layer is to determine its parameters by means of the characteristics of the overflowed surface and the overflowing environment. The most important among these parameters are the thickness of the boundary layer and the image of latitudinal and longitudinal varieties forming the boundary layer. In the case of the magnetic boundary layer of the Earth such a characteristics is the distribution of the geomagnetic field over the magnetopause [3]. This parameter, like the thickness of the magnetopause, is especially variable due to regular changes in the velocity and density of the solar wind plasma and the frozen interplanetary magnetic field transported by the plasma. As the gas-dynamic pressure of the solar wind depends on its perturbation value its change is especially well manifested in the distance from the Earth to the critical point R_0 of the magnetosphere. As far as this linear parameter is changing the thickness of the magnetopause must be changing as well. Nevertheless, in some cases this effect might be leveled by the change in the electric conductivity of the solar wind. It means that the thickness of the magnetopause might not always be in correlation with the R_0 parameter. The image of variation of the latter is especially made obvious by the numerical model [8], the theoretical basis of which is described in the work [9]. However, this model, like other theoretical models, is not able to clearly determine the thickness of the magnetopause. The main reason for such a circumstance is gaps of the theoretical models and limited capacity of the analytical methods for solving the MHD equation systems. In this viewpoint the numerical methods have certain advantage, though they have quite significant disadvantage as they provide only retrospective analysis. Therefore, in case of the changes of the parameters of the solar wind it is impossible to forecast the nature of changes in the magnetopause parameters. In this respect we assume that the so called Schwec successive approximation method is more effective compared to other methods [10]. It enables to receive an image of the thickness of meridional and equatorial magnetopause and the magnetic field distribution in it in a clear analytical form [3,11,12]. In these works, for simplification of the Zhigulev equation system of the first and second category MHD boundary layer, the so called wedge-like model of magnetosphere and the Parker kinematic model were used. These models primarily determined the field of the velocities of the plasma near the critical point of the magnetosphere [13]. It is noteworthy that the Parker model and also its generalization in three-dimensional event have been very popular for modeling the annihilation process of the geomagnetic field at the dayside boundary of the magnetosphere [14].

Thus, the central area of the magnetopause at the dayside of the magnetosphere represents a main energy channel, by means of which the structures inside the magnetosphere are supplied

with corpuscular flow from the solar wind. This process also involves gigantic funnel-shaped structures, polar cusps. By means of them the particles of the solar wind easily reach to the polar ionosphere. However, here the bulk of these particles are lost. Consequently, polar lights and aurora are observed. Only a few protons and electrons of the solar wind reach the magnetosphere structures from the solar wind. We may suppose that a structure similar to the MHD boundary layer may be formed also at the boundary of the polar cusp, in which formation of global geomagnetic storms is most probable due to the nature of the plasma flow. Therefore, the laminar approximation and consequently the use of equations of the MHD boundary layer are quite uncertain here.

2. The basic principles and initial equation

As we mentioned above, with its abilities the Parker kinematic model is quite effective as it enables to determine the velocity field of the ideal flow of the incompressible plasma near the critical point of the overflowing body. This very model has enabled to determine the parameters of the quasi-stationary meridional magnetopause [3,11,12]. As the velocity field was stationary the time dependence value has entered the induction equation of this magnetic field by means of different models of impulsive time variation in the electric conductivity of the solar wind. Furthermore, by the Shwec successive approximation method the parameters of the MHD boundary layer were determined in the same way: thickness and distribution of magnetic and electric fields over the magnetopause, and the velocity of the electromagnetic drift. However, these works do not involve any survey of the problem of the energy balance between the magnetopause and the dayside of the magnetosphere, modeling of which is the purpose of our work. For this reason qualitative admission was made, according to which during the changes of the parameters of the solar wind the magnetopause and the focal part of the dayside of the magnetosphere are considered as a closed system. It means that within some limits in this area the law of constancy of energy is quite admissible. It is natural that such an admission is quite inaccurate approximation compared to the real circumstances. At the same time, as it will be seen, it has adequate results with regard to the experimental data.

Thus, we may admit that in the focal area of the magnetosphere the sum of the energy accumulated in the MHD boundary layer of the Earth and the energy of the surface magnetospheric global DCF-current is unchanged during the perturbation of the solar wind. It is supposed, that the components of the summarized energy are the energies of the magnetic flow and the magnetic field and the energy of the corpuscular flow penetrated into the magnetosphere. It is clear, that in spite of the perturbation value of the solar wind some partial changes in the full energy will always take place. It means that the intensity of the DCF-current may change at the expense of the variation in the distribution of the magnetic field over the magnetopause. However, increase of the DCF-current certainly causes intensification of the processes inside the magnetosphere.

Such an image enables to use physical analogy at the hydrodynamic boundary layer, inside of which for assessment of the energy changes there are two effective parameters: the thickness of

the boundary layer and the thickness of loss of the mechanical impulse. For the MHD boundary layer, as the analogy of these parameters, two characteristics were used: 1) δ_a - the thickness of displacement of magnetic field induction; 2) δ_b - the thickness of magnetic energy displacement [3]. According to the explanation the thickness of displacement of magnetic field induction shows the thickness of the induction flow loss by means of comparing the distribution of the magnetic field to the corresponding distribution of the ideal profile in the latitudinal section of the magnetopause. In addition, the thickness of the energy loss of the magnetic field shows the thickness of the lost energy layer by comparing it to the ideal distribution. Generally, these parameters are defined by the following expressions:

$$\delta_a = \int_0^{\infty,\delta_H} \left(1 - \frac{H}{H_0}\right) dx, \qquad (1)$$

$$\delta_b = \int_0^{\infty,\delta_H} \left(1 - \frac{H^2}{H_0^2}\right) dx, \qquad (2)$$

where the x -coordinate from the critical point of the magnetosphere is directed to the sun, and the magnetic field induction–H, the characteristic value of which is H_0, is directed alongside the extreme force line of the geomagnetic field. The upper boundary of integration may be replaced by the finite thickness of the MHD boundary layer only in case when this parameter is defined in analytically clear form. Such a possibility is given by the Schwec successive approximation method. In the approximation of the wedge-like model of the magnetosphere the above mentioned parameters were determined for the first time by this method and this have been the only attempt to use them so far. However, in the previous results the impulsive time variation of either the electric resistance of the solar wind plasma, or the parameter depended on it - the magnetic viscosity were not considered. The further obtained experimental data proved the possibility of anomalous increase of the electric resistance of the solar wind that has been used in modern computer experiments [6]. Therefore, it is obvious that qualitative and quantitative corrections of the data works [11,15,16] carried out earlier are necessary.

MHD equations involve magnetic viscosity λ_m as a coefficient that is defined by σ specific electric conductivity (c is light speed):

$$\lambda_m = \frac{c^2}{4\pi\sigma}, \qquad (3)$$

Let us use the following expressions for modeling of the impulsive time variation of this parameter during perturbation of the solar wind:

$$1)\ \lambda_m = \lambda_{0m}[1+\beta\sin(\pi t/\tau_0)];\quad 2)\ \lambda_m = \lambda_{0m}e^{-\frac{t}{\tau_0}};\quad 3)\ \lambda_m = \lambda_{0m}(1-e^{-\frac{t}{\tau_0}}), \qquad (4)$$

where λ_{0m} is the value characterizing the magnetic viscosity, τ_0 - the time characterizing the impulsive variation of the magnetic viscosity, β - the coefficient of the impulsive strengthening. It is obvious that the first model corresponds to the periodic perturbation of magnetic viscosity, and the rest of the models are physically similar and show the change of the electric conductivity of the plasma from the finite to the ideal and vice versa.

Let us not take into account the curvilinearity of the extreme force line of the geomagnetic field on the dayside and direct the *y* axis from the critical point of the magnetosphere to the periphery. In case of such admission for determining topologic image of nonstationary distribution of the magnetic field in the Zhigulev first category plane boundary layer we may use a single-component equation of magnetic induction

$$\frac{\partial H_y}{\partial t}+u\frac{\partial H_y}{\partial x}+v\frac{\partial H_y}{\partial y}-H_y\frac{\partial v}{\partial y}=\lambda_m\frac{\partial^2 H_y}{\partial^2 x}. \qquad (5)$$

According to the Shwec successive approximation analytical method suppose that the value of the Earth's dipole magnetic field in the lower boundary of the magnetopause is constant and gradually decreases in latitudinal direction of the δ_H thickness of the magnetic boundary layer. Thus, we have the following boundary conditions for the (5) equation

$$H_y=H_0,\ \text{when}\ x=0;\quad H_y=0,\quad \text{when}\ x=\delta_H. \qquad (6)$$

Near the critical point of the magnetosphere the velocity field of the noncompressible plasma is determined by the Parker kinematic model [13]

$$u=-\alpha x,\qquad v=\alpha y, \qquad (7)$$

where α is the reverse value of the time characteristic for the overflow of the magnetosphere day side. Thus, by means of (6) and (7), e.g. in case of the (4.1) model, we will have the equation

$$\frac{\partial H_y}{\partial t}-\alpha x\frac{\partial H_y}{\partial x}-\alpha H_y=\lambda_{0m}\left[1+\beta\sin(\pi t/\tau_0)\right]\frac{\partial^2 H_y}{\partial x^2}. \qquad (8)$$

In the (6) boundary conditions, for solving the (8) equation, also the corresponding equations of the (4.2) and (4.3) models and for gaining information on the determination scheme of the magnetopause thickness we may refer to the works [3,11,12]. Therefore, it is quite sufficient to present quasi-stationary expressions of the distribution of the magnetic field over the meridional magnetopause and the boundary layer thickness ($'$ means the time derivative)

(4.1) $\lambda_m=\lambda_{0m}[1+\beta\sin(\pi t/\tau_0)]$

$$\frac{H_y}{H_0}=\left(1-\frac{x}{\delta_H}\right)+\lambda_{0m}^{-1}\left[1+\beta\sin(\pi t/\tau_0)\right]^{-1}\times\left[\left(\frac{\delta_H'}{\delta_H^{\,2}}\frac{x^3}{6}-\frac{\delta_H' x}{6}\right)+\alpha\left(\frac{x^3}{3\delta_H}-\frac{x^2}{2}+\frac{\delta_H x}{6}\right)\right], \qquad (9)$$

$$\delta_H=\left(\frac{6\lambda_{0m}}{\alpha}\right)^{1/2}\left[1+\frac{\alpha^2\beta}{\alpha^2+\pi^2/\tau_0^2}\left(\sin\left(\pi\frac{t}{\tau_0}\right)-\frac{\pi}{\alpha\tau_0}\cos\left(\pi\frac{t}{\tau_0}\right)+\frac{\pi}{\alpha\tau_0}e^{(-\alpha t)}\right)\right]^{1/2}. \qquad (10)$$

(4.2) $\lambda_m=\lambda_{0m}e^{-\frac{t}{\tau_0}}$

$$\frac{H_y}{H_0}=\left(1-\frac{x}{\delta_H}\right)+\lambda_{0m}^{-1}e^{\frac{t}{\tau_0}}\left[\left(\frac{\delta'_H}{{\delta_H}^2}\frac{x^3}{6}-\frac{\delta'_H}{6}x\right)+\alpha\left(\frac{x^3}{3\delta_H}-\frac{x^2}{2}+\frac{\delta_H}{2}x\right)\right] \quad (11)$$

$$\delta_H=(6\lambda_{0m}\alpha^{-1})^{1/2}\left[e^{-\alpha t}+\left(1-\frac{1}{\alpha\tau_0}\right)^{-1}\left(e^{-\frac{t}{\tau_0}}-e^{-\alpha t}\right)\right]^{1/2}, \quad (12)$$

(4.3) $\lambda_m=\lambda_{0m}(1-e^{-\frac{t}{\tau_0}})$

$$\frac{H_y}{H_0}=(1-\frac{x}{\delta_H})+\lambda_{0m}^{-1}\left((1-e^{-\frac{t}{\tau_0}})\right)^{-1}\left[(\frac{\delta'_H}{{\delta_H}^2}\frac{x^3}{6}-\frac{\delta'_H}{6}x)+\alpha(\frac{x^3}{3\delta_H}-\frac{x^2}{2}+\frac{\delta_H}{6}x)\right], \quad (13)$$

$$\delta_H=(6\lambda_{0m}\alpha^{-1})^{1/2}\left[\left(1-e^{-\alpha t}\right)+\left(1-\frac{1}{\alpha\tau_0}\right)^{-1}\left(e^{-\frac{t}{\tau_0}}-e^{-\alpha t}\right)\right]^{1/2}. \quad (14)$$

3.Physical analysis

By means of the (9)-(14) expressions it is possible to use the (1) and (2) expressions and determine their corresponding parameters by the magnetopause thickness. The results obtained before did not take into account the perturbation nature of the solar wind, possibility of which is given by the variation of the boundary conditions. By this way the qualitative analysis becomes easier, purpose of which is to show the so called North-South of the interplanetary magnetic field (IMF), as we have marked the B_y component, the variation of the value and direction in case of the (6) conditions changes in the image of the magnetic field distribution over the magnetopause. Such an analysis is interesting for qualitative consideration of a dynamical image of strong geomagnetic perturbations. It is known that when B_y is directed in the anti-parallel direction (i.e. to the South) of the geomagnetic field the reconnection of the force lines of the IMF and the geomagnetic field boundary may occur. Consequently, it will be followed by erosion of the magnetosphere boundary. In the opposite case, when B_y is directed to the North, the magnetosphere boundary is especially resistant to the invasion of the solar wind particles. Taking into account the first event of the B_y effect in the (6) boundary conditions leads to the following qualitative result: when B_y is directed to the North, addition of its value must not cause any change of the geomagnetic field profile screened on the magnetopause. However, when B_y is directed to the South, probably, the profile will qualitatively change and will resemble the profile characteristic for the Quetta MHD flow [17].

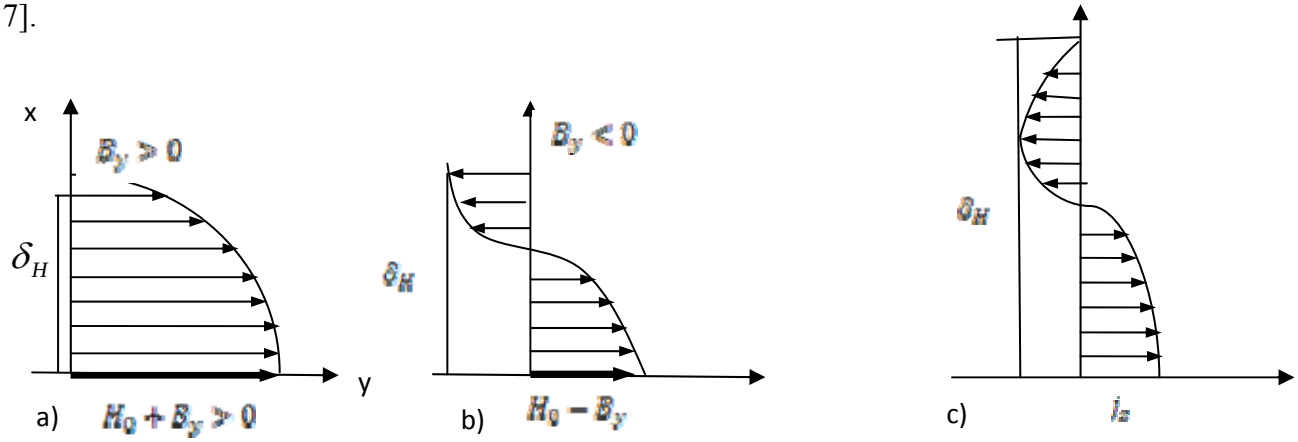

Figure 1. a) and b) The qualitative image of the geomagnetic magnetic field induction distribution over the magnetopause; c) distribution of the generated electric current for the b) case.

The above mentioned is illustrated by Figures 1a and 1b, which show corresponding profiles of varieties of B_y. The most interesting is fig. 1c. It clearly shows that the electric current generated in the magnetopause must be a partial component of the surface magnetospheric DCF-current.

The Figure 1c shows the profile of the inducted current that corresponds to the 1b event. Seemingly, like the magnetic field induction, in this case the direction of the electric current generated in the magnetopause is inverted as well. Similar behaviour must be characteristic for the corresponding component of the electric field intensity. It is obvious that formaly the electric current generated in the magnetopause is a partial component of the surface magnetospheric DCF-current. Therefore, this event is especially interesting in the viewpoint of analysis of the geomagnetic effects caused by the DCF- current intensity varieties.

Thus, the Fig.1a corresponds to the event when the IMF has a quite strong northern constituent. According to strong magnetospheric perturbation, e.g. the dynamics of the global geomagnetic storm development, this event is one of the reasons for the increase in the surface DCF- current intensity. The indicator is intensification of the screening effect in the magnetosphere boundary. Indeed, as in the $B_y > 0$ event the electric current generated in the magnetopause is parallel to the DCF-current it causes intensification in the latter. Though, meanwhile the change of the R_0 parameter may not be conspicuous. However, if the velocity and density of the solar wind increase violently, i.e. the gasodynamic pressure of the plasma increases and the magnetosphere boundary comes close to the Earth, it refers to a positive jump of the geomagnetic field. Usually it means that the initial phase of sudden commencement geomagnetic storm (SSC) is being formed. When $B_y < 0$ an opposite event, i.e. the geomagnetic field depression takes place. This event corresponds to the main phase of the geomagnetic storms. Its development is caused by the erosion of the magnetosphere boundary due to the reconnection of the force lines of the IMF and the geomagnetic field. On the other hand, it means that the effect screening the DCF- current that connects the plasma particles is weakened, due to which the intensity of the DR- the circular current inside the magnetosphere is increased [2,7]. Such a situation must be expressed by the figure 1c, according to which when there are anti-parallel and spatially distant from each other currents on the magnetopause their interaction is quite possible. It is natural that a summarized effect in the form of the global DCF- current takes place on the surface of the magnetosphere. However, due to the superposition of the partial currents which have opposite directions their contribution in the DCF- current decreases. In such a case the magnetosphere boundary moves again away from the Earth, and in the magnetosphere an injection of the additional corpuscular flow and magnetic field flux will take place. We may imagine the latter as the part of the geomagnetic field flux driven to the magnetopause, which appeared in the erosive area of the magnetosphere boundary. It is noteworthy that suggested by us the qualitative scheme of the development of the global geomagnetic storm with sudden commencement (SSC) is in principal accordance to the up-to-date global numerical model of the interaction of the magnetosphere and the solar wind [18]. This work, besides the complete simulation, considers the results of virtually strong geomagnetic storms in order to imagine the whole section dynamics of

the magnetosphere. In particular, the records of the geostationary satellite GEOS and the records of the geomagnetic field on the Earth are compared to each other. Their analyses proved complete synchronism of the effects developed in the magnetosphere and on the Earth surface. The global geomagnetic storms, besides the variation in the intensity of the geomagnetic field, are followed by other effects as well. Among them is the increase of electron concentration in the ionosphere, the main radiation belt of the Earth. In its upper F- layer this event is especially felt. This effect is especially promptly observed in the main phase of the geomagnetic storm in the polar and high-latitude ionosphere. Therefore, it was considered that the ionosphere was mainly supplied with the energy from the polar cusp. However, according to [19] in the lower D-layer of the ionosphere, in low and middle latitudes, during day time, increase of electron concentration and intensification of very low frequency electromagnetic radiation are observed. As this effect occurs with certain time delay the author of the work [19] supposes that the energy electrons are distributed from high latitudes to the low ones. However, the force lines of the geomagnetic field corresponding to the low latitudes form a boundary of the plasmasphere, the main plasma reservoir of the almost entirely closed magnetosphere. Consequently, on the dayside this ellipsoid-shape structure that represents the spatial projection of the central area of the magnetopause must be supplied with energy mainly from the focal area of the magnetosphere. Indeed, high energy electrons, concentration of which is always insignificant in unperturbed solar wind, may appear in the low latitudes as a result of reconnection of the force lines of the IMF and the geomagnetic field. Acceleration of the electrons that have penetrated into the magnetosphere from the erosive area of the magnetosphere boundary is caused by a vast electric field, the direction of which is anti-parallel to the electric field of the DCF- current in the focal area. It is natural that these fields influence on each other. In particular, according to the figure 1c the intensity of the surface magnetospheric electric field must decrease due to the weakening of the summarized field generated in the magnetopause. Consequently, the value of the electric field inside magnetosphere must increase that is equal to activation of acceleration mechanism in low energy electrons. However, it must be emphasized that such a scheme of development of the above described events is appropriate only for the dayside of the magnetosphere. However, there are up-to-date data that prove that concentration increase of the energy electrons in the low latitude ionosphere is also possible in the nightside of the plasmasphere [20]. By this time, intensification of the VLF electromagnetic radiation and short-time geomagnetic pulsation generation are observed here. This work involves a detailed morphological analysis of a similar event on the example of one concrete case. According to the conclusion, such events are connected not with the development of global geomagnetic storms but with the generation of sufficiently strong magnetic substorms in the polar area.

4.Results of numerical analysis

According to the specification of the Parker kinematic model in the stationary event the thickness of the magnetic boundary layer, as it is obvious in the corresponding analytical expressions, is constant. As the time correlation has entered the task from the magnetic viscosity

coefficient, and the equation (5) has no starting condition all its solutions (9)-(16) are quasi-stationary [16]. The admission that the thickness of the magnetic boundary layer does not vary alongside the magnetosphere boundary is quite inaccurate and it is natural that it decreases the value of the results. Though this defect is rather quantitative than qualitative. Consequently, the above mentioned must have no substantial influence on the vast MHD image of the magnetopause. In order to corroborate this fact we carried out analysis of the (9)-(14) expressions. For quantitative and qualitative assessments we used the following parameters characterizing the magnetosphere overflow: $\lambda_{0m} = 10^{12}\,\mathrm{cm^2.s^{-1}}$, $\beta = 10^2$, $\tau_0 = 500\,\mathrm{s}$ and $\alpha = \frac{V_0}{l_0} = 0.01\ \mathrm{s^{-1}}$. According to the model the last parameter is determined by the velocity characterizing the solar wind in the focal area of the magnetosphere and the linear scale of this structure: $V_0 = 2 \cdot 10^7\,\mathrm{cm.s^{-1}}$, $l_0 = 2 \cdot 10^9\,\mathrm{cm}$ [16]. In the first model, as $\sin(\pi t / \tau_0)$ the function argument varies in the interval /0-π/, increase in the magnetic viscosity is possible by two rates. Such increase is natural for perturbated solar wind in case when all the conditions for development of anomalous electric resistance in the space plasma are fulfilled. In such a case generation of either global geomagnetic storms or high latitudinal magnetospheric substorms becomes especially probable [19]. The perturbation of the second type in the magnetosphere is usually much briefer compared to the first one. Therefore, in the fig. 2 the minimal time for development of a storm is used as a characteristic of impulsive time variation of the magnetic viscosity.

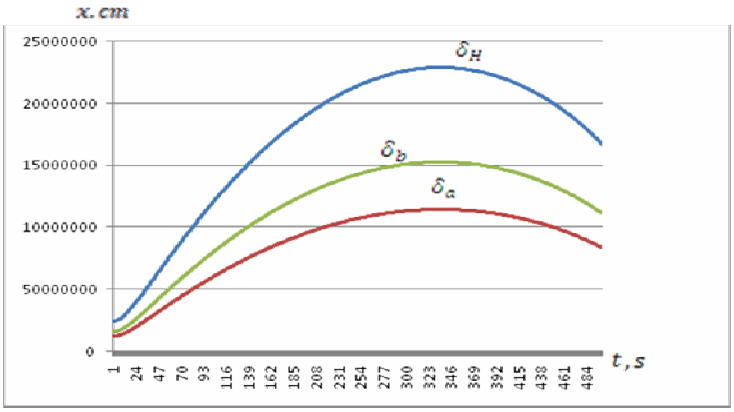

a) $\lambda_m = \lambda_{0m}[1 + \beta \sin(\pi t / \tau_0)]$

.

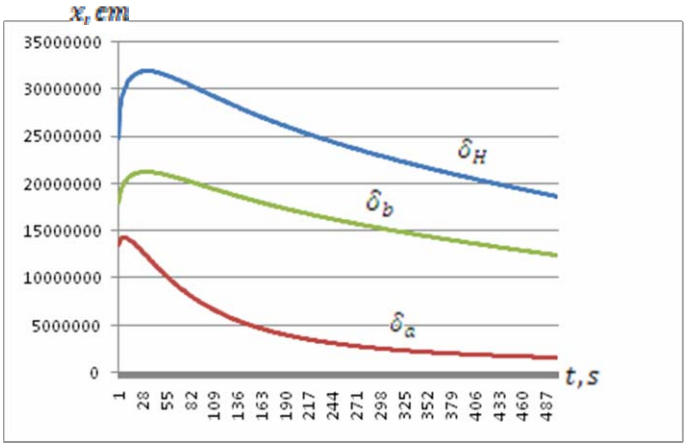

b) $\lambda_m = \lambda_{0m} e^{-\frac{t}{\tau_0}}$

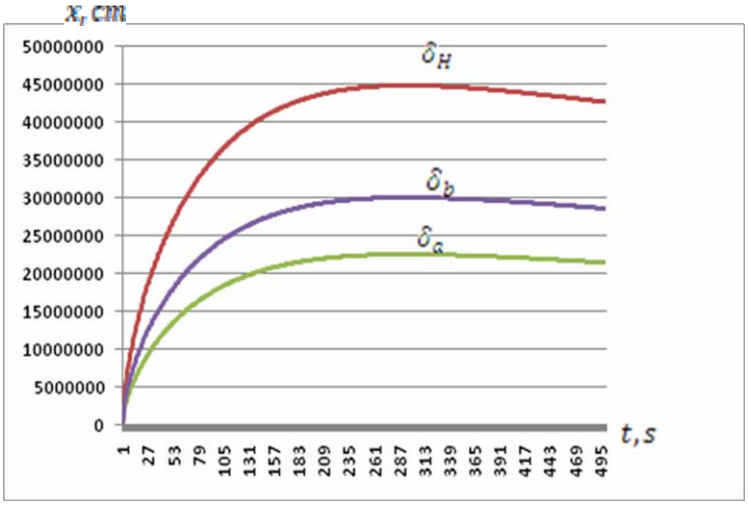

c) $\lambda_m = \lambda_{0m}(1 - e^{-\frac{t}{\tau_0}})$

Figure 2. a),b) and c)- quantity change of characteristic magnetopause parameters $\delta_H, \delta_b, \delta_a$

5.Conclusion

Interpretation of experimental data correctly is an actual problem of the magnetosphere physics. Modeling of MHD interaction effects of the solar wind and the geomagnetic field in the magnetopause is particularly connected with this problem. Mathematically, this task, is especially complex, though in the boundary layer approximation it is quite simplified. For this purpose, this work involves a theoretical model that enables to receive a clear vast MHD image of dynamic variation of the magnetopause parameters. In particular, it is possible to adequately express the physical mechanisms for energy transmission from the dayside boundary of the magnetosphere to its inner structures during the perturbation of the solar wind. The fig. 2 shows the behaviour of the thicknesses of the magnetopause, the magnetic field induction displacement and the magnetic field energy loss within the frameworks of each model of the impulsive time variation of the magnetic viscosity of the solar wind plasma. In all the three cases synchronous time variation of the magnetopause thickness and the (1) and (2) parameters was observed. The quantitative dissipation effect of the surface DCF-current during the screening process of the geomagnetic field in the magnetopause was clearly seen that may be considered as the main indicator for the physical value of the magnetopause model presented by us.

This project was carried out by grant (contract № 12/70) obtained through Shota Rustaveli National Science Foundation.

Nonprofit Edition

References

[1] Krimski G.F. Romashenko U.A. Magnetohydrodynamic model of the Magnetosphere. Investigation of Geomagn. Aeron. and Solar phys. Moscow,"Nauka",1975, v. 36, pp.174-199. (in Russian)

[2] Pudovkin M.L.,Semenov V.S. The reconnection theory and interaction of solar wind with the Earth's magnetosphere. Moscow,"Nauka", 1985, 125p. (in Russian)

[3] Kereselidze Z.A. MHD Effects of finite electric conductivity of solar wind near the Earth's Magnetosphere. Tbilisi,State Univ. Press.,1986, 122p. (in Russian)

[4] Russel C.T., Zhuang R.J., Walker L.G., Crooker N.U.. Note on the location of the stagnation point in the magnetosheath flow. Geoph. Res., Lett. 1981, v.8, pp.948-86.

[5] Crooker N.U., Siscoe G.L., Eastman T.E.,Frank L.A.,Zwiscl R.D. J.Geophys.Res.,1984, vol.89, pp.9711-19.

[6] Dorelli J.C., Hesse M., Kuznetsova M.M., Rastaetter L. A new look at driven magnetic reconnection at the terrestrial subsolar magnetopause. J. of Geophys. Res., 2010, v.109, A12216, doi:10.1029/2004JA010458.

[7] Liperovsky V.A., Pudovkin M.I. Anomalous Resistivity and double layers in the magnetospheric Plasma. Moscow,"Nauka", 1983, 183p.(in Russian)

[8] http:/pixie.spasci.com/DynMod, 2007.

[9] Shue, J.-H.; Song, P.; Russell, C. T.; Steinberg, J. T.; Chao, J. K.; Zastenker, G.; Vaisberg, O. L.; Kokubun, S.; Singer, H. J.; Detman, T. R.; Kawano, H. Magnetopause location under extreme solar wind conditions. J. of Geoph. Res., 1998,Vol. 103, Issue A8, pp. 17691-17700.

[10] Shwec M.O. About of approximate solution of same task of hydrodynamic boundary layer. Appl.Math and Mech. 1949, vol. 3, Issue XII, pp.253-266.

[11] Zhonzholadz N., Chkhitunidze M. Modeling of the Magnetic Boundary Layer in the Polar Cusp. The works compilation of Telavi State University, 2007, pp-15-19. (in Georgian)

[12] Vanishvili G.K.,Gabisonia I.A.,Kereselidze Z.A. Plasma model with variable conductivity on the boundary of day-side magnetosphere. Proceed. of Inst. of Geophys., Tbilisi, 2003, pp.285-293.ussian)

[13] Parker E.N. Comments on the reconnection rate of magnetic fields. J. Plasma Physics, 1973, v.9. p.1, pp. 49-63.

[14] Sonnerup B.U.O. and Priest E.R. Resistive MHD stagnation-point flows at a current sheet. J. Plasma phys., 1975,v.14, pp.283-294.

[15] Kereselidze Z., Chkhitunidze M. On the problem of simulation of the magnetic viscosity in the vicinity of the magnetosphere boundary. Georgian Engineering News, 2005, №2, pp.48-50.(in Russian)

[16] Kereselidze Z. Kirtskhalia V., Chkhitunidze M., Kalandadze I. On Modeling of Magnetic Boundary Layer on the Dayside Magnetosphere. Georgian International Journal of Sci. and Teq.,2008, ISSN 1939-5925,vol.1№3, pp.249-256.

[17] Sutton G.W. Sherman A. Engineering magnetohydrodynamic. McGarow-Hill Book Company , 1965.

[18] Pulkkinen A., Rastätter L., Kuznetsova M., Hesse M., Ridley M., Raeder J., Singer H.J. and Chulaki A.. Systematic evaluation of ground and geostationary magnetic field predictions generated by global magnetohydrodynamic models. J. Geophys. Res., 2010, 115, A03206, doi:10.1029/2009JA014537.

[19] Sokolov S.N. Magnetic storms and their effects in the lower ionosphere: Differences in storms of various types. Geomagnetism and Aeronomy. 2011, vol. 51, N 6, pp. 741-752.

[20] Kleimenova N.G., Kozyreva O.V., Manninen J., Raita T., Kornilova T.A., Kornilov I.A. High-Latitude Geomagnetic Disturbances during the Initial Phaze of a Recurrent Magnetic Storm (from February 27 to March 2, 2008). Geomagnetizm and Aeronomy, 2011, vol.51, N6, pp. 730-740.

(Received in final form 20 December 2012)

Магнитный пограничный слой Земли, как канал снабжения энергией процессов внутри магнитосферы

М.С. Чхитунидзе, Н.И. Жонжоладзе

Резюме

На границе магнитосферы происходит перманентное квазивязкое взаимодействие между плазмой солнечного ветра и геомагнитным полем. Подобно эффекту пересоединения силовых линий вмороженного в солнечный ветер межпланетного и земного магнитных полей, интенсивность квазивязкого взаимодействия зависит от магнитной вязкости плазмы. Аномальное возрастание величины этого параметра в МГД пограничном слое Земли, с которым отождествляется магнитопауза, зависит от уровня возмущения солнечного ветра. Исходя из необходимости явного представления динамических изменений крупномасштабной картины магнитопаузы, до настоящего времени используются различные численные и аналитические методы математического моделирования. Эффекетивность этих методов зависит от того, как удачно описывает модель передачу энергии солнечного ветра магнитосфере. Обычно, таким образом дается оценка адекватности модели относительно процесса развития различных магнитосферных явлений. В данной работе рассматривается одна из таких теоретических моделей магнитопаузы, основой которой является «магнитное» уравнение МГД пограничного слоя Жигулева, упрощенное при помощи кинематической модели Паркера для скорости плазмы. Для представления в явном виде физических механизмов, направляющих процесс передачи энергии от границы магнитосферы к ее внутренним структурам, вводятся дополнительные характеристики МГД пограничного слоя: толщины вытеснения индукции и энергии магнитного поля на магнитопаузе. При этом в «магнитном» уравнении Жигулева используются различные модели импульсного изменения во времени магнитной вязкости солнечного ветра. В результате при помощи метода последовательных приближений определена соответствующая этим моделям квазистационарная аналитическая картина изменения параметров магнитопаузы.

დედამიწის მაგნიტური სასაზღვრო ფენა, როგორც შიდამაგნიტოსფერული პროცესების ენერგომომარაგების არხი

მარინა ჩხიტუნიძე, ნინო ჟონჟოლაძე

რეზიუმე

კვაზიბლანტი ურთიერთქმედება მზის ქარის პლაზმასა და გეომაგნიტურ ველს შორის პერმანენტულად მიმდინარეობს მაგნიტოსფეროს საზღვარზე. მზის ქარის მიერ ტრანსპორტირებული საპლანეტათაშორისო მაგნიტური ველისა და დედამიწის მაგნიტური ველის ძალწირების გადაერთების ეფექტის მსგავსად, კვაზიბლანტი ურთიერთქმედების

ინტენსივობა დამოკიდებულია პლაზმის მაგნიტურ სიბლანტეზე. ამ პარამეტრის სიდიდის ანომალური ზრდა დედამიწის მჰდ სასაზღვრო ფენაში, რომელთანაც გაიგივებულია მაგნიტოპაუზა, დაკავშირებულია მზის ქარის შეშფოთების დონის ცვლილებასთან. ასეთ ვითარებაში მაგნიტოპაუზის დინამიკური სურათის განვითარების პროცესის ცხადი სახით წარმოდგენის აუცილებლობიდან გამომდინარე, აქამდე გამოიყენება მათემატიკური მოდელირების როგორც რიცხვითი, ასევე ანალიზური მეთოდები. მათი ეფექტურობა დამოკიდებულია იმაზე, თუ როგორ აღწერს მოდელი მზის ქარიდან მაგნიტოსფეროსათვის ენერგიის გადაცემის პროცესს. ჩვეულებრივ, ასე ფასდება მოდელის ადეკვატურობა შიდა მაგნიტოსფერული მოვლენების განვითარების დინამიკასთან. მოცემულ ნაშრომში განხილულია მაგნიტოპაუზის ერთ-ერთი ასეთი თეორიული მოდელი, რომელიც საფუძველს წარმოადგენს პარკერის სიჩქარეთა კინემატიკური მოდელის საშუალებით გამარტივებული ჟიგულევის მჰდ სასაზღვრო ფენის ”მაგნიტური” განტოლება. მაგნიტოსფეროს საზღვრიდან მისი შიდა სტრუქტურებისათვის ენერგიის გადაცემის პროცესის წარმმართველი ფიზიკური მექანიზმის ცხადად წარმოჩენის მიზნით შემოტანილია მჰდ სასაზღვრო ფენის ახალი მახასიათებლები: მაგნიტოპაუზაზე მაგნიტური ველის ინდუქციისა და ენერგიის გამოდევნის სისქეები. ამასთან, მაგნიტური ველის ინდუქციის განტოლებაში გამოყენებულია მზის ქარის მაგნიტური სიბლანტის დროში იმპულსური ცვლილების რამდენიმე მოდელი და მიმდევრობითი მიახლოების მეთოდის დახმარებით მიღებულია ამ მოდელების შესაბამისი მაგნიტოპაუზის პარამეტრების კვაზისტაციონარული ცვლილების ანალიზური სურათი.

Journal of the Georgian Geophysical Society,
Issue (B), Physics of Atmosphere, Ocean, and Space Plasma, v.15, 2011-2012, pp. 109-119

On the question of investigation of variations of the solar constant during the period of the severe geomagnetic storms

[1]Chkhetia A.M., [2]Gigolashvili M.S., [1]Ebralidze M.O.

[1]M. Nodia Institute of Geophysics at I. Javakhishvili Tbilisi State University, M. Alexidze 1, Tbilisi 0193, Georgia

[2]Georgian E.Kharadze Astrophysical Observatory at I. Chavchavadze State University, A. Kazbegi Ave 2a, Tbilisi 0160, Georgia.

Abstract

Still actinometrical observations in the interplanetary space, scientific workers of the Smithsonian Astrophysical Institute (USA), under his guidance of C. Abbott, obtained conclusion during the period of the severe geomagnetic storms, solar constant, as a rule, is anomalously decreased. This phenomenon is explained by Abbott like this – due to strong solar flare in solar-terrestrial interplanetary space. corpuscular cloud is ejected from the Sun. Corpuscular clouds condition Raleigh scattering of photon emission of the Sun and correspondingly, decrease of solar constant.

Comparison of variations of solar constant and intensity of the geomagnetic field in the period of large and very large magnetic storm ($\Delta Dst \leq -150$ nT) demonstrated that all considered cases can be divided into five types, according to the character of solar constant variation. From above stated experimental data follows undoubtedly that the result of Abbot's scientific school ("in the day of very large magnetic storm solar constant value, as a rule, is anomalously decreased") should be corrected so: correlation between variations of solar constant and magnetic storm is not simple.

Comparison of variations of solar constant and plasma cloud concentration of interplanetary medium, with high level of density (PCIMWHLD, $n_d \geq 25$ pr.cm $^{-3}$), revealed that variations of solar constant do not at all react at changes of PCIMWHLD. From above-stated experimental data logically follows that there aren't connection between variations of solar constant and PCIMWHLD. Hence Abbot's conception that -"due to strong solar flare in solar-terrestrial interplanetary space corpuscular cloud is ejected from the Sun. Corpuscular clouds condition Raleigh scattering of photon emission of the Sun and correspondingly, decrease of solar constant", unfortunately proved to be incorrect.

Intrudaction

Still actinometrical observations in the interplanetary space, scientific workers of the Smithsonian Astrophysical Institute (USA), under his guidance of C. Abbott, obtained conclusion during the period of the severe geomagnetic storms, solar constant, as a rule, is anomalously decreased [1]. This phenomenon is explained by Abbott like this – due to strong solar flare in solar-terrestrial interplanetary space corpuscular cloud is ejected from the Sun. Corpuscular clouds condition Raleigh scattering of photon emission of the Sun and correspondingly, decrease of solar constant.

Above – stated results of C. Abbot and his scientific school logically demand answers for two following questions:

1. If at the time of severe magnetic storm value of solar constant, as a rule, is anomalously decreased, what is main connecting link between solar activity and meteorological phenomena – electromagnetic irradiation or corpuscular radiation of the sun?

2. If C.Abbot's conception, that decrease of solar constant during severe magnetic storms is conditioned by Raleigh scattering by corpuscular cloud which is ejected from the Sun into interplanetary

space, is true then it is necessary to make a correction for change of density of interplanetary space is solar constant data by space vehicles.

Now, measurements of solar constant, which have been made in circum terrestrial cosmic space, exclude effects, which are connected with transparence of Earth atmosphere, and received results of the investigation are quite trustworthy.

The goal of the work is the following: to make our modest contribution to specification of above mentioned questions on the bases of complex synchronous measurements of solar constant, solar wind concentration in interplanetary space, and by magnetic observatories intensity of the geomagnetic field.

The following initial data was used in the process of investigation:

1. Daily average values of solar constant (SI) according to measurements made by the satellite NIMBUS 7 [2];

2. in order to characterize geomagnetic field during magnetic storm hourly values Dst-index were used [3], because Dst-index describe temporal variations of intensity of extra ionosphere current systems which occur during magnetopause (DCF) and in radiation zone (DR);

3. in order to characterize density variations of plasma clouds of interplanetary space hourly values of proton concentration (n) were taken from King's catalogue [4] (it is obvious plasma density of interplanetary space is $\rho = m_{pr} n$).

Part 1
Comparison of Variations of solar Constant and Intensity of the Geomagnetic Field during Severe Geomagnetic Storms

It is obvious, that, in order to solve the stated problem, it was necessary for investigation to compile the catalogue of severe magnetic storms during investigated period according to Dst-index. In the work [5] geomagnetic disturbances, which are classified in "Cosmic Data" [6] as magnetic storms of various intensity, during the period of 1965-1974 years, were compared with hourly values of Dst-index. It was established that cases, when Dst-index decrease in the main phase of storm fulfilled condition $\Delta Dst \leq -150$ n.T, were attributed to very large geomagnetic storms (VLGS). Hence, for investigated period, according to hourly values of Dst-index the catalog of VLGS was compiled, when Dst-index decrease in the main phase of storm fulfilled condition $\Delta Dst \leq -150$ n.T.

Comparison of variations of solar constant and intensity of the geomagnetic field in the period of VLGS revealed rather complex situation – it turned out that if in some cases VLGS value of solar constant was really decreased in a day, in other cases, its violation was observed. In order to understand such complex picture we have classified the cases according to groups, according to the character of solar constant variation in the period of VLGS duration. We have established that all considered cases could be divided into five types.

To the I types belong events, when in the period of the main phase of the geomagnetic storm, value of the solar constant undergo decreases (which coincides with results receiving by Abbott).

---

* Basic results of investigation were presented on the International conference – "2009 UN/ NASA/ESA/JAXA Workshop on Basic Space Science and the International Heliophy - sical Year 2007. Septembe r 21-25, 2009 Daejeon, Korea," p. 92.

The period analyzed by us includes temporal interval of measurements of solar constant, which were made by NIMBUS-7 from 16.11.1978 to 17.6.1992. Temporal interval of measurements, which we have investigated, includes the period between maxima of 21and 22 cycles of solar activity.

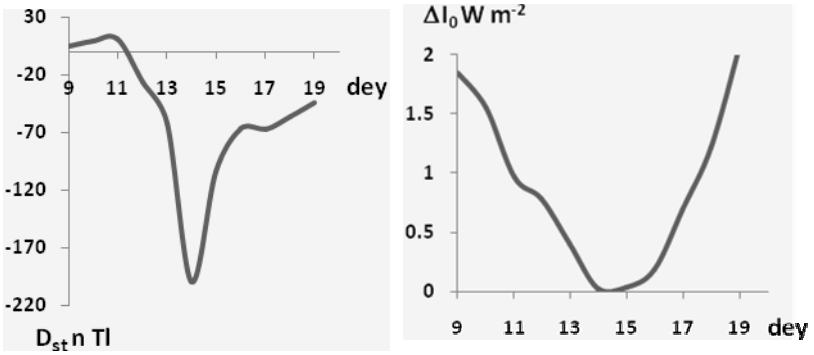

Fig.1.The example of I type interconnection (July 9-19, 1982 DR= -338 nT.)

Symbols: in figures 1-5, ordinate endwise average daily values intensity of the geomagnetic field of Dst-index; departure of solar constant (ΔI_o) from normal ($I_{o,norm}$=1370Wm^{-2}) are built up, and abscissa endwise – month days. DR is the value of Dst-index decrease in main phase of a storm, calculated according to hourly values of Dst-index.

To the II types belong events when in the period of the geomagnetic storm, value of the solar constant stays almost constant.

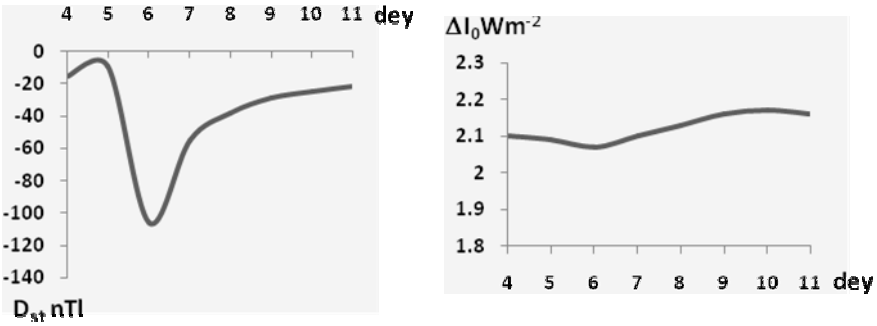

Fig.2. The example of II type interconnection (May 4-11, 1988). DR= -160 nT.

To the III types belong events, when in the period of the main phase of the geomagnetic storm, value of the solar constant undergo increases.

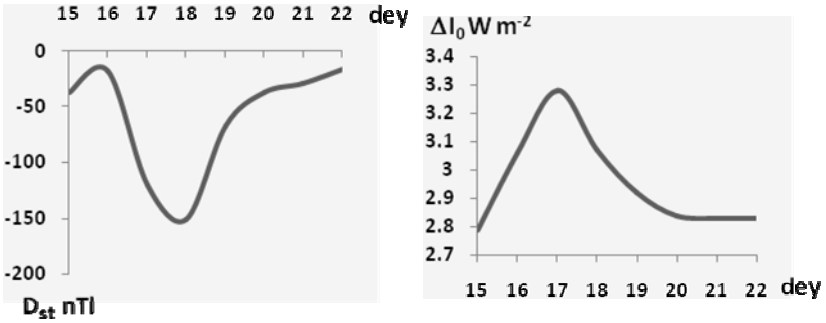

Fig.3. The example of III type interconnection (November 15-22, 1989). DR= -266 nT.

To the IV types belong events when in the period of the geomagnetic storm value of the solar constant gradually decreases.

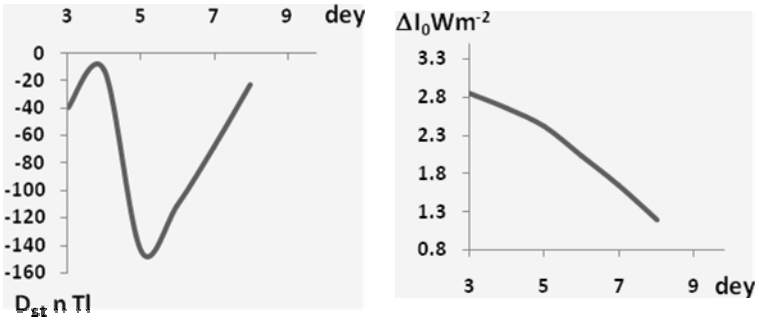

Fig.4. The example of IV type interconnection (June 3-8, 1991). DR= -219 nT.

To the V types belong events when in the period of the geomagnetic storm value of the solar constant gradually increases.

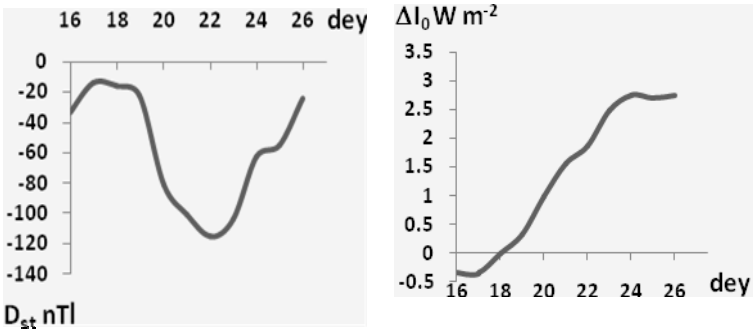

Fig.5. The example of V type interconnection (October 16-26, 1981). DR= -194 nT.

Analyzing curves of figures 1-5, we conclude that during VLGS definite, unambiguous interconnection between variations of solar constant and intensity of the geomagnetic field does not exist.

It is known that statistical method superposition of epochs (Chree's method [7,8]). is vide by used in analogous investigations in geophysics, astronomy and other sciences. Proceeding from above-said, we decided to use the method superposition of epochs too, in order to determine finally interconnection between variations of solar constant and intensity of the geomagnetic field during VLGS

In the process of the investigation, days of maximum decrease of geomagnetic field during main phase of magnetic storms were used as benchmark (zero) moment.

Fig.6 shows averaged (by the method superposition of epochs) variations of Dst-index and solar constant for VLGS observed in 1978-1992 years.

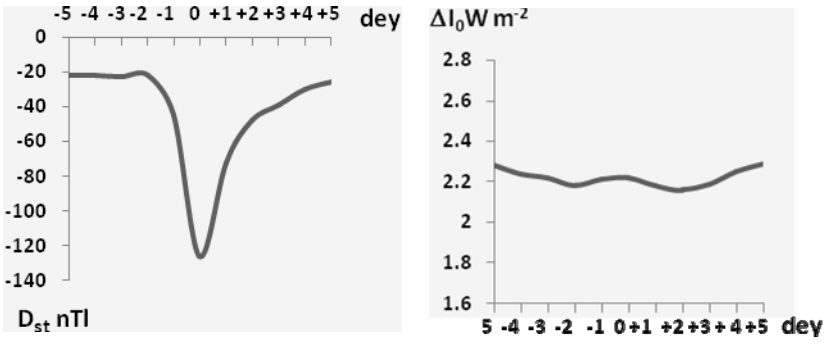

Fig.6. By the method superposition of epochs variations intensity of the geomagnetic field (Dst - index) and solar constant during VLGS in 1978-1992 years.

Fig. 6 shows that during VLGS solar constant value stays almost unchanged. Hence, the method superposition of epochs demonstrates again that during VLGS definite, unambiguous interconnection between variations of solar constant and intensity of the geomagnetic field does not exist.

Basic results of comparison of variations of solar constant and intensity of the geomagnetic field during very large geomagnetic storms (VLGS) are the following:

1. It was established that:

a) all considered cases of variations of solar constant during VLGS come to five types: in the period of main phase of the storm it decreases (I type); during storm is stays unchanged (II type); in the period of main phase of the storm it increases (III type); during the storm it gradually decreases (IV type); during the storm it gradually increases (V type).

b) By the method superposition of epochs variations intensity of the geomagnetic field and solar constant show that during VLGS value of solar constant stays almost unchanged.

Experimental facts demonstrate that during VLGS definite, unambiguous inter-connection between variations of solar constant and intensity of the geomagnetic field does not exist.

2. Conclusion of Abbot's school that "at the time of severe magnetic storms solar constant value is, as a rule, anomalously decreased", which was drown on the basis of actinometrical observations, was not corroborated.

3. It s known that VL magnetic storms (for example, E. Mustel [9]) and considerable variations of solar constant – 0,1-0,3% (for example, H. Volland [10]) may change atmospheric pressure appreciably and exert influence upon circulation processes of in terrestrial atmosphere.

Hence, when we study solar-atmospheric connection, it is logical and necessary to investigate separately those cases of observation of large and very large magnetic storms, which were not accompanied by considerable variations of solar constant and separately – considerable variations of solar constant which were not accompanied by large and very large magnetic storms.

Part 2
Comparison of variations of solar constant and plasma clouds of interplanetary medium with high level of density

Before we state results of the investigation concerning II part, we think it is necessary to clear up the role of plasma clouds of solar wind in magnetic storm formation.

It is known that classical geomagnetic storms, according to character of H – component change of geomagnetic field of middle latitude observatories (which are not influenced by auroral and equatorial electric stream), are characterized by initial phase main phase and recovery phase.

Initial phase (DCF-disturbance) is the period, during which level intensity of the geomagnetic field is higher than non-disturbance value. Amplitude of initial phase is $\Delta H \approx$ 20-40 nT and lasts from 2 to 8 hours. Basic key factor, that is responsible for DCF – disturbance formation, is plasma cloud of solar wind with high level of density [on condition that north-directed interplanetary magnetic field (I m F) $B_z > 0$].

Main phase (DR - disturbance) is characterized by sharp decrease intensity of the geomagnetic field below normal non-disturbance value. Depression difference is of the order of (50-200) nTl. Main phase of magnetic storm generally continues several hours. Basic key factor, that is responsible for DR – disturbance formation, is magnetic cloud with south-directed IMF $B_z <$ - (3-5) nT.

According to S. Akasoff and S. Chepman [11], geomagnetic storms of classical type usually consist of two forms of elementary disturbances – DCF and DR. Theoretically, each form of elementary disturbance can exist independently from each other.

Physical bases of the role of plasma parameters of solar wind in geomagnetic storm formation can be seen in detail in A. Chkhetia's monograph [12].

It follows from above stated that plasma clouds of solar wind do not participate in formation of severe geomagnetic storms. Therefore, it can be supposed, that Abbot's conception that Raleigh scattering conditions solar constant decrease during severe magnetic storms, ejected from the Sun corpuscular cloud, may not be true.

It is obvious that, in order to solve the stated problem, it is necessary for investigation to compile the catalogue of plasma clouds of interplanetary medium with high level of density (PCIMWHLD). The catalogue of PCIMWHLD was compiled based on data analysis of hourly average values of proton

concentration of interplanetary medium according to King's catalogue [4]. We selected PCIMWHLD according to the following succession:

1. For the investigated period, according to hourly average values of proton concentration (n_{ho}) of interplanetary medium, days were selected in which $n_{ho} \geq 40$ pr.cm $^{-3}$ (1).

Data selection criterion (1) indicates that in selected days increase of proton concentration exceeds minimum background average value approximately ten times.

2. Selected days which satisfied condition (1), according to King's catalogue should be full or should contain 2/3 or more hourly values (N_{ho}), it means $N_{ho} \geq 14$ ..... (2).

Satisfaction of condition (2) means that calculated, according to King's catalogue, daily average values of proton concentration of interplanetary medium are trustworthy.

3. Finally, days of PCIMWHLD were selected according to daily average values of proton concentration of interplanetary medium (n_{da}), which satisfied the condition $n_{da} \geq 20$ pr.cm $^{-3}$ ..... (3).

Satisfaction of condition (3) means that in selected days of PCIMWHLD there is no spontaneous (impulsive) increase of proton concentration of interplanetary medium.

On the basis of analysis of PCIMWHLD catalogue for investigated period we concluded the following:

1. PCIMWHLD may last 1-5 days;
2. It is advisable to divide PCIMWHLD into three subclasses:

a) Plasma clouds with high seals – 20 pr.cm $^{-3} \leq n_{da} <$ 25 pr.cm $^{-3}$;

b) Plasma clouds with very high seals – 25 pr.cm $^{-3} \leq n_{da} <$ 35 pr.cm $^{-3}$;

c) Plasma clouds with super high seals – $n_{da} \geq$ 35 pr.cm $^{-3}$.

Comparison of variations of solar constant and PCIMWHLD for investigated period revealed rather complex picture. It was found that in some cases in a day (or period) with high level density of interplanetary medium solar constant is really decreased, but in other cases its disturbances are observed. It is impossible to classify cases according to groups, character of solar constant variation in PCIMWHLD period. Picture 7 gives characteristic curves of comparison of variations of solar constant and plasma cloud concentration of interplanetary medium in the period of very high level of density ($n_{da} \geq 25$ pr.cm $^{-3}$).

Symbols: in figures 7(a, b, c, d, e), ordinates endwise average daily values of plasma cloud concentration of interplanetary space (n pr.cm $^{-3}$); Departure of solar constant (ΔI_o) from normal ($I_{o,norm}$=1370Wm^{-2}) are built up, and abscissa endwise – month days. n^{max} are maximum hourly average values of proton concentration of plasma cloud, in day (d) and hour (h)

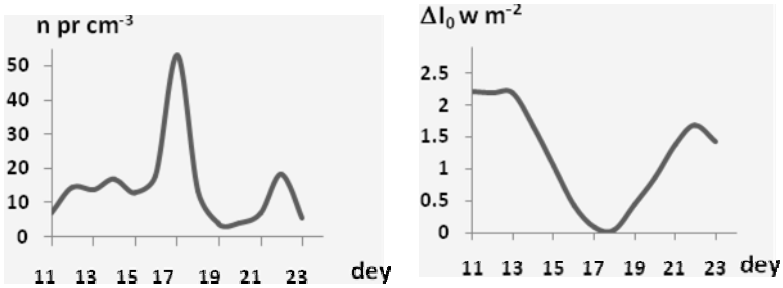

Fig.7a. Temporal interval 11-23 March, 1982 y. n^{max} =88,7 pr. см$^{-3}$, 17d, 14 h.

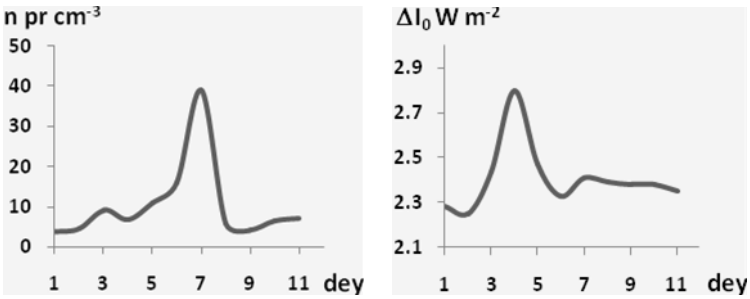

Fig.7b. Temporal interval 1-11 June, 1981 y. n^{max} =113 pr. см$^{-3}$, 7d, 18 h.

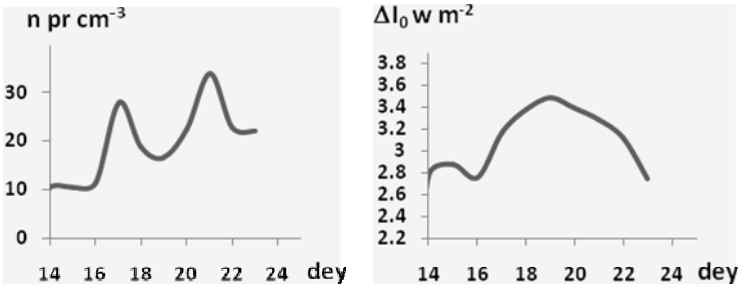

Fig.7c. Temporal interval 14-23 October, 1991 y. n^{max} = 62.2, pr. см$^{-3}$, 21d, 9 h.

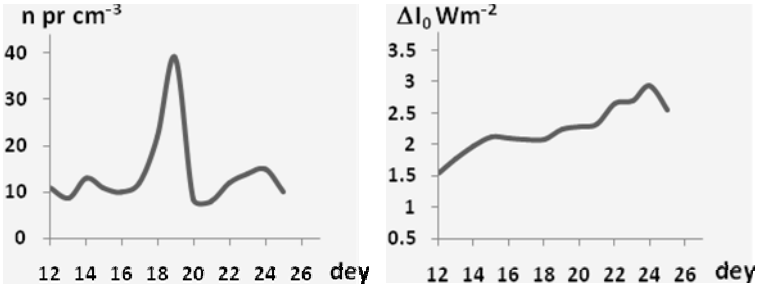

Fig.7d. Temporal interval 12-25 September, 1981 y. n^{max} =97.7, pr. см$^{-3}$, 19d, 3 h.

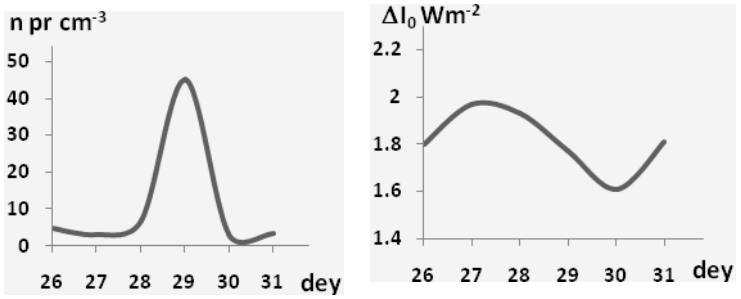

Fig.7e. Temporal interval 26-31 August, 1983 y. n^{max} =71.1, pr. см$^{-3}$, 29d, 22 h.

Fig.7 (a, b, c, d, e), Characteristic curves of comparison of variations of solar constant and plasma cloud concentration in the period of very high density level of interplanetary space.

Analyzing Fig.7 (a, b, c, d, e), we conclude that variations of solar constant do not at all react upon PCIMWHLD.

In order to solve finally the problem of relationship between variation of solar constant and plasma clouds of interplanetary medium, we decided to use the method superposition of epochs as well in our investigation, including variations intensity of the geomagnetic field level (Dst-index). In the process of investigation days with maximum values of concentration of plasma clouds of interplanetary medium, with seals $n_{da} \geq 25$ pr.cm $^{-3}$, were used as bench mark (zero) moment.

Fig.8 gives averaged (by the method superposition of epochs) variations - of plasma cloud concentration of interplanetary space, solar constant and intensity of the geomagnetic field of Dst-index (Dst-indices were investigated only in those days which were satisfying the criterion of data selection – in selected period vertical component of IMF - B_z>0).

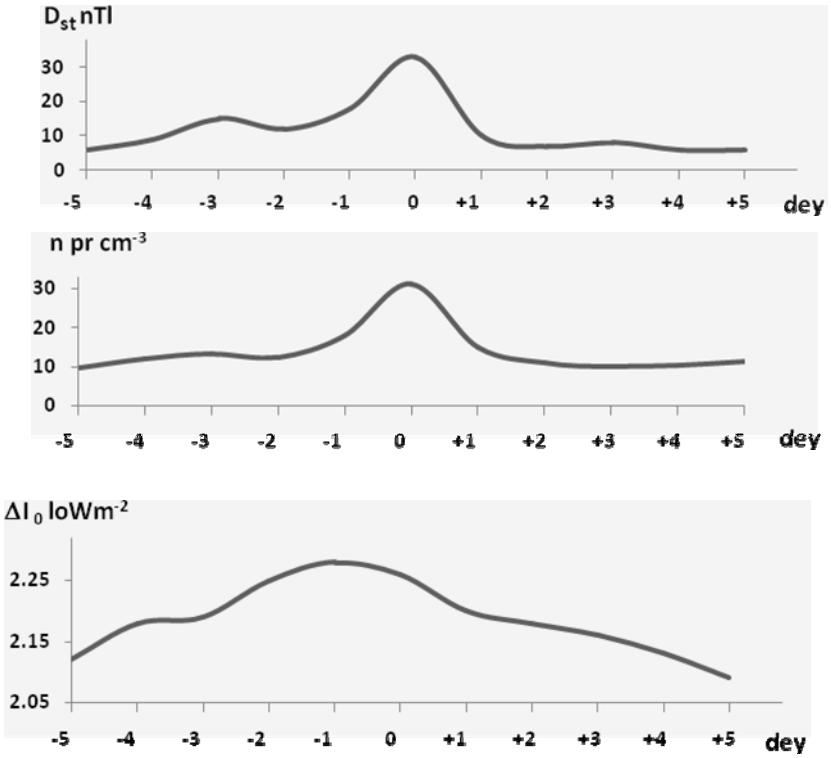

Fig.8. Averaged (by the method superposition of epochs) variations of Dst-index, of concentration PCIMWHLD ($n_{da} \geq 25$ pr.cm $^{-3}$) and solar constant for 1978-1992 years.

Curves, presented in Pic.8, allow us to conclude the following:

1. Evident correlation is observed between variations of Dst-index, PCIMWHLD and solar constant;
2. The authors think that

a) Correlation between variations of Dst-index and PCIMWHLD is casual-consequential;

b) there is no correlation between variations of solar constant and PCIMWHLD and only parallelism of proceeding of events which are called forth by third, mutual for them, reason – some X parameter, characterizing solar activity, is described (this question needs further thorough investigations).

Basic results of the authors' investigation of comparison of variations of solar constant and PCIMWHLD are the following:

1. On the basis of revealed experimental facts we conclude that:

a) Variations of solar constant do not at all react at changes of PCIMWHLD;

b) averaged (by the method superposition of epochs) variations of concentration PCIMWHLD and solar constant show that in PCIMWHLD period solar constant value, instead of decrease, increases insignificantly (ΔI_o=0,19 Wm^{-2});

We concluded that there aren't connection between variations of solar constant and PCIMWHLD;

2. it is established that Abbot's conception, that "decrease of solar constant during severe magnetic storms is conditioned by Raleigh scattering, ejected from the Sun into interplanetary space corpuscular cloud" unfortunately is not confirmed.

General Conclusions

1. Comparison of variations of solar constant and intensity of the geomagnetic field in the period of large and very large magnetic storm (ΔDst $\leq -$ 150 nT) demonstrated that all considered cases can be divided into five types according to the character of solar constant variation:

To the I types belong events, when in the period of the main phase of the geomagnetic storm, value of the solar constant undergo decreases (which coincides with results receiving by Abbott).

To the II types belong events when in the period of the geomagnetic storm, value of the solar constant stays almost constant.

To the III types belong events, when in the period of the main phase of the geomagnetic storm, value of the solar constant undergo increases.

To the IV types belong events when in the period of the geomagnetic storm value of the solar constant gradually decreases.

To the V types belong events when in the period of the geomagnetic storm value of the solar constant gradually increases.

2. With the help of the method superposition of epochs it was established that during very large magnetic storms the value of solar constant stays almost unchanged.

3. From above-stated experimental data follows undoubtedly that the result of Abbot's scientific school ("in the day of very large magnetic storm solar constant value, as a rule, is anomalously decreased") should be corrected so: correlation between variations of solar constant and magnetic storm is not simple and comes to 5 types.

4. Comparison of variations of solar constant and plasma cloud concentration of interplanetary medium, with high level of density (PCIMWHLD $n_{da} \geq 25$ pr.cm $^{-3}$), revealed that variations of solar constant do not at all react at PCIMWHLD.

5. It was established (with the help of the method superposition of epochs) that during PCIMWHLD solar constant value increases insignificantly instead of decrease (ΔI_o=0.19 Wm^{-2}).

6. From above-stated experimental data logically follows that there aren't connection between variations of solar constant and PCIMWHLD. Hence Abbot's conception that "decrease of solar constant during large magnetic storms is conditioned by Raleigh scattering, ejected from the Sun into interplanetary space corpuscular cloud", unfortunately proved to be incorrect.

7. Now it is established that solar corpuscular currents (geometric storms), as well as electromagnetic solar irradiance (change of solar constant 0.1 – 0.3%), can provoke marked changes of atmospheric pressure and influence circulation processes in terrestrial atmosphere.

Therefore, when we study solar – atmospheric connections it is logical and necessary to investigate separately cases of observation of large and very large magnetic storms which were not accompanied by solar constant considerable variations, and separately – considerable variations of solar constant which were not accompanied by large and very large magnetic storms.

References

[1] Abbot C.G. On Sterne and Dieter's Paper. "The Constancy of the Solar Constant". Smithsonian contrib. Astrophysics. V. P.13-2, 1958.

[2] NIMBUS Solar Irradiance November 1978 - June 1992. Journal Solar – Geophysical Data, USA, Number 577, part II. P. 56-70. 1992.

[3] Sugiura M., Poros D.J. Hourly values of equatorial Dst, for the years 1978 to 1992. CSFC. 1994.

[4] King J.H. Interplanetary medium data book – Supplement 3A, 1977-1985, Supplement 4, 1985-1988, Supplement 5 1988-1993. WORLD DATA CENTER "A" ROCKETS AND SATELLYTES.

[5] Porchkhidze C.D., Chkhetia A.M., Feldshtein Ja. J. Interplanetary space plasma and geomagnetic storms during the period of solar cycle, 1965-1974 years. Symposium on SolarTerrestrial physics (Tbilisi, September 1976y.) Abstract, part III. P.142-144. "Наука". Moscow. 1976. (In Russian language).

[6] Collection "Cosmic Data", monthly review. Pub. "Nauka", Moscow, for the 1965-1974 years. (In Russian language).

[7] Chree C. Phil. Trans., A212. 76. 1913.

[8] Chree C., Stayg J.M. Phil. Trans. A227. 21. 1913.

[9] Mustel E.R. On the reality of the influence of solar corpuscular streams upon the lower layer of the earth's atmosphere. Publ. N24, Astron. Counc., USSR Akad. of Sciences, Moscow. P. 5-55, 1972. (In Russian language).

[10] Volland. H. (1976) Periodic variations of the solar radiation – a possible source of solar activity – Weather effects. J. Atmos. Terr. Phys. 39. 69.1976
[11] Akasofu S.I., Chapman S.Solar-Terrestrial physics, Oxford. At the Clarendon press.P. 380. 1972.
[12] Chkhetia A.M. Monograph. The results of investigations of basic geophysical phenomena of complex problem of Solar – Terrestrial connections. Publish G C I, Tbilisi. 1998. 257 p. (In Russian language).

(Received in final form 20 December 2012)

К вопросу об исследовании вариаций солнечной постоянной в период очень больших геомагнитных бурь

Чхетия А.М., Гиголашвили М.Ш. , Эбралидзе М.О.

Реферат

Еще до проведения актинометрических наблюдений в межпланетном пространстве Аббот и возглавляемая им научная школа Смитсонианского Астрофизического института (США), пришли к выводу, что в день очень сильной геомагнитной бури величина солнечной постоянной оказывается, как правило, аномально заниженной. Аббот поддерживал точку зрения о том, что падение солнечной постоянной во время очень больших геомагнитных бурь вызвано тем, что вдобавок к нормальному Релееву рассеянию фотонной радиации Солнца молекулами земной атмосферы, во время магнитных бурь происходит дополнительное рассеяние корпускулярным облаком плазмы, выброшенным Солнцем в межпланетное пространство.

Сопоставление вариаций - солнечной постоянной и напряженности геомагнитного поля в период больших и очень больших геомагнитных бурь (Δ Dst$\leq$-150нТл) показало, что по характеру изменения солнечной постоянной, все рассмотренные случаи можно разбить на пять типов. Из вышеизложенного экспериментального факта несомненно следует, что результат, полученный научной школой Аббота о том, что “в день очень больших магнитных бурь величина солнечной постоянной оказывается, как правило, аномально заниженной”, должен быть заменен поправкой - между вариацией солнечной постоянной и магнитной бурей связь неоднозначная.

Сопоставление вариаций – солнечной постоянной и концентрации плазменных облаков межпланетной среды с высоким уровнем плотности (ПОМССВУП, $n_{ср.\ сут.}$ =25 пр.см$^{-3}$) выявило, что вариации солнечной постоянной на ПОМССВУП вовсе не реагируют. Из вышеизложенного экспериментального факта логически следует, что между вариацией солнечной постоянной и ПОМССВУП связи вовсе не существует. Следовательно, концепция Аббота о том, что “падение солнечной постоянной во время больших магнитных бурь обусловлено Релеевым рассеянием, выброшенным Солнцем в межпланетное пространство корпускулярным облаком”, к сожалению, не подтвердилась.

ძლიერ დიდი გეომაგნიტური ქარიშხლების მიმდინარეობის პერიოდში მზის მუდმივას ვარიაციის კვლევის საკითხებისათვის

ჩხეტია ა.მ., გიგოლაშვილი მ.შ., ებრალიძე მ. ო.

რეზიუმე

ჯერ კიდევ საპლანეტათშორისო სივრცეში აქტინომეტრიული დაკვირვების ჩატარებამდე, აშშ-ის სმიტსონიანის ასტროფიზიკური ინსტიტუტის თანამშრომლების მიერ, აბოტის ხელმძღვანელობით, დადგენილ იქნა, რომ ძლიერ დიდი გეომაგნიტური ქარიშხლების მიმდინარეობის პერიოდში მზის მუდმივა, როგორც წესი, ანომალურად შემცირებულია. აბოტი ამ მოვლენას ასე ხსნიდა - მზეზე ძლიერი აფეთქების შემდეგ, მზიდან მზე-დედამიწის საპლანეტთაშორისო სივრცეში გამოტყორცნილი პლაზმური ღრუბელი განაპირობებს მზის ფოტონური გამოსხივების რელეისებურ გაფანტვას და შესაბამისად მზის მუდმივას შემცირებას.

ძლიერ დიდი გეომაგნიტური ქარიშხლების მიმდინარეობის პერიოდში (როდესაც ΔDst<-150nT), მზის მუმივას და გეომაგნიტური ველის დაძაბულობის ვარიაციათა შეპირისპირების ანალიზის შედეგად გამოვლენილ იქნა, რომ-ძლიერ დიდი გეომაგნიტური ქარიშხლების მიმდინარეობის პერიოდში მზის მუდმივასა და გეომაგნიტური ველის დაძაბულობის ვარიაციებს შორის განსაზღვრული, ერთმნიშ– ვნელოვანი კავშირი არ არსებობს. ყველა შესაძლო შემთხვევა დაიყოფილ იქნა 5 ტიპად. ზემოთ მოცემული ექსპერიმენტული ფაქტიდან უშუალოდ გამომდინარეობს, რომ აბოტის მეცნიერული ჯგუფის მიერ მიღებული შედეგი ასე უნდა ჩასწორდეს – ძლიერ დიდი გეომაგნიტური ქარიშხლების მიმდინარეობის პერიოდში მზის მუდმივასა და გეომაგნიტური ველის დაძაბულობის ვარიაციებს შორის, განსაზღვრული, ერთმნიშვნე– ლოვანი კავშირი არ არსებობს.

მზის მუდმივას და მაღალი სიმკვრივის საპლანეტათშორისო სივრცის პლაზმური ღრუბლების (სსპღ, რომელთა კონცენტრაციის საშუალო დღიური მნიშვნელობა $n>25$ სმ$^{-3}$) ვარიაციათა შეპირისპირების ანალიზის შედეგად გამოვლენილ იქნა, რომ მზის მუდმივას ვარიაციები მაღალი სიმკვრივის სსპღ არსებობას საერთოდ არ ეხმაურება. ზემოთ მოცემული ექსპერიმენტული ფაქტიდან უშუალოდ გამომდინარეობს, რომ მზის მუდმივას ვარიაციებსა და სსპღ შორის კავშირი საერთოდ არ არსებობს. ამგკარად, აბოტის კონცეფცია, რომ –"მზეზე ძლიერი აფეთქების შემდეგ, მზიდან მზე-დედამიწის საპლანე -ტთაშორისო სივრცეში გამოტყორცნილი პლაზმური ღრუბელი განაპირობებს მზის ფოტონური გამოსხივების რელეისებურ გაფანტვას და შესაბამისად მზის მუდმივას შემცირებას", სამწუხაროდ არ გამართლდა.

Journal of the Georgian Geophysical Society,
Issue (B), Physics of Atmosphere, Ocean, and Space Plasma, v.15, 2011-2012, pp. 120-136

Dynamics of vortex structures in collisionless pure and gas-discharge nonneutral electron plasmas

Nikoloz A. Kervalishvili

E. Andronikashvili Institute of Physics, 6, Tamarashvili Str., 0177 Tbilisi, Georgia,
<n_kerv@yahoo.com>

Abstract

The comparative analysis of the results of experimental investigations of the processes of formation, interaction and dynamics of vortex structures in pure electron and gas-discharge electron nonneutral plasmas taking place for the period of time much less than the electron-neutral collision time has been given. The general processes of formation and behaviour of vortex structures in these two plasmas were considered. It is shown that the existing difference in behaviour of vortex structures is caused by different initial states of nonneutral electron plasmas. The significant role of vortex structures in the processes taking place in nonneutral electron plasma is discussed.

1. Introduction

Nonneutral plasmas differ from all known states of any matter. They are the medium consisting of charged particles of only one sign. Therefore, the nonneutral plasmas have their own high electrostatic fields having the strong influence on their behaviour and stability. One more peculiarity of nonneutral plasmas that differs them from the usual neutral plasma is the absolute absence of recombination. Therefore, nonneutral plasmas can exist at any temperatures down to absolute zero. Like liquids or gases the nonneutral plasmas consist of the particles of one type, however in nonneutral plasmas the long-range electrostatic repulsive forces are dominant. Under the laboratory conditions, these plasmas can be confined only by strong magnetic fields.

Nonneutral plasma can be of electron, ion or positron type. The electron nonneutral plasma can be conditionally divided into gas-discharge nonneutral electron plasma and pure electron nonneutral plasma, differing from each other by the methods of their obtaining, by the duration of their existence, and by the experimental methods of their investigation.

The gas-discharge nonneutral electron plasma is formed at the expense of ionization of neutral gas by electrons in gas-discharge devices with the crossed electric and magnetic fields of magnetron, inverted magnetron and Penning cell types. The parameters of discharge are such that the ions are not magnetized and leave the discharge gap rapidly without collisions. At the same time, the electrons are strongly magnetized and are trapped by magnetic field. Along the magnetic field, the electrons are hold by electrostatic fields. As a result, near the anode surface, the cylindrical sheath of nonneutral electron plasma is formed, and the whole discharge voltage falls on it. In gas-discharge nonneutral electron plasma there always exist the solitary vortex structures [1-5], that play the main role in the processes of electron transport and dynamic equilibrium of electron plasma sheath. One more peculiarity of gas-discharge nonneutral electron plasma is the ejection of

electrons from the vortex structures and from the electron background surrounding them to the end cathodes along the magnetic field. The flux of electrons to the cathode always exists in the discharge and the average value of the current of these electrons reaches 50% of the value of discharge current [6,7].

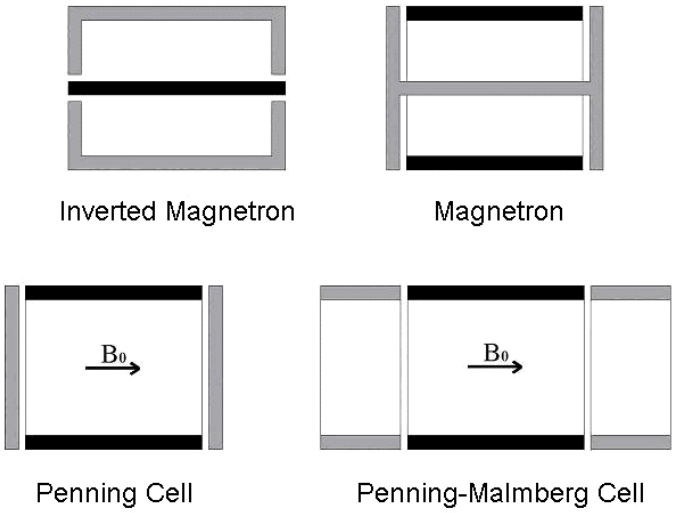

Fig.1.

In contrast to gas-discharge plasma, the pure electron plasma is formed by injection of electrons into trap with the crossed electric and magnetic fields. In most investigations, the Penning-Malmberg cell is used as a trap [8-15]. The structure of this cell is very close to Penning cell. Both of these cells (see Fig. 1) is a hollow cylindrical anode located in the longitudinal magnetic field and bounded at the ends by cathodes: flat as in the Penning cell, or in the form of short cylinders as in Penning-Malmberg cell. However, this difference in the form of cathodes is of rather high importance. In the Penning cell, the flat cathodes serve as a source of primary electrons at the expense of ion-electron emission. Therefore, the Penning cell, like a magnetron and an inverted magnetron, is used for ignition of discharge in the crossed electric and magnetic fields. In the Penning-Malmberg cell the primary electrons disappear on the cathodes under the action of the magnetic field, and the ignition of discharge in such geometry is very difficult or absolutely impossible. On the other hand, the Penning-Malmberg cell is ideally adapted for external injection of electrons and for their "extraction" from the cell after passing a certain time. Pure electron plasma in the Penning-Malmberg cell "decays" gradually, as the reproduction of electrons does not take place in it. Therefore, the vortex structures in such plasma are formed only under certain initial conditions or are formed artificially. However, after being formed, they are kept for a rather long time, more than the electron-neutral collision time.

In both electron plasmas the vortex structures are formed with the excess electron density. As the plasma is nonneutral, the excess density means that the vortex structure has its own electric field, and in the presence of external magnetic field rotates around its own axis together with rotation around the axis of experimental device. The vortex structures were investigated experimentally both, in gas-discharge electron and in pure electron nonneutral plasmas. The aim of the present work is the comparative analysis of the processes of formation, dynamics and interaction of vortex structures in these two plasmas, the search for the general mechanisms, and the explanation of the observed differences.

Before we start the analysis of the properties and behaviours of vortex structures in gas-discharge electron and pure electron nonneutral plasmas, let us stop on experimental methods of their investigation. We are not going to consider the all used experimental methods we only mention two main methods of the investigation of vortex structures in these two plasmas. These

methods are: the method of two wall probes in the gas-discharge electron plasma [1] and the method of phosphor screen diagnostic in pure electron plasma [8-15].

The method of two wall probes consists in simultaneous measurements of signals from anode and cathode wall probes during the motion of vortex structures around the axis of discharge device. It allows to observe continuously the trajectory and the charge of one or several vortex structures for a long period of time. In combination with the measurement of electron ejection from vortex structures, this method gives the possibility to determine the parameters of vortex structures, to study their formation, interaction and dynamics [1-5]. Generally speaking, this method was developed for the geometries of magnetron and inverted magnetron having internal and external cylindrical electrodes. However, its modification is applicable to the case of Penning cell [2].

The method of phosphor screen diagnostic consists in instantaneous ejection of all electrons from the trap to the phosphor screen along the magnetic field. (Sometimes, instead of phosphor screen a movable collector of electrons is used.) This method gives an instant spatial, in (r,θ) plane, pattern of the arrangement and the shapes of vortex structures in the given time moment. However, it is connected with the destruction of plasma imposing strict conditions on repeatability of the process, as each time we investigate the other structures. In order to obtain the exact pattern of the development of process in time, it is necessary to provide for each cycle not only the similar initial plasma parameters but, as well, the formation of vortex structures in one and the same place, at one and the same time, and at one and the same mode of diocotron instability. For this purpose it is necessary to impose the controlled disturbance of electron plasma. Nevertheless, even when these conditions are satisfied, some statistical straggling in the course of the processes of formation, interaction and dynamics of vortex structures still remains.

Thus, the method of phosphor screen diagnostic allows to obtain the full spatial, but statistically averaged pattern of the behaviour of vortex structures, and the method of two wall probes, on the contrary, shows not completely spatial but quite exact and continuous evolution of vortex structures in electron nonneutral plasma. In general, both methods allow to investigate rather in detail the processes of evolution and dynamics of vortex structures. This gives the possibility to make the comparison of these processes for both plasmas. On the other hand, the experimental data obtained by these methods supplement each other making it possible to have a more full pattern of the behaviour of vortex structures in electron nonneutral plasma.

The evolution and the dynamics of vortex structures in gas-discharge and pure electron nonneutral plasmas we consider in two different time intervals: (i) fast collisionless processes ($\Delta t \ll \nu_0^{-1}$) and (ii) slow processes taking place with the participation of electron-neutral collisions ($\Delta t \gg \nu_0^{-1}$). Here, ν_0 is the frequency of electron-neutral collisions. In this paper, the fast collisionless processes are considered. In section 2 the process of formation of one stable vortex structure in both plasmas is studied. In section 3 the radial displacement of vortex structures in each of plasmas is analyzed. In section 4 the process of approaching and merging of vortex structures is investigated. In sections 5 and 6 the phenomena are considered, that have place only in one of these plasmas: “vortex crystal” in pure electron plasma and “orbital instability” in gas-discharge electron plasma. In final section 7 some experimental results obtained in non-standard devices and fundamental role of vortex structures in the processes taking place in nonneutral electron plasma are discussed.

2. Formation of stable vortex structure

Let us consider the initial time interval $\Delta t \ll \nu_0^{-1}$, during which the processes of formation and evolution of vortex structures take place. In this collissionless time interval we can neglect the ionization, and, therefore, the principle difference between the gas-discharge and pure electron plasmas disappears. Here, all processes should depend only on the initial parameters of electron plasma, and the behaviour of vortex structures should be the same for both plasmas. As a starting

time interval let us take the moment of appearing the diocotron instability. The diocotron instability in all experiments is a generator of vortex structures with the exception of model experiments in pure electron plasma when the vortex structures are formed artificially.

For appearing the diocotron instability, the nonneutral electron plasma should have the shape of annular sheath (hollow column). Besides, the certain conditions should be fulfilled to excite one or another mode of diocotron instability [16-18].

In gas-discharge electron plasma the annular electron sheath is formed as a result of ionization of neutral gas by electrons. The sheath adjoins the anode surface, but between them there is always a gap of the order of electron Larmor radius. After discharge ignition, the electron density in the sheath increases until it reaches the critical value at which the diocotron instability is excited [17,18]. The minimum critical density corresponds to $l = 1$ mode. The higher is the mode, the more is the critical density of electrons. Therefore, in gas-discharge electron plasma the diocotron instability should be excited at $l = 1$ mode. The experimentally observed instability really has $l = 1$ mode (sometimes $l = 2$ mode) not only in magnetron and inverted magnetron, but as well in Penning cell in which, according to the theory, the exponentially increasing instability at $l = 1$ mode should not be excited.

The annular sheath of pure electron plasma in Penning-Malmberg cell is formed by different ways. In one of them, first, the central electron column is injected with a small seeding asymmetry at $l = 1$ mode; then, a partially hollow profile is formed by means of decreasing the applied potential [8]. By other way, from the very beginning a symmetrical partially hollow profile of electron column is formed. Such electron sheath can be unstable simultaneously for several modes of diocotron instability. For choosing a mode (usually $l = 1$ or $l = 2$) and for a good repeatability of initial conditions of experiment, a controlled initial disturbance of electron plasma is used [8]. One more way consists in the direct injection of annular electron sheath. In this case, as a source of electrons, more frequently, a photocathode is used. Here, from the very beginning, the radius and the thickness of electron ring are given. If a ring is thin the mode of diocotron instability depends on the ratio of the length of the circumference of ring to its thickness, and it can be rather great [12].

Fig.2. Hollow electron beam [19]
Distance from cathode is 1cm (left) and 8.7cm (right)

Before passing to the consideration of the processes of formation and evolution of vortex structures in both plasmas, let us note that the decay of the annular electron sheath into separate vortex structures was first observed in hollow electron beam that propagated in longitudinal magnetic field [19], and for observation of its profile, a phosphor screen located at different distances from the electron gun was used. It was shown that, beginning from a certain distance, the hollow electron beam decays into separate vortex-like current structures and besides, the neighbouring vortex structures are connected with each other by thin spiral “arms”. Fig. 2 shows the images of electron beam at different distances from the electron gun (photos are taken from [19]).

In gas-discharge electron plasma, it is more convenient to study the processes of formation and evolution of vortex structures in the geometry of inverted magnetron. In this geometry, at low pressures of neutral gas, a full cycle of the evolution of vortex structures can be observed continuously: (i) a fast collissionless process from the appearance of diocotron instability to the formation of one stable (quasistable) vortex structure, and (ii) a slow collissional process of

"decaying" the quasistable vortex structure [3,4]. When the vortex structure fully disappears, during a certain period of time before the next diocotron instability appears, only a symmetrical electron sheath remains without vortices and oscillations. The oscillograms of this periodically repeated process are shown in Fig. 3. The upper oscillogram is the oscillation of electric field on the anode wall probe. The lower oscillogram is a total electron current on the end cathodes. Here and below, the little lines on the oscillograms (to the left) indicate the initial position of the sweep trace. As is seen from the figure, the process of development of diocotron instability and of the formation of quasistable vortex structure is accompanied by the pulse of electron ejection along the magnetic field to the end cathodes.

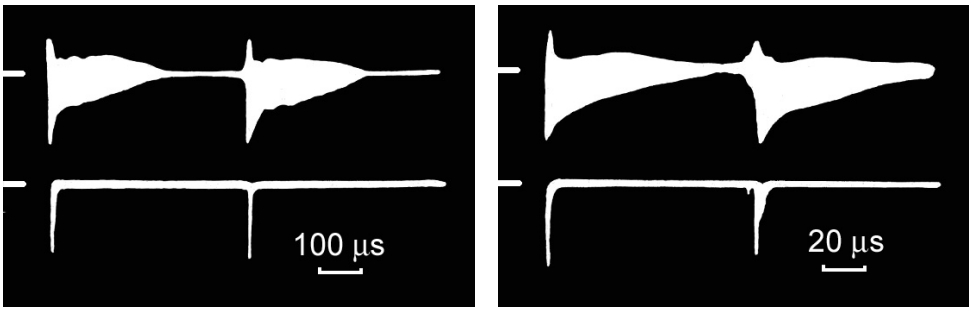

Fig.3. Diocotron instability and vortex structures in inverted magnetron [4]
$r_a = 1.0cm$; $r_c = 3.2cm$; $L = 7cm$; $B = 1.8kG$; $V = 0.9kV$; $p = 2\times10^{-6}$, $1\times10^{-5} Torr$.

Fig.4 shows the oscillograms of the fragments of this process obtained simultaneously by several oscillographs. The upper oscillograms are the oscillations of electric field on the anode wall probe, and the lower ones – on the cathode wall probe.

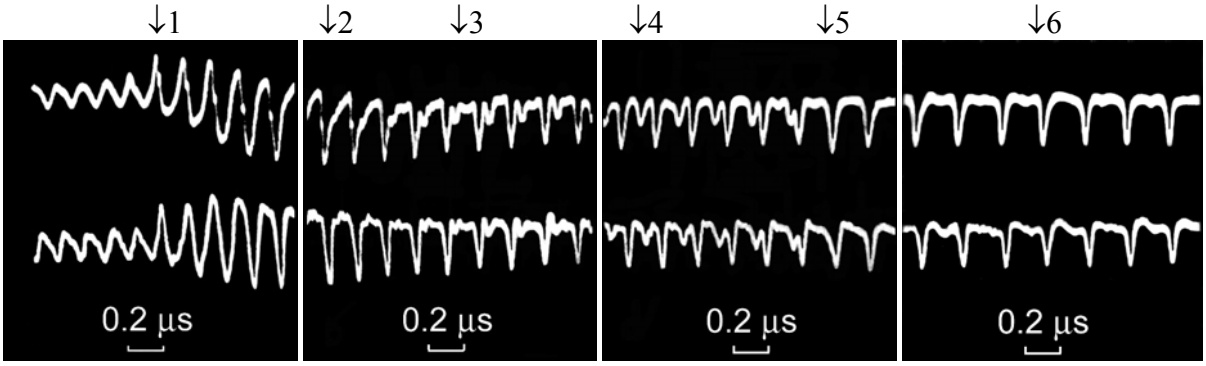

Fig.4. Formation of solitary vortex structure in gas-discharge electron plasma
$r_a = 2.0cm$; $r_c = 3.2cm$; $L = 7cm$; $B = 1.5kG$; $V = 1.0kV$; $p = 2\times10^{-5} Torr$

Let us consider in detail these oscillograms. The comparison of oscillation amplitudes on the anode and on the cathode gives evidence that the whole process takes place on one and the same drift orbit, the radial oscillations of vortex structures are absent and there is no rotation of one vortex structure about the other one. In the first part of oscillograms the strongly nonlinear oscillations of diocotron instability are seen. Then, the oscillations increase sharply and in the disturbed region of the sheath a hole (↓1) is formed. The arrow on the oscillogram denotes the place, where the described process takes place. Further, the hole widens along the azimuth, or, speaking strictly, the electrons are bunched at the point diametrically opposite to the azimuth and form a clump of electrons (↓2) followed by a tail. In the tail a lot of small irregular inhomogeneities are formed (↓3). They approach each other, merge and form one more clump (↓4), being smaller than the main one and it moves with less angular velocity. The main clump overtakes the second

clump and absorbs it (↓5). At this point, the formation of a single stable vortex structure (↓6) is completed. The formed single vortex structure continues to exist during a long period of time, much longer than the electron-neutral collision time.

It should be noted that the process of formation of a stable vortex structure beginning from the moment of formation of a hole up to the moment of merging the vortex structures (↓1 – ↓5), is accompanied by ejection of electrons along the magnetic field to the end cathodes (Fig. 3). This process is shown in more detail in Fig.5, where, like Fig.3, the upper oscillogram is the oscillations of electric field on the anode wall probe, and the lower oscillogram – a total electron current on the end cathodes.

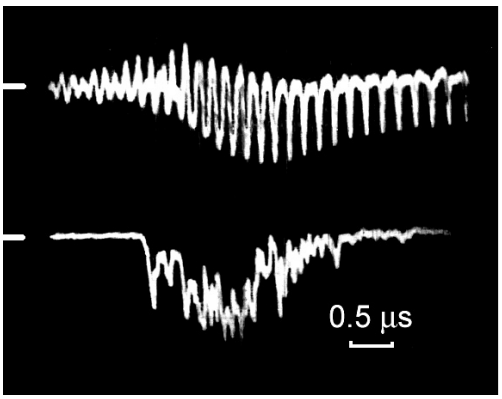

Fig.5. Vortex structure formation and ejection of electrons in inverted magnetron [3]
$r_a = 2.0cm$; $r_c = 3.2cm$; $L = 7cm$; $B = 1.5kG$; $V = 1.0kV$; $p = 1\times10^{-5}Torr$

Ejection of electrons take place from the vortex structure and from the electron background (sheath) surrounding it. As the duration of the process of vortex structure formation is less than the time of electron-neutral collisions (Δt □ ν_0^{-1}), and hence, than the time of ionization, ejection of electrons from the sheath means the decrease of the average electron density. This should lead to the decrease of the strength of electric field in the sheath and also on the drift orbit of vortex structure. The decrease of electric field on the drift orbit will increase the time of rotation of vortex structure about the axis of discharge device. Indeed, as it follows from Fig. 4, the time of rotation of vortex structure increases from 0.15μs for diocotron instability (on the left) to 0.25 μs for the formed stable vortex structure (on the right).

In pure electron plasma, the mode, at which the diocotron instability arises, depends on the initial parameters of electron annular sheath and on the external controlled disturbance of electron plasma. Instability breaks the electron ring into discrete vortex structures, the number of which is equal to the mode of diocotron instability. The vortex structures are mixed, merged (some of them decay) and besides, displaced to the trap axis [8-13]. Finally, one stable vortex structure is left, that is located on the axis of Penning-Malmberg trap. The vortex structures are always followed by filamentary tails that gradually extend, widen, and finally form the symmetric electron background, together with the decayed vortex structures. The density of this background is much less than the density of central vortex structure.

As for $l = 1$ mode, it behaves similar to other modes, although, according to the theory, the exponentially unstable $l = 1$ mode should not be excited in the geometry with the cathode radius equal to zero. Here, we will consider in more detail the process of formation of vortex structure just at $l = 1$ mode, in order to make the comparison with the gas-discharge plasma. In Fig. 6 taken from [8] the process of evolution of partially hollow electron column with a small “seeding” asymmetry is shown. Black color of the figure corresponds to the maximum of electron density.

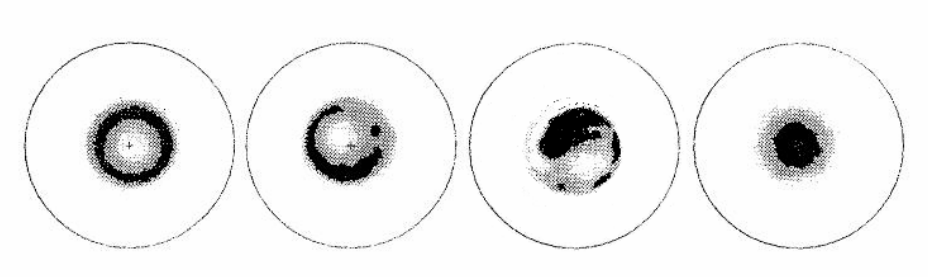

Fig.6. Formation of solitary vortex structure in pure electron plasma [8]
$t = 30, 90, 150, and 1000 \mu s$

As it is seen from the figure, first, the electron ring undergoes breaking. Then, its compression pinching takes place along the azimuth forming a dense clump, i.e. a vortex structure. The vortex structure is followed by a tail (or a arm, as it is called sometimes). On the tail some small clumps are seen, which either disappear or are merged with the main vortex structure. At last, a stable vortex structure is formed, which gradually shifts to the trap axis. At the same time, the central part of low density, on the contrary, displaces outside and diffuses along the azimuth.

Thus, the whole process of evolution from the origination of diocotron instability at $l = 1$ mode to the formation of the stable vortex structure in gas-discharge and pure electron plasmas takes place, practically, in a similar way. However, there is one significant difference: in pure electron plasma the stable vortex structure shifts to the trap axis, while in gas-discharge electron plasma it remains near the anode surface.

3. Radial drift of vortex structures

Such, ex facte diametrically opposite behaviour of vortex structures in pure electron and gas-discharge electron nonneutral plasmas can be explained on the basis of the results of experimental and theoretical investigations carried out in pure electron plasma. In [13] the evolution of a thin annular electron sheath was investigated depending on the value of its radius. An annular electron sheath was formed by a photocathode, and the result of its evolution was observed on the phosphor screen. Fig. 7 presents the photos taken from [13] that show the evolution of two thin electron rings of different radii during one and the same time interval. In both cases, as a result of diocotron instability, the ring breaks into discrete vortex structures. After a small period of mixing and merging, only one stable vortex structure and symmetrical electron background of lower density are left. If the ring radius $\left(r_i / r_a\right)$, where r_i is the average radius of annular sheath, and r_a is the anode radius, is less or of the order of 0.5, the vortex structure shifts to the center, and the background falls from the center of the trap to the wall. But if $\left(r_i / r_a\right)$ is more than 0.5, the stable vortex structure remains shifted from the trap axis, and the background reaches the wall of the trap and falls towards its center.

Now it is clear why there is a difference in the behaviour of stable vortex structure in gas-discharge and pure electron plasmas. In gas-discharge electron plasma the electron sheath adjoins the anode surface. Therefore, the formed solitary vortex structure remains as well near the anode surface. The pure electron plasma is injected, as a rule, to the central part of Penning-Malmberg trap. Therefore, the solitary vortex structure formed there is shifted to the trap axis.

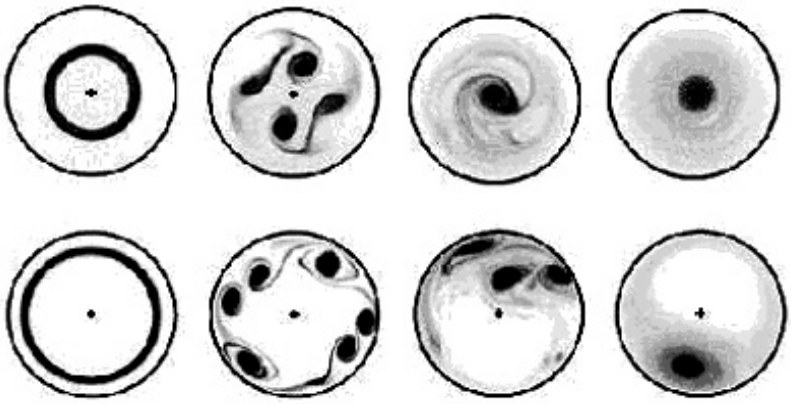

Fig.7. Time evolution of an electron rings [13]
Top: $(r_i/r_a) = 0.5$, $t = 0.01,3,10,30ms$. Bottom: $(r_i/r_a) = 0.79$, $t = 0.01,1,5,30ms$.

The mechanism of radial drift of vortex structures to the axis of Penning-Malmberg trap in pure electron plasma was investigated theoretically in [20, 21], where the motion of point vortex structure is considered in axisymmetric nonuniform electron background with the shear of velocities. The maximum density of electron background is on the trap axis. The vortex having the density more than the background density is a "clump", and the vortex having the density less than the background density is a "hole". The authors define both, the clumps and the holes as prograde or retrograde depending on the fact whether they rotate with or against the local shear. According to such definition, for the background with the maximum on the trap axis the clumps are retrograde, and the holes – prograde. The work shows that under the condition of conservation of canonical angular momentum, a clump should move up in the background gradient, i.e. to the trap axis, and a hole – down in the background gradient, i.e., radially outside. Besides, the velocity of a prograde is by an order of magnitude less than that of retrograde. The obtained results correspond well to the experimental data of [10].

Let us see how this theory is qualitatively applicable to gas-discharge electron plasma. In gas-discharge electron plasma in all three geometries of discharge device – in Penning cell, in magnetron and in inverted magnetron – the density of electron background increases towards the anode and has the maximum near the anode surface. Hence, the radial drift of vortex structures "clumps" at the expense of the gradient of electron background in gas-discharge electron plasma will be always directed to the anode. However, the vortex structures cannot approach the anode nearer than the maximum of electron background is located. Therefore, they will be at some distance from the anode surface. In all these cases, according to the definition of [21], the vortex structures "clumps" will be prograde. Therefore, the velocity of their radial drift will be much less than in pure electron plasma, when the clump drifts to the axis of the cell. In the inverted magnetron the electron sheath is paramagnetic and rotates to the direction opposite to the direction of rotation of diamagnetic sheath in the magnetron geometry, while the rotation of vortex structures in both geometries is the same. Hence, in spite of the fact that the density of sheath electrons in the inverted magnetron increases towards the axis of discharge device, the vortex structures "clumps" will be prograde.

Thus, the theory of radial shift of vortex structures at the expense of the gradient of the electron background density is in qualitative agreement with the experimental results not only in pure electron plasma but also in gas-discharge electron plasma. However, there is one uncertainty regarding the conservation of canonical angular momentum in gas-discharge electron plasma. The formation and the interaction (approach, merging) of vortex structures are accompanied by the pulsed ejection of electrons to the end cathodes along the magnetic field both, from the vortex

structures themselves and from the region of electron sheath (background) adjoined to them [1-5]. Under such conditions, it is difficult to say whether the canonical angular momentum is conserved.

It should be noted that the conditions for the ejection of electrons from the vortex structures for both nonneutral electron plasmas are not similar. At the formation and at the approach (merging) of vortex structures, as well as at the approach of the vortex structure to the trap axis the potential barrier between the vortex structure and the cathode decreases. If, at the same time, a part of the electrons of vortex structure has such a longitudinal velocity which allows them to overcome this decreased potential barrier, the ejection of these electrons to the end cathodes along the magnetic field will take place. At the consideration of collisionless situation, we should take into account the initial longitudinal electron velocity. For the pure electron plasma, it is determined by the temperature of injected electrons and by the process of filling the trap, and for the gas- discharge electron plasma – by the previous electron-neutral collisions. In general, one can assume that the conditions for the ejection of electrons in gas-discharge electron plasma are preferable.

4. Interaction of vortex structures

When in nonneutral electron plasma there exists simultaneously several vortex structures, the problem of their interaction becomes important. The interaction of vortex structures in the time interval $\Delta t \gg \nu_0^{-1}$ was studied in both plasmas.

In the pure electron plasma several stable vortex structures are formed either at the expense of diocotron instability at $l > 1$ mode, or as a result of injection of several electron columns into Penning-Malmberg trap. In the gas-discharge electron plasma at the low pressures of neutral gas, one stable vortex structure is formed as a result of diocotron instability. However, at the pressures of the order or more than $5\times10^{-5} Torr$, there exists simultaneously several vortex structures, and higher is the pressure, the more is their number. These vortex structures do not depend on each other. They move on different circular orbits with different angular velocities, and therefore, approach each other periodically. Fig. 8 shows the oscillograms depicting the process of approaching the vortex structures.

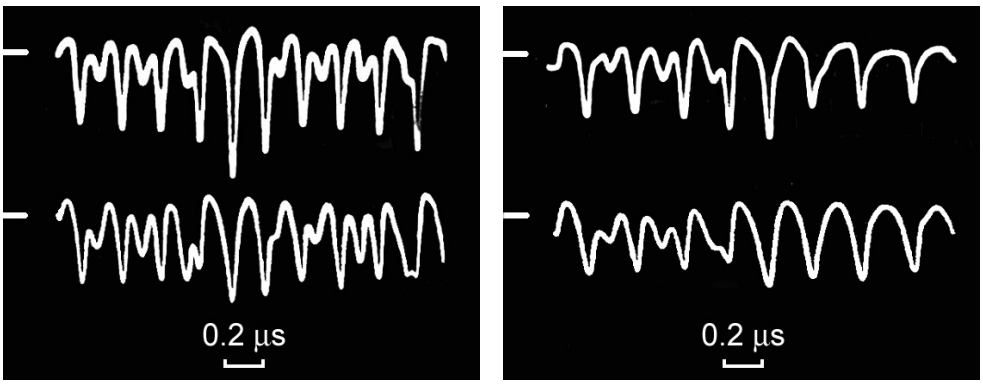

Fig.8. Approach and merging of vortex structures in magnetron
$r_a = 3.2cm$; $r_c = 1.0cm$; $L = 7cm$; $B = 1.5kG$; $V = 1.5kV$; $p = 1\times10^{-4} Torr$.

The upper oscillograms present the oscillations of electric field on the anode wall probe, and the lower - the oscillations of electric field on the cathode wall probe. On the left the process of passing of one vortex structure by the other one is shown, and on the right – the process of merging of two vortex structures. In the gas-discharge electron plasma the process of approaching the vortex structures is accompanied by the pulsed ejection of electrons to the end cathodes along the magnetic field both, from the vortex structures themselves and from the adjoining region of electron sheath (background) [1-3]. This is shown in Fig. 9, where the upper oscillograms present the oscillations of electric field on the anode wall probe, and the lower -the full current of electrons on the end

cathodes. On the left, the oscillograms are given for two vortex structures, and on the right - when the number of vortex structures is more than two.

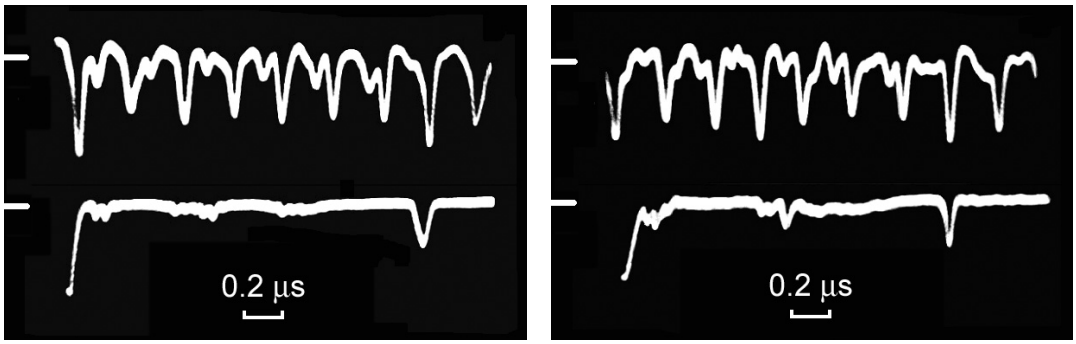

Fig.9. Approach of vortex structures in magnetron
$r_a = 3.2cm$; $r_c = 1.0cm$; $L = 7cm$; $B = 1.5kG$; $V = 1.5kV$; $p = 1\times10^{-4}Torr$.

As the vortex structures move on different drift orbits, the probability of their merging depends on how near they approach each other at passing one vortex structure by the other one. The process of merging of vortex structures and the conditions under which this takes place, were studied in detail by the experiments in pure electron plasma [9]. In these experiments, two electron columns of the given diameter and with the given distance between them were formed artificially, and then the process of their approach and merging was studied.

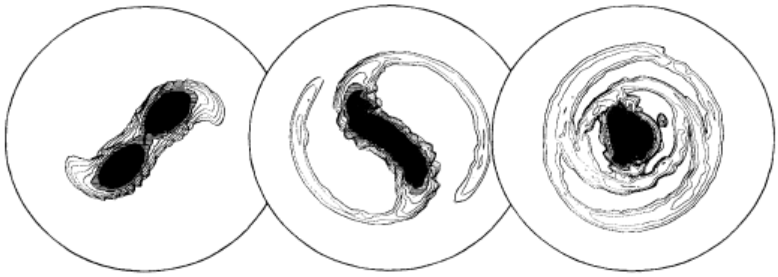

Fig.10. Merging of vortex structures [9].
$D/2R_v = 1.48$, $t = 10, 40, and\, 70\mu\sec$

Fig.10 taken from [9] shows the contours of electron densities in (r,θ) plane measured in the process of merging of two equal vortex structures. As is seen from the figure, the vortex structures are followed by the filamentary tails that are mixed and form the background of low density. It appeared that the time of merging of vortex structures depends critically on the ratio of the distance between their centers to their diameter $(D/2R_v)$. If $D/2R_v < 1.6$, the merging of vortex structures takes place for several orbital time. If $D/2R_v > 1.7$, two vortex structures make more than 10^4 rotations about each other until they merge. The measurements are in good agreement with two-dimensional fluid theory and numerical simulations.

5. "Vortex crystals" in pure electron plasma

Above we investigated the general mechanisms in the behavior of vortex structures in gas-discharge and pure electron plasmas. However, there are the phenomena observed only in one of these plasmas. First of all, this is the "vortex crystals" in pure electron plasma and the "orbital instability" in gas-discharge electron plasma.

The vortex crystals are rigidly rotating equilibrium lattices of intense vortices of small diameters in the background of lower vorticity. Such vortex crystals are formed, e.g. in the rotating vessel with superfluid helium [22], at the same time, the number of vortices in the lattice increases with the increase of the velocity of vessel rotation.

In [11] it was shown that the vortex crystals can be formed in pure electron plasma. In this experiment the layered electron column being a thin flat electron sheath reeled in a roll was injected into the trap. The strong magnetic field inhibited the mixing of layers. As a result of local diocotron instabilities, a great number of individual vortex structures (clumps) were formed. The turbulent state appearing in this case was evolved and relaxed at the expense of chaotic mixing and merging of vortex structures. A part of vortex structures decayed forming the electron background. The final state, generally, was the solitary vortex structure located at the center with approximately initial density of electrons and the electron background of low density surrounding it. The whole process took place during about 10 rotation times τ_R (the lower sequence in Fig. 11). However, sometimes, the relaxation was stopped and the individual vortex structures were located in the form of regular vortex lattice (the upper sequence in Fig. 11). Such quasistationary state lasted about $10^4 \tau_R$, after which the number of the vortex structures decreased to one located at a center of the device. The decrease of the number of vortex structures took place step-wise. After each decrease the remained vortex structures rearranged into a new rigidly rotating symmetric quasistationary configuration.

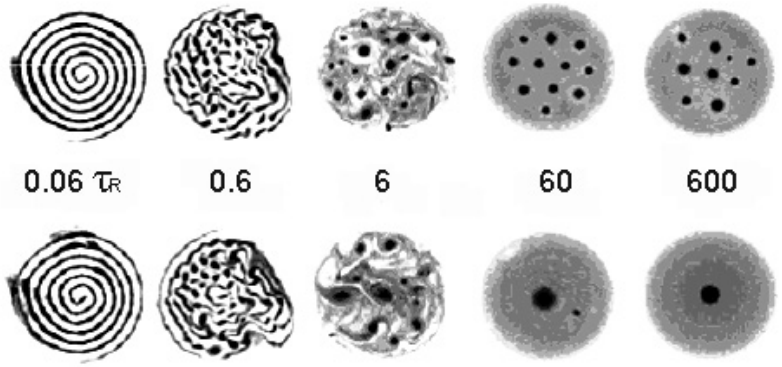

Fig.11. Relaxation of 2D turbulence to vortex crystals and to a single vortex [11]

The experimentally found [11] crystal lattices of electron vortex structures in pure electron plasma were confirmed by the numerical simulation [23] and reproduced theoretically [24]. In [11, 23, 24] it was shown that the formation of vortex crystal takes place as a result of interaction between the vortex structures (clumps) and the background of low density surrounding them.

The systematic experimental investigation of the contribution of electron background to spontaneous formation and decay of vortex crystals was given in [14,15]. In these experiments, the clumps and the background were generated separately and their superimposition formed the initial state of the system. The background of the given value and profile was formed preliminarily. Then, the clumps with the given densities and location were injected in it. This allowed to create the controllable and well-reproducible conditions of experiment. As the experiments showed, the vortex crystals are not formed in vacuum. For formation of vortex crystals, the presence of the background is necessary, and besides, the density of electron background should exceed the definite level necessary for the given number of clumps. Interaction of clumps with the background leads to the formation of annular zones around the clumps depleted of electrons. These annular zones hold the electron vortex structures in lattice points and prevent them to approach each other, even for the unequal charges of vortex structures. In Fig. 12 taken from [14] such zones are shown for three vortex structures with different charges.

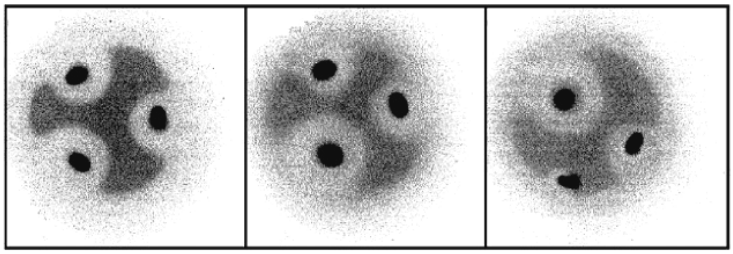

Fig.12. Ring holes around the clumps in vortex crystal [14]

Thus, the vortex crystals are formed, when the dense vortex structures (clumps) are in the electron background of low density and the level of background density has the value necessary for the given number of clumps. If the initial value of background density is not high enough, the number of clumps decreases in the process of free relaxation until the value of background is sufficient for the remained number of clumps to form a crystal. After the crystal is formed, the configuration remains quasistationary until one of the clumps disappears thanks to some dissipative processes. Disappearance of a clump destroys the stable configuration and triggers the turbulent vortex dynamics lasting until a new stable configuration is formed.

6. "Orbital instability" in gas-discharge electron plasma

In gas-discharge nonneutral electron plasma a different phenomenon is observed. At low pressures of neutral gas ($p < 10^{-5} Torr$), in magnetron geometry and in Penning cell a periodically appearing instability of orbital motion of single vortex structure was observed [1,2]. Instability manifests itself in creation of strong radial oscillations of vortex structure the frequency of which is almost by an order of magnitude less than the frequency of its orbital motion. Fig. 13 shows the oscillograms of oscillations of electric fields on the anode (the upper) and the cathode (the lower) wall probes during this instability in the magnetron geometry of the discharge device.

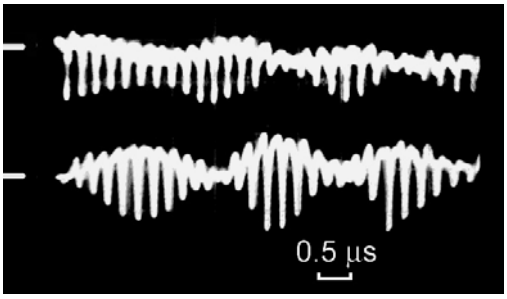

Fig.13. Orbital instability in magnetron
$r_a = 3.2cm$; $r_c = 1.0cm$; $L = 7cm$; $B = 1.2kG$; $V = 1.5kV$; $p = 5 \times 10^{-6} Torr$.

As it is seen from the figure, the vortex structure moves away from or approaches the anode periodically. As the period of radial oscillations of vortex structure is much more than the time of its rotation about the axis of the discharge device, the vortex structure makes the motion in spiral. When the vortex structure moves away from the anode, it losses a part of its electrons that escapes along the magnetic field. This is well seen in Fig 14, presenting the oscillograms of oscillations of the electric field on the cathode wall probe (the lower) and of the full electron current on the end cathodes (the upper).

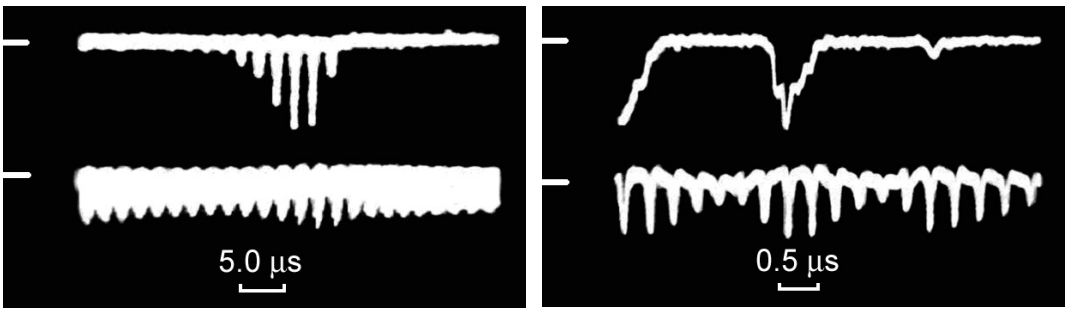

Fig.14. Orbital instability and electron ejection in magnetron
$r_a = 3.2cm$; $r_c = 1.0cm$; $L = 7cm$; $B = 1.2kG$; $V = 1.5kV$; $p = 5 \times 10^{-6} Torr$.

The amplitude of radial oscillations of vortex structure is rather large and reaches 1cm [1]. After making 5-8 radial oscillations and losing about one third of its charge, the vortex structure "calms down". The orbit of vortex structure becomes stable. However, now the radius of vortex structure orbit becomes by 5-6 mm less than it was before starting the instability. During the instability, the vortex structure is not destroyed, only its orbital motion becomes unstable. Therefore, such instability we will call "orbital instability". After completing the orbital instability, the charge of vortex structure and the radius of its drift orbit start to increase slowly, but this is already the collisional process, which continued until the instability is repeated again.

The orbital instability in Penning cell [2] takes place in the same way as in magnetron geometry, though there are some differences.

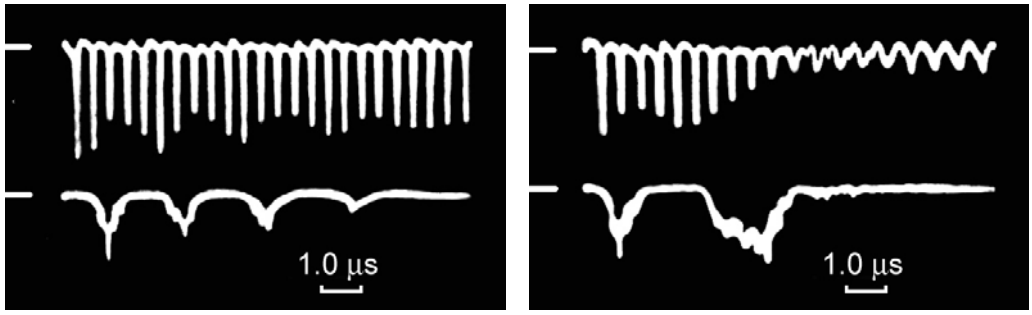

Fig.15. Orbital instability in Penning cell
$r_a = 3.2cm$; $L = 7cm$; $B = 2.0kG$; $V = 2.0kV$; $p = 6 \times 10^{-6} Torr$

The number of radial oscillations in Penning cell is more than in magnetron geometry (of the order of ten and more). The decay of radial oscillations in the Penning cell in most cases, takes place in the same way as in magnetron geometry, that is, the amplitude of radial oscillations and the amplitude of electron ejection along the magnetic field decrease gradually (Fig.15 left). Here the upper oscillogram is the oscillations of electric field on the anode wall probe, and the lower – the current of electrons on the cathodes. However, in some cases, the last ejection of electrons appears to be the greatest and the amplitude of oscillations on the anode wall probe decreases strongly (Fig.15 right). This indicates that, sometimes, the vortex structure approaches the axis of Penning cell quite close causing, thus, the great losses of electrons in the vortex structure. Then the vortex structure remains near the axis of Penning cell during the whole collisionless period. The mechanism of appearing and progressing of orbital instability is not studied yet.

7. Discussion and conclusion

We considered the processes of formation and dynamics of vortex structures taking place during the collisionless time interval in pure electron and gas-discharge electron nonneutral

plasmas. The analysis of experimental results showed that the process of formation of stable vortex structure as a result of diocotron instability at $l = 1$ mode takes place in similar way in both plasmas. If, as a result of diocotron instability several vortex structures are formed, in the process of their evolution and interaction one stable vortex structure is left finally. A great role in both plasmas is played by electron background that determines the direction of radial drift of vortex structure and the conditions of vortex crystal formation.

The difference in behaviour of vortex structures in pure electron and gas-discharge electron nonneutral plasmas is caused, mainly, by the different initial conditions. In pure electron plasma there is a wide spectrum of externally given initial conditions: the thickness, the location and the density of circular electron sheath, or the given arrangement of electron columns. Therefore, at the initial moment we can obtain any mode of diocotron instability and any number of vortex structures. However, finally, as a result of mixing and merging, one stable vortex structure is left. If a vortex crystal is formed, in this case as well the number of vortex structures decreases to one in step-wise manner.

In gas-discharge electron plasma the situation is somewhat different. Here, the cylindrical annular electron sheath is formed by natural way at the expense of collisions and ionization. Therefore, the diocotron instability develops at $l = 1$ mode, corresponding to the minimum critical electron density [17]. This leads directly to the formation of one stable vortex structure. Thus, in gas-discharge electron plasma there are not possibilities for variation of initial conditions. in contrast to the case of pure electron plasma. However, here, one can vary the geometry (magnetron or inverted magnetron) of discharge device depending on the fact in which of these geometries we can observe better one or another process.

Generally, the use of different geometries or of their modifications is very useful for carrying out the experiments. In [25] the vortex structures in magnetron geometry with dielectric end plates were studied experimentally. It was found that in such discharge device, the diocotron instability appears periodically and a quasistable vortex structure is formed. The existence of dielectric discs inhibits the ejection of electrons along the magnetic field. In this regard, the situation reminds the one taking place in pure electron plasma. Periodical formation of vortex structure and its subsequent "decay" reminds the situation connecting with gas-discharge plasma in inverted magnetron. In [26] the experimental investigation of the dispersion shifted from the axis of vortex structure in Penning-Malmberg cell was made. For creation of controllable radial electric field, a long thin wire was stretched along the cell axis, to which the displacement potential was applied. This allowed to study the process of evolution and dispersion of vortex structure depending on its intensity and applied shear. In [27] a uniform annular sheath of magnetized electrons was formed between two coaxial cylinders by means of continuous electron injection. Diocotron instability in annular electron sheath led to the formation of stable localized vortex structures of high density. In [28] the electron column was continuously injected into Penning-Malmberg cell. With the increase of electron density, the column became hollow. The diocotron instability appeared and the vortex structures were formed. However, in contrast to the case of short-time injection, when the formed vortex structures shifted to the cell axis, in the given experiment the vortex structures shifted to the region between the electron column and the anode. For simulation and studying the magnetospheric phenomena, the device was created with levitation superconducting dipole magnet for confining the pure electron plasma with magnetospheric configuration [29]. It is shown that in this device the electrons, similar to the experiments described above, are self-organized into dense stable vortex structures.

Thus, it can be assumed that the self-organizing vortex structures (clumps) in nonneutral electron plasma are one of the fundamental properties of such plasma independent of the method of its obtaining and of the geometry of confining device. Being initiated by the diocotron instability, they are formed quickly ($\Delta t \sim \nu_0^{-1}$) and exist long ($\Delta t \gg \nu_0^{-1}$).

The vortex structures have a strong influence on nonneutral electron plasma and play an important role in the processes taking place in it. One of such processes in gas-discharge electron

plasma is the ejection of electrons along the magnetic field to the end cathodes from the vortex structures and from the regions of electron sheath surrounding them.

The other physical process connected with the vortex structures is the transport of electrons across the magnetic field. As the vortex structure has its own electric field, the sheath electrons passing by the vortex structure deviate to the anode or to the cathode and thus, increase their radial shifts. When the radial shifts exceed significantly the Larmor radius of electron, there appears the neoclassical transport of electrons across the magnetic field. Besides, at the formation of stable vortex structure, at the formation and at the stepwise transformation of vortex crystals there appear many small irregular vortex structures and filamentary tails that are mixed, merged or dissipated chaotically. Thus, a turbulent state appears periodically in nonneutral electron plasma.

In conclusion, it should be noted that the Drift-Poisson equations describing the noneutral electron plasma are isomorphic to 2D Eiler equations for nonviscous incompressible fluid [16,8]. Therefore, the investigation of plasma flows, of transport mechanisms, and of the processes of formation, interaction and dynamics of vortex structures in nonneutral electron plasma is of interest not only for the physics of nonneutral plasmas and for their practical application, but also for simulation of large-scale geophysical and astrophysical phenomena.

References

[1] Kervalishvili N. A. Rotational instability of a nonneutral plasma in crossed fields E⊥H and generation of electrons of anomalously high energy. Fizika Plazmy, 1989, v. 15, N 2, pp. 174-181; Sov. J. Plasma Phys., 1989, v. 15, N 2, pp. 98-102.

[2] Kervalishvili N. A. Rotating regular structures in a nonneutral plasma in crossed electric and magnetic fields. Fizika Plazmy, 1989, v. 15, N 3, pp. 359-361; Sov. J. Plasma Phys., 1989, v. 15, N 3, pp. 211-212.

[3] Kervalishvili N. A. Evolution of nonlinear structures in nonneutral plasma in crossed fields E⊥H. Fizika Plazmy, 1989, v. 15, N 6, pp. 753-755; Sov. J. Plasma Phys., 1989, v. 15, N 6, pp. 436-437.

[4] Kervalishvili N. A. Electron vortices in a nonneutral plasma in crossed E⊥H fields. Phys. Lett. A, 1991, v. 157, Ns 6-7, pp. 391-394.

[5] Kervalishvili N. A. Solitary vortices in gas-discharge nonneutral electron plasma. J. Georgian Geophysical Society, 2005, v. 10B, pp. 93-106.

[6] Kervalishvili N. A. Effect of anode orientation on the characteristics of a low-pressure discharge in a transverse magnetic field. Zh. Tekh. Fiz., 1968, v. 38, N 4, pp. 637-645; Sov. Phys. Tech. Phys., 1968, v. 13, N 4, pp. 476-482.

[7] Kervalishvili N. A., Kortkhonjia V.P. Low-pressure discharge in a transverse magnetic field. Zh. Tekh. Fiz., 1973, v. 43, N 9, pp. 1905-1909; Sov. Phys. Tech. Phys., 1974, v. 18, N 9, pp. 1203-1205.

[8] Driscol C. F., Fine K. S. Experiments on vortex dynamics in pure electron plasmas. Phys. Fluids B, 1990, v.2, N 6, pp. 1359-1366.

[9] Fine K. S., Driscoll C. F., Malmberg J. H., Mitchell T. B. Measurements of symmetric vortex merger. Phys. Rev. Lett., 1991, v. 67, N 5, pp. 588-591.

[10] Huang X. -P., Fine K. S., Driscoll C. F. Coherent vorticity holes from 2D turbulence decaying in a background shear flow. Phys. Rev. Lett., 1995, v. 74, N 22, pp. 4424-4427.

[11] Fine K. S., Cass A. C., Flynn W. G., Driscoll C. F. Relaxation of 2D turbulence to vortex crystals. Phys. Rev. Lett., 1995, v. 75, N 18, pp. 3277-3280.

[12] Peurrung A. J., Fajans J. Experimental dynamics of an annulus of vorticity in a pure electron plasma. Phys. Fluids A, 1993, v. 5, N 2, pp. 493-499.

[13] Sarid E., Teodorescu C., Marcus P. S., Fajans J. Breaking of rotational symmetry in cylindrically bounded 2D electron plasmas and 2D fluids. Phys. Rev. Lett., 2004, v. 93, N 21, pp. 215002-1-4.

[14] Sanpei A., Kiwamoto Y., Ito K., Soga Y. Formation of a vortex crystal cell assisted by a background vorticity distribution. Phys. Rev. E, 2003, v. 68, N 1, pp. 016404-1-6.
[15] Kiwamoto Y., Hashizume N., Soga Y., Aoki J., Kawai Y. Formation and Relaxation of two-dimensional vortex crystals in a magnetized pure-electron plasma. Phys. Rev. Lett., 2007, v. 99, N 11, pp. 115002-1-4.
[16] Levy R. H. Diocotron Instability in a Cylindrical Geometry. Phys. Fluids, 1965, v. 8, N 7, pp. 1288-1295.
[17] Kervalishvili G. N. Javakhishvili J. I., Kervalishvili N. A. Diocotron instability in an annular sheath of gas-discharge nonneutral electron plasma. Phys. Lett. A, 2002, v.296, N 6, pp. 289-294.
[18] Kervalishvili N. A., Kervalishvili G. N. Quasi-stationary model of gas-discharge nonneutral electron plasma. J. Georgian Geophysical Society, 2008, v. 12B, pp. 105-124.
[19] Webster H. F. Breakup of Hollow electron beams. J. Appl. Phys. 1955, v. 26, pp. 1386-1387.
[20] Schecter D. A., Dubin D. H. E. Vortex motion driven by a background vorticity gradient. Phys. Rev. Lett., 1999, v. 83, N 11, pp. 2191-2194.
[21] Schecter D. A., Dubin D. H. E. Theory and simulation of two-dimensional vortex motion driven by a background vorticity gradient. Phys. Fluids, 2001, v. 13, N 6, pp. 1704-1723.
[22] Yarmchuk E. J., Gordon J. V. Observation of stationary vortex arrays in rotating superfluid helium. Phys. Rev. Lett., 1979, v. 43, N 3, pp. 214-217.
[23] Schecter D. A., Dubin D. H. E., Fine K. S., Driscoll C. F. Vortex crystals from 2D Euler flow: experiment and simulation. Phys. Fluids, 1999, v. 11, N 4, pp. 905-914.
[24] Jin D. Z., Dubin D. H. E. Regional maximum entropy theory of vortex crystal formation. Phys. Rev. Lett., 1998, v. 80, N 20, pp. 4434-4437.
[25] Kervalishvili N. A., Gakheladze L. R. Electron vortical structures in crossed E⊥H fields in the discharge with dielectric end walls. Proc. of the XX Int. Conf. on Phenomena in Ionized Gases, edited by Palleschi V. and Vaselly M., Pisa, Italy, 1991, v.1, pp. 226-227.
[26] Eggleston D. L. Experimental study of two-dimensional electron vortex dynamics in an applied irrotational shear flow. Phys. Plasmas, 1994, v. 1, N 12, pp. 3850-3856.
[27] Rosenthal G., Wong A. Y., Bauer B. S. Localized density clumps generated in a magnetized nonneutral plasma. Phys. Lett. A, 1992, v. 170, N 6, pp. 443-447.
[28] Pasquini T., Fajans J. Continuously injected plasma columns. In Non-neutral Plasma Physics IV, Proc. of the Workshop on Nonneutral Plasmas, edited by Anderegg F., Schweikhard L., Driscoll C. F., AIP Conf. Proc., No.606 (American Institute of Physics, New York, 2002), pp.453-458.
[29] Yoshida Z., Saitoh H., Morikawa J., Yano Y., Watanabe S., Ogawa Y. Magnetospheric vortex formation: self-organized confinement of charged particles. Phys. Rev. Lett., 2010, v. 104, N 23, pp. 235004-1-4.

(Received in final form 10 May 2012)

Динамика вихревых структур в бесстолкновительных чистой и газоразрядной ненейтральных электронных плазмах

Николоз А. Кервалишвили

Резюме

Приводится сравнительный анализ результатов экспериментальных исследований процессов формирования, взаимодействия и динамики вихревых структур в чисто электронной и газоразрядной электронной ненейтральных плазмах, происходящих за период времени, много меньший времени электрон-нейтральных столкновений. Рассмотрены общие закономерности формирования и поведения вихревых структур в этих двух плазмах. Показано, что имеющиеся различия в поведении вихревых структур обусловлены различными начальными условиями ненейтральных электронных плазм. Обсуждается вопрос об определяющей роли вихревых структур в процессах, протекающих в ненейтральной электронной плазме.

გრიგალური სტრუქტურების დინამიკა არადაჯახებად სუფთა და აირგანმუხტვად არანეიტრალურ ელექტრონულ პლაზმებში

ნიკოლოზ ა. კერვალიშვილი

რეზიუმე

წარმოდგენილია გრიგალური სტრუქტურების ფორმირების, ურთიერთქმედებისა და დინამიკის პროცესების ექსპერიმენტული კვლევების შედეგების შედარებითი ანალიზი სუფთა ელექტრონულ და აირგანმუხტვად ელექტრონულ არანეიტრალურ პლაზმებში მიმდინარე იმ დროით პერიოდში, რომელიც ბევრად მცირეა ელექტრონ-ნეიტრალთან შეჯახების დროზე. განხილულია ამ ორ პლაზმაში გრიგალური სტრუქტურების ფორმირებისა და ქცევის საერთო კანონზომიერებები. ნაჩვენებია, რომ არსებული განსხვავება გრიგალური სტრუქტურების ქცევაში განპირობებულია არანეიტრალური ელექტრონული პლაზმის სხვადასხვა საწყისი პირობებით. განიხილება საკითხი გრიგალური სტრუქტურების განმსაზღვრელ როლზე არანეიტრალურ ელექტრონულ პლაზმაში მიმდინარე პროცესებში.

Journal of the Georgian Geophysical Society,
Issue (B), Physics of Atmosphere, Ocean, and Space Plasma, v.15, 2011-2012, pp. 137-150

Dynamics of solitary vortex structure in collisional pure and gas-discharge nonneutral electron plasmas

Nikoloz A. Kervalishvili

E. Andronikashvili Institute of Physics, 6, Tamarashvili Str., 0177 Tbilisi, Georgia,
<n_kerv@yahoo.com>

Abstract

The analysis of the results of experimental investigations of equilibrium, interaction and dynamics of vortex structures in pure electron and gas-discharge electron nonneutral plasmas during the time much more than the electron-neutral collision time has been carried out. The problem of long confinement of the column of pure electron plasma in Penning-Malmberg trap is considered. The mechanism of self-sustaining long-lived stable vortex structure in gas-discharge nonneutral electron plasma is proposed. The collapse of electron sheath in gas-discharge plasma of Penning cell is described. The analysis of the interaction between the stable vortex structure and the symmetric electron sheath, as well as of the action of vortex structures on the transport of electrons along and across the magnetic field is made.

1. Introduction

In [1] the general mechanisms and the differences in the process of formation, interaction and dynamics of vortex structures in pure electron and gas-discharge electron nonneutral plasmas during a short collisionless time interval following the origination of diocotron instability were studied. The analysis of experimental results showed that the process of formation of stable vortex structure proceeds in both plasmas practically in the same way, and the observed differences connected with the different initial parameters of electron plasma. Independent of the initial number of vortex structures, at the end of the process of collisionless evolution in both plasmas only one stable vortex structure is left. However, in pure electron plasma, the vortex structure is shifted to the axis of trap, and in gas-discharge electron plasma, it remains in the electron sheath near the anode surface. The further evolution and dynamics of vortex structure takes place with the participation of electron-neutral collisions. The gas-discharge electron plasma differs from the pure electron plasma in that it exists unlimitedly long at the expense of ionization. Besides, the ionization takes place not only in plasma sheath, but also inside the vortex structure. The other characteristic feature of gas-discharge plasma is the ejection of electrons from the plasma and vortex structures to the end cathodes along the magnetic field in the form of continuous flux and periodically following pulses.

The present work deals with the comparable analysis of the behavior of vortex structures in pure electron and gas-discharge electron nonneutral plasmas in the presence of electron-neutral collisions. In section 2, the process of expansion of the column of pure electron plasma in Penning-Malmberg trap, and the problems connected with its confinement at low pressures of neutral gas are

considered. In section 3, the behavior of stable vortex structure in gas-discharge electron plasma is studied at different geometries and at different pressures of neutral gas. In section 4, the mechanism of self-sustention of long-lived stable vortex structure in gas-discharge electron plasma is considered. In section 5 the collapse of electron sheath in gas-discharge plasma in Penning cell at the pressures when the density of neutral plasma becomes comparable to the density of electron sheath is described. In final section 6, the interaction between the stable vortex structure and the symmetric electron sheath, as well as the action of vortex structure on the transport of electrons along and across the magnetic field is discussed.

2. Long confinement of pure electron plasma column

A pure electron plasma is formed by injection of electrons into Penning-Malmberg trap and, therefore, its initial state can have the arbitrary given density and shape (the central column, the hollow column, several columns shifted from the axis, etc). However, independent of the initial conditions and of the consequent collisionless processes, the initial state for the time interval $\Delta t \sim \nu_0^{-1}$ (ν_0 is the frequency of electron-neutral collisions) will be the axisymmetric picture with one vortex structure located on the axis of confinement device and the background of low density surrounding it. Under the action of electron-neutral collisions, the vortex structure (the electron plasma column) will be expanded. The velocity of expansion is proportional to the pressure of neutral gas. Consequently, one could expect a strong increase of the time of plasma confinement at the transition to very low pressures. However, the experiment did not prove such suggestion. In [2], the time of confinement (the time during which the electron density at the column center was halved) of the central column of pure electron plasma in the wide range of neutral gas pressure (He, $10^{-10} < p < 10^{-3} Torr$) was measured. It turned out that for the pressure of neutral gas $p > 10^{-7} Torr$, the time of confinement is determined by the classical mobility of electrons across the magnetic field, and at lower pressures, the time of confinement does not depend any more on the pressure [2, 3].

In this range of pressures the frequency of electron-neutral collisions becomes less than the frequency of electron-electron collisions. However, electron-electron collisions cannot be the reason of the observed expansion of electron column. Consequently, there is another process of radial transport of electrons that becomes dominant at low pressures. In [2] it was assumed that this process can be the asymmetry-induced transport. The asymmetry-induces transport in nonneutral plasma located in cylindrical symmetric trap is the transport of charged particles across the magnetic field occurred as a result of distortion of cylindrical symmetry caused by the imperfect construction of experimental device and by a small asymmetry of electric and magnetic fields. Thought his process has been studied for a long period of time, the mechanisms of such process, as well as the agreement between the considered theories and experiment have not been fully understand yet [4].

Thus, the attempt to increase the time of confinement of electron (ion) plasma in Penning-Malmberg trap at the expense of decreasing the neutral-gas pressure was not crowned with success. Nevertheless, the method was found allowing to counteract not only the radial expansion of electron plasma column, but to compress the electron column increasing multiply its density. This is the so-called “rotating wall” technique [5,6].

The description of stable state of nonneutral plasma in strong magnetic field, in cylindrically symmetric trap at low pressure of neutral gas is based on conservation of angular momentum. Small static asymmetries of trap construction, of electric and magnetic fields create the resistance to rotation of nonneutral plasma, and the condition of conservation of angular momentum leads to its expansion. To counteract this expansion the technique of rotating wall was developed, in which the rotating electric field is used for increasing the angular velocity of nonneutral plasma. This leads to the stabilization or to the decrease of the average radius of plasma column, i.e. to the increase of confinement or to the radial compression of plasma. In general case, the torque from the rotating electric field will compress the plasma if the rotating electric field frequency is larger than the

plasma rotation frequency. Here, two regimes are possible. In [5], the frequency of applied electric field was in resonance with Trivelpiece-Gould modes and was much higher than the frequency of plasma rotation. This is the "slip" regime. In [6], the other regime was used, when the frequency of applied electric field is close to the frequency of plasma rotation. In this regime, the plasma was compressed and its density was increased until the frequency of plasma rotation approaches the fixed applied frequency. This is the "low-slip" regime. In Fig.1 taken from [6], the upper part shows the process of compression of electron column under the action of rotating wall field. The lower part of the figure shows the process of expansion of the profile of column density after the field of rotating wall is detached. As it is seen from the figure, the rate of plasma expansion is much slower than the rate of compression. At continuously attached rotating wall, the compressed plasma of high density was confined in the stable state for an indefinite time (24 hours in this experiment).

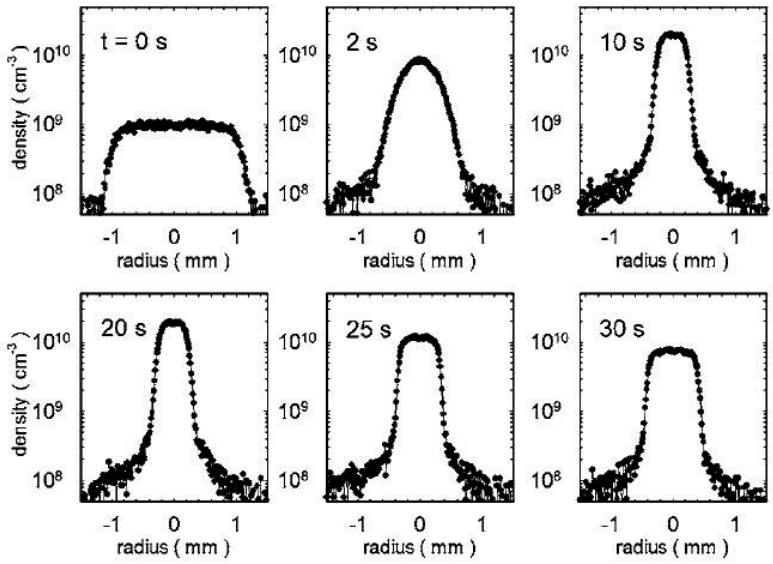

Fig.1. Evolution of the profile of electron column density
at compression (upper part) and at expansion (lower part) [6]

3. Stability of vortex structure in gas-discharge electron plasma

The behavior of vortex structures in gas-discharge electron plasma during the time much more than the electron-neutral collision time depends on the geometry of discharge device and on the pressure of neutral gas. As a result of the appearance of diocotron instability, in the geometry of inverted magnetron a stable vortex structure is formed rapidly ($\Delta t \ll \nu_0^{-1}$) and then it "decays" slowly ($\Delta t \gg \nu_0^{-1}$) [7, 8]. Hence, during the most period of time we observe one quasi-stable vortex structure, the charge of which is decreased slowly. At last, the vortex structure disappears and during some time (before appearing the next diocotron instability) the only symmetric electron sheath is left without vortices and oscillations. In Fig. 2, the oscillograms of this process are given. The upper oscillogram is the oscillations of electric field on the anode wall probe. The lower oscillogram is the full current of electrons on the end cathodes.

The process of development of diocotron instability and of formation of quasi-stable vortex structure is accompanied by the pulse of electron current along the magnetic field to the end cathodes.

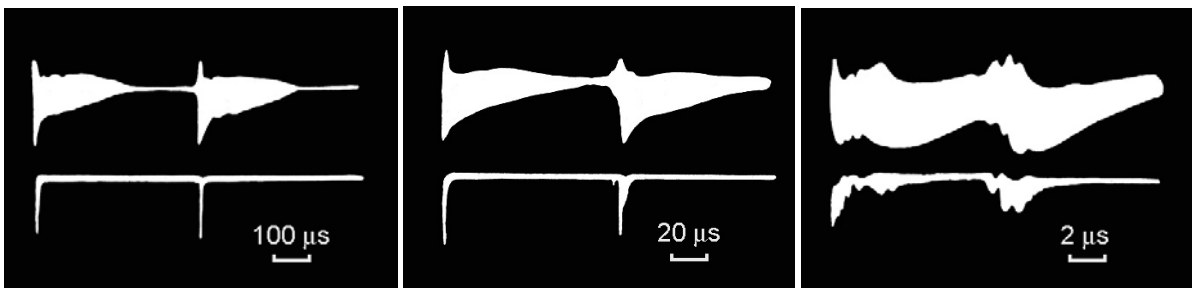

Fig.2. Diocotron instability and vortex structures in inverted magnetron [8]
$r_a = 1.0cm$; $r_c = 3.2cm$; $L = 7cm$; $B = 1.8kG$; $V = 0.9kV$; $p = 2\times10^{-6}$, 1×10^{-5}, $1\times10^{-4}Torr$.

In magnetron geometry and in Penning cell, there exists one stable vortex structure at low pressures of neutral gas. At the pressures lower than $1\times10^{-5}Torr$ (here and below the pressures of argon are given for the parameters of discharge and geometric dimensions of the device at which the experiments were made), the vortex structure approaches slowly the anode increasing gradually its own charge [9, 10]. At the definite moment of time, there arise the strong radial oscillations of the structure being accompanied by ejection of electrons to the end cathodes along the magnetic field. The period of radial oscillations of vortex structure is much more than the period of its rotation about the axis of discharge device. Therefore, during the radial oscillations the vortex structure performs a spiral motion. The ejection of electrons takes place at the moments the vortex structure moves away from the anode surface. Let us call such radial oscillations of vortex structure the orbital instability. The orbital instability continues during the time much less than the electron-neutral collision time (5-8 radial oscillations in magnetron, and about 10 – in Penning cell). As a result of orbital instability, the vortex structure losses about a third of its charge and returns to the initial (smaller) orbit. This process is repeated periodically after the interval of time much more than the electron-neutral collision time.

Fig.3. Periodically repeated orbital instability in magnetron
$r_a = 3.2cm$; $r_c = 1.0cm$; $L = 7cm$; $B = 1.2kG$; $V = 1.5kV$; $p = 6\times10^{-6}Torr$.

Fig. 3 shows the oscillograms of this process in magnetron. The upper oscillogram is the oscillations of electric field on the anode wall probe, and the lower one - the full current of electrons on the end cathodes. Here and below, the little lines on the oscillograms (to the left) indicate the initial position of the sweep trace.

Both, the average frequency of repetition of orbital instability in magnetron and the frequency of repetition of diocotron instability in inverted magnetron are proportional to the pressure of neutral gas. Both, in magnetron and in inverted magnetron, during the most period of time of periodically repeated processes the vortex structure is quasistable. The difference is in that in the inverted magnetron the charge of vortex structure decreases slowly, and in the magnetron – increases slowly. However, in the narrow range of neutral gas pressure, $(1-2)\times10^{-5}Torr$, the vortex structure in the magnetron geometry remains always stable [9]. Fig. 4 shows the

oscillograms of oscillations of electric field on the anode wall probe (upper) and on the cathode wall probe (lower) in magnetron in this range of neutral gas pressure. As it is seen from the figure, the vortex structure does not have “tails”, and its charge and orbit remain unchanged.

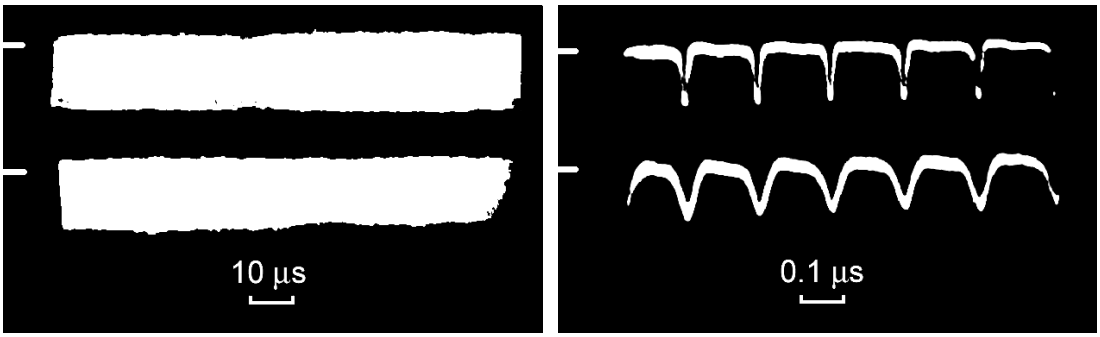

Fig.4. Stable vortex structure in magnetron
$r_a = 3.2cm$; $r_c = 1.0cm$; $L = 7cm$; $B = 1.5kG$; $V = 1.0kV$; $p = 1\times10^{-5}Torr$.

So, in gas-discharge electron plasma, in the time interval $\Delta t \gg \nu_0^{-1}$, the vortex structure in magnetron geometry exists indefinitely long and keeps its charge and dimensions despite the electron-neutral collisions. Even in the geometry of inverted magnetron where the vortex structure “decays” slowly, its expansion in time is not observed. Fig.5 shows the fragments of oscillations of electric field on the anode wall probe (upper oscillogram) in inverted magnetron taken at the moment when the stable vortex structure is fully formed (left), and at the moment close to its full decay (right). The lower oscillogram is the electron current on the end cathodes.

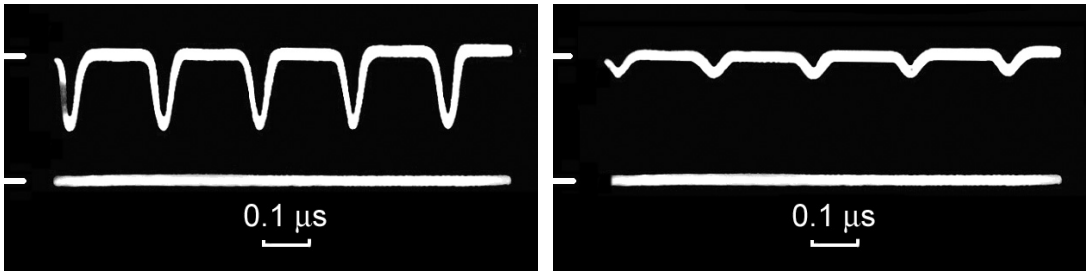

Fig.5. Decay of vortex structure in inverted magnetron
$r_a = 2.0cm$; $r_c = 3.2cm$; $L = 7cm$; $B = 1.5kG$; $V = 1.0kV$; $p = 2\times10^{-5}Torr$

4. The model of self-sustaining stable vortex structure

The stability of vortex structure at the presence of electron-neutral collisions can be connected with the simultaneous existence of two processes in the vortex structure: ionization and ejection of electrons to the end cathodes along the magnetic field. The pulses of electron current on the end cathodes appear at the formation of vortex structures, at their approach and at radial shift of vortex structure from the anode surface [7-10], i.e. the moments when the local decrease of potential barrier takes place or when the vortex structure itself shifts to the region with less potential barrier. At the same time, a part of electrons with the energy sufficient to overcome the decreased potential barrier goes to the end cathodes along the magnetic field. However, beside the pulses of electron current, there is the continuous flux of electrons from the vortex structure to the end cathodes along the magnetic field [11]. Fig. 6 taken from [11] shows the continuous flux of

electrons from the vortex structure in the case of one stable vortex structure (left) and in the case of two approaching vortex structures (right).

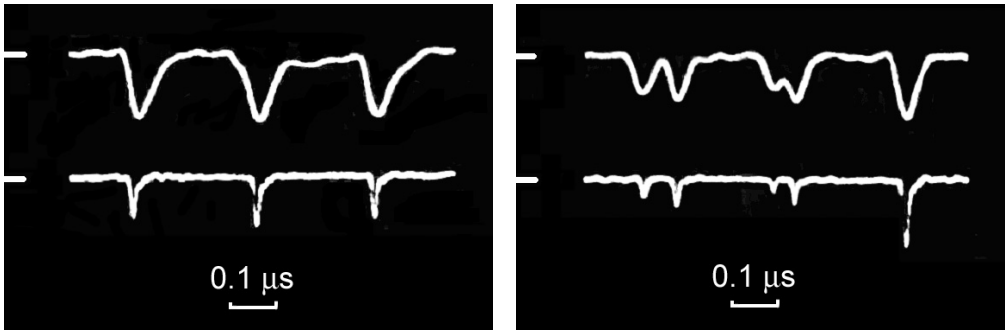

Fig.6. Continuous electron ejection from vortex structure in Penning cell [12]
$r_a = 3.2cm$; $L = 7cm$; $B = 1.9kG$; $V = 1.0kV$; $p = 1\times10^{-5}Torr$

Upper oscillograms are the signals from the anode wall probe, and lower oscillograms– the current of electrons through the narrow radial slit in the end cathode. The slit was located on the same azimuth as the wall probe and the width of slit was much less than the diameter of vortex structure. As is seen from the figure, the continues current of electrons flows from the vortex structure along the magnetic field and rotates together with the vortex structure around the axis of discharge device.

The average value of total electron current on the end cathodes is rather high and make about 50% of the value of discharge current [12,13]. Therefore, this mechanism of losing the electrons is necessary to be taken into account together with the ionization and transverse diffusion at the consideration of processes taking place both, in vortex structure and in electron sheath of discharge.

In [14] the model of stable vortex structure was proposed, in which from the periphery of vortex structure on the side nearest to the cylindrical cathode, a continuous ejection of electrons takes place to the end cathodes along the magnetic field. The ejection of electrons compensates the ionization in the vortex structure and the expansion of the vortex structure due to electron-neutral collisions. Let us consider this process in more detail. The vortex structure rotates about its own axis. Therefore, the electrons of vortex structure approach periodically the anode and the cathode. In this case, the "longitudinal energy" acquired by vortex electrons at the expense of electron-neutral collisions near the anode, can be enough for overcoming the potential barrier near the cathode after they approach the cathode. The farther are the electrons from the vortex center, the more is the value of the "longitudinal energy" acquired by electrons near the anode and the less is the potential barrier near the cathode, and consequently, the more probable is the escape of electrons along the magnetic field. The electrons originating in the vortex structure at the expense of ionization are moved to the periphery of the structure at the expense of electron-neutral collisions and go to the end cathodes along the magnetic filed by the considered mechanism. Therefore, the transverse dimension of the structure and its charge remain unchanged. If the balance between these processes is disturbed, the charge of vortex structure will increase slowly, or on the contrary, will decrease slowly. Thus, the above-considered mechanism of the balance of processes of ionization and of escape of the electrons along the magnetic field can explain the stability of vortex structure in magnetron in the range of pressure $(1-2)\times10^{-5}Torr$, the increase of the charge of vortex structure in magnetron at lower pressure and the decrease of the charge of vortex structure in inverted magnetron.

In the proposed model the electron exchange between the vortex structure and the electron sheath is absent. Consequently, the vortex structure is considered as an isolated object. Therefore, the mechanism of stabilization of vortex structure should not depend on the geometry (magnetron,

inverted magnetron, Penning cell) and on the background. However, the background, geometry and the place of location of vortex structure in the discharge gap will have an influence on the dimension and the shape of vortex structure. This is connected with the value of gradient of the containment potential along the radius of discharge device on the diameter of vortex structure. In particular, if, as a result of radial shifting the vortex structure appears in the center of Penning cell, the action of above-considered mechanism of stabilization of vortex structure will be stopped. The vortex structure will start to expand and the charge will increase. This will lead to the formation of a circular sheath, then to the diocotron instability and further to the formation of stable off-axis vortex structure. Thus, in the gas-discharge electron plasma there works not only the mechanism of self-sustention, but the mechanism of self-recovery of stable vortex structure as well.

For describing the model of stable vortex structure, let us consider two cylindrical coordinate systems: the fixed (r,θ,t) with the center on the axis of discharge device, and the moving (ρ,ϑ,t) with the center on vortex axis. For simplification of the problem let us use the planar geometry and assume that the background equals zero, i.e. the electric field between the anode and the cathode $E_o = const$. Then, for the electrons of vortex structure in the moving coordinate system (moving with the velocity of vortex structure drift $u_d = cE_o/B$), the continuity equation will have the following form:

$$\frac{\partial n_v}{\partial t} + \frac{1}{\rho}\frac{\partial}{\partial \rho}\left(\rho n_v u\right) = \nu_i n_v - \Gamma \tag{1}$$

Here n_v is the density of electrons, ν_o is the frequency of electron-neutral collisions, ν_i is the frequency of ionization, Γ is the loss of electrons along the magnetic field. Taking into account the Poisson equation and the classical transverse mobility of electrons, in the stationary case ($\partial/\partial t = 0$) equation (1) will have the following form:

$$n_v^2 + \frac{1}{\rho}\frac{\partial n_v}{\partial \rho}\int_0^\rho n_v \rho d\rho = \frac{B^2}{4\pi mc^2}\frac{1}{\nu_o}\left(\nu_i n_v - \Gamma\right) \tag{2}$$

Let us solve this problem in the following way. On the basis of experimental data, let us give the value of electron density and determine Γ. Then, using the obtained value Γ, let us find the dependence of the density of electron current to the end cathodes on the discharge radius in magnetron geometry and compare the obtained result with the experiment.

At $\rho = 0$, the electrons are not displaced on the radius, and thus, $\Gamma(\rho = 0) = 0$. Then, from (2) it follows that:

$$n_v(\rho = 0) = n_o = \frac{B^2}{4\pi mc^2}\frac{\nu_i}{\nu_o} \tag{3}$$

This value of density is close to the experimentally measured density of vortex structures [8, 9, 15]. In our model, the shape of distribution of electron density in vortex structure is not of fundamental importance and we will use the Gaussian profile of density. Then:

$$n_v = n_o \exp\left(-\frac{\rho^2}{\rho_v^2}\right) \tag{4}$$

where, ρ_v is the radius of vortex structure. Substituting (4) into (2), we will find:

$$\Gamma(\rho) = 2\nu_i n_o \left(1 - \exp\left(-\frac{\rho^2}{\rho_v^2}\right)\right) \exp\left(-\frac{\rho^2}{\rho_v^2}\right) \tag{5}$$

Now, let us use the obtained value of Γ for magnetron geometry with stable vortex structure and electron sheath (background), the density of which, according to the experimental data is about by an order of magnitude less than the density of electrons of the vortex structure. In (5), the electron losses are distributed uniformly in vortex structure circle. However, as $\omega_v >> \omega_o >> \nu_o$ (ω_o is the angular velocity of rotation of vortex structure about the axis of discharge device, and ω_v is angular velocity of rotation of vortex structure about its own axis), for distribution of electron density in vortex structure, it is not very important whether the electrons escape from the whole vortex structure circle or from any of its point. At this point there should be a minimum potential barrier along the magnetic field. Therefore, passing to the fixed coordinate system, let us assume that in the magnetron the electrons escape from vortex structure on the straight line segment connecting the vortex structure center with the center of discharge device, i.e. at the points of maximum approach of electrons near the cathode. In fixed coordinate system, the electron flux from the vortex structure will be uniformly distributed on the discharge device circle due to the rotation of vortex structure around the axis of discharge device. Hence, for Γ we can write the following relation:

$$2\pi r\Gamma(r) = 2\pi\rho\Gamma(\rho) \qquad \text{where} \quad \rho = r_v - r \tag{6}$$

r_v is the radius of the orbit of vortex structure in magnetron geometry. The density of electron current from the vortex structure on the end cathode will be equal to

$$j_e = e\Gamma(r)L/2$$

Here, L is the anode length. Finally, we will obtain:

$$j_e = \begin{cases} \left(L\nu_i n_o\right)\dfrac{r_v - r}{r}\left(1 - \exp\left(-\left(\dfrac{r_v - r}{\rho_v}\right)^2\right)\right)\exp\left(-\left(\dfrac{r_v - r}{\rho_v}\right)^2\right) & for \quad r \le r_v \\ 0 & for \quad r > r_v \end{cases} \tag{7}$$

Fig. 7 (left) shows the dependence of n_v and j_e on the radius of fixed coordinate system. Though the vortex structure is the isolated system, its influence on the electron sheath is rather great. In the sheath there is the velocity shear and each electron of the sheath passes the vortex structure many times for the collision interval. As the vortex structure has its own electric field, the sheath electrons deviate to the anode or to the cathode while passing the vortex structure. The electrons deviated to the cathode, appear in the region of low containment potential and a part of them escape to the end cathodes along the magnetic field. Thus, alongside with the electron current from the vortex structure, there is also the current of electrons from the sheath to the end cathodes. This current is located closer to the cylindrical cathode than the current from the vortex structure. The both currents are continuous and rotate together with the vortex structure around the axis of discharge device. Fig. 7 (right) shows the experimental dependence of the density of electron current along the magnetic field on the radius of end cathode in the magnetron geometry for different magnetic field in the region of neutral gas pressures, when one stable vortex structure is observed. As it is seen from the figure, the considered model of vortex structure is in qualitative agreement with the experimental results.

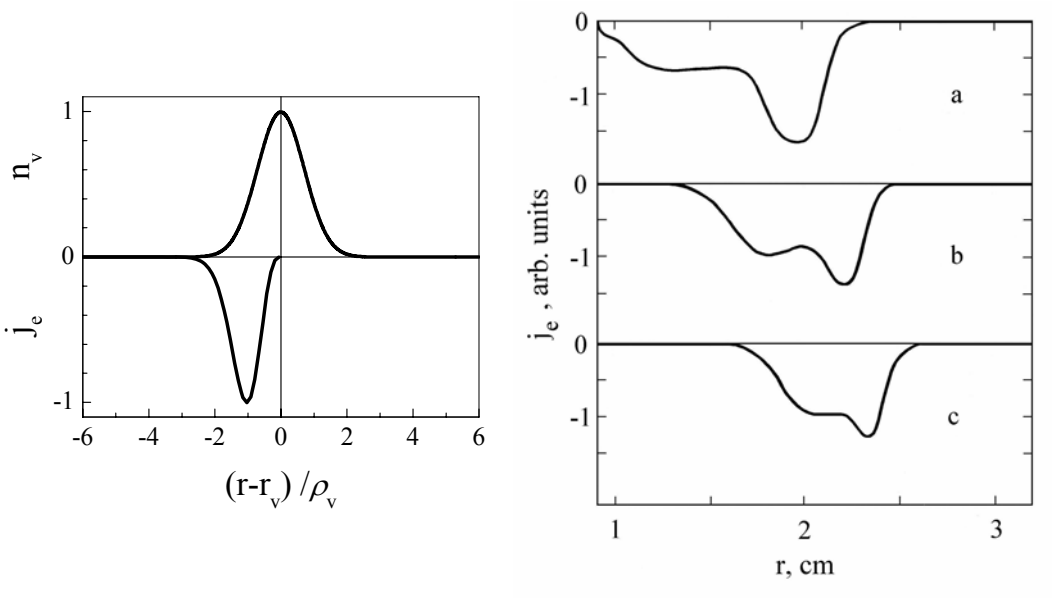

Fig.7. Continuous electron ejection from vortex structure in magnetron (right: $V = 4kV$; $p = 2\times10^{-5} Torr$; a - $B = 1.2$, b - 1.5 , c - $1.8kG$)

5. Collapse of gas-discharge electron sheath

At higher pressure of neutral gas, both, in magnetron and in inverted magnetron, there exist simultaneously several vortex structures, and higher is the pressure, the more is their number. This, probably, is caused by the fact that the decay rate of vortex structure increases with the pressure slower than the growth rate of electron density in the sheath. Consequently, the new vortex structure formed as a result of the next diocotron instability appears earlier than the preceding structure has time to decay.

Under these conditions, the interaction of vortex structures becomes the dominant process in electron plasma. It should be noted that these simultaneously existed vortex structures are not coherent. They appear at different time, move on different circular orbits with different angular velocities [9]. The vortex structures periodically approach each other, sometimes they merge, and sometimes the new structures are formed and all these processes are accompanied by ejection of electrons along the magnetic field to the endplate cathodes [7-10]. Fig.8 gives the oscillograms showing the process of approaching the vortex structures at different pressures of neutral gas. The upper oscillograms show the oscillations of electric field on the anode wall probe, and the lower – the full current of electrons on the end cathodes.

By its structure, the Penning cell is the closes analog of the Penning-Malmberg cell, as there is not a central cathode in it. However, at the pressures above $5\times10^{-5} Torr$ the average density of ions in Penning cell begins to approach the density of electrons, and in gas-discharge electron plasma in Penning cell there appear the new effects [18]. In pure electron plasma the ions are absent and such kind of problem does not arise.

In contrast to a magnetron and an inverted magnetron, in a Penning cell the ions oscillate along the radius inside the hollow cylindrical anode and, at the same time, they move slowly along the axis of a cylinder towards the end cathodes. Outside the anode sheath in the central region of a Penning cell, ions are neutralized by electrons. With the increase of neutral gas pressure the density of ions increases and, as a result, becomes comparable to the density of electrons. This is the so-called transition mode of discharge, in which the electron sheath is “enclosed” between the anode and the neutral plasma of about the same density as the sheath. In the transition mode the discharge current shows a strong nonlinear dependence on the pressure: first, it increases rapidly, passes the maximum, then decreases, passes the minimum and then again increases sharply. The electron

sheath disappears and the discharge changes abruptly to the low-voltage glow discharge in the transverse magnetic field.

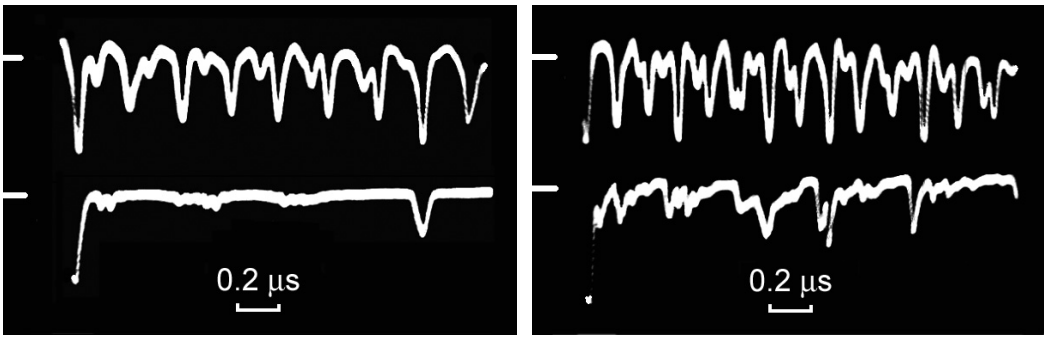

Fig.8. Approach of vortex structures in magnetron
$r_a = 3.2cm$; $r_c = 1.0cm$; $L = 7cm$; $B = 1.5kG$; $V = 1.5kV$; $p = 1\times10^{-4}, 4\times10^{-4} Torr$

The behavior of vortex structures in transition mode was studied in [18]. The experiments was carried out in modified Penning cell, in which a flat cathode was located on the one end of cylindrical anode, as in Penning cell, and on the other end a cylindrical cathode was located, as in Penning-Malmberg cell. At such modification, the characteristics of discharge and the behavior of vortex structures remain the same as in Penning cell with flat cathodes. Behind the cylindrical cathode a flat collector was placed serving for measuring the current of electrons or ions ejected along the magnetic field from the electron sheath and the neutral plasma. For observation of vortex structures a diamagnetic probe was used instead of wall anode probe. This method is described in detail in [19] and consists in that only one narrow slit is cut along the whole length of the cylindrical anode, and an insulated diamagnetic probe, consisting of several turns of rf cable, is placed around the anode. When the inhomogeneity (vortex structure) passes by the slit, the image charge induced by it overcomes the slit in the anode by the current flowing around the anode circle backwards, and generating the pulse of magnetic field registered by the diamagnetic probe. The signal from the diamagnetic probe is similar to the signal from the wall probe and therefore, it is convenient to use a diamagnetic probe for the external cylindrical electrode being under a high potential. Besides, a diamagnetic probe is capable to register abrupt changes of diamagnetic properties of electron sheath caused, e.g. by a partial or a full loss of electrons of the sheath.

The results of investigations showed that at the beginning of transition mode, the signals from collector and diamagnetic probe have the same form as in magnetron. However, starting from the pressures that correspond about to a half of a discharge current maximum, the observed pattern changes significantly. There appear the strong relaxation oscillations. Fig.9 shows the oscillograms of oscillations on the diamagnetic probe (lower), on the collector (upper left), and on the wall probe of cylindrical cathode (upper right). The similar oscillations are observed on both sides of discharge current maximum.

First of all, let us pay attention to the large positive pulses on the oscillogram of diamagnetic probe. Each pulse is caused by an abrupt increase of magnetic field due to a sharp decrease of diamagnetic properties of electron sheath as a result of a partial or a full ejection of sheath electrons to the anode. This is indicated by the physical processes taking place before and after the appearance of a pulse.

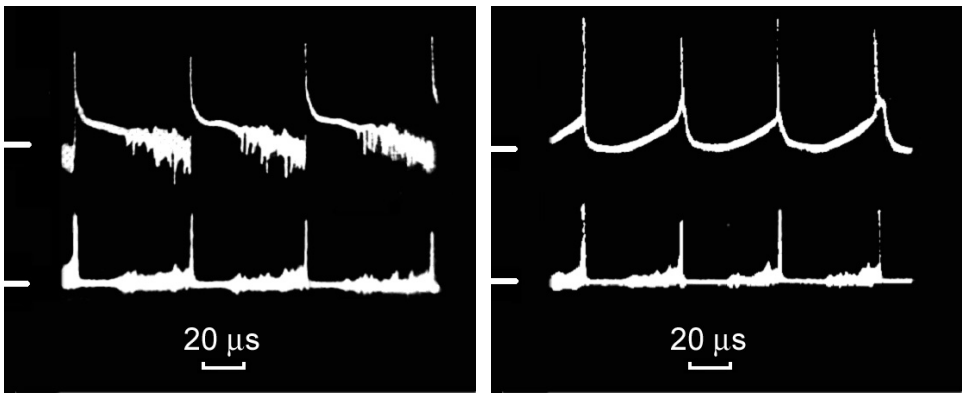

Fig.9. Collapse of electron sheath in Penning cell
$r_a = 3.2cm$; $L = 7cm$; $B = 1.0kG$; $V = 1.2kV$; $p = 1.0 \times 10^{-4} Torr$

On the oscillogram of diamagnetic probe each pulse is preceded by the oscillations connected with the motion of vortex structures. The vortex structures are formed at the moment of appearing the diocotron instability in the discharge electron sheath as in the case of low pressures of neutral gas. In the transition mode the annular electron sheath is located between the anode and the neutral plasma density of which is about equal to sheath density. The sheath density, as well as the plasma density increases in time until the diocotron instability appears and the formation of vortex structures starts. The formation and the interaction of vortex structures are accompanied by the ejection of electrons along the magnetic field to the end cathodes (upper left oscillogram in Fig.9). However, in contrast to low pressures, when the formation of vortex structures limits the increase of electron sheath density, in the transition mode the plasma density and the electron sheath density continue to increase, as is evidenced by a continuous increase of ion current on the cylindrical cathode (upper right oscillogram in Fig.9). The increase of electron sheath density at the fixed discharge voltage should be accompanied by its compression. This process will be continued until the sheath transforms into one-Larmor sheath, and its density reaches the Brillouin limit. Such sheath is unstable and the ejection of the electrons to the anode takes place causing thus the jump of magnetic field. As it is seen from the oscillograms, at the same time, on the collector and on the cylindrical cathode the large narrow pulses are observed that are caused by an abrupt increase of electric field on the cathodes. On the screened collector such pulse does not present. This confirms as well the distortion of electron sheath. The appearance of longitudinal electric field causes an increase of ion current from the plasma to the collector and a decrease of ion current to the cylindrical cathode (upper right oscillogram in Fig.9). Then, the electron sheath begins to recover. Its density increases as is evidenced by the decrease of ion current on the collector and by the increase of ion current on the cylindrical cathode. Further, the whole process is repeated. Thus, we have a periodically repeated process: the compression of electron sheath and its subsequent rapid distortion, i.e. the collapse of electron sheath. The compression of electron sheath with the increase of neutral gas pressure was discovered long ago [20]. However, in the transition mode there is not a continuous (gradual or abrupt) transition from the anode potential drop to the cathode one. In fact, the electron sheath in the transition mode "runs" periodically the complete cycle of its development from the formation of anode sheath to its maximum compression and subsequent distortion.

It should be noted that in the transition mode the vortex structures continue to be formed and to generate the electron flux along the magnetic field to the end cathodes. The formation of vortex structures is observed up to the transition to the glow discharge, while, the ejection of electrons to the end cathodes exists only up to the maximum of discharge current.

6. Discussion and conclusion

Thus, there is a certain difference in the behavior of vortex structure in pure electron and gas-discharge electron nonneutral plasmas in time interval $\Delta t \sim \nu_0^{-1}$, when the electron-neutral collisions play a significant role. In pure electron plasma the vortex structure is located on the axis of experimental device (on-axis state) and is expanded continuously until it disappears fully. For its long confinement and compression, it is necessary to use the rotating electric field - "rotating wall" technique. In gas-discharge electron plasma the vortex structure is located near the anode surface (off-axis state). This is a stable, self-organizing, self-sustaining and self-recovering structure retaining its charge and profile. In a certain sense, the vortex structure in gas-discharge electron plasma can be considered as a soliton-like structure, inside of which the formation of particles and on the periphery their removal take place.

In general, the gas-discharge electron plasma is a long existed "symbiosis" of stable off-axis vortex structure and of symmetrical electron sheath. This combination is characterized by a strong mutual effect of both components on each other and has the new surprising properties. One of them is the ejection of electrons from vortex structures and neighboring regions of electron sheath to the end cathodes. The electron ejection current is rather great, exists always and is a new mechanism of the loss of electrons from the vortex structure and electron sheath. In the vortex structure this current compensates the ionization in vortex structure and its expansion at the expense of electron-neutral collisions. In the electron sheath the electron ejection current limits the electron density. In [16,17], the model of electron sheath was considered, in which the equilibrium density of electrons is determined not by a balance between the ionization and the mobility of electrons across the magnetic field, as it was assumed earlier, but by a "critical" electron density, at which there appears the diocotron instability generating the vortex structures. The model describes well the current characteristics of discharge in the crossed electric and magnetic fields both, in magnetron geometry and in the geometry of inverted magnetron [17].

The vortex structures located in discharge electron sheath have an influence on the transport of electrons across the magnetic field. Even in the case of one stable vortex structure, the sheath electrons pass the vortex structure multiply during the mean free time. As the vortex structure has its own electric field, the sheath electrons passing by the vortex structure deviate to the anode or to the cathode increasing thus their radial shifts. When the radial shifts exceed significantly the Larmor radius of the electron, there appears the neoclassical transport of electrons across the magnetic field. At relatively high pressures of neutral gas ($p > 10^{-4} Torr$), in the discharge electron sheath there exists simultaneously several vortex structures, and the higher is the pressure, the more is their number. At a great number of vortex structures, their movement and interaction become chaotic that can lead to the turbulent transport of electrons across the magnetic field.

The electron sheath (background), in its turn, has the influence on the behavior of vortex structures, for example, on the radial drift of vortex structures and on the formation of vortex crystals.

References

[1] Kervalishvili N. A. Dynamics of vortex structures in collisionless pure and gas-discharge nonneutral electron plasmas. J. Georgian Geophysical Society, present issue.

[2] Malmberg J. H., Driscoll C. F. Long-time containment of a pure electron plasma. Phys. Rev. Lett., 1980, v. 44, N 10, pp. 654-657.

[3] Driscoll C. F., Malmberg J. H. Lenght-dependent containment of a pure electron-plasma column. Phys. Rev. Lett., 1983, v. 50, N 3, pp. 167-170.

[4] Eggleston D. L. Constraints on an empirical equation for asymmetry-induced transport. Phys. Plasmas, 2010, v. 17, N 4, pp. 042304-1-6.

[5] Anderegg F., Hollmann E. M., Driscoll C. F. Rotating field confinement of pure electron plasmas using Trivelpiece-Gould modes. Phys. Rev. Lett., 1998, v. 81, N 22, pp. 4875-4878.
[6] Danielson J. R., Surko C. M. Radial compression and torque-balanced steady states of single-component plasmas in Penning-Malmberg traps. Phys. Plasmas, 2006, v. 13, N 5, pp. 055706-1-10.
[7] Kervalishvili N. A. Evolution of nonlinear structures in nonneutral plasma in crossed fields E⊥H. Fizika Plazmy, 1989, v. 15, N 6, pp. 753-755; Sov. J. Plasma Phys., 1989, v. 15, N 6, pp. 436-437.
[8] Kervalishvili N. A. Electron vortices in a nonneutral plasma in crossed E⊥H fields. Phys. Lett. A, 1991, v. 157, Ns 6-7, pp. 391-394.
[9] Kervalishvili N. A. Rotational instability of a nonneutral plasma in crossed fields E⊥H and generation of electrons of anomalously high energy. Fizika Plazmy, 1989, v. 15, N 2, pp. 174-181; Sov. J. Plasma Phys., 1989, v. 15, N 2, pp. 98-102.
[10] Kervalishvili N. A. Rotating regular structures in a nonneutral plasma in crossed electric and magnetic fields. Fizika Plazmy, 1989, v. 15, N 3, pp. 359-361; Sov. J. Plasma Phys., 1989, v. 15, N 3, pp. 211-212.
[11] Kervalishvili N. A. Electron vortices in the nonneutral plasma of the anode sheath in the crossed E⊥H fields. Proc. of the XIX Int. Conf. on Phenomena in Ionized Gases, edited by Labat J. M., Belgrade, 1989, v.1, pp. 110-111.
[12] Kervalishvili N. A. Effect of anode orientation on the characteristics of a low-pressure discharge in a transverse magnetic field. Zh. Tekh. Fiz., 1968, v. 38, N 4, pp. 637-645; Sov. Phys. Tech. Phys., 1968, v. 13, N 4, pp. 476-482.
[13] Kervalishvili N. A., Kortkhonjia V.P. Low-pressure discharge in a transverse magnetic field. Zh. Tekh. Fiz., 1973, v. 43, N 9, pp. 1905-1909; Sov. Phys. Tech. Phys., 1974, v. 18, N 9, pp. 1203-1205.
[14] Kervalishvili N. A, Kervalishvili G. N. The mechanism of stability of long-lived, self-organized solitary vortex in nonneutral electron plasma. J. Georgian Geophysical Society, 1999, v. 4B, pp. 115-124.
[15] Kervalishvili N. A. Nonlinear regular structures in charged electron plasma in crossed field E⊥H. Zh. Tekh. Fiz., 1990, v. 60, No 2, pp. 78-84 [Sov. Phys. Tech. Phys., 1990, v. 35, No. 2, pp. 182-185].
[16] Kervalishvili G. N. Javakhishvili J. I., Kervalishvili N. A. Diocotron instability in an annular sheath of gas-discharge nonneutral electron plasma. Phys. Lett. A, 2002, v.296, N 6, pp. 289-294.
[17] Kervalishvili N. A., Kervalishvili G. N. Quasi-stationary model of gas-discharge nonneutral electron plasma. J. Georgian Geophysical Society, 2008, v. 12B, pp. 105-124.
[18] Kervalishvili N. A., Kortkhonjia V. P., Murusidze I.G.,Suramlishvili G. I. Transition mode of a nonneutral electron gas-discharge plasma in crossed electric and magnetic fields. J. Georgian Geophysical Society, 2000, v. 5B, pp. 104-111.
[19] Kervalishvili N.A., Kortkhonjia V.P. Rotational instability of the noneutral plasma of an anode sheath in crossed fields E⊥H. Fizika Plazmy, 1986, v. 12, No. 7, pp. 872-878. [Sov. J. Plasma Phys., 1986, v. 12, No. 7, pp. 503-506].
[20] Dow D.G. Electron-Beam Probing of a Penning Discharge. J. Appl. Phys., 1963, v. 34, No. 8, pp. 2395-2400.

(Received in final form 12 September 2012)

Динамика уединенной вихревой структуры в столкновительных чистой и газоразрядной ненейтральных электронных плазмах

Николоз А. Кервалишвили

Резюме

Приводится анализ результатов экспериментальных исследований равновесия, взаимодействия и динамики вихревых структур в чисто электронной и газоразрядной электронной ненейтральных плазмах, в течение времени, много большего времени электрон-нейтральных столкновений. Рассмотрена проблема длительного удержания столба чисто электронной плазмы в ловушке Пеннинга-Малмберга. Предложен механизм самоподдержания долгоживущей стабильной вихревой структуры в газоразрядной ненейтральной электронной плазме. Описан коллапс электронного слоя в газоразрядной плазме ячейки Пеннинга. Анализируется взаимодействие между стабильной вихревой структурой и симметричным электронным слоем, а также, влияние вихревых структур на перенос электронов вдоль и поперек магнитного поля.

განმხოლოებული გრიგალური სტრუქტურის დინამიკა დაჯახებად სუფთა და აირგანმუხტვად არანეიტრალურ ელექტრონულ პლაზმებში

ნიკოლოზ ა. კერვალიშვილი

რეზიუმე

წარმოდგენილია სუფთა ელექტრონულ და აირგანმუხტვად ელექტრონულ არანეიტრალურ პლაზმებში გრიგალური სტრუქტურების წონასწორობის, ურთიერთ ქმედების და დინამიკის ექსპერიმენტული კვლევების შედეგების ანალიზი მიმდინარე დროში, რომელიც ბევრად მეტია ელექტრონ-ნეიტრალთან შეჯახების დროზე. განხილულია სუფთა ელექტრონული პლაზმის სვეტის ხანგრძლივი შეკავების პრობლემა პენინგ-მალმბერგის მახეში. შემოთავაზებულია ხანგრძლივარსებული სტაბილური გრიგალური სტრუქტურის თვითდამჭერი მექანიზმი აირგანმუხტვად არანეიტრალურ ელექტრონულ პლაზმაში. აღწერილია ელექტრონული შრის კოლაპსი პენინგის უჯრედის აირგანმუხტვად პლაზმაში. გაანალიზებულია სტაბილურ გრიგალურ სტრუქტურასა და სიმეტრიულ ელექტრონულ შრეს შორის ურთიერთქმედება, ასევე გრიგალური სტრუქტურების გავლენა მაგნიტური ველის განივ და გასწვრივ ელექტრონების გადატანაზე.

Obituaries:

(1932-2012)

(1935-2012)

(1932-2012)

(1934-2011)

(1951-2012)

In 2011-2012, the Institute of Geophysics they left forever several leading specialists in the field of physics of the atmosphere and clouds and plasma physics. They all - Tamaz Salukvadze, was born into 1934; Eteri Khelaya, was born into 1935; Roman Doreuli, was born into 1932; Albert Nodia, was born into 1934, Giorgi Aburjania was born into 1951 - after end of the Physics Faculty of Tbilisi State University during several decades were occupied by scientific activity in the Department of Physics of Atmosphere of the Institute of Geophysics. Today we recall about them.

T. Salukvadze (it worked in the Institute of Geophysics in 1958-2012), E. Khelaya (1963-2012) and R. Doreuli (1962-2005), they were the specialists of high class in the field of the radar of convective clouds and artificial action on the clouds, and A. Nodia (1968-2011 - in the field of the electricity of the atmosphere and clouds. They all took direct part in the measurements, the collection and the analysis of observational data.

T. Salukvadze worked on the different posts from the senior technician to the senior scientific worker. In 1980 it protected candidate thesis. The significant contribution to the cause of the establishment of the radar structure of convective clouds made. He was the author more than 70 scientific works, including of one monograph and one invention. The rewards and the money rewards of the governments of the Soviet Union and Bulgaria were obtained for the successes in the practical activity in the region of artificial action on the hail processes in the different time.

E. Khelaya worked as junior, then senior scientific worker. In 1984 it protected candidate thesis. She made the significant contribution to the cause of the establishment of the thunderstorm and hail danger of convective clouds by radar methods. She was the author more than 60 scientific works, including of one monograph. In 1978 in the service of fight with the hail of Georgia was inculcated the developed by it radar method of the recognition of hail and rain clouds.

R. Doreuli worked as engineer, junior scientific and scientific worker. In essence it worked at the composition of the detailed maps of the fields of the distribution of hail and thunderstorm processes in Eastern Georgia on the basis of radar data. He was the author more than 40 scientific works, including of one invention. For the successful work in Georgia and Bulgaria it was rewarded with medal and money rewards.

A.Nodia worked as engineer, junior and senior scientific worker. In 1990 it protected candidate thesis. Being based on the results of field (including aircraft) and laboratory experiments, it made the significant contribution to the cause of the establishment of the electrical structure of clouds and active action on them for the purpose of the regulation of their electrical structure. He was the author more than 110 scientific works.

Professor Giorgi Aburjania suddenly passed away in Cosenza, Italy during his scientific visit at the University of Calabria within the 7th framework project of the Euro Commission, leaving his family, friends and colleagues in deep sorrow. Prof. Aburjania's was born in 1951 in Khobi, Georgia. He has graduated from V.M. Komarov secondary school of physics and mathematics in Tbilisi in 1968. In 1973 he completed the course of theoretical physics at the faculty of physics at I. Javakhishvili Tbilisi State University (TSU) with honors. In 1978 he defended the dissertation work with the degree of candidate of physical and mathematical sciences (PhD) at the institute of physics At Georgian Academy of Sciences, Tbilisi in the field of plasma physics. In 1990 he obtained the degree of doctor of physical-mathematical science with specialty "theoretical and mathematical physics" in Tbilisi State University, Georgia. At this university prof. Aburjania has prepared and read various general and special lecture courses of physics for students, post graduated students and doctoral fellows for many years. He was a head of Laboratory of Investigation of the Extraordinary Phenomena at the I. Vekua Institute of Applied Mathematics of TSU. He was Chief scientist at M. Nodia Institute of Geophysics, TSU. Well known specialist in the field of plasma physics, physics of ionosphere and magnetosphere, theories of linear, nonlinear wavy, solitary vortex structures and vortical turbulences in the dispersed media. He was an author of known monograph "Aburjania G.D. "Self-Organization of the Nonlinear Vortex Structures and the Vortical Turbulence in the Dispersive Media", Moscow, KomKniga –URSS, 2006". Pro. Aburjania worked at the leading scientific centers of Russia, Ukraine, Italy and others. Author more than 190 scientific articles, published in international impact factor and refereed scientific journal. His works were always progressive and recognized by the international scientific society. All his life he served a science nevertheless his heath condition. Prof. Aburjania was full of life, energy, with very special sense of humor. So, smiling he left us – his colleagues in deep sadness.

They all repeatedly participated in many local and international conferences.

EUROPEAN COMMISSION RESEARCH EXECUTIVE AGENCY
International Fellowships Head of Unit
B[illegible]
Legal representative of Ivane Javakhishvili Tbilisi State University

Dear Mr. Aleksandre Kvitashvili,
It is with great sadness that I have been informed today about the death of Dr. Giorgi Aburjania during a secondment as an experienced researcher in the framework of the GEOPLASMAS IRSES project.
On behalf of the Research Executive Agency and my unit, please accept our deepest and most sincere condolences. Our thoughts are with Dr. Aburjania's family, friends and colleagues at this difficult time.

Francois Willekens, Head of Unit

Dear family members of Giorgi

I knew Giorgi for almost 40 years.

Last time we met in CALABRIA couple of years ago. He loved this country, enjoyed staying there and it is impossible to believe that he passed away in this beautiful place. Giorgi was always full of life and energy, he never complained and I even do not know about any heart problems he had. He was very enthusiastic about science, was very active last years and I am very proud that we finished our first (and already last) joint paper. I will always remember him smiling, writing equations and arguing about plasma science.

Lev Zelenyi, Head of IKI - Space Research Institute

To the family of Giorgi Aburjania,

I am Gaetano Zimbardo, the Italian colleague of Giorgi. As you know, he came here for an exchange visit within the framework of a European project called Geoplasmas. Herewith I would like to give you my condolences as well as those of all the teams of the Geoplasmas project, including the project officer in Bruxelles. Many people knew Giorgi and his passing away was really shocking to us. I was always very impressed by his will to carry out research, as well as by his attachment to family and to his own country.

Gaetano Zimbardo, University of Calabria

Information for contributors

Papers intended for the Journal should be submitted in two copies to the Editor-in-Chief. Papers from countries that have a member on the Editorial Board should normally be submitted through that member. The address will be found on the inside front cover.

1. Papers should be written in the concise form. Occasionally long papers, particularly those of a review nature (not exceeding 16 printed pages), will be accepted. Short reports should be written in the most concise form not exceeding 6 printed pages. It is desirable to submit a copy of paper on a diskette.
2. A brief, concise abstract in English is required at the beginning of all papers in Russian and in Georgian at the end of them.
3. Line drawings should include all relevant details. All lettering, graph lines and points on graphs should be sufficiently large and bold to permit reproduction when the diagram has been reduced to a size suitable for inclusion in the Journal.
4. Each figure must be provided with an adequate caption.
5. Figure Captions and table headings should be provided on a separate sheet.
6. Page should be 20 x 28 cm. Large or long tables should be typed on continuing sheets.
7. References should be given in the standard form to be found in this Journal.
8. All copy (including tables, references and figure captions) must be double spaced with wide margins, and all pages must be numbered consecutively.
9. Both System of units in GGS and SI are permitted in manuscript
10. Each manuscript should include the components, which should be presented in the order following as follows:
    Title, name, affiliation and complete postal address of each author and dateline.
    The text should be divided into sections, each with a separate heading or numbered consecutively.
    Acknowledgements. Appendix. Reference.
11. The editors will supply the date of receipt of the manuscript.

CONTENTS

სარჩევი

საქართველოს გეოფიზიკური საზოგადოების ჟურნალი

სერია ბ. ატმოსფეროს, ოკეანესა და კოსმოსური პლაზმის ფიზიკა

ჟურნალი იბეჭდება საქართველოს გეოფიზიკური საზოგადოების პრეზიდიუმის დადგენილების საფუძველზე

ტირაჟი 200 ცალი

ЖУРНАЛ ГРУЗИНСКОГО ГЕОФИЗИЧЕСКОГО ОБЩЕСТВА

Серия Б. Физика Атмосферы, Океана и Космической Плазмы

Журнал печатается по постановлению президиума Грузинского геофизического общества

Тираж 200 экз

JOURNAL OF THE GEORGIAN GEOPHYSICAL SOCIETY

Issue B. Physics of Atmosphere, Ocean and Space Plasma

Printed by the decision of the Georgian Geophysical Society Board

Circulation 200 copies